Durability of Novel C-S-H-based Nanocomposites and Secondary Hydrated Cement Phases

Rahil Khoshnazar

Thesis submitted to the
Faculty of Graduate and Postdoctoral Studies
in partial fulfillment of the requirements
for the Doctorate in Philosophy degree in
Civil Engineering

Department of Civil Engineering
Faculty of Engineering
University of Ottawa

To my beloved parents and sister

Abstract

Issues concerning mechanisms of durability of hydrated cement phases in aggressive environments were studied. The possibility of using organic compounds in order to modify the micro- and nanostructure of the calcium-silicate-hydrate (C-S-H) phases was also investigated. Pure cement-based hydrated phases were synthesized and characterized by several analytical techniques such as X-ray diffraction, thermal gravimetric analysis, Fourier transform infrared spectroscopy and scanning electron microscopy. Compacted samples of the synthetic hydrated cement phases were also prepared and used for the assessment of durability and mechanical properties. This doctoral thesis is comprised of several research chapters which can be categorized into two main parts. The first part focuses on the development of novel organically modified C-S-H systems. The second part involves the mechanisms underlying the volume stability of phase pure sulfoaluminate and related phases. A brief description of each part is as follows:

- *development of novel organically modified C-S-H systems:* The mechanisms of interaction of organic compounds with the nanostructure of C-S-H systems were studied. A model for the nanostructure of the resulting composite systems was proposed. In addition, the organically modified systems were tested for length-change, calcium-ion leaching and diffusion of isopropanol. Dynamic mechanical analysis and microindentation techniques were also used to determine the mechanical performance. Evidence of the superior engineering performance of the novel organically modified C-S-H systems was provided.
- *mechanisms of the volume stability of sulfoaluminate and related phases:* Volume stability and change in the microstructure of the synthetic ettringite, monosulfate and thaumasite was critically examined in de-ionized water as well as in highly concentrated gypsum- or lime-water. A new dissolution-based mechanism for the expansion of these phases was proposed. The volume stability of multicomponent systems comprised of the C-S-H-based system (prepared in part I) and these sulfate-based hydrated phases was also investigated. It was suggested that the systems containing the modified C-S-H rather than the phase pure C-S-H had better resistance to crack growth and disintegration originating from the presence of ettringite or thaumasite.

Acknowledgements

I would like to express my deepest gratitude to my supervisor, Dr. James J. Beaudoin (Researcher Emeritus at the National Research Council, Canada (NRC) and Adjunct Professor at the University of Ottawa) for his continuous support, insightful advice and warm encouragement throughout my doctoral program. He has a wealth of knowledge of cement science and has been generously available for scientific discussions. It has been a privilege to work with him on this intriguing subject.

I would also like to gratefully thank Dr. Laila Raki (Senior Researcher at NRC) for her thoughtful comments and suggestions on my research. She made me familiar with the interesting aspects of clay minerals and helped enrich the chemistry perspective presented within this thesis. A special thank you is also extended to Dr. Rouhollah (Aali) Alizadeh (CEO at Giatec Scientific) for his willingness to share his experiences regarding the application of nanotechnology in the study of cement-based materials.

This doctoral research also benefited from scientific discussions with researchers at NRC: Drs. Pierre-Claver Nkinamubanzi, Jon Makar, Taijiro Sato, Patrick Grattan-Bellew and Jean-Francois Masson. The advice of Dr. Sagrario Martínez Ramírez and Dr. María Teresa Blanco-Varela (from Spanish National Research Council) on the synthesis procedure of pure thaumasite is also acknowledged. Thanks also to my examination committee members Drs. Jason Weiss, Pouria Ghods, Beatriz Martin-Pérez, and Mamadou Fall for their suggestions on the current work.

I am highly thankful to Messrs. Gordon Chan, Jim Margeson, Ken Trischuk, Peter Collins, Dave Edwards, Bruce Baldock, Omran Madani, Glenden Pye and Mses. Sladana Bundalo-Perc, Malgosia Kanabus-Kaminska, Ana Delgado and Helen Yew (laboratory technical officers at NRC) for their training on various experimental techniques. Their assistance made it possible to implement my novel ideas. The technical assistance of my colleagues (Ms. Dan-Tam Nguyen and Mr. Pouya Pourbeik) is also acknowledged.

I am also grateful to my fabulous family and friends for their continued support, encouragement and patience during this journey.

The experimental program of this thesis was conducted at the laboratories of the National Research Council, Canada (NRC). I would also like to acknowledge the financial support provided by an NSERC discovery grant on –"Nanostructural tailoring of cement systems for sustainability". I was also partially supported by scholarships and assistantships at the University of Ottawa. The travel grants provided by both the NSERC and the University of Ottawa enabled me to present my research achievements at several international conferences and universities. The NETZSCH Company is also acknowledged for providing the trial version of Peak Separation software for the thermal analysis.

Contents

Chapter 1

Introduction and Objectives

1.1 Introduction

Concrete is the most widely used material in the construction industry. It is estimated that more than 1 m^3 of concrete per person is produced annually world-wide [1]. Numerous studies have been carried out, in the last century, to improve the characteristics of concrete materials. Significant advances have been achieved in the design and implementation of concrete structures. However, despite documented progress, the issue of concrete durability still remains as one of the major challenges for the sustainable engineering solutions [2-12]. The exposure of concrete infrastructure to aggressive solutions, e.g. those containing chloride and sulfate ions, leads to significant damage every year [13-18]. Recent deterioration of the reinforced concrete foundations of two Canadian arctic buildings due to thaumasite formation is an example. Expansion and premature loss of structural integrity in the buildings was so severe that some of the columns had to be replaced after a two-year service period [17].

Map cracking due to alkali-silica reactivity is another issue leading to serious damage to the concrete structures [2, 6, 9]. The cyclic freezing and thawing of water may also result in large expansions that lead to deterioration of concrete structures through internal cracking. The frost damage problem has been aggravated by the use of de-icing salts that results in the progressive scaling of concrete surfaces [1]. It is estimated that deterioration of concrete results in billions of dollars of repair costs to the North American infrastructure [19].

Hydrated Portland cement - the principal binder in concrete - plays an important role in most of the durability related problems. Calcium Silicate Hydrate (C-S-H), the primary binding phase in cement paste, is a major contributor to the important properties of hardened concrete such as strength, volume stability, and durability [20]. Secondary phases, e.g. sulfoaluminate phases, can also have a significant role in determining the durability of concrete structures [21-28]. A clear understanding of the mechanisms responsible for the durability of the hydration products and the development of new construction materials with improved durability is, therefore, strategic for enhancing the service-life of concrete structures.

1.2 Objectives

The current doctoral thesis was designed to explore new methods for enhancing the durability and sustainability of cement-based materials. Two approaches were considered; the development of novel organically modified C-S-H systems with enhanced durability, and the investigation of the mechanisms underlying durability and volume stability of secondary hydrated cement phases, especially sulfoaluminate and related phases, in the aggressive solutions. Several studies have been conducted, during the past few years, on the development of organically modified C-S-H systems and the assessment of the physico-chemical behavior of these systems [29-43]. In spite of the numerous studies, the mechanisms of interaction of organic compounds with the nanostructure of C-S-H systems are not clearly understood. In addition, a comprehensive assessment of the engineering performance of the resulting C-S-H systems is still lacking. The ultimate goal of using organic compounds for the modification of C-S-H systems is to improve the durability and mechanical properties of the C-S-H-based materials. Selected organic compounds with this potential can be used as chemical admixtures in cement-based construction materials. It is argued that this can contribute to the construction of more sustainable concrete infrastructure. The first part of this research (chapters 4 to 11) was designed to contribute towards the attainment of this goal.

The mechanism of volume stability of the sulfoaluminate and related phases is the focus of the second part of this doctoral research (chapters 12 to 15). It is well-known that presence

of the calcium sulfoaluminate phases (ettringite and monosulfate) in concrete can contribute to expansion and cracking of concrete elements. The primary mechanism of these expansions, however, has been the subject of considerable debate for more than 40 years. The second part of this research comprises a substantial contribution towards the resolution of this debate. The mechanism of expansion of pure synthetic thaumasite, which is structurally similar to ettringite, was also investigated in this research for the first time. The efficiency of the modification of C-S-H with organic compounds in improving the volume-stability of multicomponent samples comprised of both the C-S-H-based systems and these secondary hydrated cement phases was also studied in the last chapter. Specific objectives for each chapter are stated as follows:

Chapter 2. To critically examine published information and identify any controversial issues relevant to the mechanisms of interaction of organic compounds with the nanostructure of C-S-H as well as those underlying the durability and engineering performance of hydrated cement phases,

Chapter 3. To select appropriate experimental techniques for the study of the key problems identified in chapter 2,

Chapter 4. To investigate the mechanisms of interaction of nitrobenzoic acid isomers with the micro- and nano-structure of C-S-H systems and to propose a model for the nanostructure of C-S-H/nitrobenzoic acid composite systems,

Chapter 5. To study the durability and mechanical properties of C-S-H/nitrobenzoic acid composite systems synthesized in chapter 4,

Chapter 6. To explore the characteristics and engineering performance of C-S-H/aminobenzoic acid composite systems and compare them with those obtained for the C-S-H/nitrobenzoic acid composite systems investigated in chapters 4 and 5,

Chapter 7. To examine the change in the mechanical performance of C-S-H systems modified with nitro- or amino-benzoic acid isomers under dynamic loading at elevated temperatures,

Chapter 8. To study the fatigue behaviour of the phase pure and organically modified C-S-H systems,

Chapter 9. To study the influence of selected organic polymers and compounds on the nanostructure and engineering performance of C-S-H system,

Chapter 10. To investigate the volume stability of C-S-H/polyaniline composites (prepared using an in-situ polymerization technique) in potentially aggressive salt solutions,

Chapter 11. To investigate possible mechanisms contributing to the mechanical stability of C-S-H/polyaniline composite systems at elevated temperatures,

Chapter 12. To propose a new mechanism underlying the expansion of calcium sulfoaluminate phases,

Chapter 13. To explore the possible damage to the microstructure of ettringite due to drying with the solvent-exchange technique,

Chapter 14. To explore the possible damage to the microstructure of monosulfate due to drying with the solvent-exchange technique,

Chapter 15. To investigate the mechanisms of expansion of thaumasite in aqueous solutions and compare these mechanisms with those proposed for ettringite. It is also intended to investigate the mechanisms of expansion of multicomponent systems composed of ettringite or thaumasite with the C-S-H-based systems, and determine the efficiency of the use of organically modified C-S-H systems rather the phase pure C-S-H system in reducing the expansions,

Chapter 16. To provide a summary of the research achievements and a list of recommendations for future study.

1.3 Overview

The current doctoral thesis is composed of 16 chapters. Each chapter has the format of a research paper, and includes an abstract, introduction, experimental program, results and discussion, concluding remarks and references. Chapters 4 to 11 focus on the development, characterization and durability assessment of novel organically modified C-S-H systems. The nature of the interactions of various organic compounds with the micro- and nano-

structure of C-S-H systems was investigated. The efficiency of the organically modified C-S-H systems for improved durability and sustainability of cement-based materials was also assessed. Chapters 12 to 15 include the synthesis of pure selected secondary hydrated phases (ettringite, monosulfate and thaumasite), and examination of a novel mechanism underlying their expansion in aqueous solutions.

An overview of chapters 2 to 15 is provided:

Chapter 2. The literature review includes a brief description of the microstructure and characteristics of Calcium-Silicate-Hydrate (C-S-H) systems, organically-modified C-S-H-systems and the secondary phases in cement paste. The role of each phase as it relates to the durability of concrete structures is also provided.

Chapter 3. The application of various experimental techniques in cement science is described. The techniques for the synthesis of pure cement-based hydrated phases are also provided.

Chapter 4. The mechanisms of interaction of nitrobenzoic acid isomers with the nanostructure of C-S-H systems were investigated in this chapter. C-S-H systems with various concentrations of nitrobenzoic acid isomers were synthesized using a pozzolanic reaction technique. The resulting composite systems were characterized by the X-ray diffraction, thermal gravimetric analysis, Fourier transform infrared spectroscopy and scanning electron microscopy techniques. BET nitrogen surface area measurements were also obtained. A model for the nanostructure of the C-S-H/nitrobenzoic acid systems was proposed.

Chapter 5. The durability and mechanical performance of the C-S-H/nitrobenzoic acid systems prepared in chapter 4 were studied in this chapter. Compacted porous bodies of the C-S-H/nitrobenzoic acid systems with a porosity of about 30% were prepared, and data from the length-change measurements and calcium ion leaching in aggressive aqueous salt solutions was obtained. Mass-change of the compacted samples due to the diffusion of isopropanol into their porous structure was also measured. In addition, the microindentation technique was used to assess the creep modulus and the hardness of the samples. Evidence was provided on the contribution of the nitrobenzoic acid isomers to the durability and mechanical performance of the C-S-H-based composite systems.

Chapter 6. C-S-H/aminobenzoic systems were synthesized and characterized by the X-ray diffraction and Fourier transform infrared spectroscopy. BET nitrogen surface area measurements were also made. The length-change of the compacted samples in LiCl and $MgSO_4$ solutions, their mass-change in isopropanol as well as their microindentation creep measurements were determined. It was shown that the C-S-H systems modified with aminobenzoic acid had improved volume stability and microindentation creep modulus.

Chapter 7. Dynamic mechanical thermal analysis (DMTA) was employed to assess the dynamic mechanical stability of the C-S-H systems modified with nitro- or amino-benzoic acid isomers upon heating. Evidence was provided on the structural role of nitrobenzoic acid isomers in these composite systems. The role of aminobenzoic acid isomers, however, was not as significant.

Chapter 8. Fatigue behaviour of the phase pure C-S-H and C-S-H systems modified with nitrobenzoic acid isomers was studied by the dynamic mechanical analysis (DMA) technique. The effect of the Ca/Si ratio and hydration time of the phase pure C-S-H was also considered. The organically modified C-S-H systems and those with lower Ca/Si ratios or increased hydration time had higher resistance to change of their storage modulus and fracture under repetitive loading.

Chapter 9. Possible intercalation of organic polymers in the interlayer region of C-S-H systems as reported by Matsuyama and Young [29-32] indicated that these polymers likely have potential to improve the engineering performance. Accordingly, three different polymers (polyvinyl alcohol, polyacrylic acid and polymethylmethacrylate) were selected for the preparation of the C-S-H-based composite systems. The volume stability and mechanical properties were assessed. Several other organic compounds with the potential application for use as chemical admixtures were also selected. No significant evidence of the interaction of the organic polymers/compounds with the nanostructure of C-S-H was obtained except for that incorporating the higher concentration of an organosilane compound. In most cases, the resulting systems had poor volume stability/mechanical properties.

Chapter 10. The C-S-H/polyaniline nanocomposites were synthesized for the first time by Alizadeh et al. [41] using an in-situ polymerization technique. In this chapter, the volume stability of these nanocomposites was assessed in various aggressive salt solutions. The damage to the microstructure of the samples was also assessed using various analytical techniques. It was suggested that the C-S-H/polyaniline nanocomposites had superior volume stability in the test solutions. The improvement was more pronounced for the samples with a higher Ca/Si ratio of the host C-S-H.

Chapter 11. The mechanisms underlying the mechanical stability of C-S-H/polyaniline nanocomposites were discussed in this chapter. The preliminary test results had been reported by Alizadeh in 2009 [44]. Additional discussions relevant to the mechanisms underlying the stability of these nanocomposites at elevated temperatures were provided in the current study.

Chapter 12. The mechanisms of expansion of sulfoaluminate phases in cement paste have been debatable for more than 40 years. In this chapter, pure ettringite and monosulfate were synthesized and compacted into porous samples. The length-change of these samples in de-ionized water as well as in aqueous solutions saturated with lime or gypsum was determined. A dissolution mechanism was suggested for the length-change measurements. Evidence of the changes in the pH of the solutions and changes occurring in the crystalline structure and morphology of the samples was provided in support of a proposed dissolution mechanism.

Chapter 13. Drying of pure ettringite samples using the solvent-exchange technique was investigated in this chapter. Three different alcohol-based solvents (methanol, ethanol and isopropanol) were selected. The mechanism of dehydration of ettringite and any possible interaction between the organic solvents and the microstructure of ettringite were investigated using various analytical techniques. Evidence was obtained on the damaging effect of methanol. These effects were, however, limited for the isopropanol.

Chapter 14. A similar study to that in chapter 13 was performed on pure monosulfate containing 12 moles of hydrate water (AF-12) in order to elucidate the mechanism of drying of this phase, further understand its microstructure and explore any possible

interaction between the organic solvents and the microstructure of monosulfate. It was suggested that dehydration of AFm-12 to AFm-10 occurs readily in any of the organic solvents. In addition, application of isopropanol for a limited time had the least damaging effect compared to that caused by methanol or ethanol.

Chapter 15. Several investigations have been published with a focus on the mechanisms of formation of thaumasite in cement-based systems. The published investigations on the mechanisms of expansion of thaumasite are, however, very limited. Pure thaumasite was synthesized in this chapter and length-change measurements were made in de-ionized water and in aqueous solutions containing a high concentration of gypsum or lime. Possible mechanisms of the expansions were discussed based on a comparison with those suggested in chapter 12 for the expansion of ettringite. In addition, multicomponent compacted samples comprised of 10% of ettringite or thaumasite and 90% of C-S-H-based systems were prepared and length-change measurements obtained. The efficiency of the modification of the C-S-H system with nitrobenzoic acid in reducing the expansions was also considered. It was suggested that the proposed dissolution mechanism plays a significant role in the length-changes observed. Modification of C-S-H with the nitrobenzoic acid isomers was also effective in increasing the service-life of the multicomponent systems in the test solutions.

References

1. K. Scrivener and R. Kirkpatrick, “Innovation in use and research on cementitious material,” *Cement and Concrete Research*, 38, pp. 128-136, 2008.
2. T. Ahmed, E. Burley, S. Rigden and A. I. Abu-Tair, “The effect of alkali reactivity on the mechanical properties of concrete,” *Construction and Building Materials*, 17, pp. 123-144, 2003.
3. J. Grandet, “of high performance concrete in relation to external chemical,” in Y. Mailer (Ed.), *Attack High Performance Concrete from Material to Structure*, E & FN Spon, London: 234-238, 1992.

4. D. Hobbs, "Thaumasite sulfate attack in field and laboratory concretes: implications for specifications," *Cement and Concrete Composites*, 25, pp. 1195–1202, 2003.

5. M. A. Hussain and S. R. Sumadi, "Durability of high performance concrete in seawater," in *Symposium on Industrial Technology and Engineering*, Malaysian Science and Technology congress, 1999.

6. V. Jensen, "Alkali–silica reaction damage to Elgeseter Bridge, Trondheim, Norway: a review of construction, research and repair up to 2003," *Materials Characterization*, 53, pp. 155- 170, 2004.

7. S. T. Lee, D. H. Lee, S. S. Kim, K. P. Park, H. S. Jung, D. K. Kim and B. Y. Kim, "Magnesium sulfate attack of mortars containing GGBFS with different fineness levels," in *The 3rd ACF International Conference-ACF/VCA*, pp. 1069-1075, 2008.

8. F. Li, Y. Yuan and C. Li, "Corrosion propagation of prestressing steel strands in concrete subject to chloride attack," *Construction and Building Materials*, 25, pp. 3878-3885, 2011.

9. H. Marzouk and S. Langdon, "The effect of alkali-aggregate reactivity on the mechanical properties of high and normal strength concrete," *Cement and Concrete Composites*, 25, pp. 549-556, 2003.

10. P. Mehta, "Sulfate Attack on Concrete: Separating Myths from Reality," *Concrete International*, 22, pp. 57-61, 2000.

11. A. Neville, "The confused world of sulfate attack on concrete," *Cement and Concrete Research*, 34, pp. 1275-1296, 2004.

12. M. O'Connell, C. McNally and M. G. Richardson, "Biochemical attack on concrete in wastewater applications: A state of the art review," *Cement and Concrete Composites*, 32, pp. 479-485, 2010.

13. H. Mingyu, L. Fumei and T. Mingshu, "The thaumasite form of sulfate attack in concrete of Yongan Dam," *Cement and Concrete Research*, 36, pp. 2006-2008, 2006.

14. R. Dong, B. Ma, X. He, H. Zhu and J. Wei, "Sulfate Attack on Concrete in an Inland Salt Lake Environment," *Journal of China University of Geosciences*, 17, pp. 342-348, 2006.

15. A. Leemann and R. Loser, "Analysis of concrete in a vertical ventilation shaft exposed to sulfate-containing groundwater for 45 years," *Cement and Concrete Composites*, 33, pp. 74-83, 2011.

16. Y. Parka, J. Suhb, J. Lee and Y. Shin, "Strength deterioration of high strength concrete in sulfate environment," *Cement and Concrete Research*, 29, pp. 1397-1402, 1999.

17. J. A. Bickley, R. T. Hemmings, R. D. Hooton and J. Balinsky, "Thaumasite related deterioration of concrete structures," In: Proceedings of the Concrete Technology: Past, Present and Future - ACI SP, pp. 144-8: 159-75, 1994.

18. N. I. Fattuhi and B. P. Hughes, "Effect of acid attack on concrete with different admixtures or protective coating," *Cement and Concrete Research*, 13, pp. 655-665, 1983.

19. NCHRP Report 577, "Guidelines for the selection of snow and ice control materials to mitigate environmental impacts," Transportation Research Board, Washington, D.C..

20. T. D. Ciach, J. E. Gillott, E. G. Swenson and P. J. Sereda, "Microstructure of calcium silicate hydrates," *Cement and Concrete Research*, 1, pp. 13-25, 1971.

21. Skalny, J., Marchand, J., and Odler I. (Eds), Sulfate attack on concrete. Modern Concrete Technology Series, 10, E. & F. Spon, London., 2002.

22. F. P. Glasser, "The stability of ettringite," in Delayed Ettringite Formation, Eds Scrivener K., Skalny J., Switzerland, pp. 43-64, 2002.

23. H. Taylor, Cement Chemistry. 2nd Edition, London: Thomas Telford Publication, 1997.

24. P. Mehta, "Sulfate Attack on Concrete - A Critical Review" in Materials Science of Concrete III. Ed. J. Skalny, The American Ceramic Society, Westerville, OH, pp. 105-130, 1992.

25. M. Santhanam, M. D. Cohen and J. Olek, "Sulfate attack research - whither now?," *Cement and Concrete Research*, 31, pp. 845-851, 2001.

26. H. F. Taylor, C. Famy and K. L. Scrivener, "Delayed ettringite formation," *Cement and Concrete Research*, 31, pp. 683-693, 2001.

27. B. A. Clark and P. W. Brown, "The formation of calcium sulfoaluminate hydrate compounds - Part I," *Cement and Concrete Research*, 29, pp. 1943-1948, 1999.

28. B. A. Clark and P. W. Brown, "The formation of calcium sulfoaluminate hydrate compounds - Part II," *Cement and Concrete Research*, 30, pp. 233-240, 2000.

29. H. Matsuyama and J. F. Young, "Intercalation of Polymers in Calcium Silicate Hydrate: A New Synthetic Approach to Biocomposites?," *Chemistry of Materials*, 11, pp. 16-19, 1999.

30. H. Matsuyama and J. F. Young, "Synthesis of calcium silicate hydrate/polymer complexes: Part I," *Journal of Materials Research*, 14, pp. 3379-3388, 1999.

31. H. Matsuyama and J. F. Young, "Synthesis of calcium silicate hydrate/polymer complexes: Part II," *Journal of Materials Research*, 14, pp. 3389-3396, 1999.

32. H. Matsuyama and J. F. Young, "The formation of C-S-H/polymer complexes by hydration of reactive β-dicalcium silicate," *Concrete Science and Engineering*, 1, pp. 66-75, 1999.

33. Popova, G. Geoffroy, M.-F. Renou-Gonnord, P. Faucon and E. Gartner, "Interactions between polymeric dispersants and calcium silicate hydrates," *Journal of the American Ceramic Society*, 83(10), pp. 2556-2560, 2000.

34. F. Merlin, H. Lombois, S. Joly, N. Lequeux, J.-L. Halary and H. Van-Damme, "Cement-polymer and clay-polymer nano- and meso-composites: spotting the difference," *Journal of Materials Chemistry*, 12, p. 3308-3315, 2002.

35. J. Minet, S. Abramson, B. Bresson, A. Franceschini, H. Van Damme and N. Lequeux, "Organic calcium silicate hydrate hybrids: a new approach to cement based nanocomposites," *Journal of Materials Chemistry*, 16, pp. 1379-1383, 2006.

36. J. Minet, S. Abramson, B. Bresson, C. Sanchez, V. Montouillout and N. Lequeux, "New layered calcium organosilicate hybrids with covalently linked organic functionalities," *Chemistry of Materials*, 16, pp. 3955-3962, 2004.

37. A. Franceschini, S. Abramson, V. Mancini, B. Bresson, C. Chassenieux and N. Lequeux, "New covalent bonded polymer-calcium silicate hydrate composites," *Journal of Materials Chemistry*, 17, pp. 913-922, 2007.

38. S. C. Mojumdar and L. Raki, "Preparation and properties of calcium silicate hydrate-Poly(vinyl Alcohol) nanocomposites materials," *Journal of Thermal Analysis and Calorimetry*, 82, pp. 89-95, 2005.

39. S. C. Mojumdar and L. Raki, "Preparation, thermal. spectral and microscopic studies of calcium silicate hydrate-poly(acrylic acid) nanocomposites materials," *Journal of Thermal Analysis and Calorimetry*, 85, pp. 99-105, 2006.

40. S. C. Mojumdar and L. Raki, "Synthesis, thermal and structural characterization of nanocomposites for potential applications in construction," *Journal of Thermal Analysis and Calorimetry*, 86, pp. 651-657, 2006.

41. R. Alizadeh, J. Beaudoin, L. Raki and V. Terskikh, "C-S-H/polyaniline nanocomposites prepared by in-situ polymerization," *Journal of Materials Science*, 46(2), pp. 460-467, 2011.

42. F. Pelisser, P. J. Gleiz and A. Mikowski, "Effect of poly(diallyldimethylammonium chloride) on nanostructure and mechanical properties of calcium silicate hydrate," *Materials Science and Engineering: A*, 527(26), pp. 1045-1049, 2010.

43. F. Pelisser, P. J. Gleiz and M. Peterson, "Synthesis of calcium silicate hydrate/polymer complexes," *IBRACON Structures and Materials Journal*, 4(5), 2011, pp. 695-708.

44. R. Alizadeh, Nanostructure and engineering properties of basic and modified calcium silicate hydrate systems, PhD thesis, University of Ottawa, 2009.

Chapter 2

Overview of Hydrated Cement Phases

Several hydrated phases are formed during the reaction of cement with water. A summary of research progress on the characteristics and engineering performance of these phases is provided in this chapter. The focus is on those of the calcium silicate hydrate (C-S-H) phases, C-S-H-based nanocomposites as well as the calcium-sulfoaluminate phases relevant to the objectives of the current thesis. A more specific literature review will be provided in the introduction section of each of the following chapters.

2.1 Calcium-silicate-hydrate (C-S-H)

Portland cement normally contains four major phases: tricalcium silicate (C_3S), dicalcium silicate (C_2S), tricalcium aluminate (C_3A) and tetra-calcium aluminoferrite (C_4AF).[1] A variety of hydrates are formed when these phases react with water. Calcium-silicate-hydrate (C-S-H) is the primary hydrate phase. It occupies up to about 60% by volume of the hydration products in hydrated cement paste, and is a major contributor to most of its principal properties such as strength, volume stability, and durability [1]. C-S-H in hydrated cement paste is known to have an amorphous or a poorly crystalline structure. Its exact composition and microstructure is, however, uncertain and variable. The hyphens indicate that no specific stoichiometry is implied.

[1] Mineralogical notations of C, S, A and F are often used, in cement chemistry, for CaO, SiO_2, Al_2O_3 and Fe_2O_3, respectively.

2.1.1 Characteristics of C-S-H

Various descriptions can be used for the characterization of C-S-H systems as a material. The primary ones that are relevant to this research are provided in this section.

Ca/Si ratio

The molar ratio of CaO to SiO_2 (Ca/Si ratio) is a principal parameter in the characterization of C-S-H. It is possible to calculate the Ca/Si ratio of the C-S-H by determining the amount of calcium hydroxide [2] and unreacted materials in the hydrated cement paste using analytical methods such as thermal gravimetric analysis or quantitative X-ray diffraction. The Ca/Si ratio in calcium silicate hydrates usually covers a range from 0.7 to 2.0 [3]. The C-S-H formed due to the hydration of C_3S and C_2S in the hydrated cement paste normally has an average of about 1.7 [4]. The formation of C-S-H with low Ca/Si ratio is also possible when the hydrated C_3S is decalcified, e.g. by leaching of the calcium in either de-ionized water or ammonium nitrate [5, 6]. Examples of SEM micrographs of synthetic C-S-H (using the precipitation technique) with Ca/Si ratio of 0.8 and 1.5 are presented in Figure 2-1.

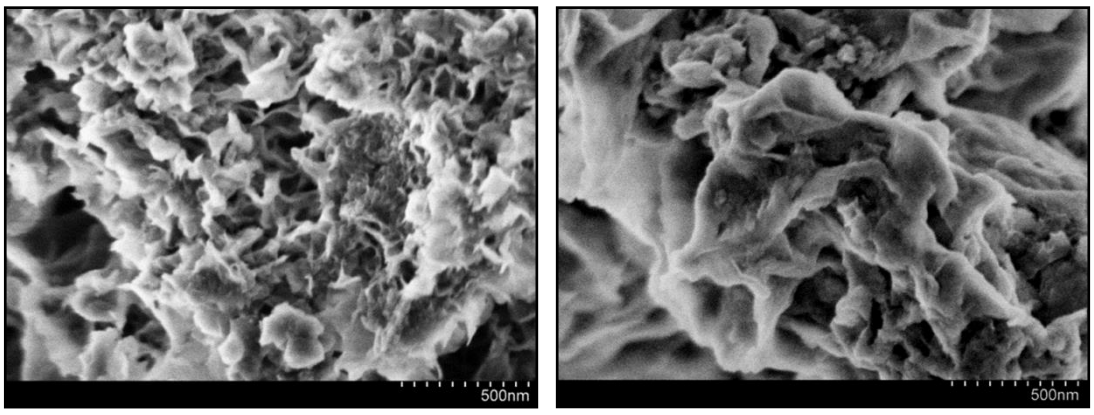

Figure 2-1- SEM micrograph of synthetic C-S-H with Ca/Si = 0.8 (left) and 1.5 (right)

Taylor categorized C-S-H systems as C-S-H (I) and C-S-H (II) for Ca/Si ratios below and above 1.5 [7-9]. Many other studies, however, distinguished various differences for the phase transition that occurs at the Ca/Si ratio of 1.0 within the composition range of C-S-H (I) [10-17]. The most significant changes in the structure of C-S-H with decreasing

the Ca/Si ratio are the longer silicate chains and the increase in the distance between the layers of C-S-H, i.e. X-ray basal-spacing [18]. The nitrogen BET surface area of the synthetic C-S-H also increases noticeably when the Ca/Si < 1.0. These characteristics have been shown to affect the physico-chemical behavior of C-S-H [17].

Aging effects (e.g. silicate polymerization) and the degree of hydration in hardened C_3S paste are dependent on the Ca/Si ratio of C-S-H systems [19]. Richardson and Groves [19] reported that the Ca/Si ratio of C_3S paste, measured by the transmission electron microscopy (TEM) analysis, was 1.71 ± 0.05, 1.77 ± 0.20, 1.74 ± 0.13 and 1.75 ± 0.05 after 1 month, 3 months, 3.5 years and 26 years, respectively.

State of water in C-S-H systems

Water is a key ingredient in cement paste. A minimum water content is required for the completion of the hydration reactions of Portland cement. It also provides the microstructural stability of the hydrated phases after the setting of cement paste. The presence of water in the pore structure, however, is usually considered as a concern for the durability of concrete structures. It facilitates the movement of aggressive ions into the concrete. The freezing of water into ice crystals is also known to cause disruptive volume changes. The role of water and its nature in hydrated cement paste is complex and has been controversial for decades.

The classification of the state of water in cement paste is generally based on the location where it is held and, the nature of its bonding with the solid structure. Various techniques such as nuclear magnetic resonance (NMR), dynamic mechanical analysis (DMA) and helium inflow techniques have been used to differentiate the role of water in various structural locations in the cement paste and also in the synthetic C-S-H systems [17, 20-22]. Although several investigations have attempted to separate the various forms of water, the dividing line between them is not completely clear [23, 24].

It has been suggested by Pellenq et al. [25] that the C-S-H lamellae are held together by an electrostatic force. The interlamellar space is also filled with quasi-immobile water molecules, and the calcium ions that are bonded to the C-S-H layer by partially covalent bonds. In addition to the water vapor in the pores, it is suggested by Ramachandran et

al. [26] that water can exist in various forms e.g. capillary water (in voids larger than 5 nm), adsorbed water (held by hydrogen bonds on the surface of the hydrated particles) and interlayer water. The discussion and debate about the latter (water that is associated with the nanostructure of C-S-H and is strongly held) still continues [27-29]. A recent investigation by Alizadeh [17] has provided additional evidences on the structural role of the interlayer water in the nanostructure and on the engineering performance of C-S-H systems. Alizadeh et al. [30] suggested that water molecules in the interlayer region of C-S-H systems act as restraints in the silicate structure, and contribute to some of the elastic properties of C-S-H.

Silicate polymerization

The silicate tetrahedra of the C-S-H structure are flanked on both sides of the Ca-O sheets (See section 2.1.2). They can be present in the form of dimers, dreierketten or a chain of dreierketten. Silicate polymerization, i.e. the mean length of silicate chains, is usually used to describe the connectivity of silicate chains in the C-S-H systems. The polymerization of silicate chains is often determined by the ^{29}Si NMR technique. The chemical shift of a silicon atom which is bonded to n bridging oxygen, Q^n, is generally used in the technique for the interpretation of the results. In the absence of Q^3, the mean silicate chain-length is normally calculated from the Q^2/Q^1 intensity ratio as following [31]:

$$\textit{mean silicate chain-length} = 2\,(1 + Q^2/Q^1) \qquad (2\text{-}1)$$

Polymerization of C-S-H is significantly affected by its compositional Ca/Si ratio. Chen et al. [31] suggested that the silicate chain-length increases significantly from 2.6 to 9.2 units as the Ca/Si ratio decreases from about 1.44 to 0.92 in synthetic C-S-H systems.

It has been suggested that incorporation of supplementary cementitious materials in hydrated cement paste results in the formation of secondary C-S-H with a relatively low Ca/Si ratio (about 1.0) [7, 32]. The degree of silicate polymerization is likely to be higher in this type of C-S-H. This results in different characteristics of the C-S-H formed [33] which may also account for some of the enhanced durability aspects of the concrete using pozzolanic materials.

Dolado et al. [34] also investigated the Q^n distributions versus the time evolution for the C-S-H systems with Ca/Si = 0.7, 1, 1.4 and 2 using a molecular dynamic modeling approach. These researchers suggested that the number of Q^0 species was reduced more slowly in the C-S-H systems with higher Ca/Si ratio.

Silicate polymerization is also affected by the humidity and temperature. The C-S-H in moist cured cement paste samples contained virtually all dimers, whereas pastes cured at the low relative humidity conditions (RH < 10%) had a greater degree of polymerization [35]. This effect was not noticeable in aged samples. Okada et al. [36] also suggested that C-S-H samples prepared at temperatures above 120 ºC are highly polymerized at all Ca/Si ratios ranging from 0.3 to 2.0. Richardson and Groves [19] suggested that the degree of hydration also affected the mean chain-length. They reported that a 10%-hydrated C_3S paste sample had a silicate mean chain-length of about 2.0. This value was increased linearly to about 2.5 at 85% and about 5.0 at 100% hydration.

Dehydration of C-S-H systems is also known to affect their degree of polymerization. Alizadeh [17] examined the ^{29}Si NMR spectra of the synthetic C-S-H with Ca/Si ratio of 0.8 and 1.2 upon dehydration. He suggested that the Q^2/Q^1 ratio of the samples was significantly increased when their mass-loss exceeded 5%. The formation of new Q^2 sites during dehydration is schematically presented in Figure 2-2. Yu and Kirkpatrick [37] also studied the effect of elevated temperatures up to 1000 °C on synthetic C-S-H systems. Q^3 and even Q^4 chemical shifts were observed in various samples after heat treatment at 250 °C.

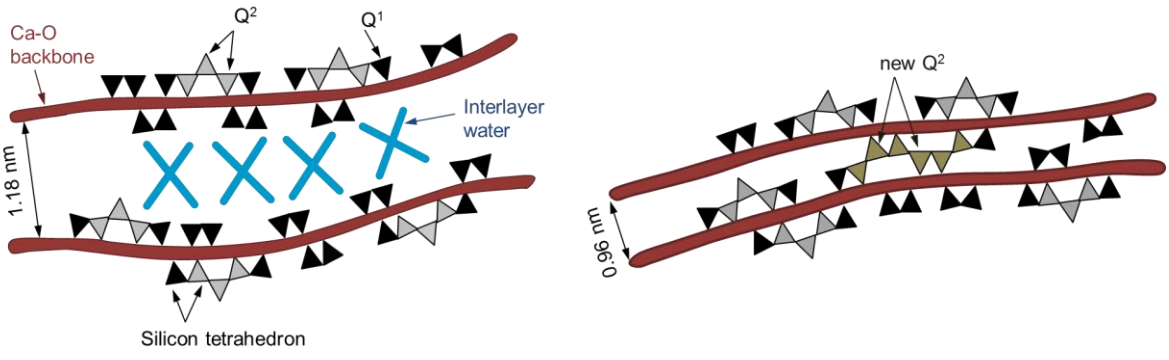

Figure 2-2- Formation of new Q^2 sites in the C-S-H structure from the initial Q^1 sites upon the removal of the interlayer water [17]

Wieker et al. [38], for the first time, applied ^{29}Si NMR to study the structure of various tobermorites[2]. Most of the samples were prepared at high temperatures and by the dehydration of other forms of tobermorite. Their results indicated a high degree of polymerization with the presence of Q^3 site even at the Ca/Si ratio of 1.0. The observed Q^3 sites were attributed to the bridging tetrahedra connected between the layers by hydrogen bonds. These results were expected because of the effect of heat treatment on the increase of degree of silicate polymerization. The decrease in the intensity of Q^1 (end groups) contributed to the condensation of the single chains due to dehydration.

Relationship of C-S-H with more highly ordered phases

Many naturally occurring crystalline calcium (alumino) silicate hydrates are of interest to cement chemists either because they are formed hydrothermally, as in deep oil wells, in autoclaved or hot-pressed materials, or because their structures are very useful in modeling the considerably variable and uncertain structure of C-S-H systems in cement paste [39]. Taylor [8, 40] suggested, in the early 1950's, that the short-range order structure of C-S-H can be related to the structure of crystalline compounds with a silicate-chain repeat distance of 0.73 nm in one direction. The crystal structure of Maddrell's salt (isostructural with β-wollastonite) was also determined by Dornberger-Schiff et al. at the same time period [41]. It was found that β-wollastonite has infinite chains of SiO_3^{2-} repeating at the intervals of three tetrahedra referred to as dreierketten. Repeating intervals for the Ca-O polyhedra are 0.365 nm (half of that for the silicate chain) considering the type of the silicate dreierkette's linkage to the Ca-O layer. Water molecules and calcium ions also fill the space between these layers.

Among various calcium silicate hydrates, 1.4 nm tobermorite ($C_5S_6H_9$ approx.) and jennite ($C_9S_6H_n$), which can be formed at temperatures below 100 °C, appear to provide a much closer structural relationship to the C-S-H gel in hydrated Portland cement. Both of these minerals have a layered structure. The layers are derived from those in CH by substantial distortions of the Ca-O layer and replacement of some or all of the hydroxyl ions by silicate. There are two peaks in the XRD pattern of C-S-H in the region of 0.3 nm and near

[2] The structure of tobermorite is discussed in the following section.

0.18 nm which correspond to important repeat distances in the Ca-O parts of these structures and also of CH [7].

The crystal structure of 1.4 nm tobermorite was resolved by Bonaccorsi et al. [42]. A schematic presentation of a tobermorite layer is shown in Figure 2-3. As shown in the figure, the crystal structure of 1.4 nm tobermorite consists of complex layers with the chemical composition of $[Ca_4Si_6O_{16}(OH)_2(H_2O)_4]^{2-}$. It has a central Ca-O sheet with silicate chains on both sides, which are kinked with a periodicity of three tetrahedra; these chains are called dreierketten, or wollastonite-like chains. The silicate chains that belong to adjacent layers, however, are not condensed into double chains as in 1.1 nm tobermorite. They are shifted by b/2 with respect to one another; the layers are also further apart, with the extra interlayer space occupied by H_2O molecules and Ca^{2+} ions. Jennite is another crystalline calcium silicate hydrate that has dreierkette silicate chains, but it has a much higher Ca/Si ratio than tobermorite. Details of the structure of jennite are described in [39].

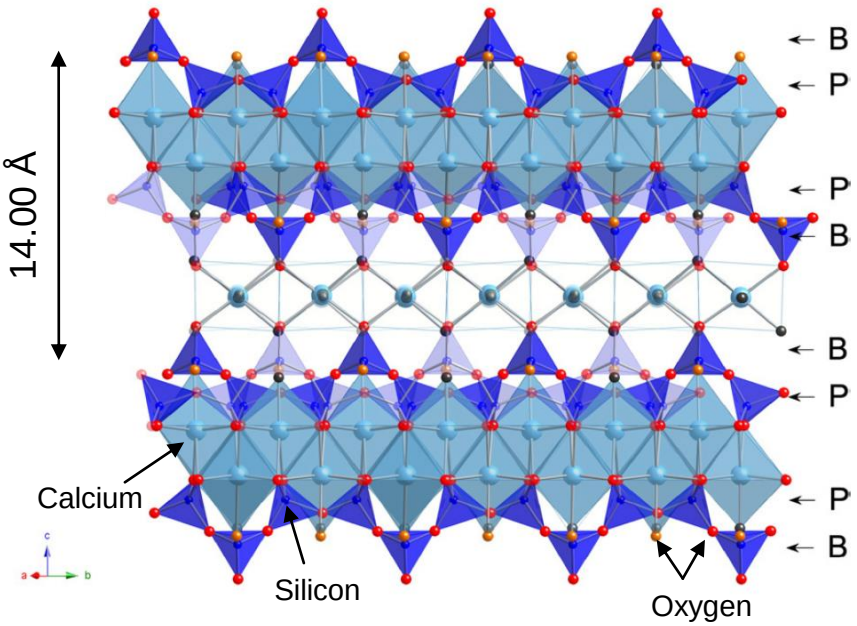

Figure 2-3- Schematic diagram of dreierkette chains present in 1.4 nm tobermorite. The directly connected silicate tetrahedron is called paired (P) and the silicate tetrahedron connecting two paired tetrahedra is called a bridging (B) tetrahedron. It should be noted that the two sets of chains in the central part of the figure are not linked. They are offset from one another by b/2 [39].

2.1.2 C-S-H models

The proposed models for C-S-H can be categorized into two main categories; structure-based models and composition-based models. The former mainly describes the structure of the C-S-H systems, and the latter mainly deals with the chemical composition of these systems. Some of the features of the most important models in each category are described in the following section.

Structure-based models

A model for the poorly crystalline structure of hardened Portland cement paste was proposed by Powers and Brownyard in 1946. This model, known as P-B model [43], was developed primarily based on mass-change measurements at varying humidity and temperature. It was intended to clarify the role of water within the structure of the cement paste. Based on this model, water could be present in two forms; 'evaporable' and 'non-evaporable'. Evaporable water was referred to as water lost under d-drying conditions i.e. over the vapor pressure of dry ice at -79 °C, while non-evaporable water was the remaining water that could be removed by heating up to 1000 ºC. The evaporable water was also categorized as 'gel water' and 'capillary water'.

The P-B model was almost generally accepted until Feldman and Sereda proposed their model in 1968 [44]. This model was further clarified in 1970 in a comparison with previous models [45]. The Feldman-Sereda (F-S) model was developed based on nitrogen surface area and porosity measurements, and isotherms for mass-, length- and modulus of elasticity-change at different humidity conditions. Evidence of a layered model for C-S-H gel was provided. It was also suggested that the water in the interlayer region had a structural role, and the adsorption-desorption curve for the water in this state was irreversible. The schematic picture of the C-S-H in the F-S model is presented in Figure 2-4 [45]. Feldman's later investigation on the diffusion of helium into the C-S-H gel at various humidity conditions provided more clear evidence of the layered nature of the C-S-H gel [46]. A recent study by Alizadeh [17] on the nanostructure and mechanical properties of C-S-H systems further supports the layered structure of C-S-H, and the structural role of the interlayer water.

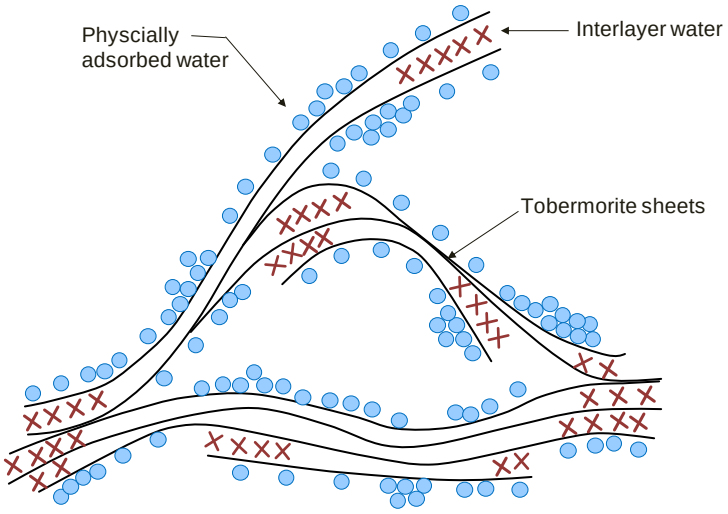

Figure 2-4- Feldman-Sereda model for the structure of C-S-H in hardened Portland cement paste [45]

The P-B and the F-S models have had many followers over the years. These models, however, have also been the source of many discussions and debates [45-50]. Some nanostructural models for the C-S-H in hydrated Portland cement have been recently developed. They, however, are not capable of describing all the C-S-H features, especially the nature and the role of the interlayer water [27-29, 51-53].

Composition-based models

The composition-based models for C-S-H have been developed to describe the molecular structure of C-S-H (i.e. the silicate anions, their arrangement and other molecular bonds in the C-S-H structure). These models were proposed based on X-ray diffraction, microscopic and spectroscopic methods and rarely were concerned with mechanical properties.

The first dreikette-based model for C-S-H was proposed by Bernal et al. in 1952 [54]. It was suggested in this model that the hydrated C_3S contained similar products to the C-S-H formed in dilute suspension which had a layered fibrous structure associated with 1.1 nm tobermorite. Taylor and Howison [55] suggested that the generally accepted Ca/Si ratio of 0.83 for tobermorite could be increased by the removal of some of the 'bridging' tetrahedra and replaced by interlayer Ca^{2+} ions [13, 31, 56-62]. A few other studies proposed that the C-S-H had a structure related to that of jennite [55]. In jennite, half of the oxygen atoms from the central Ca-O part of the C-S-H layer are shared with OH^- groups, whereas in

tobermorite all the oxygen atoms are shared with the infinite parallel rows of silicate chains.

Taylor [63] suggested that the C-S-H in cement paste had a disordered layer structure and was a mixture of structures of both 1.4 nm tobermorite and jennite (T/J model). This provided an explanation for the high Ca/Si ratio of C-S-H in cement paste (1.7 to 2.0). It was shown that dimeric 1.4 nm tobermorite and jennite type structures could, respectively, have a Ca/Si ratio of about 1.25 and 2.25 at early ages. In addition, the ratio of water to calcium of the C-S-H at 11% relative humidity (RH) was in the range suggested by the models. Richardson and Groves [19] further explained the generalized model incorporating the features of the tobermorite-jennite composition (T/J) or the tobermorite-'solid solution' calcium hydroxide (T/CH). It was predicted that the very old C-S-H entirely consisted of jennite-like units. The initial carbonation of C-S-H in cement paste, however, resulted in the loss of calcium from the J unit, and leaving a C-S-H with entirely T-like units. Recent investigations by Pourbeik et al. [64] provided further evidence in support of the T-J model for the structure of synthetic C-S-H and that in cement paste. This research was based on the mechanical performance of synthetic tobermorite, jennite and other C-S-H-based systems rather than the physico-chemistry of these systems.

Cong and Kirkpatrick investigated the nanostructure of C-S-H prepared by two different methods; hydration of β-C_2S, and the aqueous reaction of silica fume and calcium oxide [59, 60, 65]. The ^{29}Si NMR spectroscopy was conducted on the C-S-H samples with Ca/Si ratios of 0.6 to 1.54. The results provided more evidence on the presence of Ca-OH and Si-OH bonds in the C-S-H. The frequency of these bonds, however, depended on the Ca/Si ratio. These researchers proposed a 1.4 nm defect-tobermorite structure for C-S-H in which some of the bridging tetrahedra are missing (Figure 2-5). The chains are short, and they may tilt, rotate or be displaced along the b-axis.

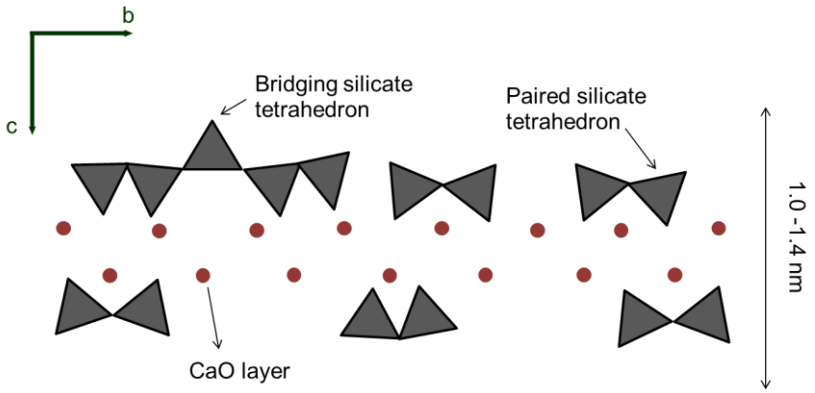

Figure 2-5- Defect-tobermorite model for C-S-H [58]

2.1.3 Preparation of C-S-H

The C-S-H in the hydrated Portland cement is mainly formed from the hydration of C_3S or β-C_2S according to the Equations 2-2 and 2-3. It, however, incorporates various elements. The reaction product can be decalcified with ammonium nitrate in order to achieve almost pure C-S-H [31]. This type of C-S-H usually has an average Ca/Si ratio of about 1.7.

$$2(3CaO.SiO_2) + 6H_2O \rightarrow 3CaO.2SiO_2.3H_2O + 3Ca(OH)_2 \quad (2\text{-}2)$$

$$2(2CaO.SiO_2) + 4H_2O \rightarrow 3CaO.2SiO_2.3H_2O + Ca(OH)_2 \quad (2\text{-}3)$$

Synthetic C-S-H can be obtained using pozzolanic reaction or precipitation techniques. Pozzolanic reaction method includes the mixing of lime and silica in excess water. In the precipitation method, a calcium salt (most commonly calcium nitrate) is mixed with a soluble silicate salt (e.g. sodium silicate). The C-S-H precipitate is, then, filtered and washed with the lime-water.

2.1.4 Mechanical properties of C-S-H

Mechanical properties, e.g. modulus of elasticity and creep, have been rarely investigated on synthetic or phase pure C-S-H. The lack of experimental evidence for the mechanical performance of C-S-H is partially due to the fact that the materials are prepared in the powder form which is not a suitable state for most engineering investigations.

The mechanical properties of C-S-H with various Ca/Si ratios were explored by Beaudoin and Feldman [66]. It was shown that the intrinsic modulus of elasticity (modulus of elasticity at zero porosity, E_0) was likely to be independent of the Ca/Si ratio and the degree of polymerization. The mechanical properties of the C-S-H in cement paste were also investigated by a nano-indentation technique using an atomic force microscope (AFM) instrument [67]. It was suggested that two types of C-S-H existed in hydrated Portland cement; low density and high density C-S-H which had a volume fraction of 30 and 70%, respectively [68]. It was also proposed that the intrinsic elasticity of the C-S-H systems would be decreased during a decalcification process.

Plassard et al. [58] also determined the elastic modulus of C-S-H with various Ca/Si ratios prepared on the surface of a calcite crystal in sodium silicate solution using an AFM technique. It was shown that the elastic modulus increased at higher Ca^{2+} values with an inflection point at the concentration of about 8 mmol/l which could correspond to a Ca/Si ratio of 1.1 [69].

Alizadeh [17] investigated the mechanical properties of C-S-H systems with various Ca/Si ratios at different humidity conditions and temperatures using dynamic mechanical thermal analysis (DMTA) technique. It was shown that the mechanical properties of C-S-H were dependent on its Ca/Si ratio. The storage modulus (E') of the C-S-H systems decreased and their internal friction (tan δ) values increased by increasing the Ca/Si ratio of the specimens. A unique multi-stage change in the stiffness and internal friction of C-S-H systems similar to cement paste was observed as samples were conditioned to moisture contents lower than 11% RH. It was suggested that the adsorbed and interlayer water molecules contributed significantly to the dynamic mechanical properties of C-S-H. Those in the interlayer region acted as restraints to the silicate structure. It was also suggested that mechanisms such as collapse of the C-S-H structure, cross-linking of silicate sites and the interaction of dehydrated interlayer calcium ions with the silicate structure possibly contributed to the variations in E' and tan δ at various drying stages.

The elastic properties of C-S-H systems have also been estimated by the dynamic molecular modeling and free energy minimization techniques [70]. It has been suggested, based on the models of Hamid [71] and Merlino [72] for tobermorite systems, that the

average Young's modulus values could increase from 63.5 to 89 GPa consistent with the increase in Ca/Si ratio from 0.83 to 1.0. This is contrary to the experimental values obtained by Alizadeh [17]. Manzeno et al. [73], however, also investigated the mechanical properties of crystalline C-S-H systems using lattice dynamic simulations. They suggested that both shear modulus (G) and elastic modulus (E) values decrease (although very scattered) when the Ca/Si ratio increases.

The source of the cohesion forces in C-S-H systems has not been clearly determined yet. It is likely that, although van der Waals and capillary forces partially contribute to the cohesion of such materials [74], the major factor that keeps the layers stable results from the iono-covalent properties of chemical bonds in the interlayer region. Calcium ions and water molecules are strongly localized in this situation [70].

2.1.5 Durability of C-S-H

It is known that C-S-H plays a significant role in durability of hydrated cement paste. It occupies a high volume percentage of the paste, and is involved in most of the durability issues of cement-based materials. It is, for example, a primary phase associated with the alkali-silica reactions. Lime-leaching from the C-S-H systems or magnesium interactions in these systems is also considered as important durability associated issue [75]. There are, however, very few investigations performed on the durability of synthetic or phase pure C-S-H. These are important for elucidating the key factors responsible for the durability of hardened cement paste.

2.2 C-S-H-based nanocomposites

Development of advanced construction materials with enhanced mechanical properties and durability has always been of interest to the construction engineers and material scientists. The general class of nanocomposite materials has, consequently, been a fast-growing area of research. Amongst all the potential nanocomposite precursors, those based on clay and layered silicates have been more widely investigated possibly because the starting clay materials are readily available, and also because their intercalation chemistry has been

extensively studied [76-78]. Noticeable improvements in the properties of clay materials, especially their resistance to swelling, have been achieved due to the incorporation of organic molecules [79-81]. Enhanced performance of organically modified cement-based nanocomposites has also been reported [25]. The number of investigations on these nanocomposites, however, is very limited. In this section, the polymer/layered silicate nanocomposites, which are promising in cement science, are first reviewed. Then, some of the related characteristics of C-S-H-based nanocomposites are presented.

2.2.1 Polymer/layered silicate nanocomposites

The incorporation of layered silicates into polymer matrices has been known for more than 50 years [82]. The interest in clay-based nanocomposites materials, however, became highlighted after publication of a report by a research group in Toyota corporation on the formation of Nylon-6/Montmorillonite in 1990 [83]. Since then, this new class of composite materials has been extensively developed and characterized [84-87]. The intent of these investigations was to improve the properties of polymers (e.g. modulus of elasticity and strength) by the formation of a nanocomposite. A layered silicate structure was generally used in these investigations. Montmorillonite, a member of the smectite group of clays, was the most commonly used layered silicate. Hectorite and saponite were also other popular choices [76].

Structure of nanocomposites

Any physical mixture of a polymer and a layered silicate material does not necessarily form a nanocomposite. When the polymer is unable to intercalate the silicate sheets, a phase-separated composite is obtained, whose properties are in the similar range as for traditional microcomposites [85, 88]. A schematic presentation of these microcomposites is shown in Figure 2-6(a). It has been observed that poor physical attraction of organic and inorganic phases in addition to the particle agglomeration may result in the poor mechanical properties of these microcomposites [89].

Beyond the traditional microcomposites, two forms of the polymer/layered silicate composites can be achieved depending on the nature of the component used and the preparation method (Figure 2-6(b) and 2-6(c)) [85]:

a. *Intercalated nanocomposite*: the extended polymer chain is inserted in the interlayer region without destroying the layered crystal structure of the silicate. The result, therefore, is a well ordered multilayer structure of alternating polymeric and inorganic layers with a repeat distance between them. This type can form a flocculated nanocomposite when the hydroxylated edge-edge interaction of silicate layers occurs.

b. *Exfoliated (or delaminated) nanocomposite*: the silicate layers are separated and individually dispersed in the continuous polymer matrix. The average distance between the layers depends on the polymer content.

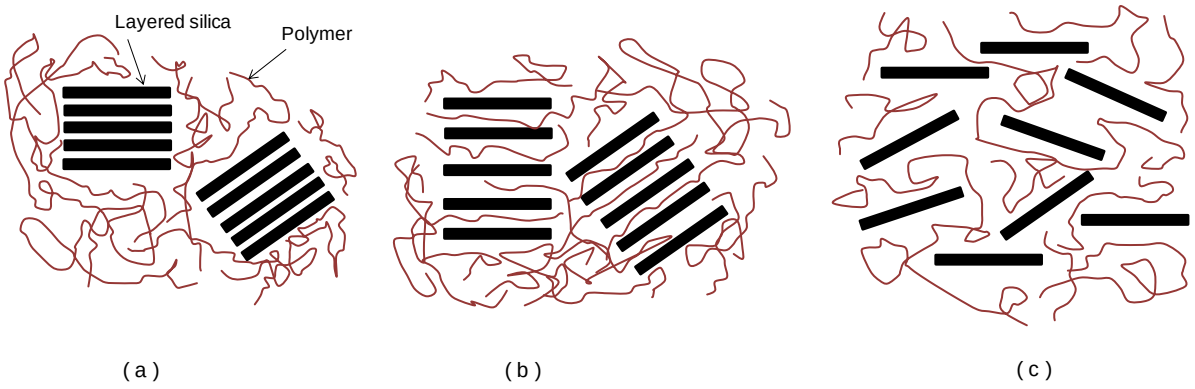

Figure 2-6- Possible composite materials formed by the interaction of polymer and layered silicate; (a) traditional microcomposite, (b) intercalated nanocomposite, and (c) exfoliated nanocomposite [85].

Synthesis of nanocomposites

There are four principal methods for preparing polymer/layered silicate nanocomposites depending on the starting materials and processing technique [76, 85, 90]:

a. *In-situ intercalative polymerization*: It was the first method used to synthesize polymer/clay nanocomposites based on polyamide 6. In this method, the layered silicate is initially swollen in the monomer solvent. The monomers are intercalated into the galleries of layered silicate. The polymerization reaction is, then, initiated either by heat, radiation or the use of an initiator.

b. *Intercalation of polymer from the solution*: The layered silicate is initially swollen in the solvent. The polymer is, then, added to the solution, and intercalates between the silicate layers. The solvent is, finally, removed by either vaporization or by precipitation.

c. *Melt intercalation*: The layered silicate is blended with the molten polymer. If the materials are compatible, the polymer can enter into the interlayer of silicate structure, and form intercalated or exfoliated nanocomposites.

d. *Template synthesis (sol-gel technology):* The layered silicates are formed within an aqueous solution containing the polymer and the silicate building blocks. During this process, the polymer aids the nucleation and growth of the inorganic host crystals and gets trapped within the layers as they grow. This method is widely used for the synthesis of layered double hydroxide (LDH)-based nanocomposites [91, 92], but it is not very common in the synthesis of layered silicate nanocomposites. A reason possibly is that the synthesis of clay minerals generally requires high temperatures which decompose the polymers. Another problem is also the aggregation tendency of the growing silicate layers.

Characterization of nanocomposites

The characterization of the nanocomposite and the extent of interaction can be studied by various techniques. X-Ray Diffraction (XRD), Nuclear Magnetic Resonance (NMR) spectroscopy, Fourier Transform Infrared (FTIR) spectroscopy and Transmission Electron Microscopy (TEM) are among most practically applied methods in this regard. In the

intercalated specimens, there is usually an increase in the interlayer space that can be detected by XRD [17].

The possibility of chemical bonding between the polymer and the layered silicate structure are usually investigated by NMR and FTIR. The ^{13}C, ^{29}Si and ^{1}H atoms have been of interest in NMR studies of polymer/layered silicate nanocomposites [93]. The FTIR technique also provides information on the type of chemical bonds. TEM also allows a qualitative understanding of the internal structure of the nanocomposites, and can directly provide information in real space, in a localized area, on morphology and defect structures [94, 95].

2.2.2 C-S-H/polymer nanocomposites

The main ideas for the synthesis of polymer modified nanocomposites have been originally developed in clay science [85]. Similar applications in cement science are relatively new and still limited. The first intercalated C-S-H systems were developed by Matsuyama and Young in 1999 [96-99]. These researchers used a range of anionic, cationic and neutral polymers such as poly(acrylic acid), poly(methacrylic acid), poly(4-vinyl benzyl trimethylammonium chloride) and poly(vinyl alcohol) for the modification of the C-S-H systems. It was suggested that the polymers intercalated into the interlayer region of C-S-H depending on the Ca/Si ratio. Intercalation of anionic polymers was more pronounced in C-S-H systems with higher Ca/Si ratios (especially Ca/Si > 1.3). For the cationic polymers, however, the intercalation was favored when Ca/Si < 1.0. The intercalation was also dependent on the type and the amount of polymer used. An increase of about 1.5 nm in the interlayer spacing was achieved for example in the intercalation of poly(methacrylic acid) (0.36 g/g of calcium nitrate salt) in the C-S-H system made from the double precipitation of the mentioned calcium salt and sodium silicate nanohydrate salt solution with Ca/Si ratio of 1.3. Considerable expansion of the basal-spacing of the C-S-H system (about 1 nm) was also observed due to the intercalation of poly(acrylic acid) with the concentration of 0.31 g/g of calcium nitrate salt in a C-S-H system with Ca/Si = 1.3. The change in the basal-spacing of C-S-H systems due to the poly(vinyl alcohol) intercalation, however, was not significant [97]. The method used for the synthesis of C-S-H-based nanocomposites

also affects the intercalation of polymer in the C-S-H structure. Larger expansion of the basal-spacing of C-S-H systems was observed when the precipitation method is used for the synthesis compared to using the pozzolanic reaction technique [99].

There is not a general agreement on the possibility of achieving an intercalated C-S-H structure. Popova et al. [100] and Merlin et al. [101], in separate studies, examined the possibility of the formation of intercalated C-S-H/polymer nanocomposites using various types of polymers. Their results did not show any significant change in the interlayer spacing as detected by XRD technique. ^{29}Si NMR did not show any change in the silicate polymerization either. It was suggested that a "mesocomposite" is formed during this interaction in which the polymer interacts with the stacking of C-S-H lamellae, and is also adsorbed on the surface of the spacing between "C-S-H stacks".

Mojumdar and Raki, however, synthesized and characterized C-S-H/poly(vinyl alcohol) and C-S-H/poly(acrylic acid) nanocomposites using the precipitation method [102-104]. An increase of about 0.20 nm was observed in the interlayer spacing as well as broadening of this peak in XRD patterns of the nanocomposites suggesting the development of both intercalated and exfoliated nanocomposite materials. In a recent investigation, Alizadeh et al. [105] also successfully synthesised C-S-H/polyaniline nanocomposites using the in-situ technique. The C-S-H host systems had Ca/Si ratio of 0.8 and 1.2. These were synthesized using the pozzolanic reaction method.

Another type of C-S-H/polymer nanocomposite has been successfully developed recently by Minet et al. [106] and Franceschini et al. [107]. Organic groups of these nanocomposites were covalently attached to the inorganic part of C-S-H via Si-C bonds as shown in Figure 2-7. Modified polymers were used containing silane functions that could be incorporated in the silicate chain of the C-S-H. The basal-spacing increased due to the occurrence of these covalent bonds in the interlayer region. The increase in the basal-spacing was linearly correlated with the length of the alkyl chains [108].

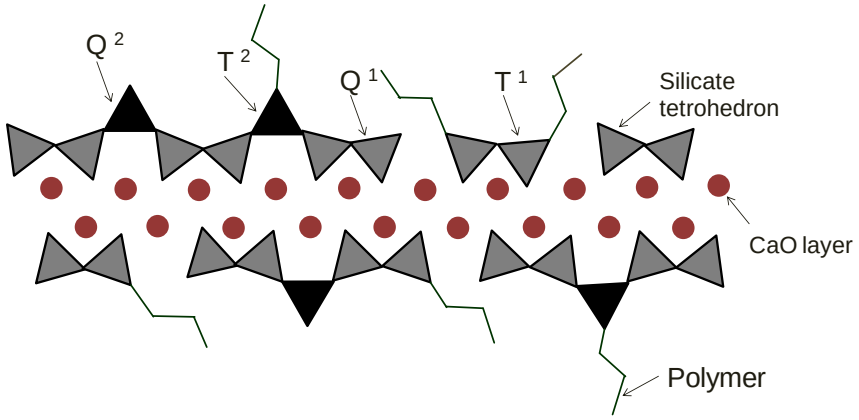

Figure 2-7- Microstructural model for the covalent bonded C-S-H/polymer nanocomposite suggesting the linkage of organotriethoxysilane to the end chain (Q^1) and middle chain (Q^2) silicate sites. This created new silicate sites referred to as T^1 and T^2, respectively [106]

2.2.3 Durability and mechanical properties of C-S-H-based nanocomposites

It has been suggested by Pellenq et al. [25] that the modulus of elasticity of C-S-H can be increased by as much as 40-100% when organically modified. A recent study, however, indicated that the elastic modulus (as measured using an indentation technique) decreased in the polymer modified C-S-H nanocomposite possibly due to the lower packing density [109]. This study, however, does not compare the engineering properties at similar porosity levels.

It is noted that most published investigations on the C-S-H-based nanocomposites are associated with the synthesis technique and chemical characterization of these materials. Only few investigations have been reported on the durability and mechanical properties of these novel systems. As the final aim of the development of these systems is to apply them in the construction industry, a link between the chemistry of organically-modified materials and their engineering performance is needed.

2.3 Secondary hydrated cement phases

Various hydrated phases are formed when Portland cement reacts with water. Calcium silicate hydrates (C-S-H), formed due to the hydration of C_3S or C_2S, are the primary phases, as previously mentioned. Several other hydrates, however, are also formed which can play important roles in the mechanical properties and durability of cement-based systems. These phases mainly include calcium hydroxide and the sulfoaluminate phases. Their microstructure and role in the durability of cement-based materials are discussed in this section.

2.3.1 Calcium hydroxide

Calcium hydroxide (CH) is one of the hydrated phases in Portland cement paste. It is formed during the hydration of the silicate phases, and occupies about 20% to 25% of the solid volume in the hardened cement paste. It has a hexagonal-prism morphology, and usually forms large crystals [75]. CH is known to have a layered structure as shown in Figure 2-8. The calcium atoms are octahedrally coordinated. The oxygen atoms are also coordinated tetrahedrally. The interlayer forces are weak with negligible hydrogen bonding.

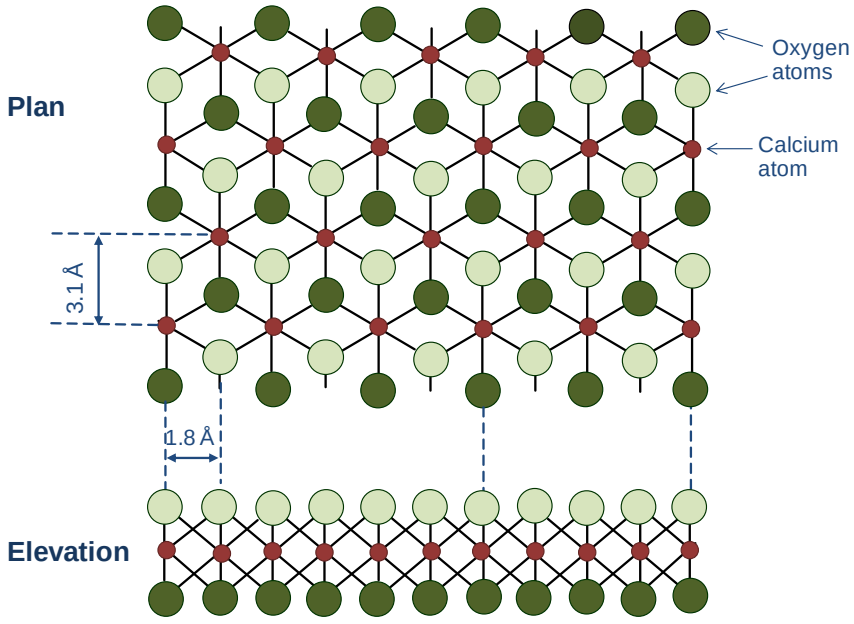

Figure 2-8- Structure of a single layer of $Ca(OH)_2$. A hydrogen atom, not shown, completes the tetrahedral coordination of each oxygen atom [7, 110].

Calcium hydroxide is readily soluble in water and is very susceptible to hydrolysis and leaching. When most of the CH has been leached out, lime-leaching from other cementitious components exposes them to decomposition. If this process still continues, it leaves behind silica and alumina gels with little or no strength [75]. According to Terzaghi [111], the strength of a concrete that had lost about a fourth of its original lime content was about one-half of the original one. In addition to the deterioration of mechanical performance, the leachates usually interact with CO_2 present in the air, and form calcium carbonate on the surface. This is undesirable from an aesthetic point of view [75]. It is also suggested that lime-leaching from hydrated cement paste may cause expansion. The mechanisms underlying this expansion are discussed in [112, 113].

2.3.2 Sulfoaluminate phases

Two common forms of calcium sulfoaluminate phases present in the hydrated cement paste include ettringite ($3CaO.Al_2O_3.3CaSO_4.32H_2O$) and monosulfate ($3CaO.Al_2O_3.CaSO_4.12H_2O$). These phases are important as they influence the durability of cement-based materials in sulfate environments. The detailed structure of these phases is discussed afterwards.

Ettringite

Ettringite ($3CaO.Al_2O_3.3CaSO_4.32H_2O$) is usually formed due to the hydration of aluminate phases during the early ages of hydration of Portland cement [7]. Its formation is a key factor in the setting process of the cement paste. Ettringite, however, normally converts to monosulfate as the cement hydration continues [114]. Ettringite is known to have a column and channel-like structure in which the columns have the empirical chemical formula of $[Ca_3Al(OH)_6.12H_2O]^{3+}$, and the SO_4^{2-} anions and water molecules occupy the intervening channels [115]. The crystalline structure of ettringite is presented in Figure 2-9. As it is shown in the figure, each of the columns in the ettringite structure is a chain of Al and Ca polyhydra (one of Al and three of Ca). It is estimated that about two out of the 32 water molecules of ettringite are located in the intercolumnar space. 12 water molecules are located in the main apices, and 12 in the additional apices of the trigonal prisms of Ca

polyhedra. The remaining six water molecules (in the form of hydroxyl groups) are also linked between the Ca and Al polyhedral [115-117].

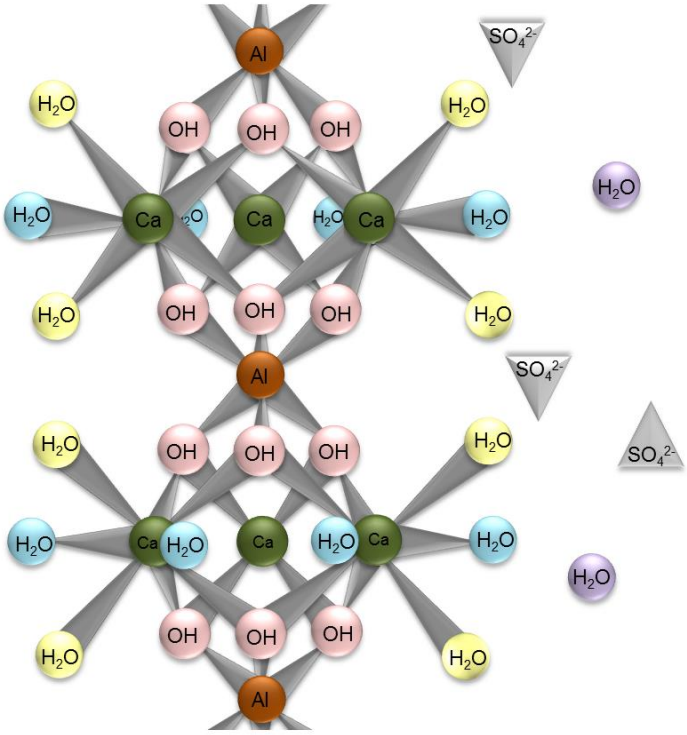

Figure 2-9- Crystalline structure of ettringite [114]

Several methods have been proposed in the literature for the synthesis of ettringite. An efficient method developed by Struble and Brown [118] includes reacting stoichiometric amounts of aluminum sulfate ($Al_2(SO_4)_3$) solution and 10% sugar solution of calcium oxide (CaO). The XRD pattern of synthetic ettringite is presented in Figure 2-10. The main peak at 9.73 Å corresponds to the intercolumnar space in the ettringite structure. Ettringite is also known to have a needle shaped morphology as shown in Figure 2-11. It is, however, noted that the size of needles is dependent of the synthesis procedure and the properties of the reactant materials.

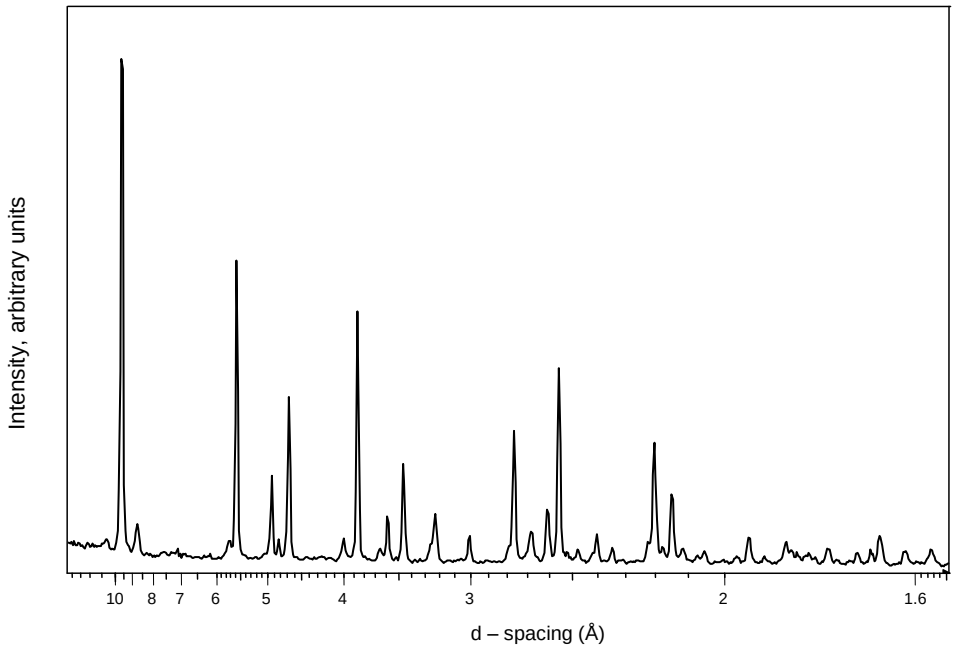

Figure 2-10- XRD pattern of synthetic ettringite

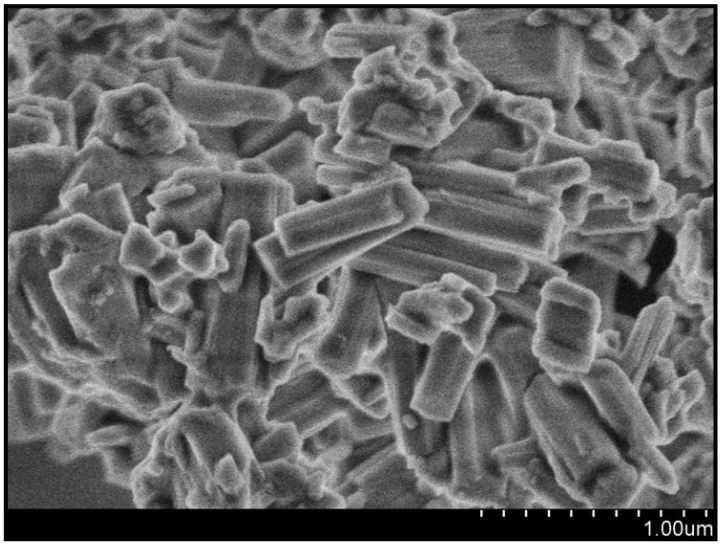

Figure 2-11- SEM micrograph of synthetic ettringite

Monosulfate

During the hydration of Portland cement, ettringite eventually transforms into the monosulfate hydrate phase. Monosulfate ($3CaO.Al_2O_3.CaSO_4.12H_2O$) has a lamellar crystalline structure. Its main layers are composed of $[Ca_2Al(OH)_6]^+$, and the SO_4^{2-} anions and water molecules are located between the layers [119]. Monosulfate phases can be synthesized either by reacting C_3A and ettringite or by reacting C_3A and gypsum as reported in the literature [120]. Synthesis of monosulfate is, however, very difficult and sensitive to the synthesis time, temperature, filtering and drying methods. Several precursors are, thus, needed to succeed in achieving pure monosulfate. An effective method of synthesis of monosulfate was proposed by Kuzel [121]. It includes reacting the stoichiometric amounts of tricalcium aluminate (C_3A) and calcium sulfate ($CaSO_4.2H_2O$) in excess water, and heating at 150 °C for four days.

An XRD pattern of synthetic monosulfate with 12 molecules of water (AFm-12) is presented in Figure 2-12. The main basal-spacing at 8.93 Å is, however, varied in monosulfate phases with varying numbers of water molecules. The basal-spacing of monosulfate with 16 water molecules (AFm-16) is reported to be located at 10.3 Å, which is reduced to 9.5, 8.93, 8.15 and 7.95 Å for monosulfate phases with 14, 12, 10 and 8 water molecules, respectively [7, 122]. Monosulfate is also known to form platey hexagonal crystals under the ideal crystallization conditions as shown in Figure 2-13.

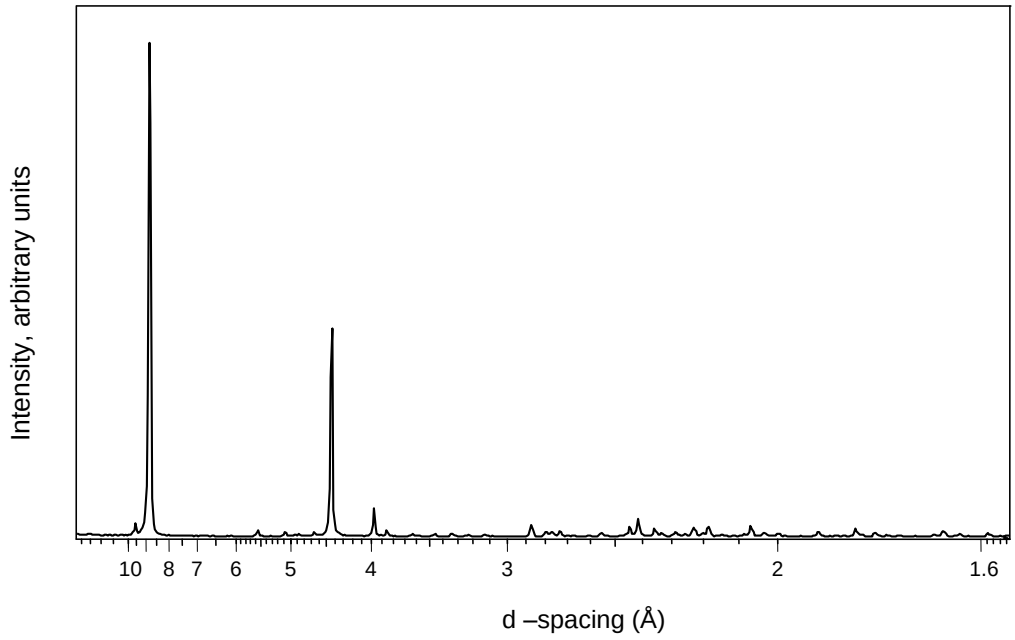

Figure 2-12- XRD pattern of synthetic monosulfate (AFm-12)

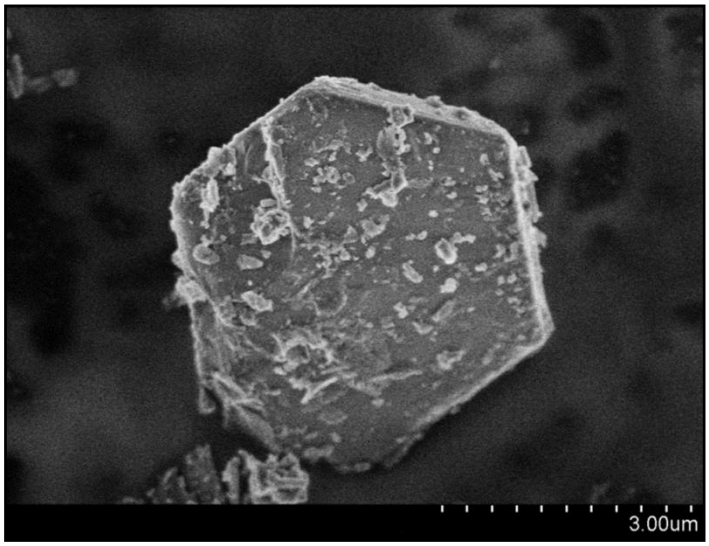

Figure 2-13- SEM micrograph of synthetic monosulfate

Thaumasite

Thaumasite is a form of calcium-silicate-sulfate-carbonate hydrate phase with the approximate formula of $3CaO.SiO_2.CO_2.SO_3.15H_2O$ which has close crystallographic similarities to ettringite [123]. The Si is in place of Al in the columns, and carbonate ions in place of water molecules in the intercolumn region. More details of the crystalline structure of thaumasite are discussed by Edge and Taylor [124].

Thaumasite can be formed in cement paste as a result of reaction between sulfate ions and the C-S-H systems in the presence of carbonate ions [125]. It has been observed that temperatures below 15 °C, particularly between 0 and 5 °C, are more favorable for the formation of thaumasite [126]. It is possibly due to the higher solubility of calcium carbonate at lower temperatures.

Synthesis of pure thaumasite has been attempted by several researchers [118, 127-130]. Only a few of them, however, were able to successfully prepare pure thaumasite. An efficient method is described by Blanco-Varela et al. [129]. This method includes mixing two sugary solutions; a calcium oxide solution, and a solution of sodium salts of silicate, sulfate and carbonate with non-stoichiometric concentrations. The resulting mixture is, then, kept at low temperatures (about 5 °C) for several weeks to form the thaumasite crystals. The XRD pattern of synthetic thaumasite is presented in Figure 2-14. As discussed, it resembles that of ettringite (Figure 2-10). Thaumasite can also form long needle-shape crystals as are presented in Figure 2-15.

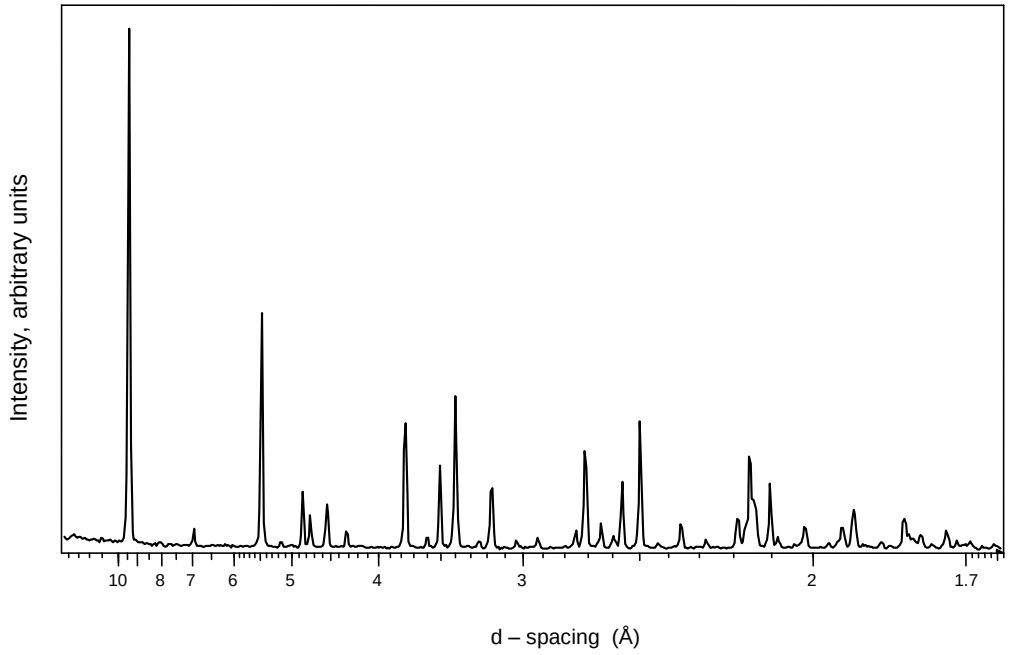

Figure 2-14- XRD pattern of synthetic thaumasite

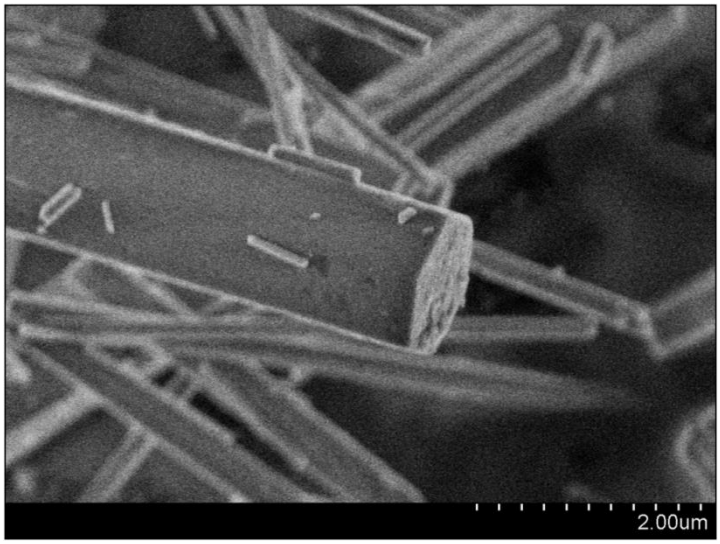

Figure 2-15- SEM micrograph of synthetic thaumasite

Other phases may also form during the hydration of Portland cement. These phases, however, are present in minor amounts in the hardened Portland cement paste. They are not included in this investigation.

2.3.3 Role of sulfoaluminate phases in the durability of cement-based systems

Sulfoaluminate phases in the Portland cement paste and their potential for producing expansion are directly linked to the durability problems of concrete structures in the sulfate rich environments. The formation of ettringite in high-concentrated sulfate environments has been widely accepted as a primary cause of expansion referred to as sulfate attack [131-134]. Monosulfate can react with sulfate ions, in the presence of Ca^{+2} and moisture, and form ettringite according to the following equation:

$$4CaO.Al_2O_3.SO_3.12H_2O + 2Ca^{2+} + SO_4^{2-} + 24H_2O \rightarrow 6CaO.Al_2O_3.3SO_3.32H_2O \qquad (2\text{-}4)$$

The anisotropic growth of ettringite crystals is then believed to be expansive. The ettringite formed can fill the pores or come into contact with pore boundaries in the hardened cement paste. When the pores are filled, formation of additional ettringite will cause additional tensile stress to the cement-based structure and results in its cracking [125, 135-137].

There is, however, no general agreement on the theories of expansion of ettringite. Mehta [138-140], reported that the expansion of ettringite does not necessarily occur in the presence of high sulfate concentrations. He attributed the expansion of ettringite crystals of colloidal dimensions to the imbibition of liquid water. The observed expansion in this case could be considerably greater than the expansions due to the ettringite formation itself [139]. Other proposed mechanisms include the expansion of ettringite associated with the osmotic forces, similar to those responsible for the swelling of the clay particles [141]. Further understanding of the mechanisms of expansion is essential in improving the durability of concrete infrastructure.

Investigations on thaumasite formation are more recent and much fewer than those on the ettringite and monosulfate phases. Although the first studies on the deterioration of cement-based materials in sulfate environments go back to 1892 [142], the first thaumasite formation was reported in 1965 in two sanitary sewer pipes in the USA. However, it was

not until 1998 that thaumasite formation began receiving significant attention, when it was found that the buried elements of a thirty-year old highway bridge in the UK had been damaged as a result of thaumasite sulfate attack [143]. The investigations on the phase pure thaumasite is also very limited due to the difficulty in synthesising this phase. It is, therefore, valuable to study the microstructure of phase pure thaumasite, and to provide information of its behaviour in various environmental conditions.

2.4 Key questions

Numerous investigations have been published on the durability of cement-based construction materials. There are, however, several uncertainties regarding the primary causes underlying the durability problems as well as the possibility of the development of novel construction materials with enhanced durability. A brief summary of the problems that are not fully resolved yet are as follows:

1- What are the mechanisms of interaction of organic compounds with the micro- and nano-structure of C-S-H systems?

2- What are the key parameters affecting the possibility of the interaction of organic compounds with the nanostructure of C-S-H systems?

3- Is the modification of C-S-H nanostructure with organic compounds effective in improving the durability and mechanical properties of the C-S-H-based systems?

4- What are the primary mechanisms underlying the expansion of sulfoaluminate phases in cement paste?

5- Are the mechanisms of expansion of thaumasite and the damage due to these expansions similar to those associated with the expansion of ettringite?

6- Is improving the nanostructure of C-S-H effective in reducing the damage due to the presence of ettringite or thaumasite in concrete structures?

These questions are among the important issues which are addressed in this doctoral thesis. Details of the experimental procedure designed to provide insight into the mechanisms of

damage relevant to the durability of cement-based phases and novel mitigation techniques will be presented in the following chapters.

References

1. T. D. Ciach, J. E. Gillott, E. G. Swenson and P. J. Sereda, "Microstructure of calcium silicate hydrates," *Cement and Concrete Research*, 1, pp. 13-25, 1971.
2. V. S. Ramachandran, "Differential thermal method of estimating calcium hydroxide in calcium silicate and cement pastes," *Cement and Concrete Research*, 9(6), pp. 677-684, 1979.
3. I. G. Richardson, "The nature of C-S-H in hardened cements," *Cement and Concrete Research*, 29, pp. 1131-1147, 1999.
4. J. Skalny and S. Mindess, Materials science of concrete, Vol. 1, 1989: American Ceramic Society.
5. C. Carde, G. Escadeillas and R. Francois, "Use of ammonium nitrate solution to simulate and accelerate the leaching of cement pastes due to deionized water," *Magazine of Concrete Research*, 49(181), pp. 295-301, 1997.
6. F. Lea, "The action of ammonium salts on concrete," *Magazine of Concrete Research*, 17(52), pp. 115-116, 1965.
7. H. Taylor, Cement Chemistry. 2nd Edition, London: Thomas Telford Publication, 1997.
8. H. Taylor, "Hydrated calcium silicates: part I. Compound formation at ordinary temperatures," *Journal of the Chemical Society*, pp. 3682-3690, 1950.
9. J. A. Gard and H. W. Taylor, "Calcium Silicate Hydrate (II)," *Cement and Concrete Research*, 6, pp. 667-678, 1976.
10. H. Stade and W. Wieker, "Zum aufbau schlecht geordneter alciumhydrogensilicate. I. Bildung und eigenschaften einer schlecht geordneten calciumhydrogendisilicatphase," *Zeitschrift für Anorganische und Allgemeine Chemie*, 466, pp. 55-70, 1980.

11. M. Grutzeck, A. Benesi and B. Fanning, "Silicon-29 magic-angle spinning nuclear magnetic resonance study of calcium silicate hydrates," *Journal of the American Ceramic Society*, 72, pp. 665-668, 1989.

12. I. Klur, B. Pollet, J. Virlet and A. Nonat, "C-S-H structure evolution with calcium content by multinuclear NMR," in 2nd International conference on NMR spectroscopy of cement based materials, pp. 119-141, 1998.

13. A. Nonat, "The structure and stoichiometry of C-S-H," *Cement and Concrete Research*, 34, pp. 1521-1528, 2004.

14. K. Garbev, P. Stemmermann, L. Black, C. Breen, J. Yarwood and B. Gasharova, "Structural features of C-S-H(I) and its carbonation in air- A Raman spectroscopic study-Part I: fresh phases," *Journal of the American Ceramic Society*, 90(3), pp. 900-907, 2007.

15. A. Nonat, "Interactions between chemical evolution (hydration) and physical evolution (setting) in the case of tricalcium silicate," *Materials and Structures*, 27(4), pp. 187-195, 1994.

16. A. Nonat and X. Lecoq, "The structure, stoichiometry and properties of C-S-H prepared by C3S hydration under controlled condition," in NMR Spectroscopy of Cement Based Materials, edt. Colombet, A. R. Grimmer, H. Zanni, P. Sozzani, Springer-Verlag, Berlin Heidelberg, pp. 197-207, 1998.

17. R. Alizadeh, Nanostructure and engineering properties of basic and modified calcium silicate hydrate systems, PhD Thesis, University of Ottawa, 2009.

18. J. J. Beaudoin, L. Raki and R. Alizadeh, "A ^{29}Si MAS NMR study of modified C-S-H nanostructures," *Cement and Concrete Composites*, 31, pp. 585-590, 2009.

19. I. G. Richardson and G. W. Groves, "Models for the composition and structure of calcium silicate hydrate (C-S-H) gel in hardened tricalcium silicate pastes," *Cement and Concrete Research*, 22, pp. 1001-1010, 1992.

20. F. Radjy and E. J. Sellevold, "Internal friction peaks due to adsorbed and capillary water in microporous substances," *Nature Physical Science*, 241, pp. 133-135, 1973.

21. A. J. Bohris, U. Goerke, P. J. McDonald, M. Mulheron, B. Newling and B. Le Page, "A broad line NMR and MRI study of water and water transport in Portland cement pastes," *Magnetic Resonance Imaging*, 16(5/6), pp. 455-461, 1998.

22. L. Miljkovic, D. Lasic, J. C. MacTavish, M. M. Pintar, R. Blinc and G. Lahajnar, "NMR studies of hydrating cement: A spin-spin relaxation study of the early hydration stage," *Cement and Concrete Research*, 18(6), pp. 951-956, 1988.

23. R. F. Feldman and V. S. Ramachandran, "Differentiation of interlayer and adsorbed water in hydrated Portland cement by thermal analysis," *Cement and Concrete Research*, 16, pp. 607-620, 1971.

24. R. F. Feldman and P. J. Sereda, "A datum point for estimating the adsorbed water in hydrated Portland cement," *Journal of Applied Chemistry*, 13, pp. 375-382, 1963.

25. R. J.-M. Pellenq, N. Lequeux and H. Van Damme, "Engineering the bonding scheme in C-S-H: The iono-covalent framework," *Cement and Concrete Research*, 38, pp. 159-174, 2008.

26. V. S. Ramachandran, R. F. Feldman and J. J. Beaudoin, Concrete Science, Heyden, 1981.

27. H. Jennings, "Refinements to colloid model of C-S-H in cement: CM-II," *Cement and Concrete Research*, 38, pp. 275-289, 2008.

28. J. J. Beaudoin and R. Alizadeh, "Discussion of the paper 'Refinements to colloid model of C-S-H in cement: CM-II,' by Jennings H. M.," *Cement and Concrete Research*, 38(7), pp. 1026-1027, 2008.

29. H. M. Jennings, "Reply to the discussion by J. J. Beaudoin and R. Alizadah of the paper "Refinements to colloid model of C–S–H in cement: CM-II" by H.M. Jennings," *Cement and Concrete Research*, 38(7), pp. 1028-1030, 2008.

30. R. Alizadeh, J. J. Beaudoina and L. Raki, "Mechanical properties of calcium silicate hydrates," *Materials and Structures*, 44, pp. 13-28, 2011.

31. J. J. Chen, J. J. Thomas, H. F. Taylor and H. M. Jennings, "Solubility and Structure of Calcium Silicate Hydrate," *Cement and Concrete Research*, 34(9), pp. 1499-1599, 2004.

32. Z. Wu and J. F. Young, "The hydration of tricalcium silicate in the presence of colloidal silica," *Journal of Materials Science*, 19, pp. 3477-3486, 1984.

33. K. Luke, "Phase studies of pozzolanic stabilized calcium silicate hydrates at 180 °C," *Cement and Concrete Research*, 39, pp. 1725-1732, 2004.

34. J. S. Dolado, M. Griebel and J. Hamaekers, "A Molecular Dynamics Study of Cementitious calcium-silicate-hydrate (C-S-H) gels," *Journal of the American Ceramic Society*, 90(12), pp. 3938-3942, 2007.

35. D. E. Macphee, E. E. Lachowski and F. P. Glasser, "Polymerization effects in C-S-H: implications for Portland cement hydration," *Advances in cement research*, 1(3), pp. 131-137, 1988.

36. Y. Okada, H. Ishida and T. Mitsuda, "^{29}Si NMR spectroscopy of silicate anions in hydrothermally formed C-S-H," *Journal of the American Ceramic Society*, 77(3), pp. 765-768, 1994.

37. P. Yu and R. J. Kirkpatrick, "Thermal dehydration of tobermorite and jennite," *Concrete Science and Engineering*, 1, pp. 185-191, 1999.

38. W. Wieker, A.-R. Grimmer, A. Winkler, M. Tarmak and E. Lippmaa, "Solid-state high-resolution ^{29}Si NMR spectroscopy of synthetic 14Å, 11and 9Å tobermorites," *Cement and Concrete Research*, 12, pp. 333-339, 1982.

39. I. G. Richardson, "The calcium silicate hydrates," *Cement and Concrete Research*, 38, pp. 137-158, 2008.

40. H. F. Taylor, "Tobermorite, jennite and cement gel," *Zeitschrift für Kristallograohie,* 202, pp. 41-50, 1992.

41. K. Dornberger-Schiff, F. Liebau and E. Thilo, "Über die Kristallstruktur des $(NaAsO_3)_x$, des Maddrellschen Salzes und des β-Wollastonits," *Die Naturwissenschaften*, 41(23), pp. 551, 1954.

42. E. Bonaccorsi, S. Merlino and A. R. Kampf, "The crystal structure of tobermorite 14 Å (Plombierite), a C-S-H phase," *Journal of the American Ceramic Society*, 88(3), pp. 505-512, 2005.

43. T. C. Powers and T. L. Brownyard, "Studies of the physical properties of hardened Portland cement paste," *ACI Journal Proceedings*, vol. 43, p. 101, p. 249, p. 469, p. 549, p. 669, p. 845 and p. 933, 1946 to 1947.

44. R. F. Feldman and P. J. Sereda, "A model for hydrated Portland cement paste as deduced from sorption-length change and mechanical properties," *Materials and Structures*, 1(6), pp. 509-520, 1968.

45. R. F. Feldman and P. Sereda, "A new model for hydrated Portland cement and its practical implications," *Engineering Journal*, 53(8-9), pp. 53-59, 1970.

46. R. F. Feldman, "The flow of helium into the interlayer spaces of hydrated Portland cement paste," *Cement and Concrete Research*, 1(3), pp. 285-300, 1971.

47. S. Brunauer, I. Odler and M. Yudenfreund, "The new model of hardened Portland cement," *Highway Research Record*, 328, pp. 89-101, 1970.

48. R. F. Feldman and P. J. Sereda, "Discussion of 'The new model of hardened Portland cement paste' by Brunauer et al.," *Highway Research Record*, 328, pp. 101-103, 1970.

49. R. F. Feldman, "Assessment of experimental evidence for models of hydrated Portland cement," *Highway Research Record*, 370, pp. 8-24, 1972.

50. M. Daimon, S. A. Abo-El-Enein, G. Rosara, S. Goto and R. Kondo, "Pore Structure of Calcium Silicate Hydrate in Hydrated Tricalcium Silicate," *Journal of the American Ceramic Society*, 60(3-4), pp. 110-114, 1977.

51. P. D. Tennis and H. M. Jennings, "A Model for Two Types of C-S-H in the Microstructure of Portland Cement Pastes," *Cement and Concrete Research*, 30(6), pp. 855-863, 2000.

52. A. J. Allen, J. J. Thomas and H. M. Jennings, "Composition and density of nanoscale calcium-silicate-hydrate in cement," *Nature Materials*, 6(4), pp. 311-316, 2007.

53. C. Plassard, E. Lesniewska, I. Pochard and A. Nonat, "Investigation of the surface structure and elastic properties of calcium silicate hydrates at the nanoscale," *Ultramicroscopy*, 100, pp. 331-338, 2004.

54. J. D. Bernal, J. W. Jeffery and H. F. Taylor, "Crystallographic research on the hydration of Portland cement. A first report on investigations in progress," *Magazine of Concrete Research*, 4(11), pp. 49-54, 1952.

55. H. F. Taylor and J. W. Howison, "Relationships between calcium silicates and clay minerals," *Clay Minerals Bulletin*, 3(16), pp. 98-111, 1956.

56. H. G. Kurczyk and H. E. Schwiete, "Concerning the hydration products of C_3S and β-C_2S," in Proceeding of the 4th International Symposium on the Chemistry of Cement, vol. 1, 349-358, 1962., 1962.

57. D. L. Kantro, S. Brunauer and C. H. Weise, "Development of surface in the hydration of calcium silicates. II. Extension of investigations to earlier and later stages of hydration," *The Journal of Physical Chemistry*, 66, pp. 1804-1809, 1962.

58. H. Stade and W. Wieker, "On the structure of ill-crystallized calcium hydrogen silicates. II. A phase consisting of poly-and disilicate," *Z. Anorg. Allg. Chem.*, 470, pp. 69-83, 1980.

59. X. Cong and R. J. Kirkpatrick, "^{29}Si MAS NMR study of the structure of calcium silicate hydrate," *Advaned Cement Based Materials*, 3, pp. 144-156, 1996.

60. X. Cong and R. J. Kirkpatrick, "^{17}O MAS NMR investigation of the structure of calcium silicate hydrate gel," *Journal of the American Ceramic Society*, 79, pp. 1585-1592, 1996.

61. M. Grutzeck, "A new model for the formation of calcium silicate hydrate (C-S-H)," *Materials Research Innovations*, 3, pp. 160-170, 1999.

62. M. W. Grutzeck, S. Kwan, J. L. Thompson and A. Benesi, "A sorosilicate model for calcium silicate hydrate (C-S-H)," *Journal of Materials Science Letters*, 18, pp. 217-220, 1999.

63. H. Taylor, "Proposed structure for calcium silicate hydrate gel," *Journal of the American Ceramic Society*, 69(6), pp. 464-467, 1986.

64. P. Pourbeik, J. J. Beaudoin, R. Alizadeh and L. Raki, "Mechanical property–porosity relationships of layered calcium silicate hydrate phases" *Materials and Structures*, 46(9), pp 1489-1495, 2013.

65. X. Cong and R. J. Kirkpatrick, "^{29}Si and ^{17}O NMR Investigation of the Structure of Some Crystalline Calcium Silicate Hydrates," *Advanced Cement Based Materials*, 3, pp. 133-134, 1996.

66. J. J. Beaudoin and R. F. Feldman, "Dependence of degree of silica polymerization and intrinsic mechanical properties of C-S-H on C/S ratio," in 8th International Congress on the Chemistry of Cement, Brazil, Vol. 3, 337-342, 1986.

67. G. Constantinides and F.-J. Ulm, "The effect of two types of C-S-H on the elasticity of cement-based materials: Results from nanoindentation and micromechanical modeling," *Cement and Concrete Research*, 34, pp. 67-80, 2004.

68. G. Constantinides, F. -J. Ulm and K. Van Vliet , "On the use of nanoindentation for cementitious materials," *Materials and Structures*, 36(3), pp. 191-196, 2003.

69. H. H. Steinour, "The reactions and thermochemistry of cement hydration at ordinary temperature," in 3rd International Symposium on the Chemistry of Cements, pp. 261-289, 1954.

70. R. J.-M. Pellenq, A. Gmira and H. Van Damme, "Stability and elastic properties of tobermorite, a model of cement hydrate at the nano-scale," in *MS&T'07,* Advances in Cement-Based Materials, Detroit, Michigan, pp. 1-12, 2007.

71. S. Hamid, "The crystal structure of the 11 Å natural tobermorite $Ca_{2.25}[Si_3O_{7.5}(OH)_{1.5}].1H_2O$," *Zeitschrift fur Kristallographie*, 154, pp. 189-198, 1981.

72. S. Merlino, E. Bonaccorsi and T. Armbruster, "Tobermorites: their real structure and order-disorder (OD) character," *American Mineralogist*, 84, pp. 1613-1621, 1999.

73. H. Manzano, J. S. Dolado, A. Guerrero and A. Ayuela, "Mechanical properties of crystalline calcium-silicate-hydrates: comparison with cementitious C-S-H gels," *physica Status Solidi (a)*, 204(6), pp. 1775-1780, 2007.

74. R. J.-M. Pellenq and H. Van Damme, "Why does concrete set? The nature of cohesion forces in hardened cement-based materials," *MRS Bulletin*, 29(5), pp. 319-323, 2004.

75. P. K. Mehta and P. J. Monteiro, Concrete; Microstructure, Properties and Materials, 3rd edition, McGraw-Hill, 2006.

76. S. Pavlidou and C. D. Papaspyrides, "A review on polymer–layered silicate nanocomposites," *Progress in Polymer Science*, 33, pp. 1119-1198, 2008.

77. C. A. Bower, "Studies on the form and availability of organic soil phosphorous," *IOWA Agricultural Experiment Station Research Bulletin*, 362, pp. 39-42, 1949.

78. L. W. Carter, J. G. Hendricks and D. S. Bolley, Elastomer reinforced with modified clay (assigned to National Lead Co.)., United States Patent No. 2,531,396, 1950.

79. A. Somwangthanaroj, W. Ubankhlong and W. Tanthapanichakoon, "Solid-state mechanical properties of polypropylene/nylon6/clay Nanocomposites," *Journal of Applied Polymer Science*, 118, pp. 538-546, 2010.

80. P. Natkanski, P. Kustrowski, A. Bialas, Z. Piwowarska and M. Michalik, "Controlled swelling and adsorption properties of polyacrylate/montmorillonite composites," *Materials Chemistry and Physics*, 136, pp. 1109-1115, 2012.

81. H. Frenkel and I. Shainberg, "The Effect of Hydroxy-Al and Hydroxy-Fe Polymers on Montmorillonite Particle Size," *Soil Science Society of America Journal*, 44(3), pp. 626-629, 1980.

82. J. W. Cho and D. R. Paul, "Nylon 6 nanocomposites by melt compounding," *Polymer*, 42, pp. 1083-1094, 2001.

83. A. Okada, M. kawasumi, A. Usuki, T. Kurauchi and O. Kamigaito, "Synthesis and properties of nylon-6/clay hybrids," in Polymer based molecular composites (edt. Schaefer D.W., Mark J. E.), MRS Symposium Proceedings, Pittsburgh, Vol. 171, pp. 45-50, 1990.

84. B. K. Theng, Formation and properties of clay-polymer complexes, Elsevier, 1979.

85. M. Alexandre and P. Dubois, "Polymer-layered silicate nanocomposites: preparation, properties and uses of new class of materials," *Materials Science and Engineering*, 28, pp. 1-63, 2000.

86. S. S. Ray and M. Okamoto, "Polymer/layered silicate nanocomposites: a review from preparation to processing," *Progress in Polymer Science*, 28, pp. 1539-1641, 2003.

87. P. C. LeBaron, Z. Wang and T. J. Pinnavaia, "Polymer-layered silicate nanocomposites: an overview," *Applied Clay Science*, 15, pp. 11-29, 1999.

88. G. Beyer, "Nanocomposites: a new class of flame retardants for polymers," *Plastics, Additives and Compounding*, 4(10), pp. 22-27, 2002.

89. E. P. Giannelis, "Polymer layered silicate nanocomposites," *Advanced Materials*, 8, pp. 29-35, 1996.

90. Y. C. Ke and P. Stroeve, Polymer-layered silicate and silica nanocomposites, 1st ed., Elsevier, 2005.

91. O. C. Wilson Jr., T. Olorunyolemi, A. Jaworski, L. Borum, D. Young, A. Siriwat, E. Dickens, E. Oriakhi and M. Lerner, "Surface and interfacial properties of polymer-intercalated layered double hydroxide nanocomposites," *Applied Clay Science*, 15, pp. 265-279, 1999.

92. C. O. Oriakhi, I. V. Farr and M. M. Lerner, "Thermal characterization of poly(styrene sulfonate)/layered double hydroxide nanocomposites," *Clays and Clay Minerals*, 45, pp. 194-202, 1997.

93. S. Yariv, H. Cross (edt.), "Chapter 6. J. Sanz and J. M. Serratosa, Nuclear magnetic resonance spectroscopy of organo-clay complexes," in Organo-clay complexes and interactions, New York, Marcel Dekker Inc., 2002.

94. J. Ma, J. Xu, J.-H. Ren, Z.-Z. Yu and Y.-W. Mai, "A new approach to polymer/montmorillonite nanocomposites," *Polymer*, 44, pp. 4619-4624, 2003.

95. A. B. Morgan and J. W. Gilman, "Characterization of polymer–layered silicate (clay) nanocomposites by transmission electron microscopy and X-ray diffraction: a comparative study," *Journal of Applied Polymer Science*, 87, pp. 1329-1338, 2003.

96. H. Matsuyama and J. F. Young, "Intercalation of Polymers in Calcium Silicate Hydrate: A New Synthetic Approach to Biocomposites?," *Chemistry of Materials*, 11, pp. 16-19, 1999.

97. H. Matsuyama and J. F. Young, "Synthesis of calcium silicate hydrate/polymer complexes: Part I," *Journal of Materials Research*, 14, pp. 3379-3388, 1999.

98. H. Matsuyama and J. F. Young, "Synthesis of calcium silicate hydrate/polymer complexes: Part II," *Journal of Materials Research*, 14, pp. 3389-3396, 1999.

99. H. Matsuyama and J. F. Young, "The formation of C-S-H/polymer complexes by hydration of reactive β-dicalcium silicate," *Concrete Science and Engineering*, 1, pp. 66-75, 1999.

100. A. Popova, G. Geoffroy, M.-F. Renou-Gonnord, P. Faucon and E. Gartner, "Interactions between polymeric dispersants and calcium silicate hydrates," *Journal of the American Ceramic Society*, 83, 10, pp. 2556-2560, 2000.

101. F. Merlin, H. Lombois, S. Joly, N. Lequeux, J.-L. Halary and H. Van Damme, "Cement-polymer and clay-polymer nano- and meso-composites: spotting the difference," *Journal of Materials Chemistry*, 12, pp. 3308-3315, 2002.

102. S. C. Mojumdar and L. Raki, "Preparation and properties of calcium silicate hydrate-poly(vinyl Alcohol) nanocomposites materials," *Journal of Thermal Analysis and Calorimetry*, 82, pp. 89-95, 2005.

103. S. C. Mojumdar and L. Raki, "Preparation, thermal spectral and microscopic studies of calcium silicate hydrate-poly(acrylic acid) nanocomposites materials," *Journal of Thermal Analysis and Calorimetry*, 85, pp. 99-105, 2006.

104. S. C. Mojumdar and L. Raki, "Synthesis, thermal and structural characterization of nanocomposites for potential applications in construction," *Journal of Thermal Analysis and Calorimetry*, 86, pp. 651-657, 2006.

105. R. Alizadeh, J. Beaudoin, L. Raki and V. Terskikh, "C-S-H/polyaniline nanocomposites prepared by in situ polymerization," *Journal of Materials Science*, 46(2), pp. 460-467, 2011.

106. J. Minet, S. Abramson, B. Bresson, A. Franceschini, H. Van Damme and N. Lequeux, "Organic calcium silicate hydrate hybrids: a new approach to cement based nanocomposites," *Journal of Materials Chemistry*, 16, pp. 1379-1383, 2006.

107. A. Franceschini, S. Abramson, V. Mancini, B. Bresson, C. Chassenieux and N. Lequeux, "New covalent bonded polymer-calcium silicate hydrate composites," *Journal of Materials Chemistry*, 17, pp. 913-922, 2007.

108. J. Minet, S. Abramson, B. Bresson, C. Sanchez, V. Montouillout and N. Lequeux, "New layered calcium organosilicate hybrids with covalently linked organic functionalities," *Chemistry of Materials*, 16, pp. 3955-3962, 2004.

109. F. Pelisser, P. J. Gleiz and A. Mikowski, "Effect of poly(diallyldimethylammonium chloride) on nanostructure and mechanical properties of calcium silicate hydrate," *Materials Science and Engineering: A*, 527(26), pp. 1045-1049, 2010.

110. F. D. Tamas, A. K. Sarkar and D. M. Roy, Hydraulic Cement Pastes: Their Structure and Properties, UK: Cement and Concrete Association, 1974.

111. R. D. Terzaghi, "Concrete deterioration in a shipway," *Journal of American Concrete Institute*, 19(10), pp. 977-1005, 1948.

112. J. Marchand, J. J. Beaudoin and M. Pigeon, "Influence of $Ca(OH)_2$ dissolution on the properties of cement systems," Materials Science of Concrete-Sulfate Attack Mechanisms, American Ceramic Society, pp. 283-293, 1999.

113. J. Marchand, D. P. Bentz, E. Samson and Y. Maltais, "Influence of Calcium Hydroxide Dissolution on the Transport Properties of Hydrated Cement Systems," in Materials Science of Concrete: Calcium Hydroxide in Concrete, Special Volume, Proceedings. American Ceramic Society. Workshop on the Role of Calcium, Florida, pp. 113-129, 2001.

114. S. N. Ghosh, Advances in Cement Technology: Chemistry, Manufacture and Testing, 2nd Edition, New Delhi, India: Tech Books International, 2002.

115. E. A. Moore and F. W. Taylor, "Crystal structure of ettringite," *Acta Crystallographica Section B: Structural Science*, 26, pp. 386-393, 1970.

116. N. N. Skoblinskaya and K. G. Krasilnikov, "Change in the crystal structure of ettringite due to dehydration. Part 1," *Cement and Concrete Research*, 5, pp. 381-394, 1975.

117. N. N. Skoblinskaya, K. G. Krasilnikov, L. V. Nikitina and V. P. Varlamov, "Change in the crystal structure of ettringite due to dehydration. Part 2," *Cement and Concrete Research*, 5, pp. 419-432, 1975.

118. L. J. Struble and P. W. Brown, "An evaluation of ettringite and related compounds for use in the solar energy storage," NBSIR 82-253, USA, US Dept. of Commerce, pp. 11, 1982.

119. R. Allmann, "Refinement of the hybrid layer structure $[Ca_2Al(OH)_6]^+.[1/2SO_4.3H_2O]^-$," *Neues Jahrbuch fur Mineralogie Monatsheft*, pp. 136-144, 1977.

120. I. Odler and S. Abdul-Maula, "Possibilities of quantitative determination of the AFt-(ettringite) and AFm-(monosulfate) phases in hydrated cement pastes," *Cement and Concrete Research*, 14(1), pp. 133-141, 1984.

121. H. J. Kuzel, "Synthesis and X-Ray Study of the Crystalline Composition $3CaO.Al_2O_3.CaSO_4.12H_2O$," *Neues Jahrbuch Mineral Monatsh*, 7, pp. 193-197, 1965.

122. L. Zhang and F. P. Glasser, "Critical examination of drying damage to cement paste," *Advances in Cement Research*, 12(2), pp. 79-88, 2000.

123. D. Mcconnell and J. Murdoch, "Crystal chemistry of ettringite," *Mining Magazine*, 33, pp. 59, 1962.

124. R. A. Edge and H. F. Taylor, "Crystal Structure of Thaumasite, $[Ca_3Si(OH)_6.12H_2O](SO_4)(CO_3)$," *Acta Crystallographica B*, 27, pp. 594-601, 1971.

125. Skalny, J., Marchand, J., and Odler I. (Eds), Sulfate attack on concrete. Modern Concrete Technology Series, 10,, E. & F. Spon, London., 2002.

126. M. Santhanam, M. D. Cohen and J. Olek, "Sulfate attack research-whither now?," *Cement and Concrete Research*, 31, pp. 845-851, 2001.

127. S. Martinez-Ramirez, M. T. Blanco-Varela and J. Rapazote, "Thaumasite formation in sugary solutions: Effect of temperature and sucrose concentration," *Construction and Building Materials*, 25, pp. 21-29, 2011.

128. J. Aguilera, M. T. Blanco Varela and T. Va´zquez, "Procedure of synthesis of thaumasite," *Cement and Concrete Research*, 31, pp. 1163-1168, 2001.

129. M. T. Blanco-Varela, P. M. Carmona-Quiroga, I. F. Sáez del Bosque and S. Martínez-Ramírez, "Role of organic admixtures on thaumasite precipitation," *Cement and Concrete Research*, 42(7), pp. 994-1000, 2012.

130. T. Matschei, Thermodynamics of Cement Hydration, PhD thesis, University of Aberdeen, 2007.

131. W. C. Hansen, "Attack on Portland cement concrete by alkali soils and waters - A critical review," *Highway Research Record*, 113, pp. 1-32, 1966.

132. I. Odler and M. Gasser, "Mechanism of sulfate expansion in hydrated Portland cement," *Journal of the American Ceramic Society*, 71, pp. 1015-1020, 1988.

133. B. Mather, "A Discussion of the Paper 'Mechanism of Expansion-Associated Ettringite Formation' by P.K. Mehta," *Cement and Concrete Research*, 3, pp. 651-652, 1973.

134. W. C. Hansen, "A Discussion of the Paper 'Scanning Electron Microscopic Studies of Ettringite Formation' by P.K. Mehta," *Cement and Concrete Research*, 6, pp. 595-596, 1976.

135. G. W. Scherer, "Crystallization in pores," *Cement and Concrete Research*, 29, pp. 1347-1358, 1999.

136. G. W. Scherer, "Stress from crystallization of salt," *Cement and Concrete Research*, 34, pp. 1613-1624, 2004.

137. R. J. Flatt and G. W. Scherer, "Thermodynamics of crystallization stresses in DEF," *Cement and Concrete Research*, 38, pp. 325-336, 2008.

138. P. K. Mehta, "Mechanism of Expansion Associated with Ettringite Formation," *Cement and Concrete Research*, 3, pp. 1-6, 1973.

139. P. K. Mehta and F. Hu, "Further evidence for expansion of ettringite by water adsorption," *Journal of the American Ceramic Society*, 61, pp. 179-181, 1978.

140. P. K. Mehta and S. Wang, "Expansion of ettringite by water adsorption," *Cement and Concrete Research*, 12, pp. 121-122, 1982.

141. T. Thorvaldson, "Chemical Aspects of the Durability of Cement Products," in Proceedings of the 3rd International Symposium on the Chemistry of Cement, Cement and Concrete Association, London, p. 463, 1952.

142. W. Michaelis, "Cement Bacillus," *The Engineering Record*, 110, 1892.

143. D. Hobbs, "Thaumasite sulfate attack in field and laboratory concretes: implications for specifications," *Cement and Concrete Composites*, 25, pp. 1195-1202, 2003.

Chapter 3

Experimental Program

The experimental techniques in the study of cement-based materials are now well established. Some of the techniques used for the characterization, and the assessment of durability and engineering performance of hydrated cement phases are described in this chapter. It should be noted that each of these techniques has its own benefits and limitations. A combination of these techniques, therefore, should be employed in order to provide greater confidence in the conclusions made about the structure and behavior of the cementitious materials. The details of synthesis of cement-based phases, humidity conditioning and preparation of the compacted samples are also presented in this chapter. More specific details of the experiments for each part of the thesis are explained in the relevant chapters.

3.1 Experimental techniques

A description of the most common experimental technics used in this research for the study of cement-based systems is presented in this section. These techniques are categorized into two parts: those used for the characterization and those used for the assessment of durability and engineering performance.

3.1.1 Characterization techniques

X-ray Diffraction

The X-ray diffraction (XRD) technique is one of the most commonly used methods in cement chemistry. As each crystal has a unique X-ray pattern, the XRD technique is an effective tool for the characterization of crystalline materials. In a crystalline structure, various atoms are located in a repeating order which results in the formation of similar atomic planes. The distance between these planes is referred to as d-spacing. X-ray beams give constructive interference when they hit different parallel layers. The diffracted beams can be detected if they are in phase. This occurs according to Bragg's law:

$$n\,\lambda = 2\,d\,sin\theta \qquad (3\text{-}1)$$

in which λ is the wavelength of the X-ray (e.g. about 0.15 nm for copper), d is the distance between the atomic planes, θ is the angle between the incidence beam and the normal to the reflecting lattice plane, and n is an integer called order of reflection (Figure 3-1).

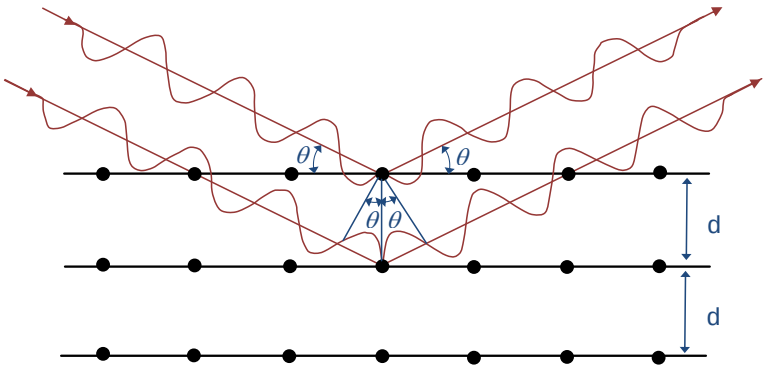

Figure 3-1- Diffraction of X-rays expressed by Bragg's law [1]

In order to identify the compounds of a sample, the powder diffraction pattern is recorded using a diffractometer. These data are, then, compared with the standard line patterns available for various compounds in the powder diffraction file (PDF) database. This file is updated annually by the international center for diffraction data (ICDD). In practice, the appearance of the three most intense characteristic lines from the PDF line pattern is sufficient to indicate the existence of a crystalline phase in a material. However, a prior

knowledge of the class of the investigated materials and the chemical analysis data is of significant value [1].

Thermal analysis

A chemical compound may be decomposed or experience a phase transition when it is subjected to heating. Bulk water, for example, is gradually lost at temperatures up to 100 ºC. Calcium hydroxide is also decomposed at about 400 º C. The thermal analysis technique determines the physical or chemical changes of a compound due to the thermal treatment as a function of temperature. It may be conducted by measurement of the decrease in the mass of the compound during heating or by the estimation of the heat that is adsorbed or generated through an endothermic or exothermic change of the compound. These measurements are referred to as thermal gravimetric analysis (TGA) and differential thermal analysis (DTA), respectively. Differential mass-loss measurements can be used to estimate the amount of each chemical compound. Various types of materials can also be identified based on the heat flow during the physicochemical changes.

Scanning electron microscopy

The Scanning Electron Microscopy (SEM) technique is used to investigate the morphology and surface characterization of materials by capturing images at the micro or nano scale. In this technique, a focused beam of electrons strikes the surface of the material. The surface interactions result in the emission of secondary and backscattered electrons as well as X-rays and other responses. The electrons are collected and converted to an image of the surface. Any compound, as long as it is electrically conductive, can be examined by this technique. The contrast formed by the collected electrons originates from the difference in surface topography and composition. Both secondary electrons (SE) and backscattered electrons (BSE) modes provide imaging facility. The SE mode is dominated by topographic contrast, whereas the BSE mode mainly detects atomic density which helps differentiate regions rich in a specific atom. It is also possible to collect the X-rays emitted from the surface. This technique which is referred to as energy dispersive X-ray spectroscopy (EDX)

enables elemental analysis and the detection of different atoms in the compound. EDX imaging facilitates estimation of the distribution of various elements in the compound.

Fourier Transform Infrared Spectroscopy

Fourier Transform Infrared Spectroscopy (FTIR) is a powerful technique for the identification of the chemical bonds of molecules. It has different applications in the areas of determination of molecular structure and identification of chemical components of a mixture of either organic or inorganic materials. This technique can be applied for the investigation of materials in the solid, liquid, or gaseous state. The principle of this technique is that molecular bonds vibrate at various frequencies depending on the type of atoms and bonds. The adsorption of the energy of the infrared portion of the electromagnetic spectrum by a molecular bond can change the vibration state of a chemical bond from ground state (lowest frequency) to an excited state. The energy required for this transition is unique for each bond and, thus, can be used for the identification of various bonds in the molecules.

Nitrogen surface area

The surface area of cement-based compounds can be estimated from the nitrogen gas sorption isotherm based on the Brunauer, Emmett and Teller (BET) theory. It is assumed that the surface of the porous material is like an array of adsorption sites, and each site is capable of adsorbing one or more molecular layers. The mathematical form of this theory is as follows [2, 3]:

$$\frac{p}{x(p-p_0)} = \frac{1}{x_m c} + \frac{c-1}{x_m c}\frac{p}{p_0} \tag{3-2}$$

where p is the existing vapor pressure, p_0 is the pressure of saturated vapor, x is the quantity of vapor adsorbed at vapor pressure p, x_m is the monolayer capacity of adsorbate per unit quantity of solid, and C is a constant related to the heat of adsorption. The BET equation (Eq. 3-2) shows that the surface area of the adsorbent should be equal to the

summation of the area covered by all the molecules required to fill the first layer of the adsorbent. The surface area of the solid can, therefore, be evaluated by:

$$S = \frac{A_m x_m N}{M} \tag{3-3}$$

where N is the number of molecules in a gram-molecular weight (6.022×10^{23}), M is the molecular weight of the adsorbed gas, and A_m is the surface area covered by a single adsorbed molecule (16.2×10^{-16} cm^2 per molecule of nitrogen) [2, 3]. Eq. 3-3 can also be used in the volumetric form. In this form, x_m is expressed in volume per volume of adsorbate, and M is the molecular volume of the adsorbed gas which is equal to 22.414 l in the standard temperature and pressure condition ($T = 0°C$ and $P = 1\ atm$).

3.1.2 Engineering performance techniques

Dynamic mechanical analysis (DMA)

Dynamic Mechanical Analysis (DMA) is widely used in polymer science to record elastic modulus and damping or melting points of polymers [4]. It has also been used in cement science in order to provide information on the states of water in hydrated cement phase [5-7], and in the synthetic C-S-H systems [8]. The DMA technique involves the analysis of the response of a specimen under an oscillating force. It can also combine the information with temperature response which is referred to as Dynamic Mechanical Thermal Analysis (DMTA).

Applying an oscillating stress on a viscoelastic specimen (that is still in the elastic region) results in an oscillating strain response in that specimen which lags with stress by an angle δ. The tan δ, which is referred to as internal friction, is a function of frequency of the applied stress [9]. Consider a sinusoidal load that is applied on a sample in the form of

$$\sigma = \sigma_{\max} \sin(\omega t) \tag{3-4}$$

where σ is the stress at time t, σ_{max} is the maximum stress and ω is the angular frequency of the oscillation. If the stress remains within the elastic region of the material, the strain response will also be in a sinusoidal form which can be expressed as

$$\varepsilon = \varepsilon_{max} \sin(\omega t - \delta) \tag{3-5}$$

where ε is the strain at time t, ε_{max} is the maximum strain and δ is the phase difference angle (Figure 3-2).

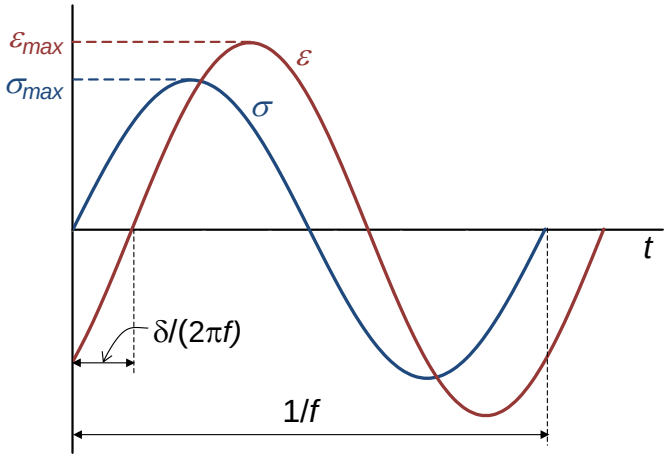

Figure 3-2- Phase difference between the stress and strain in a viscoelastic material subjected to sinusoidal oscillation

The storage modulus (E') and the loss modulus (E'') of the specimen are, then, calculated based on the maximum stress (σ_{max}), maximum strain (ε_{max}) and the phase difference angle (δ) [4]:

$$E' = (\sigma_{max} / \varepsilon_{max}) \cos\delta$$
$$E'' = (\sigma_{max} / \varepsilon_{max}) \sin\delta \tag{3-6}$$

The storage modulus is an indication of the elasticity of material. Loss modulus, also known as the viscous modulus, determines the loss of energy due to internal friction and motions. The complex modulus (E^*) is defined as

$$E^* = E' + iE'' \tag{3-7}$$

The tangent of the phase angle (tan δ), also referred to as damping angle, is an indicator of how efficiently the material loses energy due to molecular rearrangements and internal friction. It can be calculated by Equation 3-8. It is known that tan δ of a sample is independent of its geometry.

$$\tan\delta = \varepsilon'' / \varepsilon' = E'' / E' \tag{3-8}$$

Microindentation

The microindentation technique has been successfully used to assess the creep rate and the hardness of monophasic cement-based systems. In this technique, a load (P) is applied through a probe to the surface of a specimen, and is increased to its maximum value (P_{max}). This maximum load is held on the specimen for a given period of time. This results in the penetration of the probe tip to the surface of the specimen. The specimen will, then, be unloaded. The amount of the applied load, the penetration depth (h) with a maximum value of (h_{max}) and the time are recorded during this test. A schematic of the load versus penetration depth obtained by the microindentation technique on a synthetic C-S-H specimen is presented in Figure 3-3.

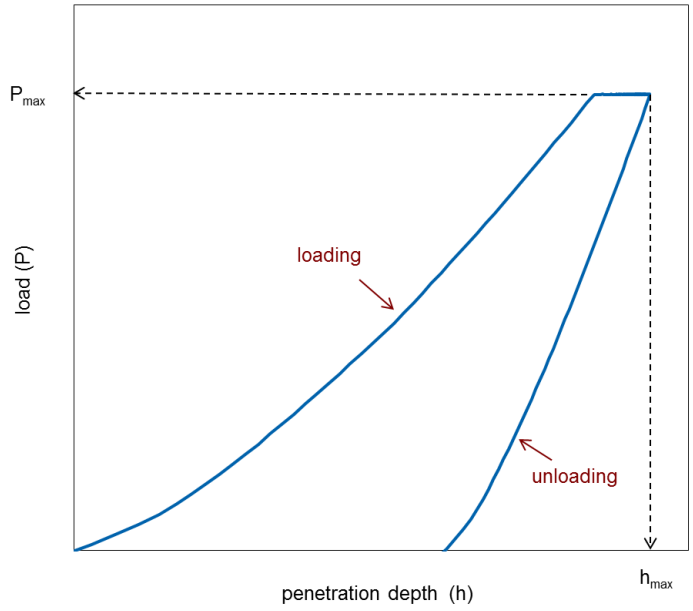

Figure 3-3- Load versus penetration depth determined by the microindentation technique

Several suggestions have been proposed to determine the mechanical performance of the test specimen based on these parameters. Microindentation creep modulus as suggested by Vandamme and Ulm [10] and indentation hardness are used in the current study. The creep modulus is inversely related to the creep of the specimens. It is calculated by the following procedure:

The creep is determined by curve fitting of the indentation-depth versus time curves under loading by equation $\Delta h(t) = x_1 \ln(x_2 t + 1) + x_3 t + x_4$. The creep modulus ($C$) is, then, calculated from $C = P_{\max} / (2 a_u x_1)$ where $a_u = (a_c / \pi)^{1/2}$. a_c is the projected area of contact between the indenter probe and the indenter surface. It is determined using the Oliver and Pharr method [11] as a function of the maximum indentation depth ($\Delta h(t) = 24.5 h_{\max}^2 + k_1 h_{\max}^1 + k_2 h_{\max}^{1/2} + k_3 h_{\max}^{1/4} + ... + k_8 h_{\max}^{1/128}$ where k_n is a constant). The indentation hardness (H) is also obtained by $H = P / a_c$.

Length-change measurements

The Tuckerman extensometer has been successfully used to measure the length-change of cement-based systems under various external on internal stimuli [12-14]. It has very good accuracy (1 microstrain), and therefore can be used for the length-change measurements of small specimens. A schematic picture of this extensometer is shown in Figure 3-4. The sample (number 1 in the figure) is put on a holder (5), and is held against the knife edges (2 and 3) by a light spring (4). The optical system consists of two mirrors: a fixed one (6) and a titling one (7). The latter is on the face of a rocking lozenge. The whole set-up is supported by a stand (8). The tilting of the mirror is correlated to the length-change of the sample, and is monitored using an auto-collimator (Figure 3-5).

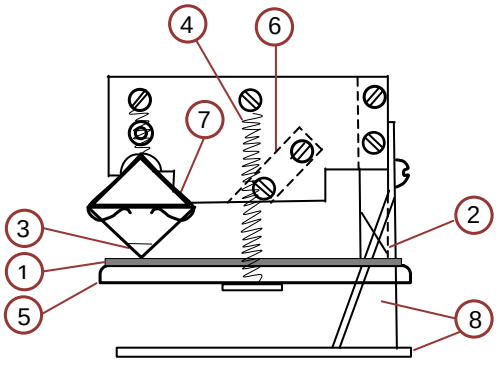

Figure 3-4- Tuckerman extensometer [13]

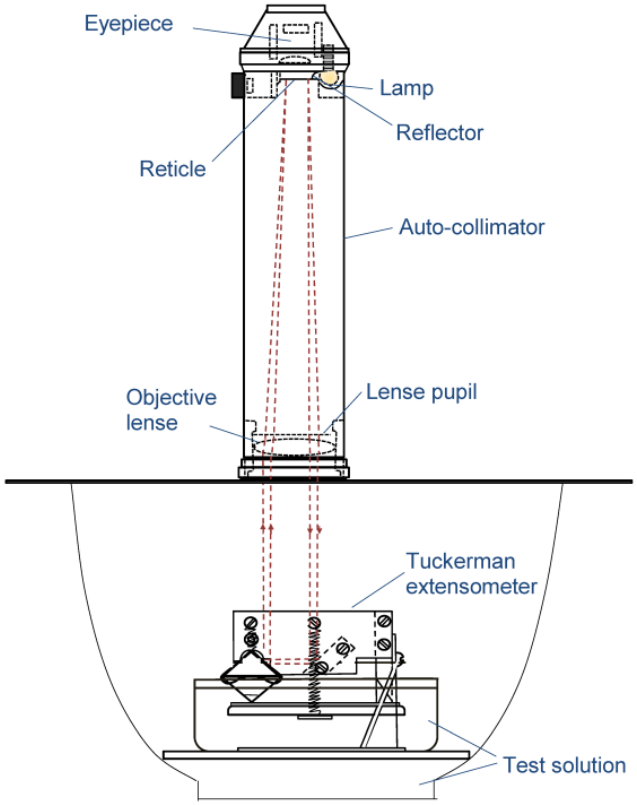

Figure 3-5- Relationship of autocollimator and an extensometer [15]

Mass-change in isopropanol

It was previously suggested that diffusion of isopropanol in saturated cement paste samples can be successfully used to evaluate resistance of the samples to the chloride diffusion [16]. An experimental set-up was designed in the current study to evaluate the rate of diffusion of isopropanol in the compacted samples of the C-S-H-based systems. This was based on the mass-change measurements of the compacted samples following the immersion in the isopropanol. The test set-up is schematically presented in Figure 3-6. A small stainless steel basket was attached to a balance by steel wires, and immersed in 450 ml of anhydrous isopropanol (Reagent grade, Fischer Scientific). A compacted sample (32 mm in diameter and 1 mm thickness) was placed in the basket at the depth of 20 mm from the free surface of the isopropanol solution, and its mass-change was monitored until a plateau was achieved (about 2 hours).

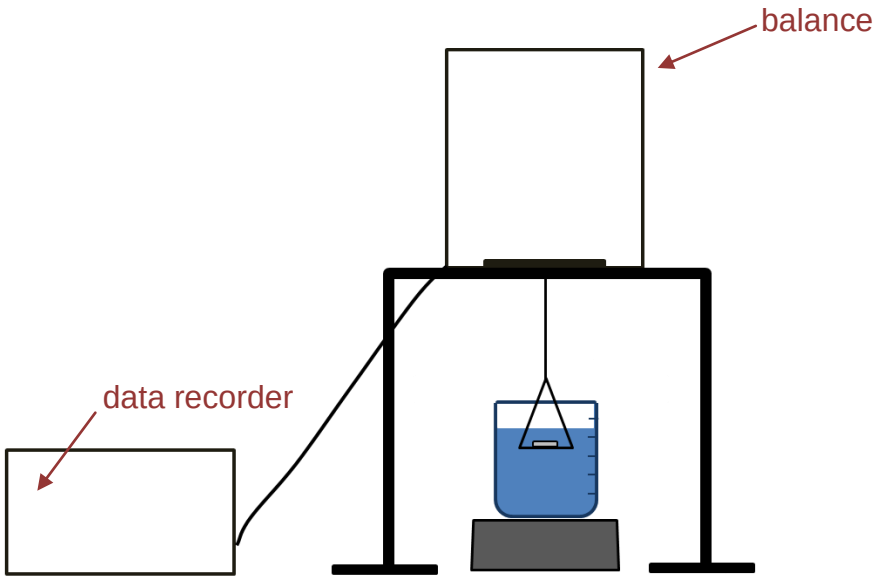

Figure 3-6- Schematic of the set-up used for the isopropanol diffusion measurements

3.2 Materials

Individual hydrated cement-based phases were synthesized and characterized prior to being used for the assessments of durability and mechanical properties. The synthesis method, humidity conditioning and the compaction technique are described in the following sections. Reagent grade chemicals as received by the producers were used for the synthesis as well as for the preparation of the test solutions.

3.2.1 Synthesis of pure phases

C-S-H-based systems

Phase pure C-S-H (Ca/Si = 1.5) was synthesized using the pozzolanic reaction technique. It included the reaction of stoichiometric amounts of calcium oxide and colloidal silica in excess water (water/solid mass ≈ 10) for 21 days. Calcium oxide was obtained by calcining calcium carbonate (reagent grade, Fisher Scientific) at 900 °C for 24 hours. Reactive

colloidal silica (CAB-O-SIL®, grade M-5) was also provided by Cabot Corporation. Powders of calcium oxide and colloidal silica were first dry-mixed in a high density polyethylene (HDPE) bottle. De-ionized out-gassed water was, then, added to the solid mixture to initiate the pozzolanic reaction. The solution was agitated for 21 days at room temperature (about 24 °C). It was, then, filtered and dried under vacuum for four hours. The gel-like product was conditioned in sealed desiccators at the relative humidity of 11% (over saturated lithium chloride solution) for 40 days. The equilibrium of the samples was confirmed by the thermal analysis and mass-loss measurements. A similar method was used to synthesize the organically modified C-S-H systems. The organic compounds were, however, added to the mixing water. The organic compound used included 2-, 3- and 4-nitrobenzoic acid, 3- and 4-aminobenzoic acid, octadecylamine, oxalic acid, malonic acid, adipic acid, lauric acid, aminolauric acid, stearic acid, 3-aminopropyltriethoxysilane, vinyltrimethoxysilane, polyvinyl alcohol, polyacrylic acid and polymethylmethacrylate. A wide range of concentration of the organic compounds was used. These included from 0.01 mol. to 0.70 mol. of the organic per mol. of calcium of the host C-S-H. The greatest interaction for most the organic compounds and C-S-H was achieved for the organic/Ca = 0.01. Additional details of each organically modified C-S-H system will be provided in the relevant chapter.

In addition to the organically modified C-S-H-based systems mentioned above, C-S-H/polyaniline nanocomposites were used in this study for the assessment of durability. These nanocomposites were used as synthesized by Alizadeh et al. through an in-situ polymerization technique. A detailed procedure of this technique was provided by these researchers [17]. A summary of it is as follows: The C-S-H/aniline system (Ca/Si ratio of 0.8 and 1.2) was prepared using a pozzolanic reaction technique. The aniline monomer was pre-dissolved in the mixing water. The mixture was hydrated for 90 days. It was then filtered and dried to get the powder. The C-S-H/aniline powder was then mixed in water. Ammonium persulfate was added to it as the initiator for the polymerization reaction. The solution was stirred for three days at room temperature. The final material was washed, filtered, and then vacuum-dried. All the powders were kept in desiccators at the relative humidity of 11% to be equilibrated before conducting the experiments.

Secondary hydrated cement phases

Monosulfate **-** Monosulfate was synthesized by a method proposed by Kuzel [18]. It consisted of reacting stoichiometric amounts of tricalcium aluminate (C_3A) and gypsum ($CaSO_4.2H_2O$) in an excess amount of water in a hydrothermal pressure vessel. The C_3A clinker used was obtained from the CTL group (Skokie, IL). It was ground, and passed through a 150 μm sieve (#100) before being used for the synthesis. Reagent grade gypsum supplied by the Caledon Laboratories Ltd. was used. The mixture of C_3A and gypsum solution was heated in an oven at 150 °C for four days. The pressure vessel was, then, removed from the oven, and the excess water was discharged after reaching equilibrium at room temperature. The remaining solid was placed in a desiccator and dried over a saturated lithium chloride solution, at 11% relative humidity, for 24 h.

Ettringite - Ettringite was synthesized by a method described by Struble and Brown [19] which consisted of reacting stoichiometric amounts of aluminum sulfate ($Al_2(SO_4)_3$) solution and calcium oxide (CaO) solution. The 98% aluminum sulfate hydrate (supplied by Aldrich chemical company) was used as one of the starting materials. The calcium oxide was also obtained by calcining reagent grade calcium carbonate at 900 °C for 24 h. The aluminum sulfate solution was prepared in de-ionized water, and the calcium oxide solution was prepared in a 10% sucrose solution. The two solutions were then mixed, and stirred for 60 h at room temperature. The resulting mixture was filtered and dried in a vacuum drying cell at room temperature for 24 h.

Thaumasite - Thaumasite was synthesized by a method developed by Blanco-Varela et al. [20]. Two sugary solutions (10% by mass) were prepared in this method: Solution 1 which contained calcium oxide (CaO), and solution 2 which contained sodium salts of silicate, sulfate and carbonate (Na_2SiO_3, Na_2SO_4 and Na_2CO_3). The salt concentrations for each solution are summarized in Table 3-1. Both solutions were kept at 5 °C for 5 h. They were, then, mixed, and the mixture was stored at 5 °C for 3 months. The mixture was, then, washed with de-ionized water and filtered. The filtered material was kept in a desiccator at 11% RH to be equilibrated.

Table 3-1- Salt concentration for the synthesis of thaumasite [20]

	Solution 1	Solution 2		
Reagent	CaO	Na_2SiO_3	Na_2SO_4	Na_2CO_3
Mass (g)	5.05	1.83	7.1	1.59
Volume/solvent	250 ml/(water + 25 g sucrose)	250 ml/(water + 25 g sucrose)		

3.2.2 Humidity conditions

All the powders were conditioned at a relative humidity of 11% to reach equilibrium prior to the test. It is known that there is, theoretically, only a monolayer of adsorbed water on the surface of the C-S-H particles at the 11% RH in addition to the interlayer water [13].

3.2.3 Characterization of pure phases

All the synthetic pure phases were characterized using the XRD, TGA-DSC, SEM-EDX and FTIR techniques described in section 3.1.1. The specific test details for each technique will be provided in the relevant chapters.

3.2.4 Preparation of the compacted samples

A rigid body of the powdered material is required for the volume stability and dynamic mechanical analysis experiments. In this study, powders were compacted in a steel mould consisting of a cylinder and two closely fitting pistons (Figure 3-7). Two types of moulds were used depending on the requirements for each experiment; a circular mold was used for the length-change and mass-change measurements, and the rounded rectangle for the DMA experiments. The cross-section of the prepared samples is shown in Figure 3-8.

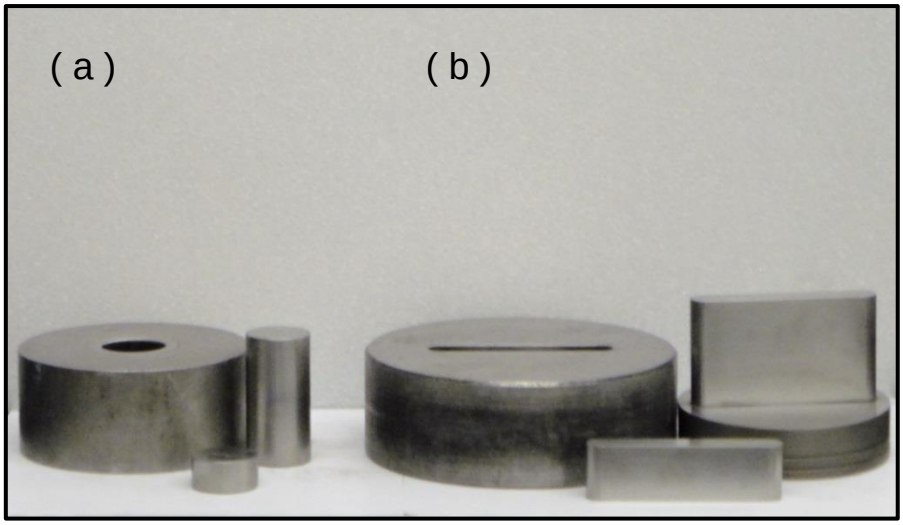

Figure 3-7- Compaction mould used - (a) circular and (b) rounded rectangle type

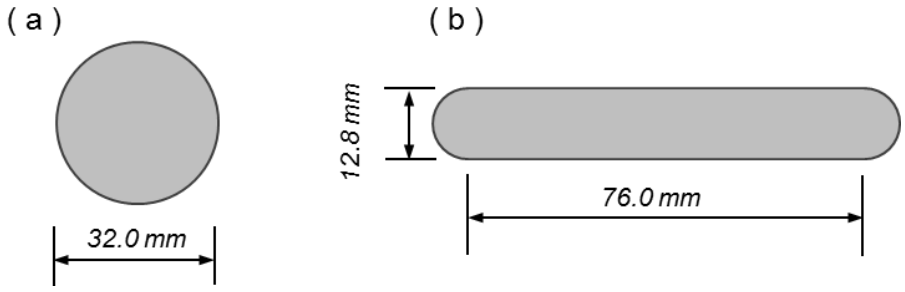

Figure 3-8- Cross-section of the compacted samples: (a) circular and (b) rounded rectangle type (thickness was about 0.9 to 1.2 mm)

In order to prepare the compacted samples, the mould is mounted vertically, and the powder is placed in the cylinder by tamping with the edge of a spatula against the top edge of the cylinder. It is very important to have a flat surface for the powder to achieve a uniform thickness throughout the compacted sample. The top piston is, then, placed in the cylinder and the assembly is mounted in a compression machine. The pressure is increased gradually to the required value, maintained at that value for about 10 s, and then is released. The compacted sample is finally removed by pressing out the pistons.

The compaction procedure in this study was performed on the powders conditioned at 11% RH. The powders were very fine passing through a 150 μm (# 100) sieve. The

pressure of the compression machine was adjusted to reach a porosity of about 30% for the compacted C-S-H-based systems. This porosity level was selected as a typical hydrated Portland cement paste sample (w/c = 0.40) has a porosity of 26-30% [17]. As the mechanical properties and durability of porous materials are dependent of their porosity values [8], the porosity of the compacted samples was determined using the helium porosimetry method. The details of the helium porosimetry technique are described later.

The secondary hydrated phases were compacted to reach a porosity of about 10%. This was selected so that the samples would have a greater resistance to disintegration during the length-change measurements in the test solutions.

Helium porosimetry

A helium pycnometer was used for the helium porosimetry measurements. A total of about five compacted circular samples were put in the pycnometer. Helium gas was allowed to flow into the test cell. All small pores of the specimens were instantly filled with the helium gas, and the solid volume of specimens could be measured based on the gas laws and the assumption of an ideal gas. The porosity of the samples was then estimated knowing the solid volume and the apparent volume. A schematic of the helium porosimetry equipment is presented in Figure 3-9.

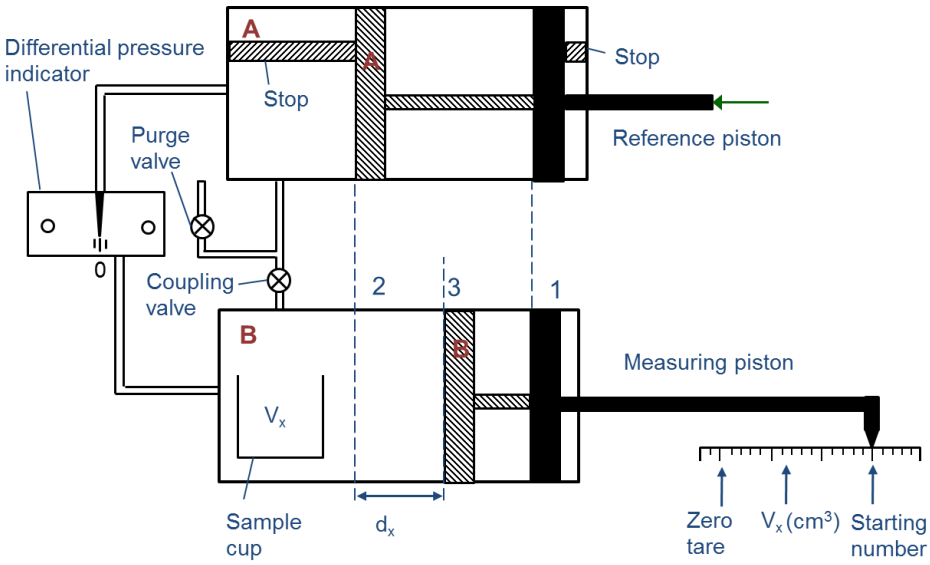

Figure 3-9- A schematic of the helium pycnometer [21]

References

1. V. S. Ramachandran and J. J. Beaudoin (edt.), Handbook of Analytical Techniques in Concrete Science and Technology, William Andrew, 2000.
2. S. J. Gregg and K. S. Sing, Adsorption, Surface area and Porosity, London: Academic Press Inc., 1967.
3. T. C. Powers and T. L. Brownyard, "Studies of the physical properties of hardened Portland cement paste," *Research Laboratories of the Portland Cement Association Bulletin*, 22, 1948.
4. J. Ferry, Viscoelastic Properties of Polymers, New York, Chapters 5-7: Wiley, 1980.
5. F. Radjy, A thermodynamic study of the system hardened cement paste and water and its dynamic mechanical response as a function of temperature, PhD Thesis, Technical Report No. 90, Department of Civil Engineering, Stanford University, 1968.
6. F. Radjy and C. W. Richards, "Effect of curing and heat treatment history on the dynamic mechanical response and the pore structure of hardened cement paste," *Cement and Concrete Research*, 3, pp. 7-21, 1973.
7. F. Radjy and E. J. Sellevold, "Internal friction peaks due to adsorbed and capillary water in microporous substances," *Nature Physical Science*, 241, pp. 133-135, 1973.
8. R. Alizadeh, Nanostructure and engineering properties of basic and modified calcium silicate hydrate systems, PhD Thesis, University of Ottawa, 2009.
9. K. Menard, Dynamic Mechanical Analysis - A practical introduction, CRC Press LLC, 1999.
10. M. Vandamme, F.-J., Ulm "Nanogranular origin of concrete creep," *Proceedings of the National Academy of Sciences*, 106(26), pp. 10552-10557, 2009.
11. W.C. Oliver, G.M. Pharr, "An improved technique for determining hardness and elastic modulus using load and displacement sensing indentation experiments," *Journal of Materials Research*, 7, pp. 1564-1583, 1992.

12. R. F. Feldman and P. J. Sereda, "A model for hydrated Portland cement paste as deduced from sorption-length change and mechanical properties," *Materials and Structures*, 1(6), pp. 509-520, 1968.

13. R. F. Feldman, P. J. Sereda and V. S. Ramachandran, "A study of length changes of compacts of Portland cement on exposure to H_2O," *Highway Research Record*, 62, pp. 106-118, 1964.

14. I. Soroka and P. J. Sereda, "The Structure of Cement-stone and the Use of Compacts as Structural Models," In Proceedings of the 5th International Symposium on the Chemistry of Cement, Tokyo, Vol. III, pp. 67-73., 1968.

15. AMINCO, American Instrument Company, Ultra modern instrumentation for precise physical measurement, Bulletin 2160, April 1948.

16. R. F. Feldman, "Diffusion measurements in cement paste by water replacement using propan-2-ol," *Cement and Concrete Research*, 17, pp. 602-612, 1987.

17. R. Alizadeh, J. Beaudoin, L. Raki and V. Terskikh, "C-S-H/polyaniline nanocomposites prepared by in situ polymerization," *Journal of Materials Science*, 46(2), pp. 460-467, 2011.

18. H. J. Kuzel, "Synthesis and X-Ray Study of the Crystalline Composition $3CaO.Al_2O_3.CaSO_4.12H_2O$," *Neues Jahrbuch Mineral Monatsh*, 7, pp. 193-197, 1965.

19. L. J. Struble and P. W. Brown, "An evaluation of ettringite and related compounds for use in the solar energy storage," NBSIR 82-253, USA, US Department of Commerce, p. 11, 1982.

20. M. T. Blanco-Varela, P. M. Carmona-Quiroga, I. F. Sáez del Bosque and S. Martínez-Ramírez, "Role of organic admixtures on thaumasite precipitation," *Cement and Concrete Research*, 42(7), pp. 994-1000, 2012.

21. Beckman instructions, Model 930, Air comparison pycnometer, Beckman Instruments, INC., 1971.

Chapter 4

Interaction of 2-, 3- and 4-Nitrobenzoic Acid with the Structure of Calcium-Silicate-Hydrate Systems

Possible interaction of nitrobenzoic acid with the structure of calcium-silicate-hydrate (C-S-H) was critically investigated in this chapter. Phase pure C-S-H and C-S-H with 2-, 3- or 4-nitrobenozic acid (0.01 and 0.02 mol. per mol. of Ca) were synthesized, and characterized by the X-ray diffraction, thermal analysis, Fourier transform infrared spectroscopy and scanning electron microscope techniques. Nitrogen adsorption measurements were also performed to estimate the surface area of the samples. A model for the nanostructure of C-S-H/nitrobenzoic acid systems was proposed. All types of nitrobenzoic acid with the lower concentration of nitrobenzoic acid were able to fill the defects on the surface of the C-S-H layers, block access to the space between the stacked C-S-H layers, and possibly partially intercalate the layered structure. The C-S-H-based samples prepared with different types of nitrobenzoic acid compounds, however, had different characteristics. The interaction of organic and inorganic phases was limited in the systems incorporating the higher concentration of nitrobenzoic acid. Accumulation of nitrobenzoic acid on the surface or at the edge of the C-S-H layers or between the stacked C-S-H layers occurred in these systems.

4.1 Introduction

Performance enhancement of cement-based materials is desired in order to produce more sustainable concrete construction. Most of the studies have focused on the Calcium-

Silicate-Hydrate (C-S-H) as it is the predominate phase and influences many of the properties of cement paste. The modification of the C-S-H nanostructure using organic compounds was first suggested by Matsuyama and Young in 1999 [1-4]. These researchers investigated the influence of several anionic, cationic and non-ionic polymers, and suggested the possibility of the intercalation of selected organic compounds in the interlayer region of C-S-H. It was observed that the intercalation of polymers in the C-S-H interlayer region is dependent on the type and concentration of the polymers as well as the Ca/Si ratio of the host C-S-H. The formation of organically modified C-S-H nanocomposites was also reported by Mojumdar and Raki [5-7], Alizadeh et al. [8] and Pelisser et al. [9-10].

After more than a decade of investigation on the interaction of organic compounds with the nanostructure of C-S-H, the nature of these interactions is still debatable. Although earlier reports provided evidence on the intercalation of polymers in the interlayer region of C-S-H [1-4], separate studies by Popova et al. [11] and Merlin et al. [12] indicated that the interlayer region of C-S-H is unlikely to be altered by the polymers investigated. The polymer was, however, adsorbed in significant amounts on the surface or in the void space left by lamellae 'stacks' [12]. Minet et al. [13, 14] also suggested that small-sized organotrialkoxysilane molecules might be intercalated in the C-S-H layers. Phase separation, however, would occur for the large-sized organic compounds. Franceschini et al. [15] also suggested that only polymers with trialkoxysilane groups are able to be incorporated in noticeable amounts in the C-S-H structure. These polymers could form a specific linkage with the silicate chain in C-S-H. They, however, would not modify the interlayer region. In addition, Pelisser et al. [9] reported that poly-(diallyldimethyl-ammonium chloride) could partially intercalate the C-S-H interlayer region. The remainder of this organic compound was adsorbed on the "surface" or in "the void space left by the C-S-H particles".

Most investigations on the formation of C-S-H-based nanocomposites were conducted with the use of relatively large molecular-sized organic compounds. The reports on the application of small-sized molecules for these purposes are very limited and not comprehensive. Matsuyama and Young [1] suggested that small organic molecules (e.g. glycerol, propanediol, ethylene glycol, succinic acid and maleic acid) were not intercalated

in the interlayer region of C-S-H. The results by Minet et al. [13], however, provided evidence of the intercalation of small-sized organic molecules which have a trialkoxysilane functional group.

The focus of the current chapter is on the possible interaction of nitrobenzoic acid with the micro- and nanostructure of C-S-H. Nitrobenzoic acid has a small molecular size, and was successfully intercalated into the nanostructure of layered double hydroxides [16]. It was also previously suggested that nitrobenzoic acid can influence the hydration kinetics of C_3S [17]. The nature of the interaction of these organics with the structure of C-S-H is, however, still unknown. C-S-H systems modified with various concentrations of 2-, 3- and 4-nitrobenzoic acid were synthesized and characterized in this chapter. The next chapter will focus on the assessment of durability and engineering performance of these systems.

4.2 Experimental program

4.2.1 Materials

Phase pure C-S-H and C-S-H/nitrobenzoic acid systems with Ca/Si = 1.5 was synthesized using the pozzolanic reaction technique as described in chapter 3. The effect of either of 2-, 3- and 4-nitrobenzoic acid (reagent grade, supplied by Sigma-Aldrich) was investigated. The concentration of nitrobenzoic acid was 0.010 moles or 0.020 moles per mole of Ca. Two additional mixtures with 0.015 moles and 0.030 moles of 4-nitrobenzoic acid per mole of Ca were also prepared and used in a few experiments.

4.2.2 Characterization techniques

All the samples were tested by the XRD, TGA, FTIR and SEM techniques. The nitrogen adsorption measurement was also conducted and used for the surface area determination. The detailed test methods are as follows:

XRD - The X-ray diffraction pattern of the samples was acquired using a Scintag XDS 2000 diffractometer (CuK_α radiation). A 2θ range of $4^\circ < 2\theta < 15^\circ$, a step size of 0.03° and a 5 second count interval was used to detect the changes in the basal-spacing (d_{002}) peak.

TGA - A TA Instrument SDT Q-600 was used for the thermal analysis. About 20 mg of the sample was heated from the ambient temperature (about 24 °C) to 1000 °C at a rate of 10 °C/min under the flow of nitrogen gas (10 ml/min). The derivative mass-loss was obtained using Universal Analysis 2000 software.

FTIR – Fine powders were mixed with potassium bromide, and compacted into a disk of 10 mm diameter using a 10 ton load. FTIR spectra were collected on a Tensor 27 spectrometer in direct transmission mode between 4000 and 400 cm^{-1}. Each FTIR spectrum represented the average of 50 scans at 4 cm^{-1} resolution. Air was used as a background for the measurements.

SEM – SEM images were collected using a Hitachi S-4800 Field Emission Scanning Electron Microscope. The surface structure images were acquired using a beam current of 10 mA at 3.2×10^{-16} J (2 kV) at the working distance of 4 mm.

Nitrogen adsorption - A Quantachrome instrument NOVA 2200e surface area and pore size analyzer was used for the nitrogen adsorption measurements. The samples were vacuum dried at 110 °C for three hours prior to starting the measurements. Then, the nitrogen BET (Brunauer-Emmett-Teller) surface area was performed on each sample.

4.3 Results and discussion

4.3.1 X-ray diffraction

The C-S-H/NBA samples prepared with either 2-, 3- or 4-nitrobenzoic acid (NBA/Ca = 0.01) had a similar basal-spacing (d_{002}) of 1.17 nm (Figure 4-1). Although this d-spacing was slightly higher than that observed for the phase pure C-S-H (d_{002} = 1.10 nm), it was much lower than what was expected for the intercalated nanocomposites considering an average value of about 0.61 nm for the thickness of nitrobenzoic acid molecule. It is, however, possible that the nitrobenzoic acid molecules were oriented parallel to the CaO layers in the nanostructure of C-S-H. In this case, an increase of less than 0.10 nm in the d_{002} of the samples could be expected. In addition, it is known that silicate tetrahedra are mainly in the form of dimers in the structure of C-S-H with Ca/Si = 1.5. The nitrobenzoic

acid molecules could possibly fill the gaps between the silicate tetrahedra dimers resulting in a lower increase in the d_{002} of the resulting samples. An additional d-spacing of about 1.13 nm was also detected in the XRD pattern of the sample incorporating 3-nitrobenzoic acid with the NBA/Ca of 0.01. It is possible that this sample was composed of two different phases; an intercalated phase forming a nanocomposite and a phase in which the C-S-H layers were just slightly altered by the presence of the 3-nitrobenzoic acid. The interaction of organic and inorganic phases in the latter, however, is less than that in the former.

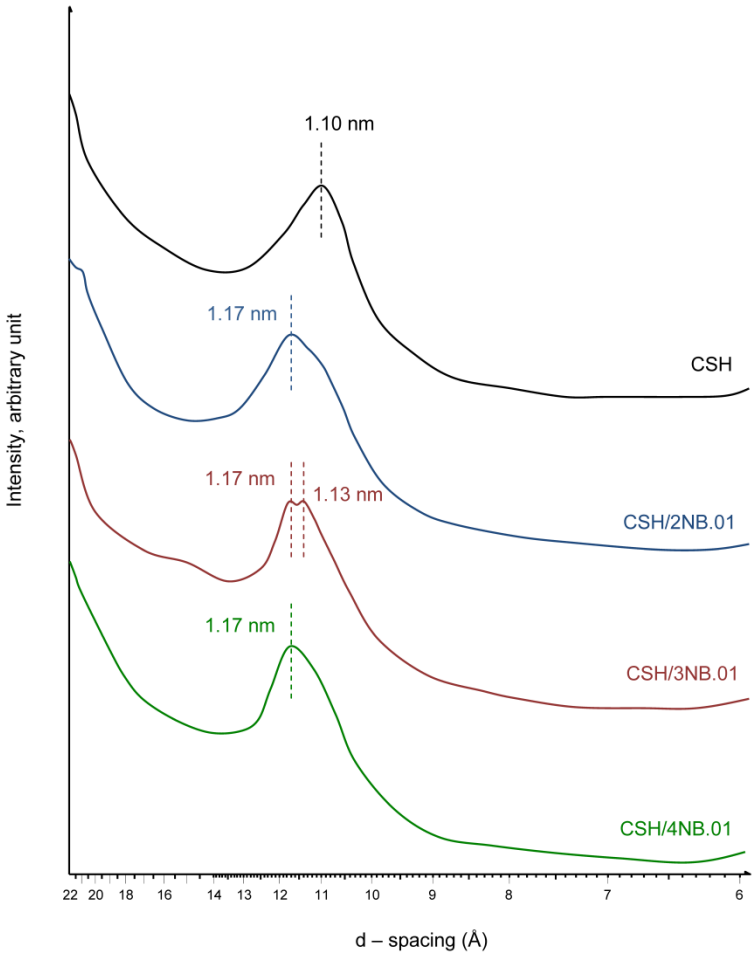

Figure 4-1- XRD pattern of the phase pure C-S-H and C-S-H/NBA (NBA/Ca=0.01)

The basal-spacing (d_{002}) of the samples with NBA/Ca ratio of 0.02 was lower than that for the samples with NBA/Ca ratio of 0.01 (Figure 4-2). This could be an indication of less interaction of the organic and inorganic phases in the samples with higher amounts of nitrobenzoic acid. Preparation of two additional samples with 4NBA/Ca ratios of 0.015 and

0.03 provided more information of how the d_{002} value of the samples incorporating 4-nitrobenzoic acid would be eventually reduced by the gradual increase in the concentration of the nitrobenzoic acid. The d_{002} of the C-S-H/4NBA sample with 4NBA/Ca = 0.03 was ultimately almost identical to that of the phase pure C-S-H. It is suggested based on the XRD patterns that partial intercalation of the nitrobenzoic acid was likely achieved in the samples with NBA/Ca = 0.01. Higher concentrations of nitrobenzoic acid, however, prevented the intercalation of the organics. In this case, the nitrobenzoic acid may have altered the edge of the C-S-H layers resulting in a slight increase in the basal-spacing of the sample.

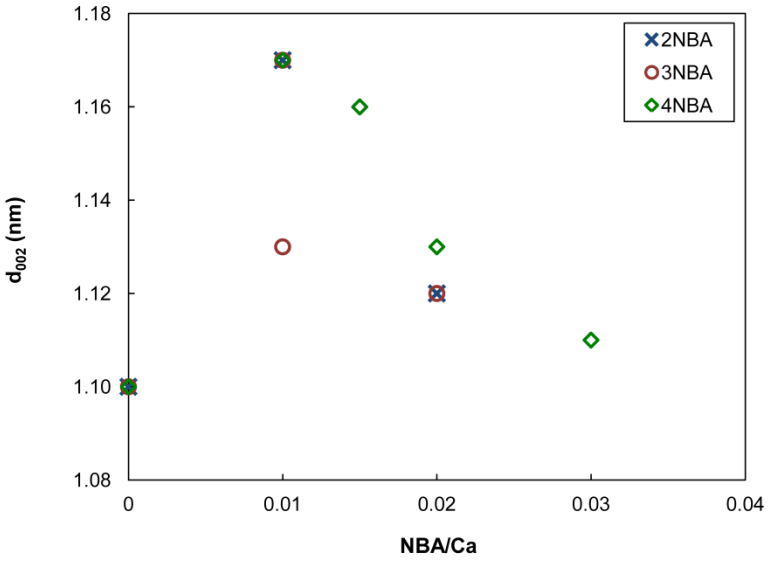

Figure 4-2- basal-spacing (d_{002}) of the phase pure C-S-H and the C-S-H/NBA samples with various concentrations of nitrobenzoic acid

It is also noted that the intensity of the XRD peaks was very similar in the phase pure C-S-H and the C-S-H/NBA samples regardless of the type and concentration of nitrobenzoic acid. No evidence of the significant change in any crystallinity of the samples due to the incorporation of the nitrobenzoic acid was obtained.

4.3.2 Thermal gravimetric analysis

The phase pure C-S-H and the C-S-H/NBA samples were heated up to 1000 °C, and the mass-loss curves and their derivative were analyzed. It was observed that the removal of water from the samples with nitrobenzoic acid (NBA/Ca = 0.01) occurred at relatively higher temperatures compared to that in the phase pure C-S-H. The location of the maximum peak corresponding to the gradual removal of water from the structure of C-S-H-based samples is presented in Figure 4-3. It was observed that the peak location was increased from about 90 °C in the phase pure C-S-H to about 99 °C in the C-S-H/NBA samples with NBA/Ca = 0.01, regardless of the type of nitrobenzoic acid. This possibly occurred because the nitrobenzoic acid molecules may have blocked the interlayer region and the space between the stacked layers of C-S-H. The peak, however, shifted back to its original location in the C-S-H/NBA samples with NBA/Ca = 0.02. This is consistent with the XRD results, and is an indication of limited interaction of nitrobenzoic acid molecules with the nanostructure of C-S-H, and possible phase separation due to the relatively high amount of organics.

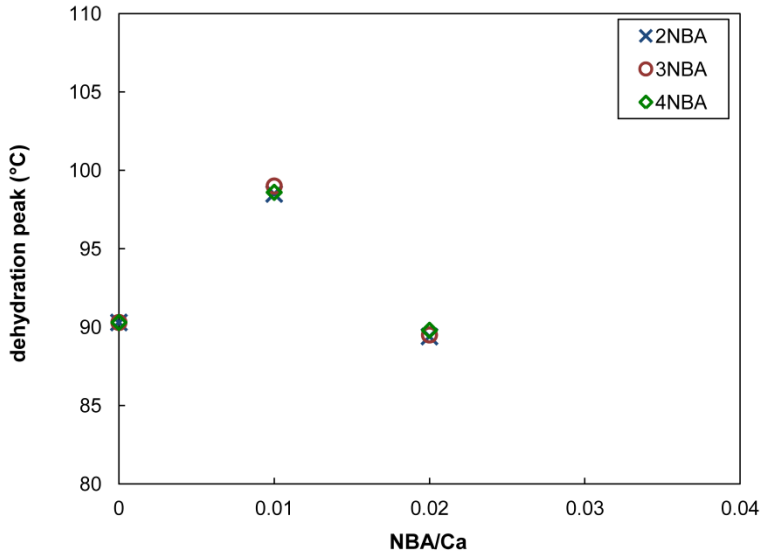

Figure 4-3- Temperature of occurrence for the maximum dehydration peak of the mass-loss derivative curve due to the heating of the phase pure C-S-H and the C-S-H/NBA samples

The mass-loss percentage of the phase pure C-S-H and the C-S-H/NBA samples was also estimated by the TGA, and no significant difference was observed. This does not support the suggestion by Merlin et al. [12] that the slight increase in the basal-spacing of the organo-C-S-H samples could be due to a higher interlamellar hydration degree.

In addition, about 2.0% of unreacted lime was detected by the TGA in either the phase pure C-S-H or the C-S-H/NBA samples. The presence of unreacted lime is common in the synthetic C-S-H with Ca/Si ratios of 1.54 and higher [18]. No significant evidence of the presence of higher amounts of unreacted lime was, however, observed in the samples incorporating nitrobenzoic acid. It is, therefore, suggested that higher concentrations of nitrobenzoic acid possibly only resulted in the organic/inorganic phase separation, and did not interfere with the pozzolanic reaction.

4.3.3 Fourier transform infrared spectroscopy

The FTIR spectra of the phase pure C-S-H and the C-S-H/NBA samples are presented in Figure 4-4. The peaks at the frequencies of about 820 cm^{-1} and 988 cm^{-1} in the FTIR spectra of the phase pure C-S-H are assigned to the Si-O stretching of Q^1 and Q^2 tetrahedra, respectively [18]. The peak at 820 cm^{-1} was reduced in intensity, and appeared as a shoulder at about 821 cm^{-1} in the sample with 2-nitrobenzoic acid (NBA/Ca = 0.01) due to the interaction of the 2-nitrobenzoic acid molecule with the Q^1 tetrahedra in the nanostructure of the host C-S-H. The band at the frequency of about 988 cm^{-1} also shifted to 989 cm^{-1}. The change in the location of these peaks in the sample incorporating 3-nitrobenzoic acid (NBA/Ca = 0.01) was small. Two additional peaks, however, were detected at the frequencies of 729 and 1365 cm^{-1}. These peaks, respectively, correspond to the symmetric out of plane wagging and symmetric stretching of NO_2 in the 3-nitrobenzoic acid [19]. This is in conformity with the XRD pattern of Figure 4-1 which suggests the formation of a phase with a limited interaction of organic and inorganic in addition to the nanocomposite phase in the sample with 3-nitrobenzoic acid (NBA/Ca = 0.01). The location of the peaks corresponding to the Si-O stretching of Q^1 and Q^2 was altered, and shifted to the frequencies of about 826 cm^{-1} and 985 cm^{-1} due to the interaction with the

4-nitrobenzoic acid (NBA/Ca = 0.01). No evidence of the presence of unreacted organic was detected in this sample.

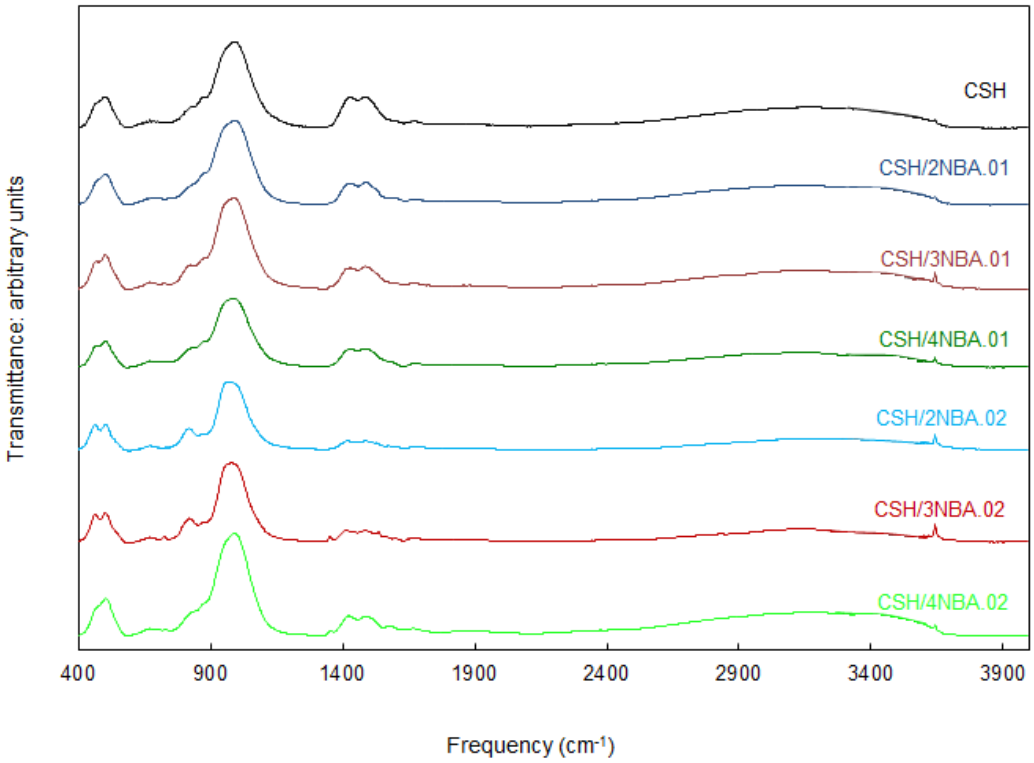

Figure 4-4- FTIR spectra of the phase pure C-S-H and the C-S-H/NBA samples with various concentrations of nitrobenzoic acid

The location of the peaks corresponding to the Si-O stretching of Q^1 and Q^2 in the C-S-H/NBA samples with NBA/Ca = 0.02 was very similar to that in the phase pure C-S-H likely due to the limited interaction of the organic and inorganic phases in these samples. The only exception was the shift of the peak at 988 cm^{-1} in the phase pure C-S-H to 959 cm^{-1} in the sample with 2-nitrobenzoic acid (NBA/Ca = 0.02). The relative intensity of the Q^2/Q^1 peak was also lower in the samples with 2- or 3-nitrobenzoic acid (NBA/Ca = 0.02) compared to the phase pure C-S-H and other C-S-H/NBA samples. It is, therefore, suggested that the silicate tetrahedra are more in the form of dimers in the samples incorporating higher amounts of 2- or 3-nitrobenzoic acid. Additional peaks also appeared in the FTIR spectra of the C-S-H/NBA samples with NBA/Ca = 0.02 likely due to the presence of unreacted organics. The peak at the frequencies of 840 cm^{-1}, 825 and 825 cm^{-1} in the spectra of the samples incorporating 2-, 3-, and 4-nitrobenzoic acid corresponds to

the symmetric out of plane wagging of NO_2. The peaks at 1369 cm^{-1}, 1352 and 1349 cm^{-1} are assigned to the symmetric stretching of NO_2, and those at 1535 cm^{-1}, 1539 and 1575 cm^{-1} refer to the asymmetric stretching of NO_2 in 2-, 3- and 4-nitrobenzoic acid, respectively.

4.3.3 Scanning electron microscopy

The SEM micrographs of the phase pure C-S-H as well as C-S-H/NBA samples with NBA/Ca = 0.01 are presented in Figure 4-5. No significant change in the morphology of the samples was observed due to the incorporation of nitrobenzoic acid. The morphology of the samples with NBA/Ca = 0.02 was also very similar. However, traces of unreacted organics were detected by the Energy Dispersive X-ray technique (EDX) on the sample with 4-nitrobenzoic acid (NBA/Ca = 0.02). This is an indication of the separation of organic and inorganic phases in this sample.

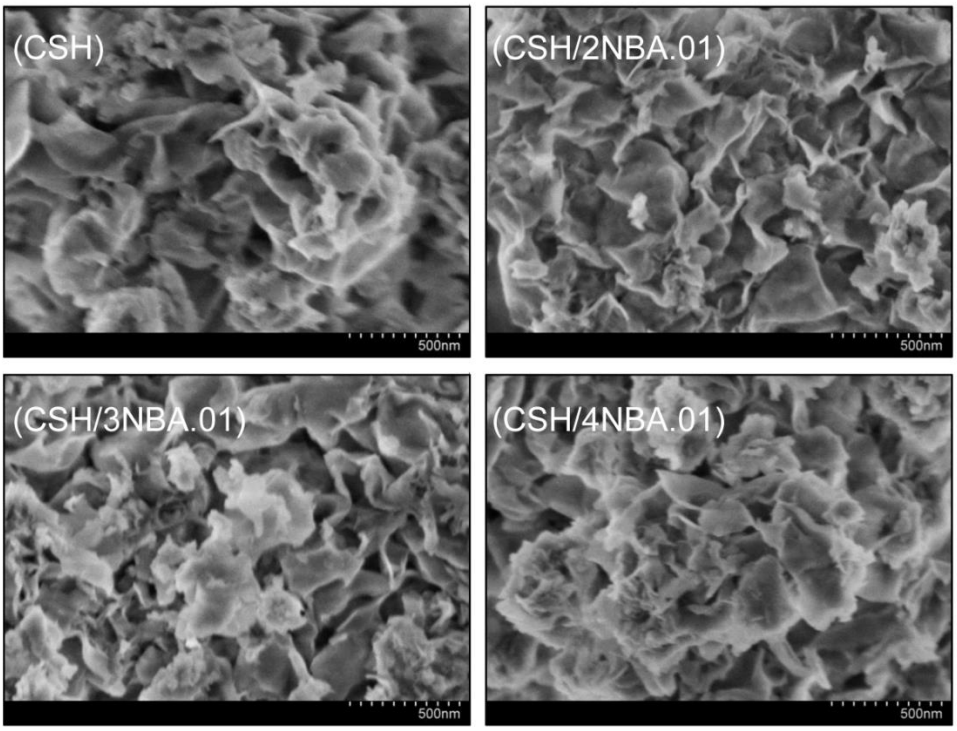

Figure 4-5- SEM micrographs of the phase pure C-S-H and the C-S-H/NBA samples with NBA/Ca = 0.01

4.3.4 Surface area

The surface area measurements for the C-S-H/NBA samples with NBA/Ca = 0.01 was considerably lower than that for the phase pure C-S-H (Figure 4-6). It was suggested based on the significant difference in the surface area of these phases that the nitrobenzoic acid molecules were able to adsorb on the exterior surface of the C-S-H layers and fill the surface defects in the structure of C-S-H. As the nitrogen molecules are unable to penetrate the interlayer region of C-S-H [20], no conclusion could be made on the possible presence of nitrobenzoic acid in the interior surface of the layers based on the nitrogen adsorption measurement. The difference in the surface area of the phase pure C-S-H and the C-S-H/NBA samples with NBA/Ca = 0.01 was more pronounced for the sample incorporating the 4-nitrobenzoic acid compared to those with 2- or 3-nitrobenzoic acid. This may be due to the symmetry in the location of the nitro and carboxylate group in the structure of 4-nitrobenzoic acid. The 4-nitrobenzoic acid isomer, therefore, has a higher potential to cover the surface defects and to block the spaces between the stacked C-S-H layers compared to 2- and 3-nitrobenzoic acid isomers.

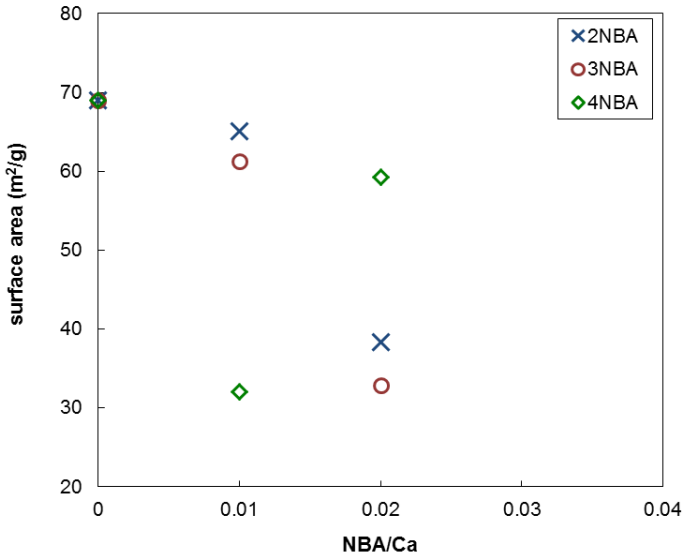

Figure 4-6- BET surface area of the phase pure C-S-H and the C-S-H/NBA samples with various concentrations of nitrobenzoic acid

The surface area detected by the nitrogen adsorption were lower for the samples with 2- or 3-nitrobenzoic acid (NBA/Ca = 0.02) compared to those for the samples with NBA/Ca = 0.01 (Figure 4-6). The sample with 4-nitrobenzoic acid (NBA/Ca = 0.02), however, had a higher surface area compared to the sample with lower concentration of nitrobenzoic acid. It is likely due to the organic/inorganic phase separation in the sample with higher concentration of 4-nitrobenzoic acid as also evidenced by the SEM/EDX examination. It appears, based on these results and those obtained by the other techniques, that the interaction of 2- and 3- nitrobenzoic acid with the nanostructure of C-S-H would be limited when the NBA/Ca = 0.02. These organics, however, are still able to interact with C-S-H at the micro-level. Organic/inorganic phase separation, however, occurred at both the micro- and nano-scale for the sample with 4-nitrobenzoic acid (NBA/Ca = 0.02).

4.3.5 A model for the C-S-H/NBA system

A schematic representation of the possible interaction of nitrobenzoic acid with the structure of C-S-H is suggested in Figure 4-7. The Feldman-Sereda model [20] was used for the nanostructure of C-S-H. It is suggested, based on the results of various characterization techniques of this study, that the nitrobenzoic acid molecule with the concentration of NBA/Ca = 0.01 is able to interact with the structure of C-S-H in five different ways. These include:

1- intercalation in the interlayer region where the silicate tetrahedra is missing in the layered structure of C-S-H,
2- intercalation in the interlayer region so that the orientation of the benzene group is parallel to the layers,
3- adsorbed on the exterior surface of the layers,
4- adsorbed at the edge of the layers, and
5- adsorbed between the stacked C-S-H layers.

The numbers in the above list also correspond to the locations in the model presented in Figure 4-7(a).

The adsorption of nitrobenzoic acid on the exterior surface of the layers, at the edge of the layers and between the stacked C-S-H layers is still possible when NBA/Ca = 0.02.

However, the interaction of the organic and inorganic phase is limited, and accumulation of the organic phase possibly occurs (see Figure 4-7(b)).

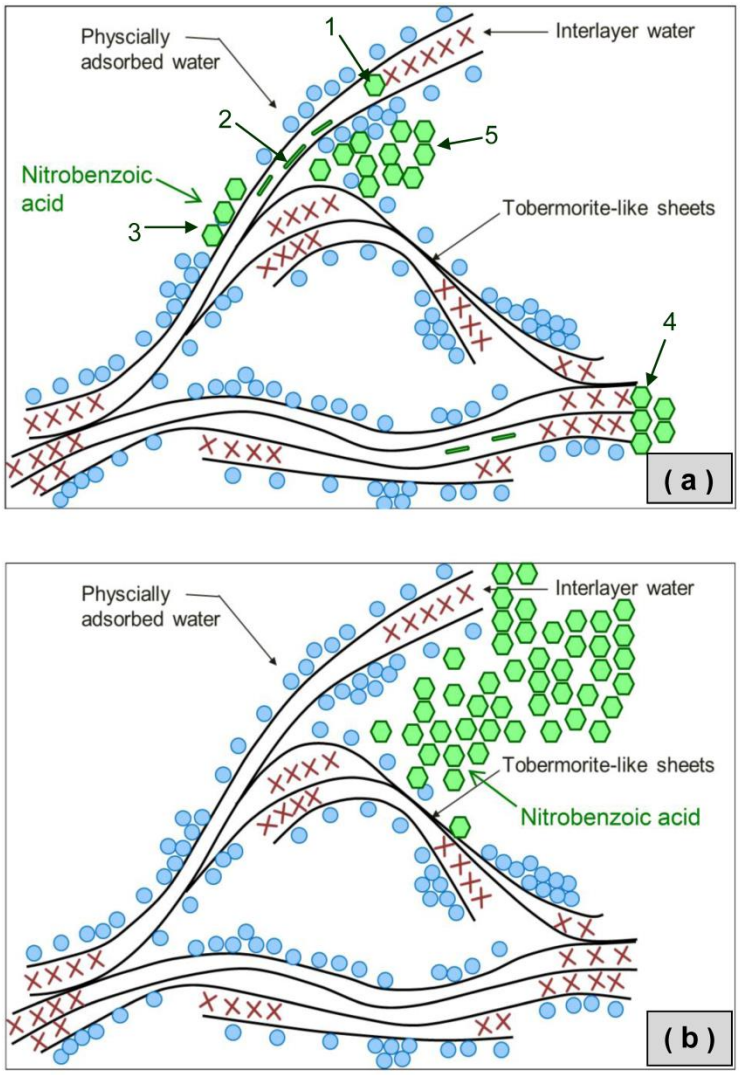

Figure 4-7– Schematic representation of the C-S-H/NBA system, (a) NBA/Ca = 0.01, (b) NBA/Ca = 0.02. Numbers in (a) refer to the location of NBA molecules. The location of the accumulation of NBA molecules is indicated in (b).

4.4 Conclusions

The influence of 2-, 3- and 4-nitrobenzoic acid on the structure of C-S-H was investigated. Evidence was obtained that nitrobenzoic acid with the concentration of NBA/Ca = 0.01 was able to fill/modify the defects on the exterior surface of the C-S-H layers, block the spaces between the stacked C-S-H layers, and possibly partially intercalate the interlayer region.

This resulted in a slight increase in the basal-spacing of the resulting materials, and improved their resistance to dehydration. The interaction of nitrobenzoic acid with the C-S-H structure is reduced, and the organic/inorganic phase separation occurs when higher concentrations of nitrobenzoic acid are used. It was also observed that the 4-nitrobenzoic acid (NBA/Ca = 0.01) was the most effective of the organic molecules investigated to interact with the C-S-H structure. Phase separation, however, was more likely to occur in the composite material when the concentration of the 4-nitrobenzoic acid was relatively high.

References

1. H. Matsuyama and J. F. Young, "Intercalation of polymers in calcium silicate hydrate: A new synthetic approach to biocomposites?," *Chemistry of Materials*, 11, pp. 16-19, 1999.
2. H. Matsuyama and J. F. Young, "Synthesis of calcium silicate hydrate/polymer complexes: Part I," *Journal of Materials Research*, 14, pp. 3379-3388, 1999.
3. H. Matsuyama and J. F. Young, "Synthesis of calcium silicate hydrate/polymer complexes: Part II," *Journal of Materials Research*, 14, pp. 3389-3396, 1999.
4. H. Matsuyama and J. F. Young, "The formation of C-S-H/polymer complexes by hydration of reactive β-dicalcium silicate," *Concrete Science and Engineering*, 1, pp. 66-75, 1999.
5. S. C. Mojumdar and L. Raki, "Preparation and properties of calcium silicate hydrate-poly(vinyl Alcohol) nanocomposites materials," *Journal of Thermal Analysis and Calorimetry*, 82, pp. 89-95, 2005.
6. S. C. Mojumdar and L. Raki, "Preparation, thermal. spectral and microscopic studies of calcium silicate hydrate-poly(acrylic acid) nanocomposites materials," *Journal of Thermal Analysis and Calorimetry*, 85, pp. 99-105, 2006.
7. S. C. Mojumdar and L. Raki, "Synthesis, thermal and structural characterization of nanocomposites for potential applications in construction," *Journal of Thermal Analysis and Calorimetry*, 86, pp. 651-657, 2006.

8. R. Alizadeh, J. Beaudoin, L. Raki and V. Terskikh, "C-S-H/polyaniline nanocomposites prepared by in situ polymerization," *Journal of Materials Science*, 46(2), pp. 460-467, 2011.

9. F. Pelisser, P. J. Gleiz and A. Mikowski, "Effect of poly(diallyldimethylammonium chloride) on nanostructure and mechanical properties of calcium silicate hydrate," *Materials Science and Engineering: A*, 527(26), pp. 1045-1049, 2010.

10. F. Pelisser, P. J. Gleiz and M. Peterson, "Synthesis of calcium silicate hydrate/polymer complexes," *IBRACON Structures and Materials Journal*, 4(5), 2011, pp. 695-708.

11. Popova, G. Geoffroy, M.-F. Renou-Gonnord, P. Faucon and E. Gartner, "Interactions between polymeric dispersants and calcium silicate hydrates," *Journal of the American Ceramic Society*, 83(10), pp. 2556-2560, 2000.

12. F. Merlin, H. Lombois, S. Joly, N. Lequeux, J.-L. Halary and H. Van Damme, "Cement-polymer and clay-polymer nano- and meso-composites: spotting the difference," *Journal of Materials Chemistry*, 12, pp. 3308-3315, 2002.

13. J. Minet, S. Abramson, B. Bresson, A. Franceschini, H. Van Damme and N. Lequeux, "Organic calcium silicate hydrate hybrids: a new approach to cement based nanocomposites," *Journal of Materials Chemistry*, 16, pp. 1379-1383, 2006.

14. J. Minet, S. Abramson, B. Bresson, C. Sanchez, V. Montouillout and N. Lequeux, "New layered calcium organosilicate hybrids with covalently linked organic functionalities," *Chemistry of Materials*, 16, pp. 3955-3962, 2004.

15. A. Franceschini, S. Abramson, V. Mancini, B. Bresson, C. Chassenieux and N. Lequeux, "New covalent bonded polymer-calcium silicate hydrate composites," *Journal of Materials Chemistry*, 17, pp. 913-922, 2007.

16. L. Raki, J. J. Beaudoin and L. Mitchell, "Layered double hydroxide-like materials: nanocomposites for use in concrete," *Cement and Concrete Research*, 34, pp. 1717-1724, 2004.

17. V. S. Ramachandran, J. J. Beaudoin and R.M. Paroli, "The effect of nitrobenzoic and aminobenzoic acids on the hydration of tricalcium silicate: a conduction calorimetric study," *Thermochimica Acta*, 190(2), pp. 325-333, 1991.

18. P. Yu, R. J. Kirkpatrick, B. Poe, P. McMillan, and X. Cong, "Structure of calcium silicate hydrate (C-S-H): Near-, mid-, and far-infrared spectroscopy," *Journal of the American Ceramic Society*, 82(3), pp. 742-748, 1999.

19. M. Samsonowicz, R. Świsłocka E., Regulska, and W. Lewandowski, "Experimental and theoretical IR, Raman, NMR spectra of 2-, 3-, and 4-nitrobenzoic acids," *International Journal of Quantum Chemistry*, 107(2), pp. 480-494, 2007.

20. R. F. Feldman and P. Sereda, "A new model for hydrated Portland cement and its practical implications," *Engineering Journal*, 53(8-9), pp. 53-59, 1970.

Chapter 5

Durability and Mechanical Properties of C-S-H/Nitrobenzoic Acid Composite Systems

The influence of nitrobenzoic acid on the nanostructure of calcium-silicate-hydrate (C-S-H) systems was investigated in the previous chapter. The focus of this chapter is on the assessment of durability and mechanical performance of the C-S-H/nitrobenzoic acid composite systems. Different nitrobenzoic acid isomers in various concentrations were studied. The C-S-H-based preparations were compacted into porous bodies. Their dimensional stability and the leaching of calcium ions in aqueous salt solutions containing Mg^{2+}, Li^{+}, Cl^{-} or SO_4^{2-} ions were evaluated. The resistance of the compacted samples to the diffusion of isopropanol was also obtained by the mass-change measurements. The microindentation technique was used also to measure the creep modulus and the hardness of the samples. Evidence was obtained that nitrobenzoic acid has the potential to significantly improve the durability and mechanical properties of the C-S-H systems. This improvement, however, only occurred in the systems with the lower concentration of nitrobenzoic acid. The systems with higher concentration of nitrobenzoic acid had poor durability and mechanical properties likely due to the limited interaction of the organic and inorganic phases in these systems.

5.1 Introduction

Calcium-silicate-hydrate (C-S-H) is the primary binding phase in hydrated Portland cement. It has been modeled as a layered silicate structure [1] with similarities to that in

smectite clays. Enhancement of the properties of C-S-H is of practical interest as it has a direct influence on the performance of cement-based materials. The use of organic compounds to modify the nanostructure of C-S-H was proposed by Matsuyama and Young in 1999 [2-5]. Although the formation of organo-smectite clay nanocomposites was previously well-established [6-10], it was the first time that a study on the possibility of the formation of C-S-H/polymer nanocomposites was reported. Expansion of the basal-spacing of C-S-H was observed, and assigned to the intercalation of selected polymers in the interlayer space of C-S-H. Not all the polymers, however, were able to intercalate depending on their type (anionic, cationic or non-ionic) and molecular size as well as on the Ca/Si ratio of the host C-S-H.

The possibility of interaction of organic compounds with the nanostructure of C-S-H has been the subject of several investigations during the past few years [11-16]. Merlin et al. [12] suggested that intercalation of polymers in the C-S-H interlayer space is very difficult to achieve. They argued that a considerable amount of polymer, however, can be adsorbed in the voids between the stacked layers of C-S-H resulting in the formation of a "meso-composite" system rather than a nano-composite system. The mechanical performance of the meso-composite systems formed, however, was not reported. The interaction of organotrialkoxysilane molecules with C-S-H was also studied by several researchers [13-15]. The nature of the chemical bonds and the nanostructure of the resulting material were critically investigated. An assessment of the engineering performance of these systems, however, was not covered.

In spite of the significant role of mechanical properties and durability of C-S-H on the service-life of concrete structures, investigations with the focus on these engineering aspects of the C-S-H/organic systems are very limited. Pellenq et al. [17] suggested the modulus of elasticity of C-S-H can be increased by as much as 40% to 100% when organically modified. Pelisser et al., however, reported that the elastic modulus decreased in the organically modified C-S-H nanocomposite [18]. The porosity of the samples, however, was not controlled in this study. It has been previously observed that the engineering properties are porosity dependent [19].

The main objective of this chapter is to assess the mechanical performance and durability of C-S-H/nitrobenzoic acid (C-S-H/NBA) nanocomposite systems. Synthesis and characterization of these systems were reported in chapters 3 and 4. A model for the nanostructure of C-S-H/NBA.01 systems (C-S-H/NBA with NBA/Ca = 0.01) and the C-S-H/NBA.02 systems (C-S-H/NBA with NBA/Ca = 0.02) was suggested. The nitrobenzoic acid, based on this model, can interact with the nanostructure of C-S-H in different ways. These include the intercalation in the interlayer space of C-S-H as well as the adsorption on the surface of the layers, at the edges of the layers or between the stacked layers of C-S-H. The interaction of organic and inorganic phases in C-S-H/NBA.02 systems, however, is very limited. Local accumulation of organics on the surface of the C-S-H layers, at the layer edges or between the stacked layers of C-S-H is expected in these systems.

Porous bodies of the samples were prepared by the compaction technique in the current study and their length-change in the concentrated solutions of magnesium chloride ($MgCl_2$), magnesium sulfate ($MgSO_4$) and lithium chloride (LiCl) solutions were monitored. The concentration of calcium ions leached out of the samples during the immersion in the LiCl and $MgCl_2$ solutions was measured and compared with the length-change measurements. Diffusion of isopropanol into the porous structure of the samples was also evaluated. The creep modulus and the hardness of the samples were determined using the microindentation technique.

5.2 Experimental program

5.2.1 Materials

Phase pure C-S-H and CSH/NBA systems (Ca/Si = 1.5) were synthesized using the pozzolanic reaction technique described in chapter 3. Either of 2-, 3- or 4-nitrobenzoic acid isomers (reagent grade, Sigma-Aldrich) with the concentration of 0.01 or 0.02 mol. per mol. of Ca was pre-mixed with water to prepare the C-S-H/NBA systems.

5.2.2 Experiments

Powders of the phase pure C-S-H and C-S-H/NBA.01 (C-S-H with 0.01 mol. of nitrobenzoic acid per mol. of Ca) systems were compacted into porous bodies in the form of circular discs (32 mm in diameter × 1 mm thick). The compaction pressure was adjusted to obtain a porosity of about 30% for all the samples as determined using a Beckman helium pycnometer to measure the solid volume [20, 21]. The powders of C-S-H/NBA.02 (C-S-H with 0.02 mol. of nitrobenzoic acid per mol. of Ca) systems were compacted with a similar load to the C-S-H/NBA.01 systems. A porosity of 15%-18% was determined for the C-S-H/NBA.02 compacted samples using the helium pycnometer method. All the compacted samples were conditioned at the 11% relative humidity for an additional two weeks to reach equilibrium. The details of the tests performed are as follows:

Length-change measurement

Rectangular prisms (5 mm × 25 mm × 1 mm) were cut from the compacted discs and mounted on modified Tuckerman extensometers (see chapter 3). These were, then, placed in small vessels containing the test solutions so that the specimens were completely immersed. Aqueous solutions of $MgCl_2$, $MgSO_4$ and LiCl with a concentration of 15 mg/l were used as the test solution. The ratio of the solid to the solution was 1 g of solid per 50 ml of the solution. The whole set-up was placed in sealed desiccators containing the same salt solution as the test solution to prevent any change in the solution level due to evaporation. The length-change of the samples in each solution was measured up to 7 days.

Calcium ion concentration

Small prisms of the compacted samples were cut and immersed in 20 ml of the LiCl or $MgCl_2$ solution (15 g/l). The solution was continuously stirred using a magnetic stirrer (Fisher Scientific) with the speed of 250 rpm. The ratio of the sample mass to the solution volume was the same as that used in the length-change measurements (1 g of solid per 50 ml of the solution). The concentration of the calcium ions released into the solution was recorded using a Metrohm Titrando titration instrument during the first 30 min after the immersion. The measurements after 30 min were not utilized due to a possible deposit of

calcite in the test solution. The calcium leaching in $MgSO_4$ was not measured because of the rapid precipitation of gypsum.

Diffusion of isopropanol

The diffusion of isopropanol into the compacted samples was evaluated by the measurement of the mass-change of the compacted samples following immersion in the isopropanol. A schematic of the test set-up is presented in Figure 3-6. A small stainless steel basket was attached to a balance by steel wires, and immersed in 450 ml of anhydrous isopropanol (Reagent grade, Fischer Scientific). The compacted circular samples (32 mm in diameter × 1 mm thick) conditioned to 11% relative humidity were placed in the basket at the depth of 20 mm from the free surface of the isopropanol solution (so that about 100 ml of the isopropanol covered the samples). The mass-change of the samples in isopropanol was monitored until a plateau was achieved at about 2 hours. It was previously suggested that diffusion of isopropanol in saturated cement paste samples can be successfully used to evaluate resistance of the samples to the chloride diffusion [22].

Microindentation measurements

The microindentation tests were performed using a CSM Instruments Indentation Tester. Measurements were conducted using a Berkovich indenter which has the same projected area-to-depth ratio as a Vickers indenter. The whole apparatus is housed in an environmental chamber. Circular compacted samples equilibrated at the relative humidity of 11% were used for the microindentation measurements.

A total of 25 indents were obtained on each sample. The indentation depth (h) was recorded as a function of time at the maximum load of 1 N for a 600 s dwell period. The loading rate was 2 N/min. The creep was determined by curve fitting of the indentation-depth versus time curves during the loading period by the following equation:

$$\Delta h(t) = x_1 \ln(x_2 t + 1) + x_3 t + x_4$$

The creep modulus, C, was then calculated from:

$$C = P_{\max} / (2 a_u x_1)$$

where $P_{\max}$ is the maximum load and $a_u = (a_c / \pi)^{1/2}$. a_c is the projected area of contact between the indenter probe and the indenter surface. It is determined using the Oliver and Pharr method as a function of the maximum indentation depth [23]. The creep modulus parameter was first introduced by Vandamme and Ulm [24]. Higher values of creep modulus of materials correspond to lower values creep rate under loading. In addition, the indentation hardness (*H*) was obtained from the software by $H = P / a_c$.

5.3 Results

5.3.1 C-S-H/NBA.01 systems

Length-change in aggressive test solutions

The length-change values of the phase pure C-S-H and C-S-H/NBA.01 systems after 1 day and 7 days of immersion in LiCl, $MgCl_2$, and $MgSO_4$ solutions are presented in Figure 5-1. It was observed that the length-change of the C-S-H/NBA.01 systems in all the test solutions was significantly lower than that of the phase pure C-S-H after 1 day of immersion. For example, the 1 day length-change values of the C-S-H with 2-, 3- and 4-nitrobenzoic acid (NBA/Ca = 0.01) was, respectively, about 18%, 20% and 40% lower than that of the phase pure C-S-H in the LiCl solution. The C-S-H system with 4-nitrobenzoic acid exhibited the lowest length-change values compared to those with 2- or 3-nitrobenzoic acid.

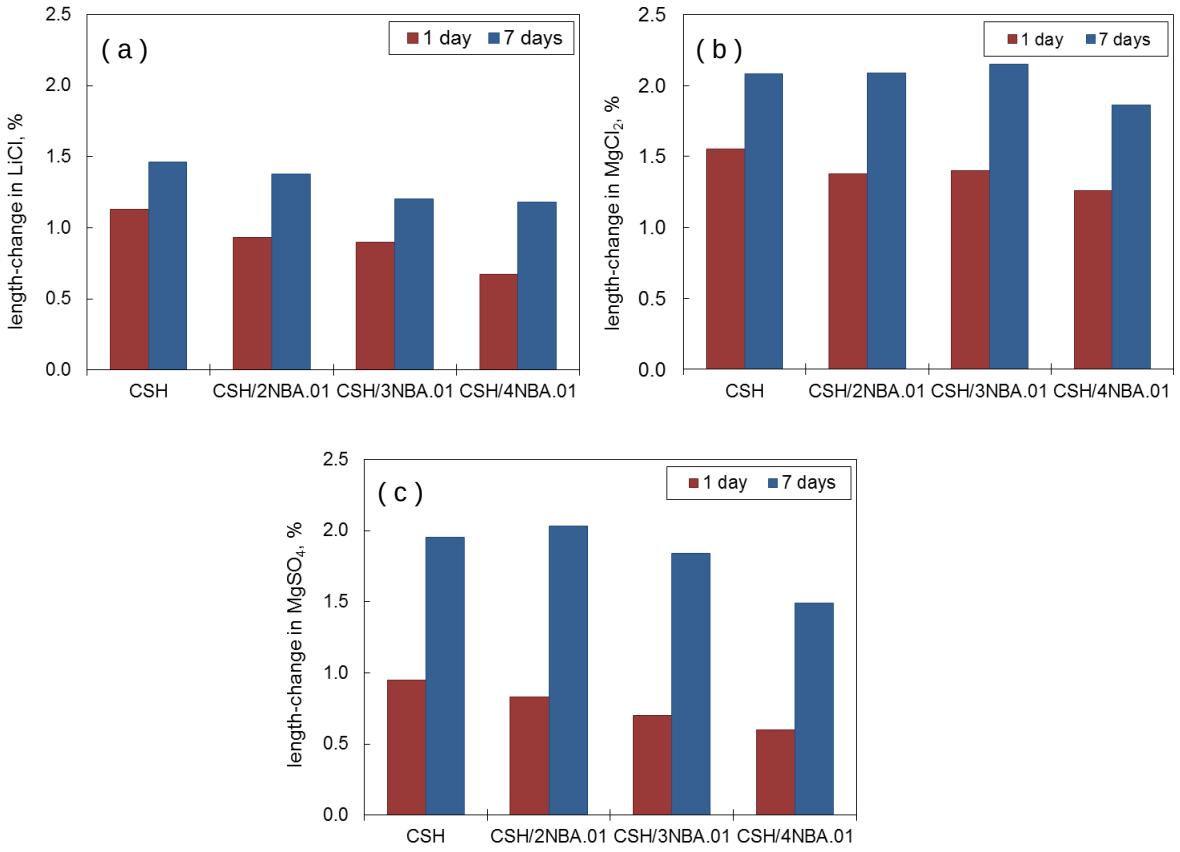

Figure 5-1- Length-change of the phase pure C-S-H and the C-S-H/NBA.01 systems after 1 d and 7 d of immersion in (a) LiCl, (b) $MgCl_2$, and (c) $MgSO_4$ solutions

Not all types of the nitrobenzoic acid were effective in limiting the length-change of the systems during the long-term exposure to the test solutions. The length-change of the C-S-H system with 2-nitrobenzoic acid was similar to that of the phase pure C-S-H after 7 days of immersion in $MgCl_2$ solution. The length-change values of this sample were even higher than that of the phase pure C-S-H after 7 days of immersion in $MgSO_4$ solution. The length-change values of the systems with 3-nitrobenozic acid were lower than those of phase pure C-S-H in all the test solutions after 7 days. The C-S-H system with 4-nitrobenzoic acid had even lower values of the length-change. The 7-day length-change of the C-S-H/4NBA.01 sample was lower than that of the phase pure C-S-H in LiCl, $MgCl_2$ and $MgSO_4$ solutions by 20%, 10% and 24%, respectively.

Calcium-leaching due to the immersion of the C-S-H-based systems in the aqueous solutions is possibly an important mechanism underlying their expansion. Penetration of

water and ionic species available in the test solution into the pore structure of the compacted samples is also a major cause of expansion. It is suggested that the nitrobenzoic acid possibly filled the gaps (due to missing bridging silicate tetrahedra), and also blocked entry into the stacked layers of C-S-H. This mechanism could possibly limit the calcium-leaching from the C-S-H layers as well as the penetration of water and ionic species into the pore structure of the C-S-H-based systems resulting in the lower length-change of the samples incorporating nitrobenzoic acid during the immersion in the test solutions. It is also suggested that the 4-nitrobenzoic acid was the most effective among other types nitrobenzoic acid possibly because of the opposite side locations of the nitro and the carboxylic groups in its structure. These functional groups are located beside each other in the structure of the 2-nitrobenzoic acid molecule. This may have resulted in the lower efficiency of the 2-nitrobenzoic acid in reducing the length-change values during the long-term immersion in the test solutions.

Calcium ion concentration

The concentration of calcium ions leached-out of the C-S-H-based systems due to the immersion in the LiCl and $MgCl_2$ solutions after 30 min is presented in Figure 5-2. These values were compared with the length-change measurements during the similar immersion conditions. It was suggested that, in general, the samples which experienced higher values of calcium leaching in a test solution also had higher values of length-change although there was not a direct correlation between the calcium leaching and the length-change measurements. The concentration of calcium ion leached-out due to the immersion of the C-S-H system with 2-nitrobenzoic acid (NBA/Ca = 0.01) was similar to that leached-out due to the immersion of the phase pure C-S-H. The leaching of calcium ions occurred due to the immersion of the C-S-H systems with 3- or 4-nitrobenzoic acid, however, was considerably lower. It is possible that these nitrobenzoic acid isomers blocked the escape boundaries of the calcium ions in the structure of C-S-H. This could be due to the presence of the nitrobenzoic acid in the interlayer space or between the stacked layers of C-S-H in these systems. They both could limit the amount of calcium ions leached-out to the solution.

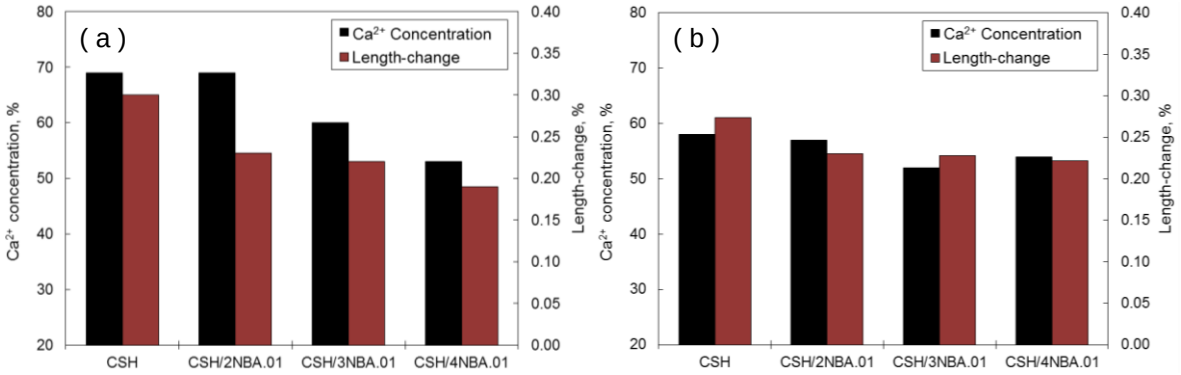

Figure 5-2- Concentration of calcium ions and length-change of the phase pure C-S-H and the C-S-H/NBA.01 systems after 30 min of immersion in (a) LiCl, and (b) $MgCl_2$ solutions

Mass-change in isopropanol

The mass-change of the C-S-H-based systems following the immersion in isopropanol is presented in Figure 5-3. In general, two distinct stages were observed in the mass-change curves of the samples: stage I, where the samples exhibited a significant mass-increase due to the diffusion of isopropanol into their pore structure, and stage II where the mass was gradually reduced due to the solvent-exchange in the pore structure of the samples and the partial removal of the interlayer water by the isopropanol. The quantity of the isopropanol diffused in the C-S-H systems with 3- or 4- nitrobenzoic acid (NBA/Ca = 0.01) in both stages was lower than that diffused in the phase pure C-S-H. It is, therefore, suggested that the size and connectivity of the pores in the structure of these systems are such that less pores are accessible to the isopropanol. In addition, a lower amount of water can be removed from the interlayer space of the C-S-H/3NBA.01 and C-S-H/4NBA.01 systems by the isopropanol. These two are a result of the blockage of the pores and entry locations of the C-S-H layers by the nitrobenzoic acid compound. In addition, it is likely that the 3- and 4-nitrobenzoic acid isomers are able to fill some of the defects in the layered structure of C-S-H. These defects could act as the escape points of the interlayer water to the larger pores. In addition, it was observed that the 4-nitrobenzoic acid was more effective than the 3-nitrobenzoic acid in “sealing” of the pore structure of C-S-H to the diffusion of isopropanol.

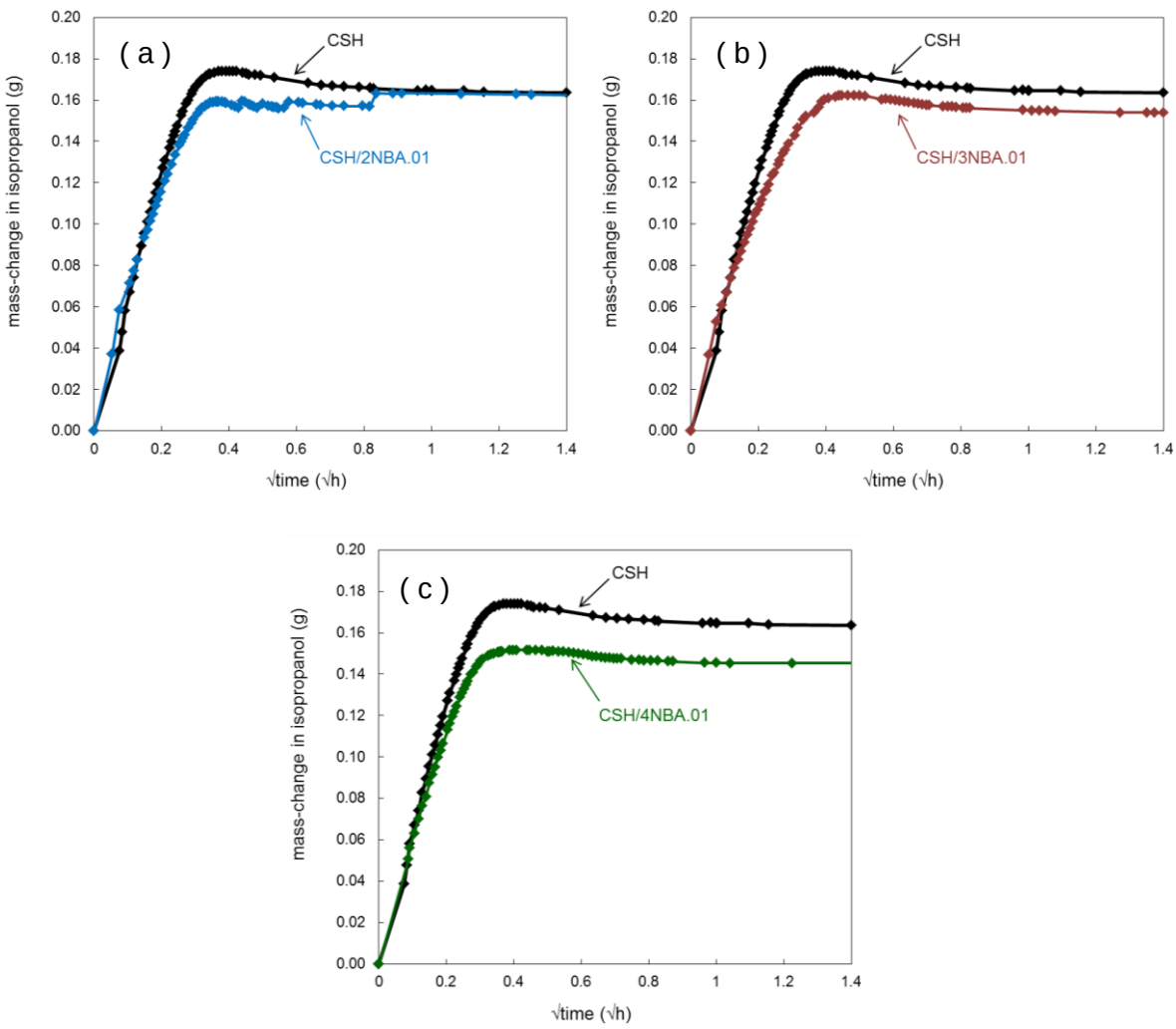

Figure 5-3- Mass-change of C-S-H/NBA.01 systems in isopropanol in comparison with that of the phase pure C-S-H. (a) C-S-H/2NBA.01, (b) C-S-H/3NBA.01 and (c) C-S-H/4NBA.01

The 2-nitrobenzoic aid was effective in reducing the diffusion of isopropanol in the C-S-H-based system during the first minutes following the immersion. More pores, however, became accessible to the isopropanol by increasing the immersion time so that the mass of the C-S-H/2NBA.01 sample was very similar to that of the phase pure C-S-H after about 45 min of immersion (Figure 5-3(a)). This is consistent with the results of the length-change measurements presented in Figure 5-1. It was shown that the C-S-H/2NBA.01 samples had lower values of length-change compared to those of the phase pure C-S-H after 1 day of immersion in the test solutions. These samples, however, had similar or higher values of length-change than the phase pure C-S-H when the immersion time was

increased to 7 days. This could be due to a rearrangement of the 2-nitrobenzoic acid molecules in the structure of C-S-H/2NBA.01 system during the increased period of immersion of the sample in the alcohol or the aqueous test solution.

Microindentation

Creep modulus and hardness data for the phase pure C-S-H and C-S-H/NBA.01 systems are presented in Figure 5-4. The creep (that varies inversely with creep modulus) of the C-S-H/NBA.01 systems was generally lower than that of the phase pure C-S-H. The sample with 4-nitrobenzoic acid (NBA/Ca = 0.01) had the lowest creep. It has been suggested that the creep of C-S-H-based materials involves the sliding of the C-S-H layers against each other [25]. The interaction of nitrobenzoic acid with C-S-H could "interlock" the C-S-H layers, and limit their sliding. This would result in lower values of creep rate of the samples with nitrobenzoic acid. The opposite location of the carboxylate and nitro groups in the 4-nitrobenozic acid molecule may contribute to the increased effect of the 4-nitrobenozic acid in limiting the sliding of the C-S-H layers and reducing the creep. The hardness of the C-S-H/4NBA.01 sample was also considerably higher than that of the phase pure C-S-H possibly due to the same mechanism. The hardness of the C-S-H/2NBA.01 sample was low. This may be due to the rearrangement of the 2-nitrobenzoic acid under long-term loading resulting in a higher ultimate indentation value.

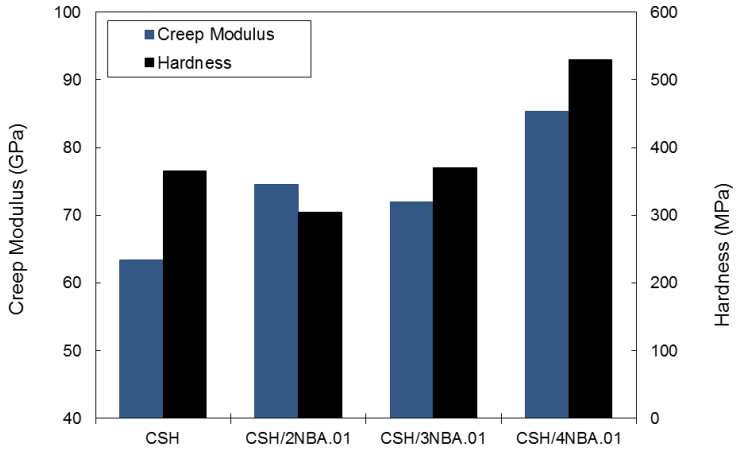

Figure 5-4- Creep modulus and hardness of the phase pure C-S-H and the C-S-H/NBA.01 systems

5.3.2 C-S-H/NBA.02 systems

Length-change in aggressive test solutions

The length-change results of the phase pure C-S-H and the C-S-H/NBA.02 systems in LiCl and $MgSO_4$ solutions are presented in Figure 5-5. The incorporation of a higher concentration of nitrobenzoic acid was not effective in reducing the length-change of the C-S-H-based systems. Especially in the $MgSO_4$ solution, the length-change of the samples with nitrobenzoic acid (NBA/Ca = 0.02) was considerably higher than those for the phase pure C-S-H. It was previously suggested that the nitrobenzoic acid compound in the C-S-H/NBA.02 systems has limited interaction with the nanostructure of C-S-H, and is mainly accumulated on the surface of the layers or between the stacked layers of C-S-H. The leaching of nitrobenzoic acid in the test solution or other possible reaction of this compound with the solution may have resulted in the significant expansion of the C-S-H/NBA.02 systems.

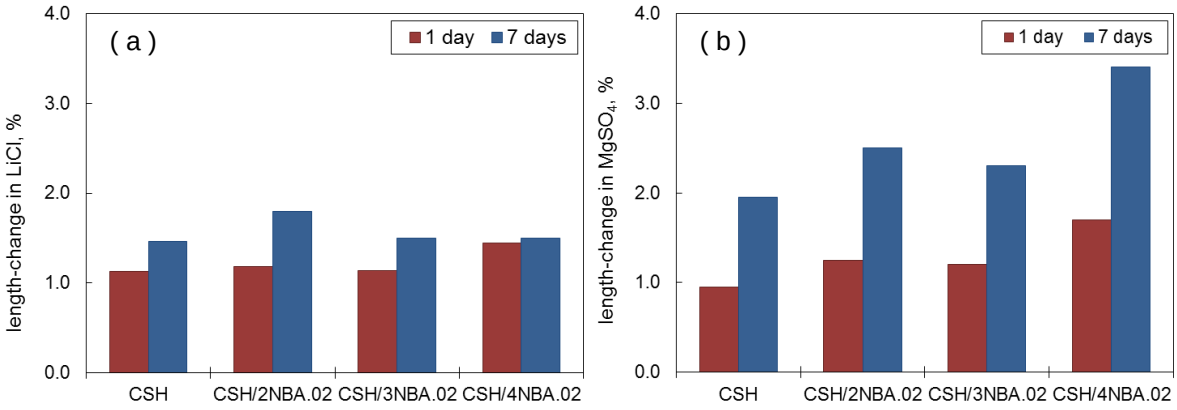

Figure 5-5- Length-change of the phase pure C-S-H and the C-S-H/NBA.02 systems after 1 d and 7 d of immersion in (a) LiCl and (b) $MgSO_4$ solutions

Calcium ion concentration

The concentration of calcium ions leached-out of the C-S-H/NBA.02 systems due to the immersion in LiCl was very similar to that of the phase pure C-S-H (Figure 5-6). The higher concentration of nitrobenzoic acid was, therefore, not effective in reducing the

calcium-leaching from the C-S-H-based systems. This may also be due to the limited interaction of organic and inorganic phases in the structure of the C-S-H/NBA.02 systems.

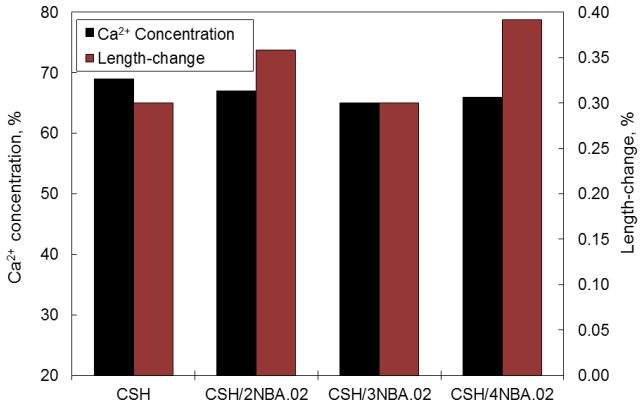

Figure 5-6- Concentration of calcium ions and length-change of the phase pure C-S-H and the C-S-H/NBA.02 systems after 30 min of immersion in LiCl solution

Mass-change in isopropanol

The mass-change values of the C-S-H/NBA.02 systems in isopropanol were lower than that of the phase pure C-S-H. Especially the mass-changes were relatively small during the second stage of the measurements. This likely occurred due to the blockage of the entries of the C-S-H layers by the nitrobenzoic acid in the structure of the C-S-H/NBA.02 systems. The mass-change measurements are in conformity with the helium pycnometer results indicating a reduced pore volume of the C-S-H/NBA.02 systems.

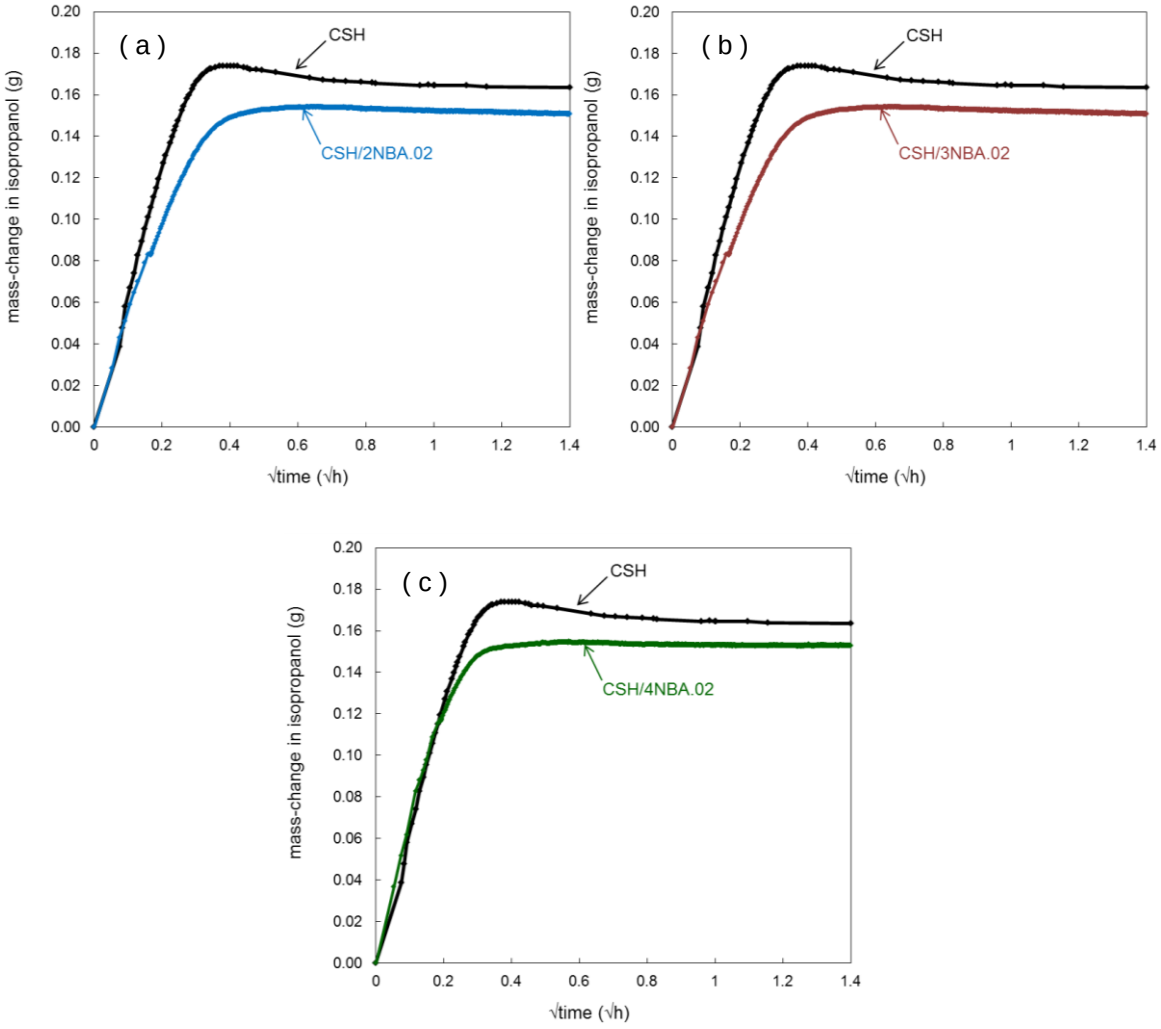

Figure 5-7- Mass-change of C-S-H/NBA.02 systems in isopropanol in comparison with that of the phase pure C-S-H. (a) C-S-H/2NBA.02, (b) C-S-H/3NBA.02 and (c) C-S-H/4NBA.02

Microindentation

The creep modulus and hardness of the C-S-H/NBA.02 systems were considerably lower than those of the phase pure C-S-H (Figure 5-8). Poor mechanical performance of these samples could also be explained by the separation of organic and inorganic phases. In addition, it was previously suggested based on the analysis of FTIR spectra that the silicate chains contain more dimers in the structure of C-S-H/NBA.02 systems (see chapter 4). This

could result in a lower resistance of the silicate sheets to sliding in these systems under the loading condition.

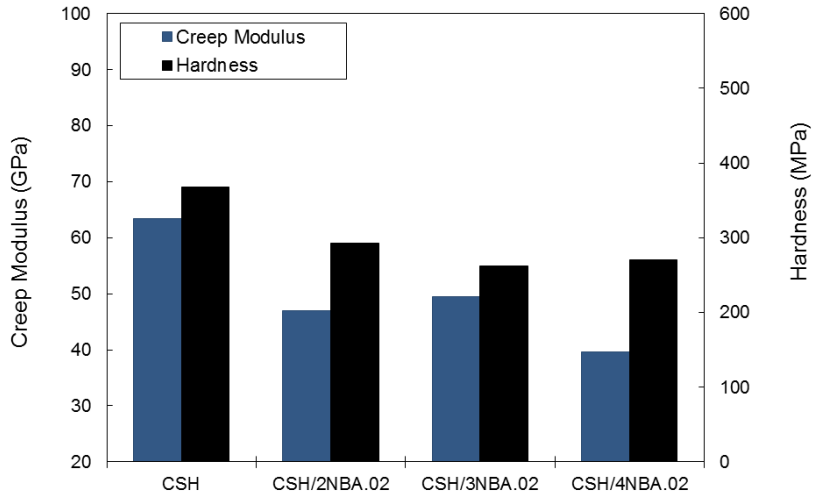

Figure 5-8- Creep modulus and hardness of the phase pure C-S-H and the C-S-H/NBA.02 systems

5.4 Concluding remarks

Durability and mechanical performance of C-S-H/NBA systems with two different concentrations of nitrobenzoic acid (NBA/Ca = 0.01 and 0.02) were investigated. The nitrobenzoic acid with the lower concentration contributed to a significant improvement of the durability and mechanical performance of the C-S-H systems. New evidence of the interaction of nitrobenzoic acid with the nanostructure of C-S-H (partial intercalation as well as surface adsorption) in these systems was consistent with the results of previous studies. The C-S-H/NBA.02 systems, however, had poor durability and mechanical performance. This could also be explained by the previous model proposed for the nanostructure of these systems. It was suggested that in this model the organic and inorganic phases have limited interaction in the structure of the C-S-H/NBA.02 systems, and nitrobenzoic acid molecules are mainly accumulated at the surface of the C-S-H layers, at the edge of the layers or between the stacked layers of C-S-H.

References

1. R. F. Feldman and P. Sereda, "A new model for hydrated Portland cement and its practical implications," *Engineering Journal*, 53(8-9), pp. 53-59, 1970.

2. H. Matsuyama and J. F. Young, "Intercalation of Polymers in Calcium Silicate Hydrate: A New Synthetic Approach to Biocomposites?," *Chemistry of Materials*, 11, pp. 16-19, 1999.

3. H. Matsuyama and J. F. Young, "Synthesis of calcium silicate hydrate/polymer complexes: Part I," *Journal of Materials Research*, 14, pp. 3379-3388, 1999.

4. H. Matsuyama and J. F. Young, "Synthesis of calcium silicate hydrate/polymer complexes: Part II," *Journal of Materials Research*, 14, pp. 3389-3396, 1999.

5. H. Matsuyama and J. F. Young, "The formation of C-S-H/polymer complexes by hydration of reactive β-dicalcium silicate," *Concrete Science and Engineering*, 1, pp. 66-75, 1999.

6. A. Okada, M. kawasumi, A. Usuki, T. Kurauchi and O. Kamigaito, "Synthesis and properties of nylon-6/clay hybrids," in Polymer based molecular composites (edt. Schaefer D.W., Mark J. E.), MRS Symposium Proceedings, Pittsburgh, Vol. 171, pp. 45-50, 1990.

7. A. Somwangthanaroj, W. Ubankhlong and W. Tanthapanichakoon, "Solid-state mechanical properties of polypropylene/nylon6/clay Nanocomposites," *Journal of Applied Polymer Science*, 118, pp. 538-546, 2010.

8. P. Natkanski, P. Kustrowski, A. Bialas, Z. Piwowarska and M. Michalik, "Controlled swelling and adsorption properties of polyacrylate/montmorillonite composites," *Materials Chemistry and Physics*, 136, pp. 1109-1115, 2012.

9. B. K. Theng, Formation and properties of clay-polymer complexes, Elsevier, 1979.

10. P. C. LeBaron, Z. Wang and T. J. Pinnavaia, "Polymer-layered silicate nanocomposites: an overview," *Applied Clay Science*, 15, pp. 11-29, 1999.

11. A. Popova, G. Geoffroy, M.-F. Renou-Gonnord, P. Faucon and E. Gartner, "Interactions between polymeric dispersants and calcium silicate hydrates," *Journal of the American Ceramic Society*, 83, 10, pp. 2556-2560, 2000.

12. F. Merlin, H. Lombois, S. Joly, N. Lequeux, J.-L. Halary and H. Van Damme, "Cement-polymer and clay-polymer nano- and meso-composites: spotting the difference," *Journal of Materials Chemistry*, 12, pp. 3308-3315, 2002.

13. J. Minet, S. Abramson, B. Bresson, C. Sanchez, V. Montouillout and N. Lequeux, "New layered calcium organosilicate hybrids with covalently linked organic functionalities," *Chemistry of Materials*, 16, pp. 3955-3962, 2004.

14. J. Minet, S. Abramson, B. Bresson, A. Franceschini, H. Van Damme and N. Lequeux, "Organic calcium silicate hydrate hybrids: a new approach to cement based nanocomposites," *Journal of Materials Chemistry*, 16, pp. 1379-1383, 2006.

15. A. Franceschini, S. Abramson, V. Mancini, B. Bresson, C. Chassenieux and N. Lequeux, "New covalent bonded polymer-calcium silicate hydrate composites," *Journal of Materials Chemistry*, 17, pp. 913-922, 2007.

16. S. C. Mojumdar and L. Raki, "Synthesis, thermal and structural characterization of nanocomposites for potential applications in construction," *Journal of Thermal Analysis and Calorimetry*, 86, pp. 651-657, 2006.

17. R. J.-M. Pellenq, N. Lequeux and H. Van Damme, "Engineering the bonding scheme in C-S-H: The iono-covalent framework," *Cement and Concrete Research,* 38, pp. 159-174, 2008.

18. F. Pelisser, P. J. Gleiz and A. Mikowski, "Effect of poly(diallyldimethylammonium chloride) on nanostructure and mechanical properties of calcium silicate hydrate," *Materials Science and Engineering: A*, 527(26), pp. 1045-1049, 2010.

19. R. Alizadeh, Nanostructure and engineering properties of basic and modified calcium silicate hydrate systems, PhD thesis, University of Ottawa, 2009.

20. I. Soroka and P. J. Sereda, "The Structure of Cement-stone and the Use of Compacts as Structural Models," In Proceedings of the 5th International Symposium on the Chemistry of Cement, Tokyo, Vol. III, pp. 67-73, 1968.

21. P. J. Sereda, R. F. Feldman, "Compact of powdered materials as porous bodies for use in sorption studies," *Journal of Applied Chemistry*, 13(4), pp. 150-158, 1963.

22. R. F. Feldman, "Diffusion measurements in cement paste by water replacement using propan-2-ol," *Cement and Concrete Research*, 17, pp. 602-612, 1987.

23. W. C. Oliver, G. M. Pharr, "An improved technique for determining hardness and elastic modulus using load and displacement sensing indentation experiments," *Journal of Materials Research*, 7, pp. 1564-1583, 1992.

24. M. Vandamme, F.-J., Ulm "Nanogranular origin of concrete creep," *Proceedings of the National Academy of Sciences*, 106(26), pp. 10552-10557, 2009.

25. D.-T. Nguyen, R. Alizadeh, J. J. Beaudoin, P. Pourbeik, L. Raki, "Microindentation creep of monophasic calcium-silicate-hydrates," *Cement and Concrete Composites*, 48, pp. 118-126, 2014.

Chapter 6

Characteristics and Engineering Performance of C-S-H/Aminobenzoic Acid Composite Systems

Calcium-silicate-hydrate/aminobenzoic acid (C-S-H/ABA) composite systems were synthesized and characterized for the first time. Each of 3- or 4-aminobenzoic acid with a concentration of 0.01 mol. per mol. of Ca was added to the C-S-H preparations during their hydration. The C-S-H/ABA systems were filtered and dried after three weeks. These were, then, characterized by X-ray diffraction, Fourier transform infrared spectroscopy and nitrogen adsorption analysis. Porous bodies were also prepared from C-S-H/ABA compacted powders and used for the length-change and mass-change measurements in different test solutions. In addition, the microindentation technique was used to determine the creep modulus and hardness of the compacted samples. It is suggested that the C-S-H/ABA systems had improved durability and enhanced mechanical properties compared to the phase pure C-S-H reference materials. The influence of the 3- and 4-aminobenozic acid on durability factors was similar. The C-S-H/3ABA, however, had superior mechanical performance.

6.1 Introduction

Calcium-silicate-hydrate (C-S-H) is the primary binding phase in the hydrated Portland cement. The improvement of properties of C-S-H is of significant interest as it can directly influence the performance of cement-based construction materials. Modification of the

nanostructure of C-S-H by organic compounds is likely to be a promising approach to achieve this goal [1-5]. Several organic compounds have been previously used successfully to modify/improve the nanostructure of smectic clays [6-9]. The use of these organics for the modification of the C-S-H structure has potential based on the similarities between the layered structure of C-S-H and that of the smectic clays [10-11].

Several studies have been conducted during the past two decades with a focus on the physico-chemistry of the C-S-H/organic systems. In spite of this work, the nature of the various types of interaction of organic compounds with the structure of C-S-H is still unclear. It was suggested by Matsuyama and Young [1-3] that certain polymers are able to intercalate the interlayer region of C-S-H systems prepared by the precipitation technique. More recent investigations, however, provided evidence that the intercalation of organic compounds in the layered structure of C-S-H is much more difficult than that in smectic clays. It was suggested by Merlin et al. [12] that this could be due to the higher charge of the layers in the C-S-H structure and the localization of the charge on the surface of the layers in the structure of C-S-H as opposed to the distribution of the charge within the layers as is the case for smectic clays. These two reasons could make the intercalation very difficult to achieve. It was, however, observed that a significant amount of the organics could be adsorbed in the stacked layers of C-S-H. In addition, it was suggested by Minet et al. [13, 14] that trialkoxysilane compounds were able to form covalent bonds with silicate tetrahedra in the structure of C-S-H. The formation of these bonds was more probable when these organic compounds had a smaller size. A comprehensive investigation of the characteristics of covalent-bonded polymer-C-S-H composites was also provided by Franceschini et al. [15]. A study of the engineering performance of these composite systems, however, is still lacking.

It was suggested in chapter 4 that different isomers of nitrobenzoic acid could be successfully used to interact with the nanostructure of C-S-H. Significant improvement of the durability and mechanical performance of the C-S-H-based systems was observed due to the incorporation of nitrobenzoic acid with the concentration of 0.01 mol. per mol. of Ca of the C-S-H (see chapter 5). Aminobenzoic acid (ABA) has a similar molecular size and structure to the nitrobenzoic acid (NBA). However, the amino group is electropositive and an activating group of the aromatic ring. This is opposite to the electronegative properties

of the nitro group resulting in deactivation of the aromatic ring in the nitrobenzoic acid molecule [16, 17]. It has been suggested that the acidity of the aminobenzoic acid isomers, increases in the order of 3ABA > 4ABA > 2ABA [17]. The acidity of the nitrobenzoic acid isomers, however, increases in the opposite order (2NBA > 4NBA > 3NBA) [16].

The main objective of this study is to explore the influence of aminobenzoic acid on the microstructure and engineering properties of C-S-H systems. The C-S-H/3ABA and C-S-H/4ABA systems were synthesized using a pozzolanic reaction technique. Their characteristics and engineering performance were compared with those obtained for the phase pure C-S-H.

6.2 Experimental program

6.2.1 Materials

Phase pure C-S-H, C-S-H/3ABA and C-S-H/4ABA systems (Ca/Si = 1.5) were synthesized using the pozzolanic reaction technique described in chapter 3. Either of 3- or 4-aminobenzoic acid (reagent grade, Sigma-Aldrich) with the concentration of 0.01 mol. per mol. of Ca (in the C-S-H) was pre-mixed with the water to prepare the C-S-H/ABA systems. The C-S-H/3ABA and C-S-H/4ABA systems had a pinkish and yellowish color, respectively, which was different from the white color of the phase pure C-S-H.

6.2.2 Experiments

All the C-S-H-based systems were characterized using X-ray diffraction (XRD), Fourier transform infrared spectroscopy (FTIR) and nitrogen adsorption analysis. Circular compacted samples of the powder were also prepared with a porosity of about 30% determined using the helium pycnometer technique [18]. Length-change of the compacted samples in $MgSO_4$ and LiCl solutions (15 g/l) was measured up to 7 days. The mass-change of the samples in isopropanol was also determined as an estimation of the resistance of the samples to the diffusion of aggressive ions. The microindentation technique was also

used to measure the creep modulus and hardness of the compacted samples. Details of the experiments are as following:

XRD - The X-ray diffraction pattern of the C-S-H-based systems was acquired using a Scintag XDS 2000 diffractometer (CuK_α radiation). The test was performed in a 2θ ranging $4^\circ < 2\theta < 15^\circ$, with a step size of 0.03° and a 5 second count interval to detect the changes in the basal-spacing (d_{002}) peak.

FTIR – FTIR spectra of the powders were collected between 4000 and 400 cm^{-1} using a Thermo scientific Nicolet™ iS™50R instrument in ATR mode. Each FTIR spectrum represented the average of 32 scans at 4 cm^{-1} resolution. Air was used as a background for the measurements.

Nitrogen adsorption - The nitrogen adsorption measurements were obtained using a Quantachrome instrument NOVA 2200e surface area and pore size analyzer. The samples were vacuum dried at 110 °C for three hours prior to starting the tests. Then, the nitrogen BET (Brunauer-Emmett-Teller) surface area analysis was performed on each sample.

Diffusion of isopropanol - The diffusion of isopropanol into the compacted samples was evaluated by the measurement of the mass-change of the samples following immersion in the isopropanol. Each compacted circular sample preconditioned to 11% relative humidity was placed in a small stainless steel basket, and immersed in 450 ml of anhydrous isopropanol (Reagent grade, Fischer Scientific). About 100 ml of the isopropanol covered the samples. The set-up was attached to a balance and a data recorder to measure the mass-change of the samples for two hours after the immersion. Diffusion of isopropanol in saturated cement paste samples was previously used successfully to evaluate the resistance of the samples to the diffusion of chloride ion [19].

Length-change measurements – Prisms (5 mm × 25 mm × 1 mm) were cut from the compacted discs and mounted on modified Tuckerman extensometers. Strains were determined with an accuracy of 1 microstrain [20, 21]. These were, then, placed in small vessels containing the test solutions so that the specimens were completely immersed. Aqueous solutions of $MgSO_4$ and LiCl with a concentration of 15 g/l were used as the test

solution. The ratio of the mass of solid to the volume of solution was 1 g of solid per 50 ml of the solution. The vessels were placed in sealed desiccators containing the same salt solution as the test solution to avoid evaporation. The length-change of the samples in each solution was measured up to 7 days.

Microindentation measurements - The microindentation tests were performed using a CSM Instruments Indentation Tester. A Berkovich indenter was used for the measurements. The whole apparatus is housed in an environmental chamber. Circular compacted samples equilibrated at a relative humidity of 11% were used for the microindentation measurements.

A total of 25 indents were obtained on each sample. The indentation depth (*h*) was recorded as a function of time (*t*) at the maximum load of 1 N for a 600 s dwell period. The loading rate was 2 N/min. The creep was determined by curve fitting of the indentation-depth versus time curves during the loading period using $\Delta h(t) = x_1 \ln(x_2 t + 1) + x_3 t + x_4$. The creep modulus, *C*, was then calculated from $C = P_{\max} / (2 a_u x_1)$ where $P_{\max}$ is the maximum load and $a_u = (a_c / \pi)^{1/2}$. a_c is the projected area of contact between the indenter probe and the indenter surface. It is determined using the Oliver and Pharr method as a function of the maximum indentation depth [22]. In addition, the indentation hardness (*H*) was obtained from the software by $H = P / a_c$.

6.3 Results

6.3.1 XRD

The XRD patterns of the phase pure C-S-H and C-S-H/ABA systems are presented in Figure 6-1. The d_{002} basal-spacing increased from 1.10 nm in the phase pure C-S-H to 1.13 nm and 1.17 nm in the C-S-H/3ABA and C-S-H/4ABA systems, respectively. An additional small peak was also observed at about 1.18 nm in the XRD pattern of the C-S-H/3ABA system. It was likely due to the occurrence of a second configuration of the 3-aminobenzoic acid molecule in the structure of C-S-H/3ABA system. The small increment in the basal-spacing might have been due to the adsorption of the aminobenzoic

acid at the entry locations of the C-S-H layers. Partial intercalation of the aminobenzoic acid was also possible because of the small size of this compound and also the relatively large number of defect locations in the structure of C-S-H with Ca/Si ratio of 1.5. The aminobenzoic acid could also be adsorbed between the stacked layers of C-S-H without any significant change in the basal-spacing. It is also noted that locations of the d_{002} basal-spacing of the C-S-H/3ABA and C-S-H/4ABA systems were similar to those observed for the C-S-H/3NBA and C-S-H/4NBA systems, respectively, reported in chapter 4. This could be expected due to the similar size and structure of the aminobenzoic acid and the nitrobenzoic acid compounds.

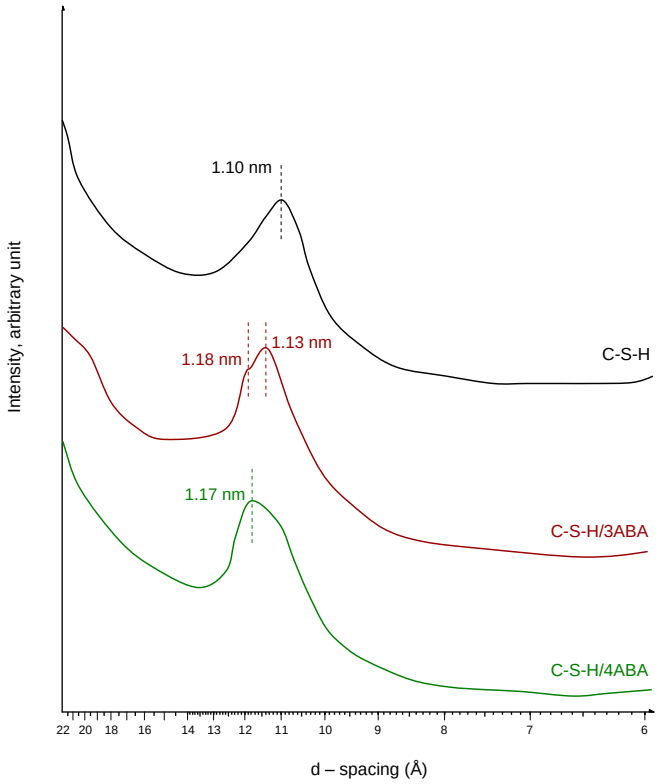

Figure 6-1- XRD patterns of the phase pure C-S-H and the C-S-H/ABA systems

6.3.2 FTIR

The FTIR spectra of the C-S-H/ABA systems were generally similar to that of the phase pure C-S-H (Figure 6-2). The peaks at the wavelengths of 820 cm^{-1} and 988 cm^{-1} in the structure of C-S-H are assigned to the Si-O stretching of Q^1 and Q^2, respectively [23]. The

locations of these peaks were shifted slightly to the lower wavelengths (816 cm^{-1} and 983 cm^{-1}) in the systems with 3- or 4-aminobenozic acid. In addition, the ratio of Q^2/Q^1 peaks are slightly larger in the C-S-H/ABA systems compared to that in the phase pure C S-H.

The peak at about 3645 cm^{-1} is sharper in the FTIR spectra of C-S-H/ABA systems compared to that in the spectra of the phase pure C-S-H. This peak is assigned to the relatively weak hydrogen-bonded interlayer water molecules [23]. The higher intensity of this peak in the spectra of the C-S-H/ABA systems could be due to some weak hydrogen bonding of the aminobenzoic acid with the structure of the host C-S-H. The peak at 1595 cm^1 in the FTIR spectra of C-S-H/4ABA can be due to the symmetric in-plane deformations of NH_2 in the structure of 4-aminobenozic acid [17]. The peaks at the wavelengths of about 460 cm^{-1} and 890 cm^{-1} likely correspond to carbonates [23]. The higher intensity of these peaks in the FTIR spectra of the phase pure C-S-H was expected due to the higher surface area of the phase pure C-S-H compared to the C-S-H/ABA systems (see section 3-3).

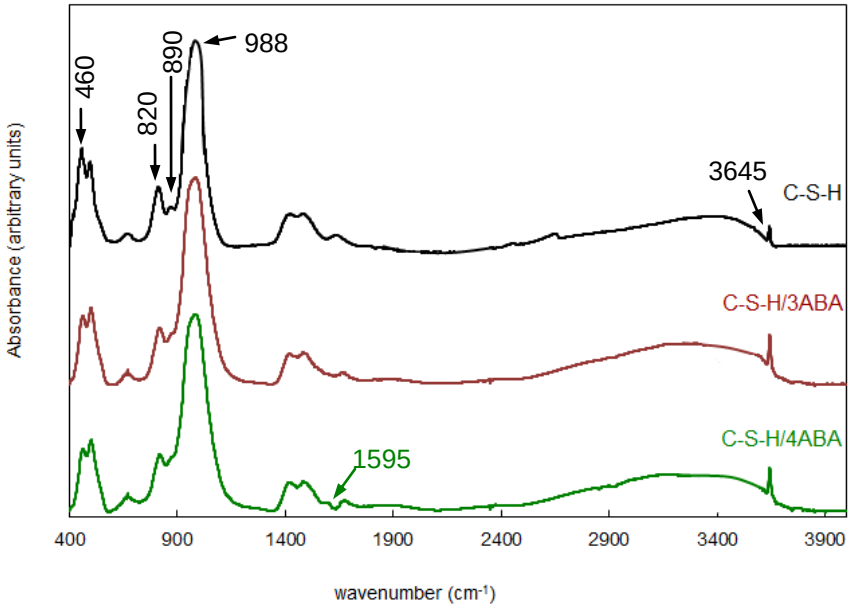

Figure 6-2- FTIR spectra of the phase pure C-S-H and the C-S-H/ABA systems

6.3.3 Nitrogen adsorption analysis

The BET nitrogen surface area of the phase pure C-S-H and the C-S-H/ABA systems is presented in Figure 6-3. The surface area values of the C-S-H systems incorporating 3- and 4-aminobenozic acid were very similar (35.6 m^2/g and 34.5 m^2/g for the C-S-H/3NBA and C-S-H/4NBA system, respectively). These values were significantly lower than that measured for the phase pure C-S-H (69.0 m^2/g). The significantly lower values of the surface area of the C-S-H/ABA systems provide evidence of the adsorption of the aminobenzoic acid on the exterior surface of the C-S-H layers, and the blockage of the pore structure of the C-S-H by this organic compound. It is also noted that the surface area values of the C-S-H/ABA systems were smaller than that previously reported for the C-S-H/3NBA (61.2 m^2/g) and larger than that for the C-S-H/4NBA system (32.0 m^2/g).

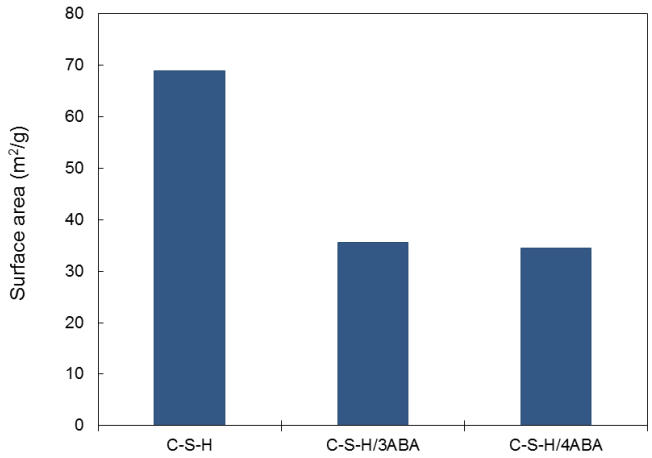

Figure 6-3- BET nitrogen surface area of the phase pure C-S-H and the C-S-H/ABA systems

6.3.4 Diffusion of isopropanol

The mass-change of the C-S-H-based systems due to the immersion in the isopropanol is shown in Figure 6-4. The increase in the mass of the C-S-H-based systems during the first 10 min after the immersion is due to the filling of the large pores by the isopropanol. The mass-reduction followed could be due to the exchange of water with the isopropanol and the removal of the interlayer water. The mass-change values of the C-S-H/3ABA and C-S-H/4ABA systems were very similar, and significantly lower than that of the phase pure C-

S-H. This could be due to filling of some defect locations in the pore structure of C-S-H by the 3- and 4-aminobenzoic acid. Fewer pores were, therefore, accessible to the isopropanol in the C-S-H/3ABA and C-S-H/4ABA systems.

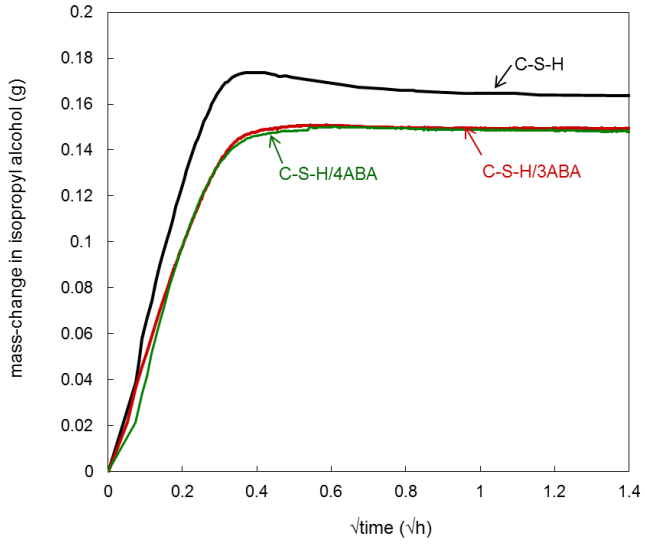

Figure 6-4- Mass-change of the phase pure C-S-H and the C-S-H/ABA systems in isopropanol

6.3.5 Length-change in the test solutions

The length-change values of the C-S-H/3ABA and C-S-H/4ABA systems in the test solutions were very similar, and significantly lower than those for the phase pure C-S-H (Figure 6-5). In the $MgSO_4$ solution, for example, the length-change values of the C-S-H systems with either of the 3- or 4-aminobenzoic acid were lower than those for the phase pure C-S-H by 28% and 36% after 1 day and 7 days of immersion, respectively. It has been suggested that leaching of calcium ions from the structure of C-S-H accompanied by the penetration of water and ionic species are the primary mechanisms of the expansion of the C-S-H-based systems in the aqueous solutions (see chapter 5). The two isomers of aminobenzoic acid likely filled the defect locations and blocked some of the pores in the structure of C-S-H. These could have limited both the mechanisms responsible for the expansions. In addition, the length-change values of the C-S-H/3ABA and C-S-H/4ABA systems were smaller than those of C-S-H/3NBA and larger than C-S-H/4NBA systems.

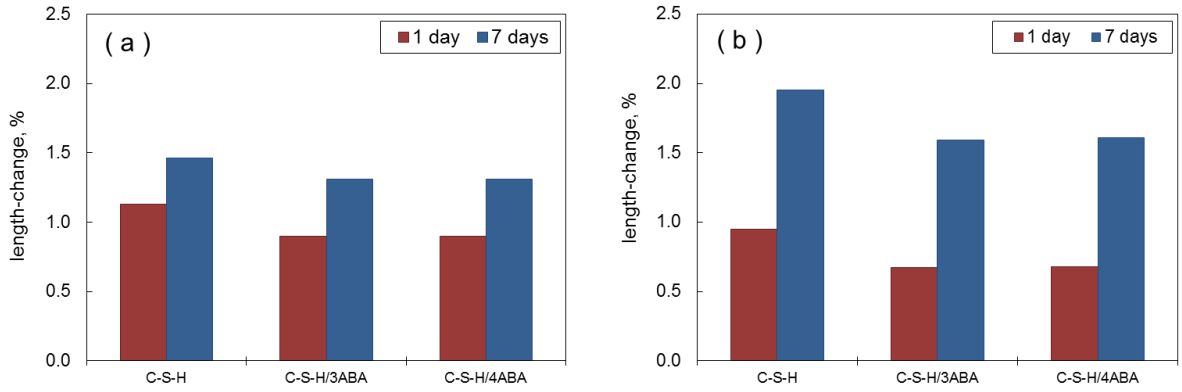

Figure 6-5- Length-change of the phase pure C-S-H and the C-S-H/ABA systems in (a) LiCl and (b) $MgSO_4$ solutions

6.3.6 Microindentation measurements

The creep modulus and the hardness of the C-S-H/ABA systems were compared with those of the phase pure C-S-H in Figures 6-6 and 6-7. It was observed that the creep modulus of the C-S-H/3ABA system (80.8 GPa) was considerably higher than those of the C-S-H/4ABA (68.8 GPa) which in turn was higher than that for the phase pure C-S-H (63.4 GPa). The same trend was observed for the hardness of these systems. It has been suggested that the sliding of the silicate sheets in the nanostructure of C-S-H is the primary mechanism responsible for the creep of C-S-H systems [24]. The use of the 3- and 4-aminobenzoic acid likely limited the sliding of the C-S-H sheets resulting in a lower creep rate (higher creep modulus) of the systems. The dipole moment and acidity of the 3-aminobenzoic acid are higher than those of the 4-aminobenozic acid [17]. This likely resulted in an increased effect of the 3-aminobenozic acid in blocking of the C-S-H sheets to sliding against each other under loading. It was previously observed in chapter 5 that the creep modulus of the C-S-H systems with 4- nitrobenzoic acid was higher than that for the C-S-H systems with 3-nitrobenzoic acid. This was also likely due to the higher dipole moments and acidity of the 4- nitrobenzoic acid compared those for 3- nitrobenzoic acid [16].

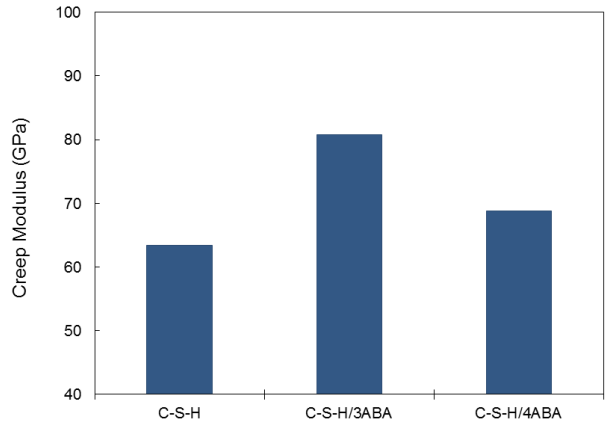

Figure 6-6- Creep Modulus of the phase pure C-S-H and the C-S-H/ABA systems

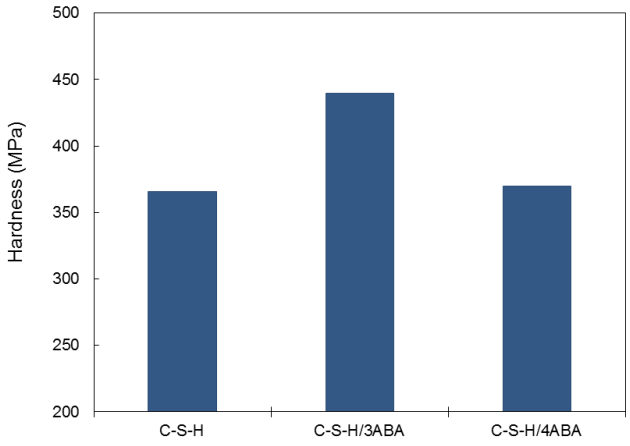

Figure 6-7- Hardness of the phase pure C-S-H and the C-S-H/ABA systems

6.4 Concluding remarks

The effect of 3- and 4-aminobenzoic acid on the microstructure, durability and mechanical performance of C-S-H systems was investigated. Evidence was obtained that these isomers of aminobenzoic acid were able to modify the microstructure of C-S-H; mainly by the adsorption on the surface of the layers and blockage of the stacked layers of C-S-H and entry locations to the interlayer region. In addition, the aminobenzoic acid compounds likely formed some weak hydrogen bonding with the structure of the host C-S-H. It was determined using nitrogen adsorption measurements that the C-S-H/3ABA and

C-S-H/4ABA systems had lower values of the surface area compared to those of the phase pure C-S-H. The durability parameters and microindentation measurements were also improved in the C-S-H/3ABA and C-S-H/4ABA systems.

References

1. H. Matsuyama and J. F. Young, "Intercalation of Polymers in Calcium Silicate Hydrate: A New Synthetic Approach to Biocomposites?," *Chemistry of Materials*, 11, pp. 16-19, 1999.
2. H. Matsuyama and J. F. Young, "Synthesis of calcium silicate hydrate/polymer complexes: Part I," *Journal of Materials Research*, 14, pp. 3379-3388, 1999.
3. H. Matsuyama and J. F. Young, "Synthesis of calcium silicate hydrate/polymer complexes: Part II," *Journal of Materials Research*, 14, pp. 3389-3396, 1999.
4. S. C. Mojumdar and L. Raki, "Synthesis, thermal and structural characterization of nanocomposites for potential applications in construction," *Journal of Thermal Analysis and Calorimetry*, 86, pp. 651-657, 2006.
5. R. Alizadeh, J. Beaudoin, L. Raki and V. Terskikh, "C-S-H/polyaniline nanocomposites prepared by in situ polymerization," *Journal of Materials Science*, 46(2), pp. 460-467, 2011.
6. A. Okada, M. kawasumi, A. Usuki, T. Kurauchi and O. Kamigaito, "Synthesis and properties of nylon-6/clay hybrids," in Polymer based molecular composites (edt. Schaefer D.W., Mark J. E.), MRS Symposium Proceedings, Pittsburgh, Vol. 171, pp. 45-50, 1990.
7. A. Somwangthanaroj, W. Ubankhlong and W. Tanthapanichakoon, "Solid-state mechanical properties of polypropylene/nylon6/clay Nanocomposites," *Journal of Applied Polymer Science*, 118, pp. 538-546, 2010.
8. P. Natkanski, P. Kustrowski, A. Bialas, Z. Piwowarska and M. Michalik, "Controlled swelling and adsorption properties of polyacrylate/montmorillonite composites," *Materials Chemistry and Physics*, 136, pp. 1109-1115, 2012.

9. P. C. LeBaron, Z. Wang and T. J. Pinnavaia, "Polymer-layered silicate nanocomposites: an overview," *Applied Clay Science*, 15, pp. 11-29, 1999.

10. H. Taylor, Cement Chemistry, 2nd Edition, London: Thomas Telford Publication, 1997.

11. R. F. Feldman and P. Sereda, "A new model for hydrated Portland cement and its practical implications," *Engineering Journal*, 53(8-9), pp. 53-59, 1970.

12. F. Merlin, H. Lombois, S. Joly, N. Lequeux, J.-L. Halary and H. Van Damme, "Cement-polymer and clay-polymer nano- and meso-composites: spotting the difference," *Journal of Materials Chemistry*, 12, pp. 3308-3315, 2002.

13. J. Minet, S. Abramson, B. Bresson, C. Sanchez, V. Montouillout and N. Lequeux, "New layered calcium organosilicate hybrids with covalently linked organic functionalities," *Chemistry of Materials*, 16, pp. 3955-3962, 2004.

14. J. Minet, S. Abramson, B. Bresson, A. Franceschini, H. Van Damme and N. Lequeux, "Organic calcium silicate hydrate hybrids: a new approach to cement based nanocomposites," *Journal of Materials Chemistry*, 16, pp. 1379-1383, 2006.

15. A. Franceschini, S. Abramson, V. Mancini, B. Bresson, C. Chassenieux and N. Lequeux, "New covalent bonded polymer-calcium silicate hydrate composites," *Journal of Materials Chemistry*, 17, pp. 913-922, 2007.

16. M. Samsonowicz, R. Świsłocka E., Regulska, and W. Lewandowski, "Experimental and theoretical IR, Raman, NMR spectra of 2-, 3-, and 4-nitrobenzoic acids," *International Journal of Quantum Chemistry*, 107(2), pp. 480-494, 2007.

17. M. Samsonowicz, T. Hrynaszkiewicz, R. Świsłocka, E. Regulska and W. Lewandowski, "Experimental and theoretical IR, Raman, NMR spectra of 2-, 3- and 4-aminobenzoic acids," *Journal of Molecular Structure*, 744-747, pp. 345-352, 2005.

18. P. J. Sereda and R. F. Feldman, "Compact of powdered materials as porous bodies for use in sorption studies," *Journal of Applied Chemistry*, 13(4), pp. 150-158, 1963.

19. R. F. Feldman, "Diffusion measurements in cement paste by water replacement using propan-2-ol," *Cement and Concrete Research*, 17, pp. 602-612, 1987.

20. R. Khoshnazar, J. J. Beaudoin, L. Raki and R. Alizadeh, "Volume stability of C-S-H/polyaniline nanocomposites in aqueous salt solutions," *ACI Materials Journal*, in-press, 2014.

21. R. F. Feldman, P. J. Sereda and V. S. Ramachandran, "A study of length changes of compacts of Portland cement on exposure to H_2O," *Highway Research Record*, 62, pp. 106-118, 1964.

22. W. C. Oliver, G. M. Pharr, "An improved technique for determining hardness and elastic modulus using load and displacement sensing indentation experiments," *Journal of Materials Research*, 7, pp. 1564-1583, 1992.

23. P. Yu, R. J. Kirkpatrick, B. Poe, P. McMillan, and X. Cong, "Structure of calcium silicate hydrate (C-S-H): Near-, mid-, and far-infrared spectroscopy," *Journal of the American Ceramic Society*, 82(3), pp. 742-748, 1999.

24. D.-T. Nguyen, R. Alizadeh, J. J. Beaudoin, P. Pourbeik, L. Raki, "Microindentation creep of monophasic calcium-silicate-hydrates," *Cement and Concrete Composites*, 48, pp. 118-126, 2014.

Chapter 7

Dynamic Mechanical Thermal Analysis of Organically Modified Calcium-Silicate-Hydrate Systems

The characteristics and engineering performance of calcium-silicate-hydrate (C-S-H) systems modified with nitrobenzoic acid (NBA) or aminobenzoic acid (ABA) were studied in the previous chapters. Evidence of the improved volume stability, durability and values of microindentation creep modulus of the C-S-H/NBA and C-S-H/ABA systems was reported. The main objective of this chapter is to evaluate the performance of the C-S-H/NBA and C-S-H/ABA systems under dynamic loading at elevated temperatures. Dynamic mechanical thermal analysis measurements, at temperatures from 26 to 300 °C and frequencies ranging from 0.25 to 2.5 Hz were obtained on the phase pure C-S-H as well as the C-S-H/NBA and C-S-H/ABA systems. It is suggested that all the isomers of nitrobenzoic acid can improve the storage modulus of the C-S-H systems both at room temperature and at the elevated temperatures. The 3-aminobenzoic acid also slightly improves the performance of the C-S-H systems upon heating. The improving effect of 4-aminobenzoic acid, however, is not as significant at higher temperatures.

7.1 Introduction

Enhancement of the engineering properties of calcium-silicate-hydrate (C-S-H) systems is of practical interest as it has a direct influence on the performance of concrete materials. The use of organic compounds to modify the structure of C-S-H appears to have potential. The organics have long been used for the modification of smectite clays. It was suggested

by Matsuyama and Young [1-3] that is it possible to interact organics with the nanostructure of C-S-H systems. These results, however, were not validated by those obtained later (see Popova et al. [4] and Merlin et al. [5]). In spite of the numerous studies, the mechanisms of interaction of organics with the structure of C-S-H are still not fully understood.

The ultimate goal of the formation of C-S-H-based composite systems is to improve the engineering performance of these systems with the objective of increasing the service-life of concrete structures. The investigations on the engineering properties of the C-S-H-based composite systems are very limited in the literature. It has been suggested by Pellenq et al. that the organically modified C-S-H systems can have increases in their modulus of elasticity values of about 40% to 100% compared to those for phase pure C-S-H [6]. A decrease in the modulus of elasticity of C-S-H systems due to the interaction with organic polymers, however, was reported by Pelisser et al. [7]. Khoshnazar et al. [8] also studied the dynamic mechanical thermal analysis of C-S-H/polyaniline composite systems with Ca/Si ratios of 0.8 and 1.2. It was suggested that the storage modulus of these systems was improved at temperatures ranging from room temperature up to about 50 °C. No improvement was, however, observed at higher temperatures.

It was recently suggested by Khoshnazar et al. [9] that different nitrobenzoic acid isomers have the potential to improve the micro and nanostructure of C-S-H. This effect, however, is dependent on the type and the concentration of nitrobenzoic acid isomers. The C-S-H/NBA systems had also improved engineering performance and durability [10]. It was also observed that aminobenzoic acid isomers can interact with the structure of C-S-H. The effect of the 3- and 4-aminobenzoic acid lies between those of the 3- and 4-nitrobenoaic acid [11]. This chapter was designed to investigate the performance of the C-S-H/NBA and C-S-H/ABA systems under dynamic loading coupled with heating. The C-S-H-based systems were synthesized and tested by the dynamic mechanical thermal analysis technique at various temperatures and frequencies. The change in the storage modulus (E') and internal friction (tan δ) was then compared for the different systems.

7.2 Experimental program

The phase pure C-S-H and C-S-H-based composite systems (with Ca/Si = 1.5) were synthesized using the pozzolanic reaction technique described in chapter 3. Either of nitrobenzoic acid (2-, 3- or 4- isomer) or aminobenzoic acid (3- or 4- isomer) with a concentration of 0.01 mol. per mol. of Ca was added to the mixing water to prepare the C-S-H/NBA and C-S-H/ABA systems. All the preparations were conditioned at a relative humidity of 11% to reach equilibrium prior to testing. The powders were, then, compacted into circular discs with a porosity of about 30% using the compaction technique described in chapter 3. Prisms with a dimension of 32 mm × 13 mm × 1 mm were then obtained by cutting the compacted samples. A Rheometrics RSA III instrument with a three-point bending feature was used to obtain the dynamic mechanical response of the samples. All the tests were performed using a strain-controlled method. The maximum strain was set at 0.01%. An initial static load of 10 g was applied on the samples to ensure the contact between the upper fixture of the instrument and the surface of the sample throughout dynamic loading. The temperature was increased from 26 to 300 ℃ at a rate of 2 ℃/min. Tests were carried out at frequencies of 0.1, 0.25, 1.0 and 2.5 Hz. The storage modulus (E') and internal friction (tan δ) of samples were recorded at each temperature and frequency.

7.3 Results and Discussion

7.3.1 C-S-H/NBA systems

The general trend of the E' curves was not significantly changed by the variation of the load frequency. The E' values obtained at the higher frequencies were only slightly higher than those obtained at the lower frequencies. The E' values for the phase pure C-S-H and C-S-H/NBA systems at two frequencies of 0.1 and 2.5 Hz are presented in Figures 7-1 and 7-2, as examples. The data obtained at the lowest test frequency (0.1 Hz) is quantitatively discussed in this chapter.

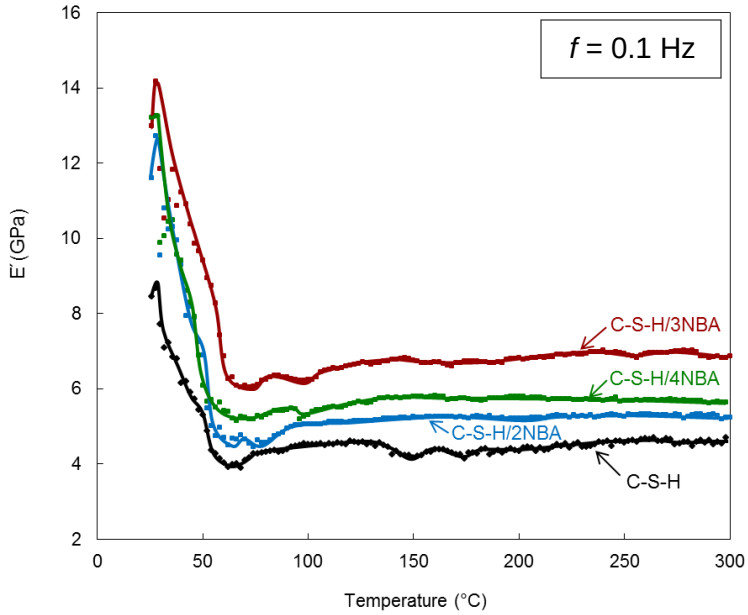

Figure 7-1- Storage modulus of the phase pure C-S-H and C-S-H/NBA systems versus temperature at the frequency of 0.1 Hz

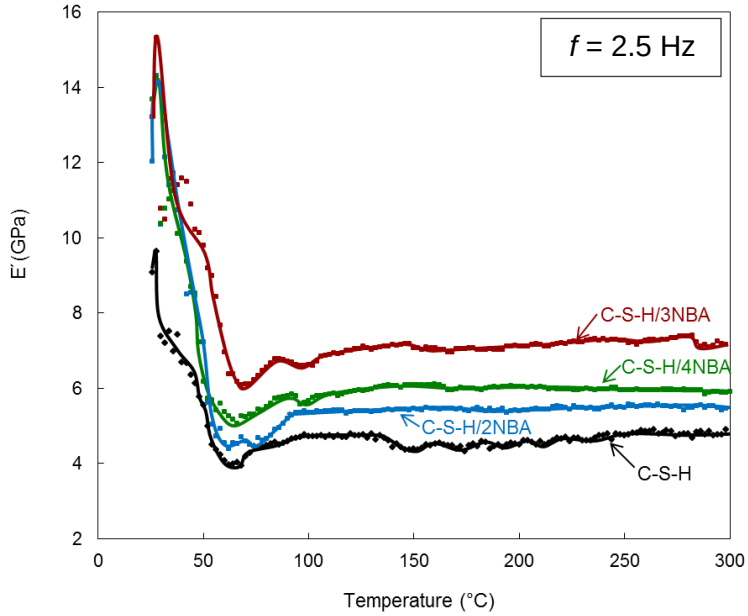

Figure 7-2- Storage modulus of the phase pure C-S-H and C-S-H/NBA systems versus temperature at the frequency of 2.5 Hz

The initial E' values of the C-S-H/NBA systems were higher than that of the phase pure C-S-H by about 36%, 53% and 55% for the systems incorporating 2-, 3- and 4-nitrobenzoic

acid, respectively (Figure 7-1). The E' values for all the C-S-H-based systems slightly increased by increasing the temperature from 26 °C to 28 °C. The increase of the E' values was significantly higher for the C-S-H/2NBA and C-S-H/3NBA systems (~ 10%) compared to that observed for the phase pure C-S-H (~ 2%). This increment was not significant for the C-S-H/4NBA system (less than 1%).

The E' values decreased gradually by increasing the temperature from 28 °C to about 60 °C. The reduction of the E' values of the C-S-H-based systems in this temperature range is known to occur due to the removal of the interlayer water from the nanostructure of C-S-H [12]. The decrease in the E' values was generally higher for the C-S-H/NBA systems compared to that observed for the phase pure C-S-H. It is possible that the nitrobenzoic acid isomers had formed hydrogen bonding with the structure of C-S-H. These bonds could break down due to the heating of the samples to about 60 °C. This likely resulted in higher decrease of the E' values for the composite systems. The E' values of the C-S-H/NBA systems, however, remained higher than that of the phase pure C-S-H at all the temperatures. The E' values were slightly recovered for all the C-S-H-based systems upon heating beyond 60 °C. This likely occurred due to the decrease of the spacing between the silicate sheets and possible cross-linking of the silicate tetrahedra [12]. The increase of the E' values was between 0.5 to 0.9 MPa for different C-S-H-based systems. No significant difference was observed between the phase pure C-S-H and C-S-H/NBA systems at this stage of drying.

The tan δ curves for the phase pure C-S-H and C-S-H/NBA systems were also generally similar at all the test frequencies. The peaks of the tan δ curves, however, were better defined at the lower frequencies as are shown in Figures 7-3 and 7-4. This is in conformity with the results previously reported by Alizadeh et al. [12]. The first peak of the tan δ curve of the phase pure C-S-H at a frequency of 0.1 Hz occurred at about 54 °C. This peak slightly shifted to higher temperatures (~ 60 °C) for the C-S-H/NBA systems. It was expected as this peak is assigned to the removal of the interlayer water in the structure of the C-S-H-based systems. The results of thermal gravimetric analysis in a previous study by the authors [9] also suggest that the removal of the interlayer water of C-S-H/NBA systems occurs at slightly higher temperatures compared to that in the phase pure C-S-H.

This peak was sharper in C-S-H/3NBA and C-S-H/4NBA systems corresponding to a larger decrease in the E' of these two systems. It was possibly due to the break-down of some hydrogen bonding between the nitrobenzoic acid isomers and the C-S-H structure in addition to the removal of the interlayer water.

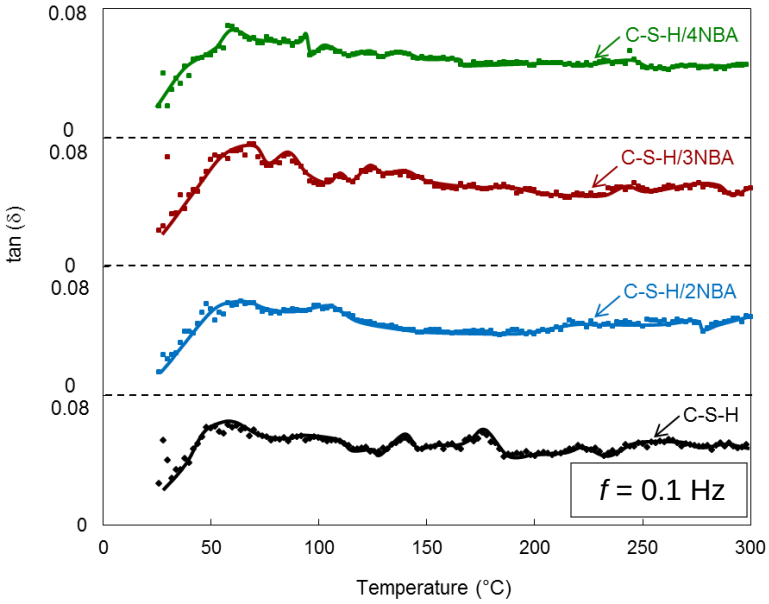

Figure 7-3- tan δ curves versus temperature the phase pure C-S-H and C-S-H/NBA systems at the frequency of 0.1 Hz

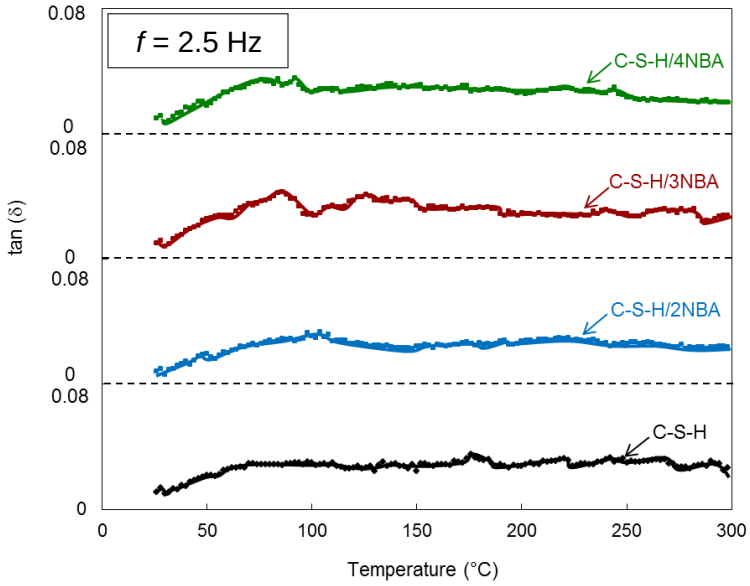

Figure 7-4- tan δ curves versus temperature the phase pure C-S-H and C-S-H/NBA systems at the frequency of 2.5 Hz

The hump at about 100 °C was better defined in the C-S-H/2NBA and C-S-H/3NBA systems (Figure 7-3). The peaks at the temperatures above 120 °C were, however, significantly diminished in intensity in the C-S-H/2NBA and C-S-H/4NBA systems. All these provide evidence on the structural role of nitrobenzoic acid isomers in the C-S-H/NBA composite systems.

7.3.2 C-S-H/ABA systems

The general trend of the E' and tan δ curves versus temperature were similar at different test frequencies. The only difference was that the E' values were slightly lower and the tan δ peaks were sharper at the lower frequencies, similar to those observed for the C-S-H/NBA systems. The E' values versus temperature for the phase pure C-S-H and C-S-H/ABA systems at a frequency of 0.1 Hz are presented in Figure 7-5. The initial E' values of the C-S-H/3ABA and C-S-H/4ABA were higher than that of the phase pure C-S-H by about 35% and 45%, respectively. The increase of the E' values that occurred by increasing the temperature from 26 to 28 °C was also observed for the C-S-H/ABA systems. The rate of the decrease of the E' values due to heating from 28 to 60 °C was higher for the C-S-H/3ABA and C-S-H/4ABA systems. The E' values for the C-S-H/3ABA system were still higher than those of the phase pure C-S-H by 18% at the end of this stage of drying. For the C-S-H/4ABA system, however, the E' values dropped to about 5% lower than those of the phase pure C-S-H. The E' of this system was then slightly recovered and reached the level of the phase pure C-S-H at about 80 °C. This value remained almost constant to the end of the test (300 °C).

The tan δ curves for the phase pure C-S-H and C-S-H/ABA systems at a frequency of 0.1 Hz are presented in Figure 7-6. The peaks of the tan δ curves were generally sharper in the C-S-H/ABA systems than those for the phase pure C-S-H at the temperatures up to 100 °C. This corresponds to the higher decrease of the E' values of the C-S-H/ABA systems in this temperature range.

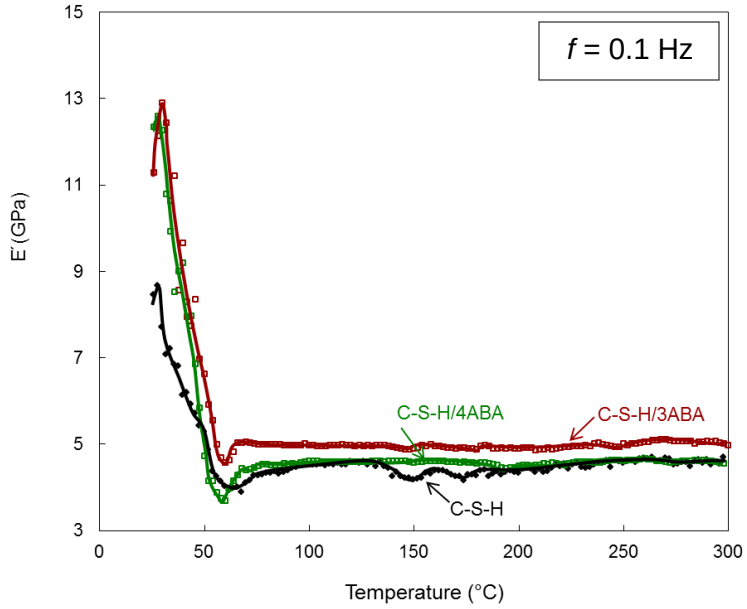

Figure 7-5- Storage modulus of the phase pure C-S-H and C-S-H/ABA systems versus temperature at the frequency of 0.1 Hz

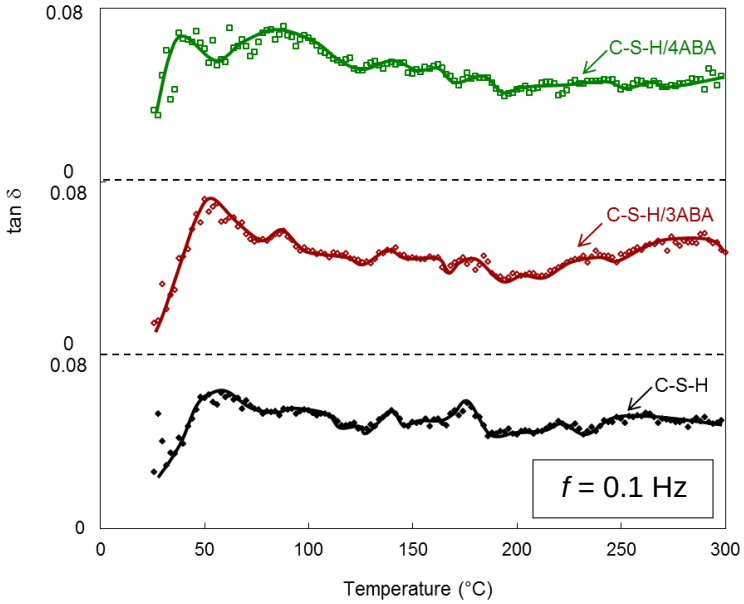

Figure 7-6- tan δ of the phase pure C-S-H and C-S-H/ABA systems versus temperature at the frequency of 0.1 Hz

7.4 Conclusions

The dynamic mechanical response of the phase pure C-S-H as well as the C-S-H/NBA and C-S-H/ABA composite systems were investigated at elevated temperature (up to 300 °C) and frequencies ranging from 0.1 to 2.5 Hz. The general response of the C-S-H-based systems is not significantly affected by the change of the frequency in the range investigated. It is also suggested that nitrobenzoic acid isomers have some structural role in the C-S-H/NBA systems. The storage modulus of the C-S-H/NBA systems remained higher than that of the phase pure C-S-H throughout the whole heating process. The initial peak of the tan δ curve was sharper in this range, and slightly shifted to higher temperatures. The aminobenzoic acid isomers also generally improved the storage modulus of the C-S-H-based systems. These compounds were not, however, as effective as the corresponding nitrobenzoic acid isomers.

References

1. H. Matsuyama and J. F. Young, "Intercalation of Polymers in Calcium Silicate Hydrate: A New Synthetic Approach to Biocomposites?," *Chemistry of Materials*, 11, pp. 16-19, 1999.
2. H. Matsuyama and J. F. Young, "Synthesis of calcium silicate hydrate/polymer complexes: Part I," *Journal of Materials Research*, 14, pp. 3379-3388, 1999.
3. H. Matsuyama and J. F. Young, "Synthesis of calcium silicate hydrate/polymer complexes: Part II," *Journal of Materials Research*, 14, pp. 3389-3396, 1999.
4. A. Popova, G. Geoffroy, M.-F. Renou-Gonnord, P. Faucon and E. Gartner, "Interactions between polymeric dispersants and calcium silicate hydrates," *Journal of the American Ceramic Society*, 83, 10, pp. 2556-2560, 2000.
5. F. Merlin, H. Lombois, S. Joly, N. Lequeux, J.-L. Halary and H. Van Damme, "Cement-polymer and clay-polymer nano- and meso-composites: spotting the difference," *Journal of Materials Chemistry*, 12, pp. 3308-3315, 2002.

6. R. J.-M. Pellenq, N. Lequeux and H. Van Damme, "Engineering the bonding scheme in C-S-H: The iono-covalent framework," *Cement and Concrete Research*, 38, pp. 159-174, 2008.

7. F. Pelisser, P. J. Gleiz and A. Mikowski, "Effect of poly(diallyldimethylammonium chloride) on nanostructure and mechanical properties of calcium silicate hydrate," *Materials Science and Engineering: A*, 527(26), pp. 1045-1049, 2010.

8. R. Khoshnazar, R. Alizadeh, J. J. Beaudoin and L. Raki, "The physico-mechanical stability of C-S-H/polyaniline nanocomposites," *Materials and Structures*, in-press, DOI: 10.1617/s11527-013-0168-4, 2013.

9. R. Khoshnazar, J. J. Beaudoin, L. Raki and R. Alizadeh, "Interaction of 2-, 3- and 4-nitrobenzoic acid with the structure of calcium-silicate-hydrate," *Materials and Structures*, under review, 2014.

10. R. Khoshnazar, J. J. Beaudoin, L. Raki and R. Alizadeh, "Durability and mechanical properties of C-S-H/nitrobenzoic acid composite systems," under review, 2014.

11. R. Khoshnazar, J. J. Beaudoin, L. Raki and R. Alizadeh, "Characteristics and engineering performance of C-S-H/aminobenzoic acid composite systems," under review, 2014.

12. R. Alizadeh, J. J. Beaudoina and L. Raki, "Mechanical properties of calcium silicate hydrates," *Materials and Structures*, 44, pp. 13-28, 2011.

Chapter 8

Fatigue Behaviour of Phase Pure C-S-H and C-S-H/Nitrobenzoic Acid Composite Systems

The main objective of this chapter is to investigate the performance of C-S-H-based systems under repetitive loading. A three-point bending set-up employing a strain-controlled condition was used for the fatigue analysis. The phase pure C-S-H and C-S-H/nitrobenzoic acid systems with a Ca/Si ratio of 1.5 were subjected to various load conditions. Comparisons were made based on the change of their storage modulus values and the number of cycles required for fracture. In addition, the phase pure C-S-H systems with various Ca/Si ratios (0.8, 1.2 and 1.5) and hydration time (from three weeks to 48 months) were prepared and tested for their dynamic response under repetitive loading. It is suggested that the C-S-H/NBA systems have higher fatigue resistance than the phase pure C-S-H with a similar Ca/Si ratio and hydration time. In addition, increasing the silicate chain length by lowering the Ca/Si ratio (e.g. in the C-S-H system with Ca/Si = 0.8) and by increasing hydration time, likely plays a significant role in improving the fatigue resistance of the phase pure C-S-H systems.

8.1 Introduction

Most concrete infrastructure is subjected to repetitive loading during its service-life. The study of the fatigue mechanisms of concrete and development of novel cement-based materials with increased fatigue-life is, therefore, of practical interest. The general performance of concrete under repetitive loading has long been studied. A few mechanisms

for the cracking and failure of concrete elements due to fatigue have also been proposed [1-3]. There are, however, still several uncertainties on how to estimate and improve the fatigue-life of concrete materials due to the complex nature of the development and propagation of cracks.

The investigations of the fatigue performance of pure hydrated cement-phases can provide the insight required to understand the mechanisms underlying their behavior. They can lead to development of novel cement-based materials with improved fatigue behaviour. In spite of the valuable results that can be provided, investigations in this field are still lacking in the literature.

Calcium-silicate-hydrate (C-S-H) is the primary binding phase in the hydrated Portland cement, and is responsible for most engineering properties of cement paste. Improvement of the fatigue performance of C-S-H has, therefore, the potential to increase the service-life of cement-based materials. It is suggested that the use of organic compounds is a promising approach to reach this goal. Although the mechanisms of interaction of high molecular-weight organic compounds with the nanostructure of C-S-H are still debatable [4-10], the results of recent studies by Khoshnazar et al. [11, 12] have provided evidence that selected low molecular-weight organic compounds, such as nitrobenzoic acid, have the potential to interact with the structure of C-S-H and significantly improve its durability as well as mechanical properties. The evidence includes data obtained using microindentation measurements.

The main objective of the current study is to assess the performance of C-S-H-based systems under repetitive bending loads. The experiments were designed to use different load conditions in order to investigate the efficiency of using nitrobenzoic acid isomers on the fatigue resistance of the C-S-H system with Ca/Si = 1.5. Additional experiments were also performed on the phase pure C-S-H systems with various Ca/Si ratios and hydration times to further investigate the effect of these parameters on the fatigue performance.

8.2 Experiments

C-S-H-based systems were prepared using the pozzolanic reaction technique described in chapter 3. The systems investigated were as follows:

- C-S-H(1.5) : phase pure C-S-H with Ca/Si ratio of 1.5, hydrated for three weeks,
- C-S-H(1.5)/NBA : C-S-H/nitrobenzoic acid composite systems with Ca/Si ratio of 1.5 and 0.01 mol. of nitrobenzoic acid (either of 2-, 3- and 4- isomers) per mol. of Ca. These systems were also hydrated for three weeks.
- C-S-H(1.5)-H48: phase pure C-S-H with Ca/Si ratio of 1.5, hydrated for 48 months,
- C-S-H(1.2)-H18 : phase pure C-S-H with Ca/Si ratio of 1.2, hydrated for 18 months,
- C-S-H(1.2)-H48 : phase pure C-S-H with Ca/Si ratio of 1.2, hydrated for 48 months and
- C-S-H(0.8)-H18 : phase pure C-S-H with Ca/Si ratio of 0.8, hydrated for 18 months.

All the preparations were conditioned at a relative humidity of 11% to reach equilibrium. The powders were, then, compacted into circular discs with a porosity of about 30% using the compaction technique described in chapter 3. Prisms with a dimension of 32 mm × 13 mm × 1 mm were then obtained by cutting the compacted samples. A Rheometrics RSA III instrument with a three-point bending feature was used to obtain the dynamic mechanical response of the samples. A time-sweep test was performed using a strain-controlled method (maximum strain = 0.01%). The change in the storage modulus (E') of the C-S-H-based systems was observed until a fracture occurred or until 200,000 cycles. Three different sets of experiments were designed. In the first set, the frequency of the dynamic load was 10 Hz and an initial static load of 50 g was applied to the specimens (the phase pure C-S-H(1.5) and C-S-H(1.5)/NBA systems) in each cycle. This load was applied to ensure that satisfactory contact between the upper fixture of the instrument and the surface of the sample during dynamic loading. The initial static load was increased to 80 g in the second experimental set-up. The test was performed on the phase pure C-S-H systems, with different Ca/Si ratios and hydration time, at frequencies of 5 and 10 Hz. The samples were subjected to a relatively medium static load in addition to the dynamic load during the test. An increased initial static load of 100 g was used in the third experimental

set-up. The test was performed at frequencies of 2, 5 and 10 Hz on the phase pure C-S-H(1.5) and C-S-H(1.5)/NBA systems. The systems were subjected to a relatively heavy static load during the whole dynamic loading. This was selected to accelerate the crack growth and failure of the C-S-H-based systems. It was previously suggested that the mechanisms of fracture of concrete are likely similar under static and dynamic loading [3].

8.3 Results and discussion

8.3.1 Fatigue behaviour of C-S-H(1.5) system

The change in the E' values by increasing the number of cycles for the phase pure C-S-H(1.5) is presented in Figure 8-1. A frequency of 10 Hz was used in these experiments. The test was repeated three times using three different values of initial static load (50, 80 and 100 g). The initial static load of 50 g was selected to ensure that a contact was provided between the upper fixture of the instrument and the surface of the sample throughout dynamic loading. The net static load was small during this experiment. The sample was subjected to a relatively medium and heavy static load in addition to the dynamic load in the experiments with increased initial static load (80 and 100 g).

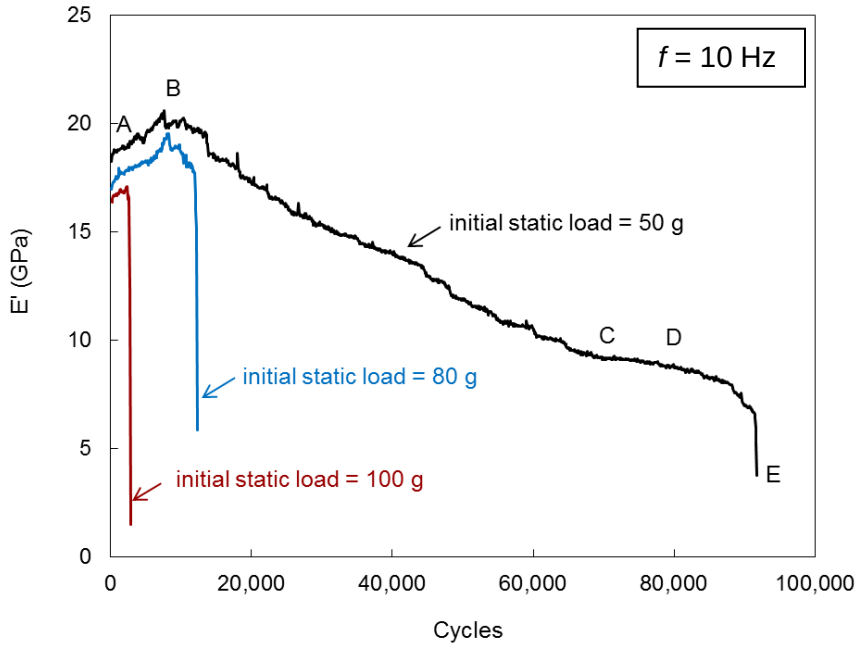

Figure 8-1- Change in the E' values of the phase pure C-S-H(1.5) systems by increasing the number of cycles, frequency = 10 Hz

The C-S-H(1.5) system, as expected, had a higher resistance to the failure when it was only dynamically loaded. Four different stages were observed in the fatigue curve of the C-S-H system in this case. In Stage I, from point A to point B, the E' of the sample increased by increasing the number of cycles. High frequency dynamic loading of the C-S-H(1.5) sample would result in sliding of the silicate sheets in the nanostructure of C-S-H. The spacing of these sheets could be slightly reduced and possible cross-linking of the silicate tetrahedra could occur as a result of this sliding during the first cycles. It ultimately increased the E' values of the C-S-H(1.5) system by about 13%.

In stage II, from point B to C, the E' of the C-S-H(1.5) system was gradually reduced to less than a half of its initial value. Further loading and sliding of the silicate sheets beyond point B could result in breaking of some silicate bonds and possibly formation of some micro-cracks in the C-S-H(1.5) sample. This resulted in a decrease of the E' of the sample. The E' values remained almost unchanged in stage III, from point C to D. It is possible that the silicate sheets in the structure of C-S-H are in a relatively stable condition. The sliding of these sheets against each other, further silicate bond breaking and crack growth was limited during this stage. Loading beyond point D, however, resulted in a significant formation and propagation of cracks and ultimately failure of the sample (point E).

Addition of a medium static load to the dynamic load of the sample resulted in a rapid break-down of the silicate bonds. The stage II was, therefore, shortened when the initial static load was increased to 80 g (Figure 8-1). The stage III was also eliminated in this case, and rapid formation and propagation of cracks resulted in a sudden failure of the sample. Application of a heavy static load in addition to the dynamic load significantly reduced the service-life of the C-S-H(1.5) sample. The fatigue curve in this case only consisted of two stages; an increase of about 7% during the first 1,000 cycles due to some rearrangement of the silicate sheets followed by a quick development and growth of micro-cracks in the sample resulting in its failure.

8.3.2 Fatigue behaviour of C-S-H(1.5)/NBA composite systems

The time sweep test at a frequency of 10 Hz and an initial static load of 50 g was performed on the C-S-H(1.5)/NBA systems (Figure 8-2). The initial E' was significantly higher for the

C-S-H(1.5)/NBA systems compared to that for the phase pure C-S-H(1.5). The increment of the initial E' of the C-S-H-based systems due to the use of 2-, 3- and 4-nitrobenozic acid isomers was 13%, 25% and 31%, respectively. The initial E' of the C-S-H(1.5)/NBA systems was increased during the first cycles. This increment (from 1 to 5% for different composite systems), however, was significantly lower than that observed for the phase pure C-S-H(1.5) (~ 13%). The E' values were, then, gradually decreased by increasing the number cycles. The rate of decrease of the E' values for the C-S-H(1.5)/4NBA system was higher than that observed for the other systems. The values of E' were, however, always slightly higher than that of the phase pure C-S-H(1.5). A slight recovery of the E' values was observed for the C-S-H(1.5)/3NBA system between the 85,000 to 97,000 cycles. This could probably have been occurred due to some cross-linking of silicate tetrahedra and possible healing of some micro-cracks at this stage of loading.

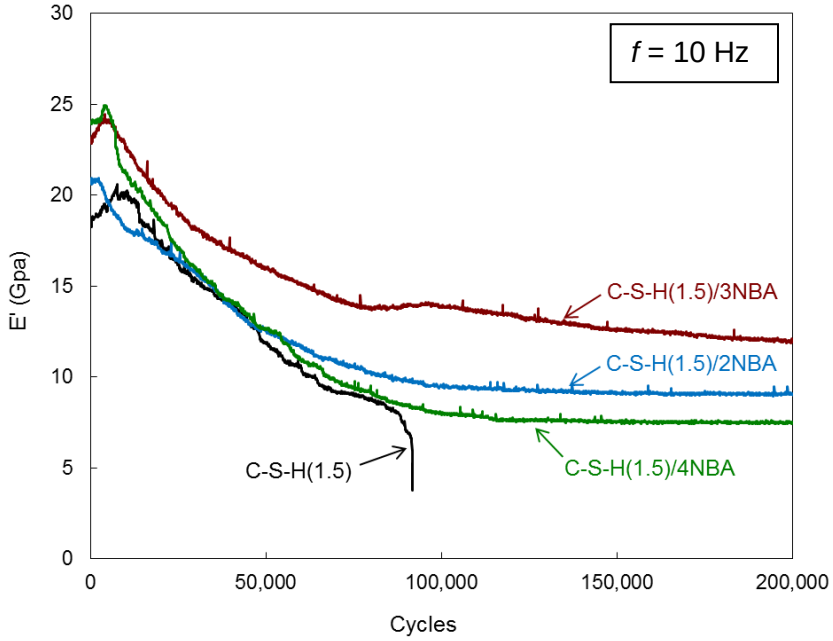

Figure 8-2- Change in the E' values of the phase pure C-S-H(1.5) and C-S-H(1.5)/NBA systems by increasing the number of cycles, frequency = 10 Hz, initial static load = 50 g

The stage III of the fatigue curve, at which the E' values remained almost constant, was significantly increased for the C-S-H/NBA systems. The stage IV (failure of the samples) was not observed up to 200,000 cycles. The test was continued up to 260,000 cycles for the C-S-H/3NBA system. No further decrease in the E' of the sample, however, was observed.

The fatigue curves for the phase pure C-S-H(1.5) and C-S-H(1.5)/NBA composite systems at the frequency of 10 Hz and initial static load of 100 g are presented in Figure 8-3. The service-life of the C-S-H(1.5)/NBA systems was significantly longer than that for the phase pure C-S-H(1.5). The crack propagation, however, occurred very quickly and the fracture was sudden for all the systems.

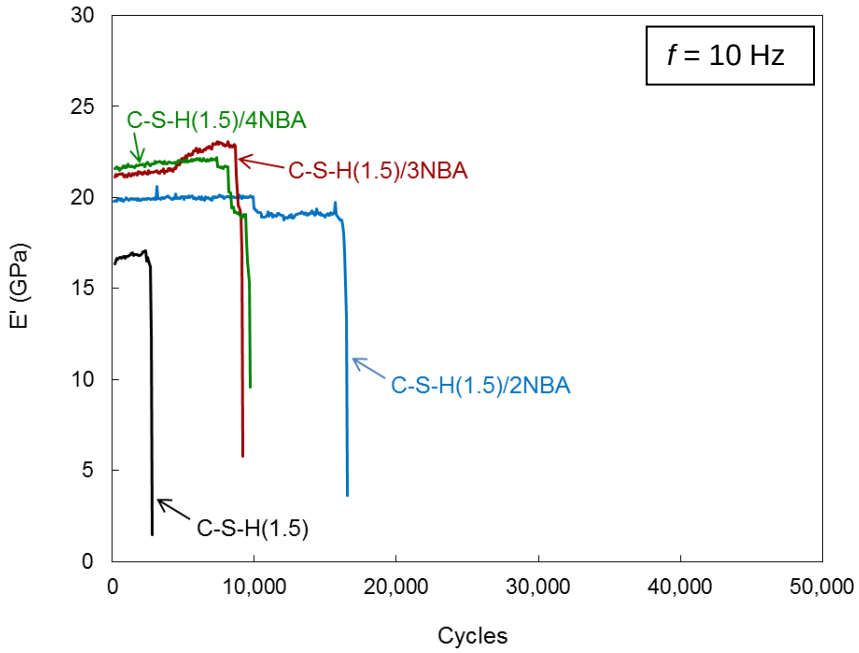

Figure 8-3-Change in the E' values of the phase pure C-S-H(1.5) and C-S-H(1.5)/NBA systems by increasing the number of cycles, frequency = 10 Hz, initial static load = 100 g

The test was repeated at frequencies of 2 and 5 Hz. The number of cycles prior to the failure (N_f) for the phase pure C-S-H(1.5) and C-S-H(1.5)/NBA systems is presented in Figure 8-4. An increased service-life was observed for all the C-S-H(1.5)/NBA composite systems compared to that for the phase pure C-S-H(1.5) at all three frequencies. The C-S-H(1.5)/2NBA composite system had the longest service-life at all different frequencies although the absolute E' values for this system were not very high during loading (see Figure 8-3 as an example).

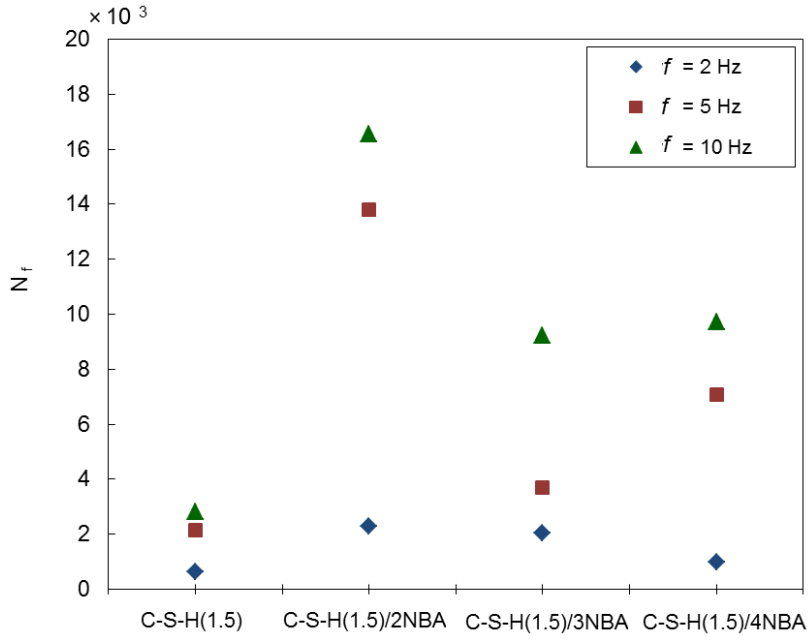

Figure 8-4- Number of cycles to failure (N_f) for the phase pure C-S-H(1.5) and C-S-H(1.5)/NBA composite system at different frequencies

8.3.3 Fatigue behaviour of phase pure C-S-H systems with various Ca/Si ratios and hydration time

The time-sweep test was performed on the C-S-H(1.5) system with an increased hydration time (48 months) as well as the C-S-H(0.8) and C-S-H(1.2) systems hydrated for 18 months and the C-S-H(1.2) system hydrated for 48 months. An initial static load of 80 g was applied in each cycle. The test was performed twice at the frequencies of 5 and 10 Hz. The results are presented in Figures 8-5 and 8-6, respectively. The fatigue curves of each sample were generally similar at the two test frequencies. The E' values obtained at the frequency of 10 Hz was, however, higher than those at frequency of 5 Hz. In addition, the changes of the E' values by increasing the number of cycles at the higher frequency were not as significant as those occurred at the lower frequency. These two results were generally expected for the C-S-H-based systems.

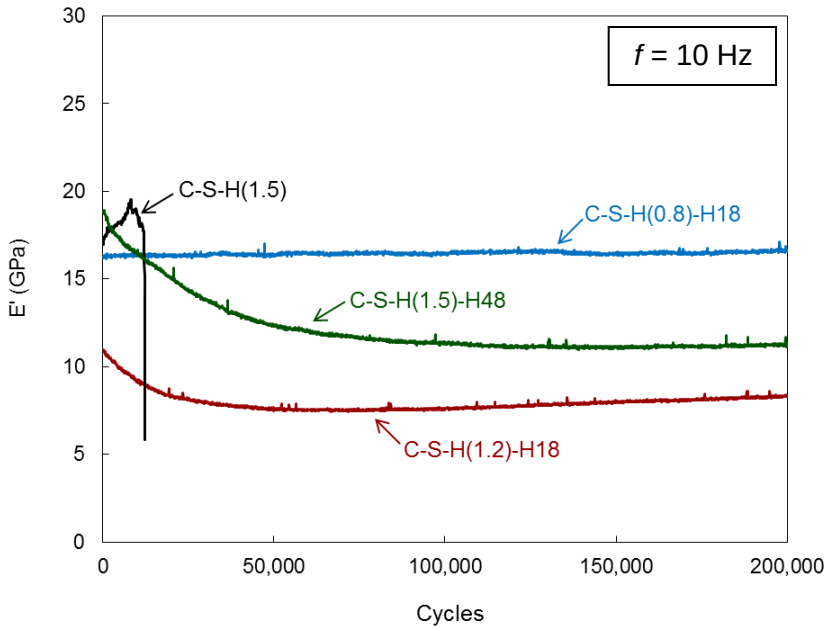

Figure 8-5- Change in the E' values of the phase pure C-S-H systems with various Ca/Si ratios and hydration time by increasing the number of cycles, frequency = 10 Hz, initial static load = 80 g

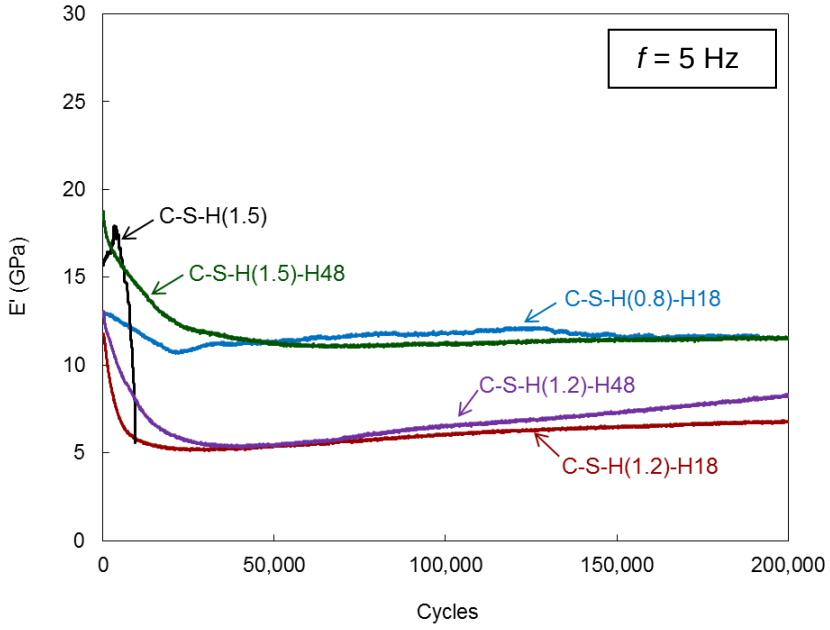

Figure 8-6-Change in the E' values of the phase pure C-S-H systems with various Ca/Si ratios and hydration time by increasing the number of cycles, frequency = 5 Hz, initial static load = 80 g

The initial E' values were higher for the C-S-H(1.5) systems hydrated for 48 months compared to those hydrated for three weeks. The initial increase in the E' values was not observed for the samples with an increased hydration time. The silicate chain-length is expected to increase by lengthening the hydration time. This likely resulted in a higher initial E' values for the C-S-H(1.5)-H48 systems. It could also lower the tendency of the aged systems to the additional increase of the E' values during the first cycles of dynamic loading. The decrease of the E' values of the C-S-H(1.5)-H48 systems was gradual up to about 40,000 and 110,000 cycles at the frequencies of 5 and 10 Hz, respectively. The E' values, then, remained almost unchanged, and no failure was observed until the end of the test. The results up to 200,000 cycles are presented in Figure 8-5 and 8-6 at the frequency of 5 and 10 Hz, respectively. The test at the frequency of 10 Hz was continued to 560,000 cycles for the C-S-H(1.5)-H48 system without any signs of failure for the sample.

The E' values of the C-S-H(1.5)-H48 system were generally higher than those of the C-S-H(1.2)-H48 system at the frequency of 5 Hz (Figure 8-6). The C-S-H(1.5)-H48 system had about 1.4% of calcium hydroxide as determined by the thermal gravimetric analysis. This likely contributed to the higher E' values of this system.

The E' values of the C-S-H(1.2)-H48 were generally higher than those of the C-S-H(1.2)-H18 at the frequency of 5 Hz. The decrease of the E' values during the loading was also slightly less and occurred at a lower rate compared to that for the C-S-H(1.2)-H18 system. In addition, the E' values of the C-S-H(1.2)-H48 system recovered by almost 40% after 200,000 cycles. The recovery of the E' values of the C-S-H(1.2)-H18 system was not as significant.

The resistance of the C-S-H(0.8)-H18 system to repetitive loading was significantly higher than that for the C-S-H(1.2)-H18 system. In addition, the E' values for the C-S-H(0.8)-H18 were almost unchanged even after 200,000 cycles at the frequency of 10 Hz (Figure 8-5). The decrease of the E' values for the C-S-H(0.8)-H18 at the frequency of 5 Hz was also considerably less than that occurred for the C-S-H(1.2)-H18 system (figure 8-6). A recovery of the E' values was also observed between 40,000 to 140,000 cycles probably due to the cross-linking of the silicate tetrahedra at this stage of loading.

It is noted that none of the C-S-H systems with increased hydration time failed or were close to failure after 200,000 cycles. Selected tests were continued to 560,000 cycles. No further decrease of the E' values was, however, observed. Additional tests are required to investigate the possibility of presence of an endurance limit for the fatigue of the phase pure C-S-H systems.

8.4 Concluding remarks

The resistance of the phase pure C-S-H systems with various Ca/Si ratios and hydration time as well as the C-S-H/NBA systems to the fatigue behavior was investigated. Evidence was obtained that both modification of C-S-H with nitrobenzoic acid and increasing the hydration time of the C-S-H systems can improve the fatigue performance. In addition, the C-S-H systems with a Ca/Si ratio of 0.8 had better performance than those with higher Ca/Si ratios. This was likely due to the increased silicate chain-length in the C-S-H(0.8) systems (i.e. fewer defects or missing bridging silica tetrahedra). Further study is needed to investigate the mechanisms of fatigue failure of the C-S-H-based systems and the presence of an endurance limit for these systems.

Reference

1. H. Horii, H. C. Shin and T. M Pallewatta, "Mechanism of fatigue crack growth in concrete," *Cement and Concrete Composites*, 14, pp. 83-89, 1992.
2. T. T. C. Hsu, "Fatigue and microcracking of concrete," *Materials and Structures*, 17(97), pp. 51-54, 1984.
3. S. P. Shah and S. Chandra, "Critical stress, volume change and microcracking of concrete," *Journal of the American Concrete Institute*, 65(9), pp. 770-781, 1968.
4. H. Matsuyama and J. F. Young, "Intercalation of Polymers in Calcium Silicate Hydrate: A New Synthetic Approach to Biocomposites?," *Chemistry of Materials*, 11, pp. 16-19, 1999.
5. H. Matsuyama and J. F. Young, "Synthesis of calcium silicate hydrate/polymer complexes: Part I," *Journal of Materials Research*, 14, pp. 3379-3388, 1999.

6. H. Matsuyama and J. F. Young, "Synthesis of calcium silicate hydrate/polymer complexes: Part II," *Journal of Materials Research*, 14, pp. 3389-3396, 1999.

7. A. Popova, G. Geoffroy, M.-F. Renou-Gonnord, P. Faucon and E. Gartner, "Interactions between polymeric dispersants and calcium silicate hydrates," *Journal of the American Ceramic Society*, 83, 10, pp. 2556-2560, 2000.

8. F. Merlin, H. Lombois, S. Joly, N. Lequeux, J.-L. Halary and H. Van Damme, "Cement-polymer and clay-polymer nano- and meso-composites: spotting the difference," *Journal of Materials Chemistry*, 12, pp. 3308-3315, 2002.

9. J. Minet, S. Abramson, B. Bresson, C. Sanchez, V. Montouillout and N. Lequeux, "New layered calcium organosilicate hybrids with covalently linked organic functionalities," *Chemistry of Materials*, 16, pp. 3955-3962, 2004.

10. J. Minet, S. Abramson, B. Bresson, A. Franceschini, H. Van Damme and N. Lequeux, "Organic calcium silicate hydrate hybrids: a new approach to cement based nanocomposites," *Journal of Materials Chemistry*, 16, pp. 1379-1383, 2006.

11. R. Khoshnazar, J. J. Beaudoin, L. Raki and R. Alizadeh, "Interaction of 2-, 3- and 4-nitrobenzoic acid with the structure of calcium-silicate-hydrate," *Materials and Structures*, under review, 2014.

12. R. Khoshnazar, J. J. Beaudoin, L. Raki and R. Alizadeh, "Durability and mechanical properties of C-S-H/nitrobenzoic acid composite systems," under review, 2014.

Chapter 9

The Interaction of Selected Organic Polymers and Compounds with Calcium-Silicate-Hydrate Systems

The efficiency of the use of relatively small molecular-sized organic compounds in order to modify the nanostructure of calcium-silicate-hydrate (C-S-H) systems was studied in the previous chapters. The influence of organic polymers is the focus of this chapter. Possible intercalation effects as reported by Matsuyama and Young [1-4] indicated that there was potential for improvement of mechanical properties. Accordingly, three different polymers, polyvinyl alcohol, polyacrylic acid and polymethylmethacrylate, in various concentrations were added to the phase pure C-S-H during its hydration. The characteristics and engineering performance of the resulting composite systems were then investigated. No evidence of the improvement of the performance of the C-S-H/polymer systems was obtained. The only exception was the C-S-H/polymethylmethacrylate system which had an improved creep modulus as determined by the microindentation technique. In addition to the properties of the C-S-H/polymer systems, the X-ray diffraction patterns and length-change measurements in LiCl solution for the C-S-H systems prepared with several other organic compounds, e.g. octadecylamine, selected dicarboxylic acids, etc. are presented in this chapter. These organic compounds were selected due to their possible application in chemical admixture formulations for cement-based materials.

9.1 Introduction

Organic compounds have been successfully used to modify the nanostructure of layered silicate minerals for more than fifty years [5]. These modifications can mainly occur by the intercalation of the organics in the interlayer space of the layered silicates as well as the surface grafting or adsorption. Significant improvement of the performance of the layered silicates and the organics was achieved due to the interaction of the organic and inorganic phases at the nano-scale [6, 7].

It has been about a decade since the possibility of interaction of organic compounds with the nanostructure of synthetic calcium-silicate-hydrate (C-S-H) systems was suggested by Matsuyama and Young [1-4]. Mechanisms of the interaction of several anionic, cationic and non-ionic polymers with the nanostructure of C-S-H systems with various Ca/Si ratios were studied. It was suggested that intercalation of a few of these polymers was possible in the interlayer region of the host C-S-H systems. The results of later investigations, however, were not in conformity with those obtained by Matsuyama and Young (see Popova et al. [8] and Merlin et al. [9] as examples). It was argued that in most the cases the organics can be adsorbed significantly between the stacked layers of C-S-H. Their intercalation in the interlayer region, however, is very limited.

The mechanisms of interaction of small molecular-sized organics (nitrobenzoic acid and aminobenzoic acid isomers) were recently investigated Khoshnazar et al. [10-13]. A model for the nanostructure of the resulting composite systems was suggested [10]. The focus was given to the durability and mechanical properties of the organically modified C-S-H systems. Evidence was reported that the appropriate concentration of the selected organics can contribute to the engineering performance of the resulting composite systems [11-13].

The main objective of this chapter is to investigate the influence of organic polymers on the nanostructure of C-S-H and their possible contribution to the durability and mechanical properties of the C-S-H-based composite systems. Three different polymers (polyvinyl alcohol (PVA), polyacrylic acid (PAA) and polymethylmethacrylate (PMM)) were selected. PVA and PAA have been successfully used in the clay science previously [14-16]. Their influence on the nanostructure of C-S-H, prepared by precipitation technique or by the hydration of β-dicalcium silicate, was also studied by Matsuyama and Young in 1999

[1, 2, 4]. The C-S-H-based systems of the current study, however, were prepared by the pozzolanic reaction technique as described in chapter 3. All these systems were characterized by the X-ray diffraction (XRD), thermal gravimetric analysis (TGA), scanning electron microscopy (SEM) techniques and BET nitrogen surface area measurements. These systems were also tested for their volume stability in $MgCl_2$ and $MgSO_4$ solutions. Microindentation creep modulus determinations were also made. In addition to the mentioned polymers, several organic compounds such as octadecylamine, selected dicarboxylic acids, etc. were also selected and used for the preparation of the C-S-H-based composite systems. Their influence on the basal-spacing and the volume stability of the C-S-H system was then determined.

9.2 Experimental program

All the C-S-H-based systems were prepared using pozzolanic reaction technique described in chapter 3. Either of polyvinyl alcohol (PVA), polyacrylic acid (PAA) or polymethylmethacrylate (PMM) with a concentration of 0.01 mol. of the monomer per mol. of Ca were added to the mixing water during the hydration of the C-S-H systems (Ca/Si = 1.5). Additional preparations with increased concentration of PVA or PAA (PVA/Ca = 0.70 or PAA/Ca = 0.50) were also synthesized. All the preparations were filtered after three weeks of hydration, then, dried under vacuum for four hours and conditioned at a relative humidity of 11% for at least 40 days to reach equilibrium. The preparations were characterized by the X-ray diffraction (XRD), scanning electron microscopy technique (SEM), thermal gravimetric analysis (TGA) and BET nitrogen surface area measurements. Compacted samples with a porosity of about 30% were also prepared as described in chapter 3. The length-change of the compacted samples in $MgCl_2$ and $MgSO_4$ solutions (15 g/l) as well as their microindentation creep modulus were also determined.

Additional organic compounds were also selected and used for the C-S-H-based preparations. These organics included: octadecylamine, selected dicarboxylic acids (oxalic acid, malonic acid and adipic acid) and selected fatty acids (lauric acid, aminolauric acid and stearic acid). Dicarboxylic acids can potentially act as a plasticizer in cement paste and fatty acids can have application as resins. These organics were used with a concentration of

0.01 mol. per mol. of Ca in the C-S-H systems. Combination of 4-nitrobenzoic acid (4NBA) and oxalic acid (OA) with two different molar ratios (4NBA/OA/Ca = 0.01/0.01/1 and 4NBA/OA/Ca = 0.005/0.005/1) was also considered to examine the compatibility of these two organics. Two different organosilanes were also selected; 3-aminopropyl-triethoxysilane (APTES) and vinyltrimethoxysilane (VTMS). The concentration of these organics was APTES/Ca = 0.01, VTMS/Ca = 0.01 and VTMS/Ca = 0.30. The organo-silanes were not added to the mixing water directly to prevent the possible immediate hydrolysis of these organics. They were added to the solid mixture of CaO and SiO_2. The water was, then, added to this mixture. No other solvent was used because of potential adverse reactions interfering with the pozzolanic reaction. All resulting composite systems were tested by the X-ray diffraction. Length-change measurements in the LiCl solution (15 g/l) were also made.

9.3 Results and discussion

9.3.1 Effect of organic polymers

XRD - The d_{002} basal-spacing of the C-S-H-based systems containing various polymers is presented in Figure 9-1. The change in the basal-spacing of the C-S-H-based systems due to the incorporation of the lower concentration of polymers was not significant. The basal-spacing of the C-S-H/PVA.01 and C-S-H/PAA.01 systems was similar (1.18 nm). It was slightly larger than the basal-spacing of the phase pure C-S-H (1.10 nm). The increase of the basal-spacing of the C-S-H/PMM.01 system was also small (0.04 nm). It is likely that the selected polymers were mainly adsorbed on the surface or at the edges of the C-S-H layers. This slightly increased the basal-spacing of the samples.

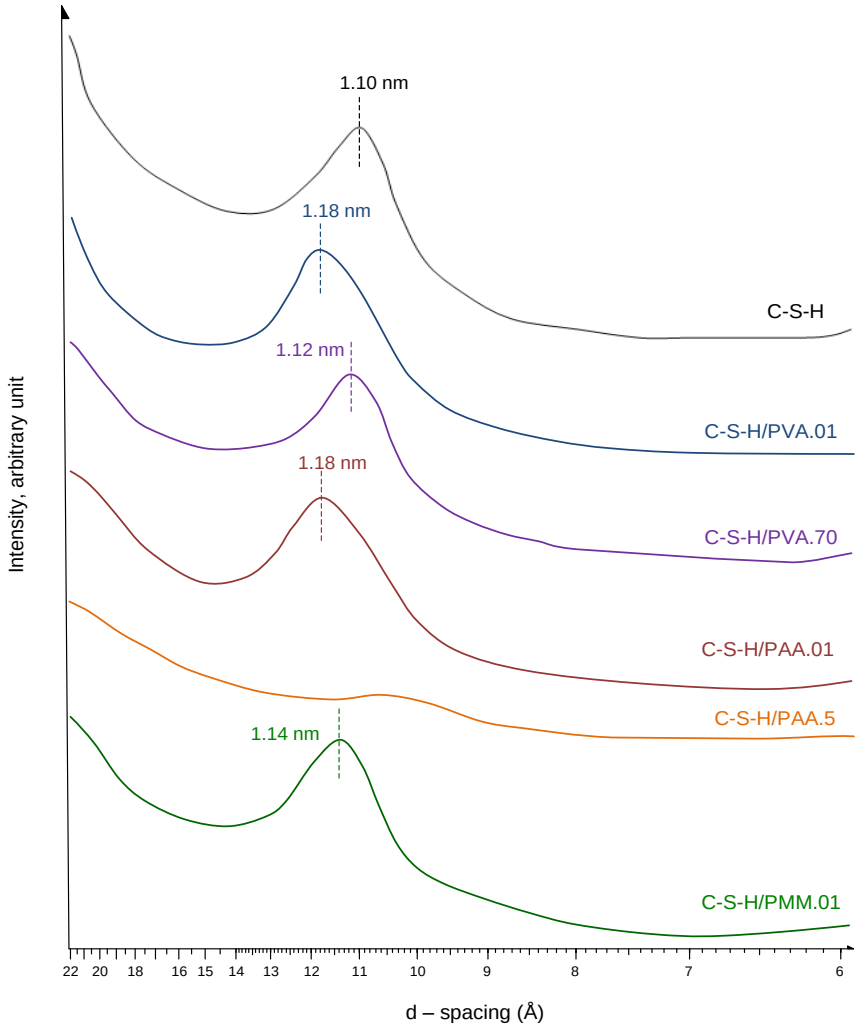

Figure 9-1- basal-spacing of the C-S-H/polymer systems

The basal-spacing of the C-S-H/PVA.70 system was almost similar to that of the phase pure C-S-H (Figure 9-1). It is likely that interaction of PVA with the C-S-H structure would be limited by increasing the concentration of PVA. Local accumulation of the PVA on the surface of the C-S-H layers or between the stacked layers of C-S-H is expected in this case, as previously suggested in chapter 4 for the C-S-H/NBA systems. The d_{002} basal-spacing corresponding to C-S-H was not detected in the XRD pattern of the C-S-H/PAA.50 system. The XRD pattern in the range of $4° < 2\theta < 60°$ for this system is compared with those of the phase pure C-S-H and C-S-H/PVA.70 systems in Figure 9-2. The peaks observed in the XRD patterns of the C-S-H/PAA.50 correspond mainly to portlandite and calcite rather than the crystalline C-S-H. It is likely that the higher concentration of PAA acted as an

inhibitor of the pozzolanic reaction. This is in conformity with the results obtained by Popova et al. [8] suggesting that the formation of C-S-H from the pozzolanic reaction was slightly inhibited due to the presence of adsorbed polymer.

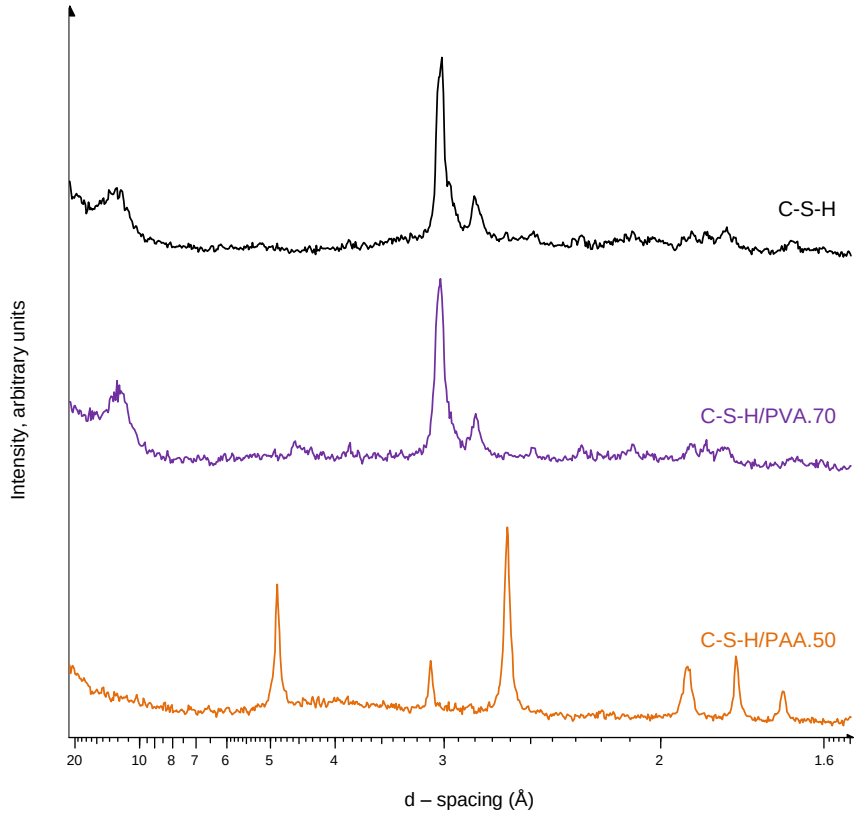

Figure 9-2- XRD pattern of the phase pure C-S-H, C-S-H/PVA.70 and C-S-H/PAA.50 systems

SEM – No significant change was detected by the SEM technique in the morphology of the C-S-H-based systems due to the incorporation of the polymers (see Figures 9-3(a) and 9-3(b) as an example). The only exception was the C-S-H/PAA.50 system (Figure 9-3(c)). Two separate components (a calcium rich and a silica rich component) rather than a C-S-H-based system were detected in the SEM micrograph of this sample. This result is in conformity with that of the X-ray diffraction and provides evidence of the interference of the higher concentration of PAA with the pozzolanic reaction. The C-S-H/PAA.50 system was not used for further characterization in this chapter as it was not considered a C-S-H-based system.

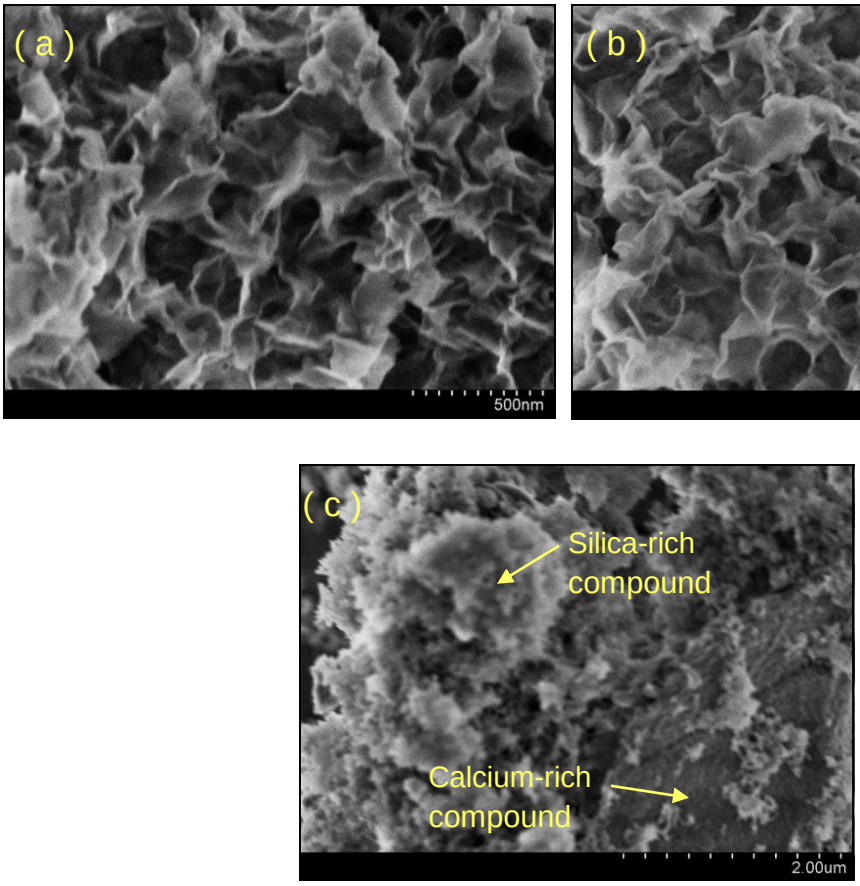

Figure 9-3- SEM micrographs of (a) phase pure C-S-H, (b) C-S-H/PVA.70 and (c) C-S-H/PAA.50

TGA – The derivative of mass-loss curves for the C-S-H-based systems are presented in Figure 9-4. The curves for the C-S-H-based systems with the lower concentration of polymers were generally similar to that for the phase pure C-S-H. An additional peak, however, was observed at about 45 °C. It is possible that these systems had slightly adsorbed moisture prior to performing the TGA test. The polymers could also have formed some weak hydrogen bonding with the C-S-H structure. Removal of this water likely resulted in the formation of a small peak at the lower temperatures of the TGA experiment.

The peak at about 220 °C in the TGA curve of the C-S-H/PVA.70 system corresponds to the decomposition of PVA. This peak has slightly shifted to the lower temperatures compared to that for pure PVA (~ 270 °C). The percentage of PVA in the C-S-H/PVA.70 systems was estimated to be about 12% based on the integration of this peak.

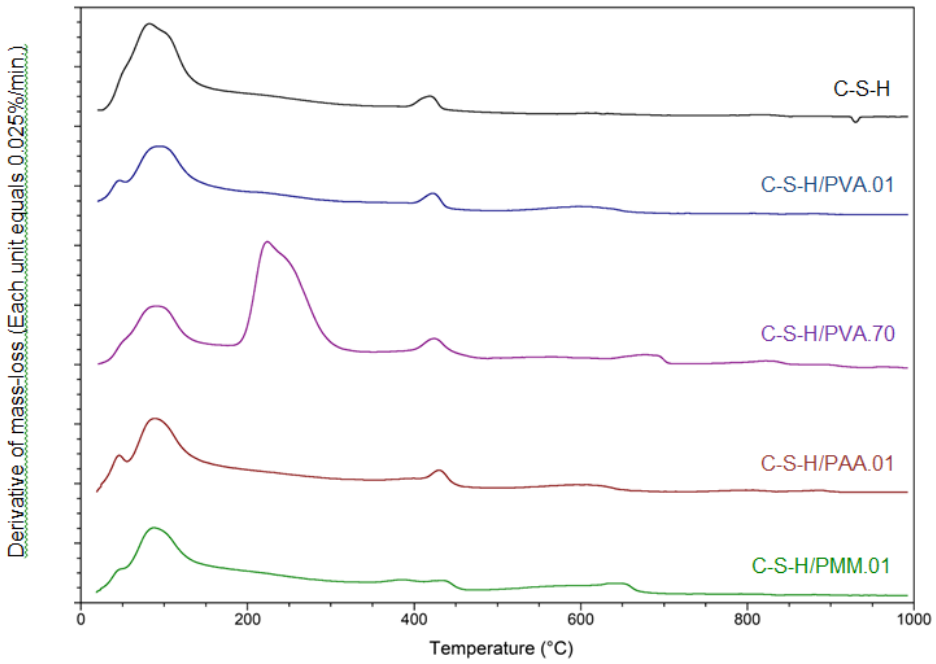

Figure 9-4- Derivative of mass-loss curves in the TGA experiment of the C-S-H/polymer systems

Surface area – All the C-S-H/polymer systems had surface area values lower than that determined for the phase pure C-S-H system (Figure 9-5). This could have occurred due to the adsorption of the polymers on the surface of the layers or between the stacked layers of C-S-H. Nitrogen has a relatively large molecular size and does not enter the interlayer region of C-S-H-based systems. No conclusion can, therefore, be made based on the nitrogen surface area measurements on the possible intercalation of the polymers.

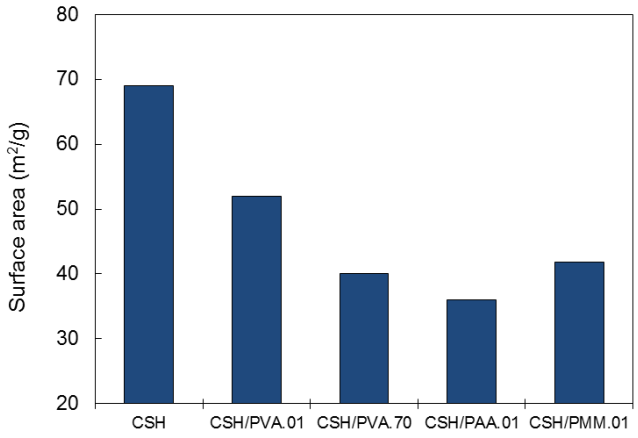

Figure 9-5- BET nitrogen Surface area measurements for the C-S-H/polymer systems

Length-change measurements – The length-change values of the C-S-H/polymer systems after 24 h of immersion in the $MgCl_2$ and $MgSO_4$ solutions are presented in Figures 9-6(a) and (b), respectively. No evidence of an improvement of the volume-stability of the C-S-H-based systems in the test solutions due to the incorporation of the polymers was obtained. The length-change values of the C-S-H/polymer systems with the lower concentration of the polymer was not significantly different from those obtained for the phase pure C-S-H. The length-change values of the C-S-H/PVA.70 system was, however, significantly high (an average of about three times higher than that for the phase pure C-S-H). The length-change values of the phase pure C-S-H and C-S-H/PVA.70 systems were also determined in de-ionized water to eliminate the influence of ionic species on the longitudinal expansions. The length-change value for the C-S-H/PVA.70 systems, however, was almost ten times higher than that determined for the phase pure C-S-H after 4 h of immersion. The significantly high length-change values of the C-S-H/PVA.70 system compared to those obtained for the phase pure C-S-H could have been occurred due to the separation of the organic and inorganic phases in the C-S-H/PVA.70 system. In addition, PVA is a water soluble polymer. The significant length-change of the C-S-H/PVA.70 system in the aqueous solutions could provide evidence of the role of dissolution in the length-change measurements (see Khoshnazar et al. [17, 18] for more details of the dissolution mechanism underlying the length-change of cement-based phases).

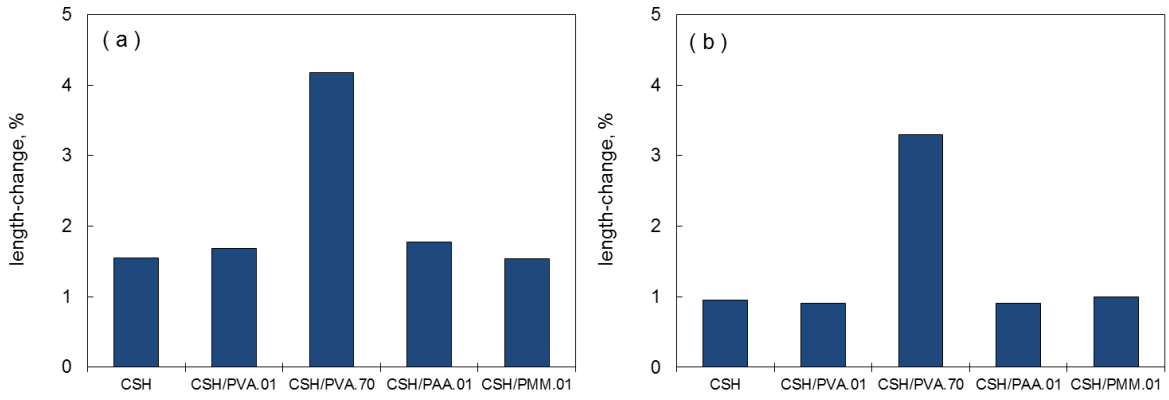

Figure 9-6- Length-change measurements for the C-S-H-based systems in (a) $MgCl_2$ and (b) $MgSO_4$ solution

Microindentation – The Creep modulus values of the C-S-H/polymer systems are presented in Figure 9-7. The C-S-H/PMM.01 system had an improved creep modulus by about 20% compared to that of the phase pure C-S-H. The creep modulus values of C-S-H-based systems prepared with other polymers were lower (corresponding to higher creep rates) than that determined for the phase pure C-S-H. The creep modulus of the C-S-H/PVA.70 system was very low (67% of that of the phase pure C-S-H). The lower values of creep modulus of the C-S-H/polymer systems can be a result of organic/inorganic phase separation in these systems. The phase separation was more likely to occur in the C-S-H system with higher concentration of PVA. The creep modulus of this system was, therefore, lower.

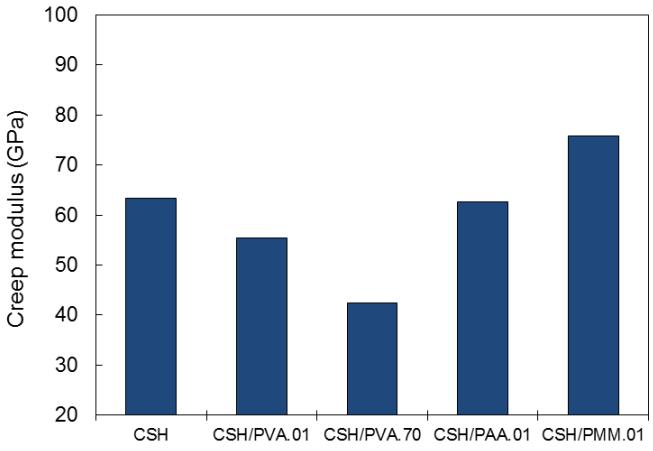

Figure 9-7- Microindentation creep modulus of the C-S-H/polymer systems

9.3.2 Effect of other organic compounds

The d_{002} basal-spacing of the C-S-H-based systems as well as their length-change measurements in the LiCl solution are presented in Table 9-1. The effect of different organic compounds was as follows:

octadecylamine: An increase of 0.13 nm was observed in the basal-spacing of the C-S-H system due to the incorporation of octadecylamine. This increment was small. It was, however, larger than that observed for the organic compounds studied in the previous chapters. Octadecylamine has a relatively long carbon chain-length. Its adsorption at the

edges of the C-S-H layers could have been contributed to a larger increase of the basal-spacing of C-S-H. Additional experiments are still required to make a conclusion about the possible intercalation of octadecylamine in the interlayer region of the host C-S-H. No evidence of an improvement of the volume stability of the C-S-H/octadecylamine.01 system in the test solution was observed (Table 9-1).

Table 9-1- d_{002} basal-spacing and length-change measurements of the C-S-H-based systems

Label	**d_{002} (nm)**	**Length-change in LiCl solution (%)**
C-S-H	1.10	1.1
C-S-H/octadecylamine.01	1.23	1.2
C-S-H/oxalic acid.01	1.13	1.1
C-S-H/malonic acid.01	1.16	2.1
C-S-H/adipic acid.01*	1.23	2.2
C-S-H/4NBA-OA.005005	1.19	1.2
C-S-H/4NBA-OA.0101	1.22	1.3
C-S-H/lauric acid.01	1.16	1.1
C-S-H/aminolauric acid.01	1.20	1.2
C-S-H/stearic acid.01*,**	1.18	1.0
C-S-H/APTES.01	1.21	2.9
C-S-H/VTMS.01	1.23	2.0
C-S-H/VTMS.30*	1.29	-

* *A porosity of 16-20% was determined by helium pycnometry for the compacted samples.*

** *An additional peak corresponding to pure stearic acid was observed in the XRD pattern of this system.*

***dicarboxylic acids**:* The basal-spacing of the C-S-H-based systems increased linearly by increasing the number of carbons in the dicarboxylic acids. The increase, however, was considerably lower than that expected for intercalated systems. The anion of oxalic acid, the smallest molecular-sized organic of this group, has a diameter of about 0.5 nm, for

example. The C-S-H/oxalic acid.01, however, had a basal-spacing of 1.13 nm which was only 0.03 nm larger than that for the phase pure C-S-H. The low increment of the basal-spacing can be due to the large number of defects in the nanostructure of C-S-H system with the Ca/Si ratio of 1.5. The anion of the organics can possibly fill these defects resulting in a lower increase of the interlayer space of the host C-S-H. It is also possible that the selected dicarboxylic acids were mainly adsorbed on the surface or at the edges of the C-S-H layers resulting in a small increase of the basal-spacing.

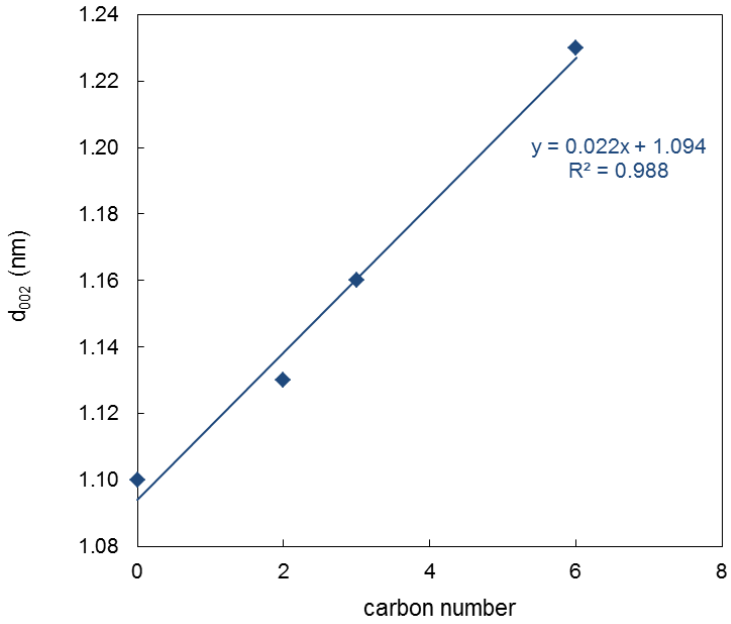

Figure 9-8- d_{002} versus carbon numbers for the C-S-H/dicarboxylic acid systems
(carbon number = 2, 3 and 6 for the oxalic acid, malonic acid and adipic acid, respectively)

The length-change values of the C-S-H/oxalic acid.01 system in the LiCl solution were similar to that of the phase pure C-S-H system (Table 9-1). The length-change values of the C-S-H/malonic acid.01 and C-S-H/adipic acid.01 systems, however, were almost two times higher. The larger basal-spacing of these systems likely facilitates the entry of water and anionic species to the interlayer region resulting in higher length-change values.

Combination of 4NBA and oxalic acid: The increase of the basal-spacing of the C-S-H systems with both 4NBA and oxalic acid was higher than that observed for those with the individual organics. The basal-spacing increased by increasing the concentration of 4NBA

and oxalic acid. The length-change measurements, however, were also higher for these systems compared to the phase pure C-S-H, C-S-H/4NBA.01 (see chapter 5) and C-S-H/oxalic acid.01 systems.

***Fatty acids**:* Incorporation of selected fatty acids also slightly increased the basal-spacing of the host C-S-H systems. The selected fatty acids, however, had a relatively large number of carbon atoms in their structure (the number of carbon atoms is 12 in lauric acid and 18 in stearic acid). The slight increase of the basal-spacing, therefore, could have been a result of alteration of the edges of the C-S-H layers. An additional peak corresponding to unreacted stearic acid crystals was also detected in the XRD pattern of the C-S-H/stearic acid.01 system. It provides evidence of the separation of organic and inorganic phases in this system. The organics of this group were not effective in limiting the length-change values.

***Organosilanes**:* The increase in the basal-spacing of the C-S-H/organosilane systems was slightly higher than that observed for most previously studied C-S-H-based systems. The basal-spacing of the C-S-H/VTMS.01 and C-S-H/VTMS.30 systems, for example, was higher than that of the phase pure C-S-H by 0.13 nm and 0.19 nm, respectively. The mechanism of interaction of organosilanes with the nanostructure of the C-S-H systems was also investigated by the Fourier transform infrared spectroscopy (FTIR) technique (Figure 9-9). The peaks at the frequencies of 889 and 957 cm^{-1} in the FTIR spectra of the C-S-H/VTMS.30 system are assigned to the Si-O stretching of Q^1 and Q^2 tetrahedra, respectively [19]. The intensity of the peak corresponding to Q^1 tetrahedra was significantly lower than that observed in the FTIR spectra of the phase pure C-S-H. The intensity of the peak corresponding to Q^2 tetrahedra was also slightly higher. In addition, a shoulder was detected at the frequency of about 1050 cm^{-1} likely due to the interaction of the silane group in the organosilane with the silicates in the structure of the host C-S-H. A similar band (at 1032 cm^{-1}) was also observed due to the interaction of silane group in the APTES with the montmorillonite clay platelet [20]. The peak at 3640 cm^{-1} was reduced in intensity in the FTIR spectra of the C-S-H/VTMS.30 system. It may have been a result of the formation of some hydrogen bonding between the hydrolyzed organosilane and the structure of the host C-S-H [20]. Additional peaks at the frequencies of 512, 756, 1400 and 1590 cm^{-1} also correspond to the presence of the organosilane in the structure of the C-S-H/VTMS.30

system. Similar peaks were also reported by Minet el. al [21] and Shanmugharaj et al. [20] due to the presence of organosilanes in the C-S-H-based systems and clay minerals, respectively. The change in the FTIR spectra of the C-S-H-based systems with the lower concentration of organosilanes was not significant. The intensity of the peak corresponding to the Si-O stretching of Q^2 tetrahedra (~ 945 cm^{-1}), however, was slightly larger than that observed in the phase pure C-S-H (see Figure 9-9).

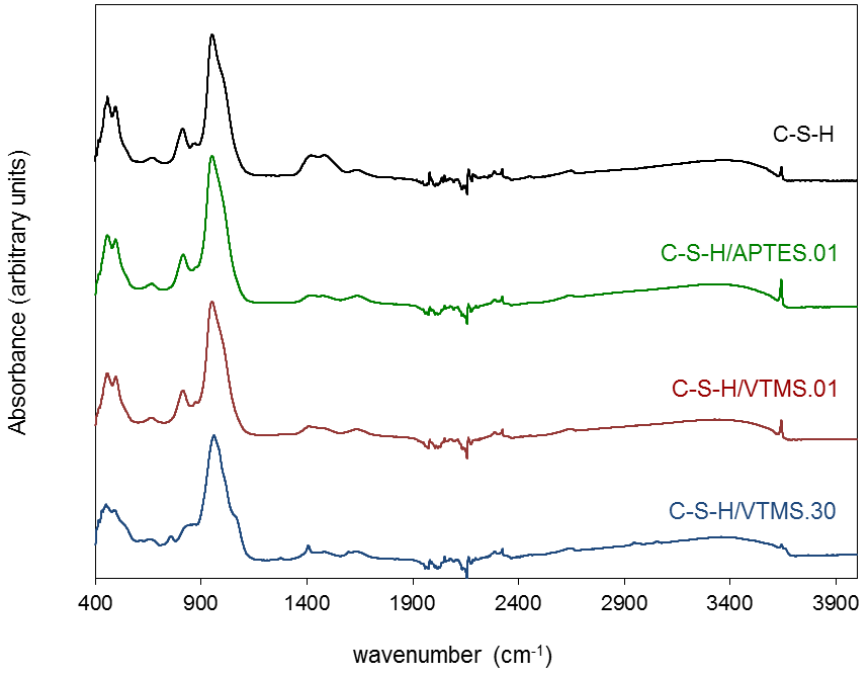

Figure 9-9- FTIR spectra of C-S-H-based systems prepared with organosilanes

The C-S-H-based systems prepared with the organosilanes had poor volume stability in the LiCl solution. The length-change values of the C-S-H/APTES.01 and C-S-H/VMTS.01 systems were higher than that for the phase pure C-S-H by about 160% and 80%, respectively (see Table 9-1). The length-change of the C-S-H/VMTS.30 system was also very fast, and the sample disintegrated within a few seconds after the immersion in the test solution.

In addition to the organic compounds of Table 9-1, pyrrole (C_4H_5N) was used in two different concentrations (0.01 and 0.30 mol. per mol. of Ca) in order to prepare the C-S-H-based systems. An increase of 0.07 nm and 0.10 nm was observed in the basal-spacing of

the C-S-H/pyrrole.01 and C-S-H/pyrrole.30 systems compared to that of the phase pure C-S-H. An attempt to synthesize the C-S-H/polypyrrole using C-S-H/pyrrole.30 and ferric chloride (as the oxidant) by an in-situ polymerization technique was not successful. A similar method was previously used successfully in clay science to prepare conductive polypyrrole/montmorillonite nanocomposites [22-23]. Additional tests are still required to make a conclusion about the possibility of formation of C-S-H/polypyrrole nanocomposites. It is, however, suggested that the preparation of these nanocomposites would be much more difficult than the clay-based nanocomposites possibly due to the higher charge density of the layers in C-S-H systems compared to that in clays [9].

9.4 Conclusions

The influence of three different polymers (PVA, PAA and PMM) on the nanostructure and engineering performance of C-S-H systems was investigated. It is suggested that the selected polymers can be adsorbed between the stacked layers of C-S-H, on the surface or at the edges of the layers. No significant evidence of their intercalation in the interlayer region of the host C-S-H, however, was obtained. In addition, the higher concentration of the polymers acted as inhibitor of the pozzolanic reaction. These results are in conformity with those reported by Popova et al. [8]. In addition, the C-S-H/polymer systems had relatively poor volume stability and mechanical properties likely due to the separation of the organic and inorganic phases in their structure. The C-S-H/PMM.01 system, however, had an improved microindentation creep modulus.

The influence of several other organic compounds (octadecylamine, dicarboxylic acids, fatty acids, organosilanes, etc.) on the X-ray diffraction pattern and the length-change of the C-S-H systems was also investigated. The increase of the basal-spacing of the C-S-H-based systems was relatively small. No evidence of the improvement of the C-S-H systems was obtained due to the use of these organic compounds. The organosilane with the higher concentration, however, likely interacted with the silicate tetrahedra through the silane group, as detected by the FTIR. The volume stability of this system, however, was very poor.

References

1. H. Matsuyama and J. F. Young, "Intercalation of polymers in calcium silicate hydrate: A new synthetic approach to biocomposites?," *Chemistry of Materials*, 11, pp. 16-19, 1999.

2. H. Matsuyama and J. F. Young, "Synthesis of calcium silicate hydrate/polymer complexes: Part I," *Journal of Materials Research*, 14, pp. 3379-3388, 1999.

3. H. Matsuyama and J. F. Young, "Synthesis of calcium silicate hydrate/polymer complexes: Part II," *Journal of Materials Research*, 14, pp. 3389-3396, 1999.

4. H. Matsuyama and J. F. Young, "The formation of C-S-H/polymer complexes by hydration of reactive β-dicalcium silicate," *Concrete Science and Engineering*, 1, pp. 66-75, 1999.

5. J. W. Cho and D. R. Paul, "Nylon 6 nanocomposites by melt compounding," *Polymer*, 42, pp. 1083-1094, 2001.

6. A. Somwangthanaroj, W. Ubankhlong and W. Tanthapanichakoon, "Solid-state mechanical properties of polypropylene/nylon6/clay nanocomposites," *Journal of Applied Polymer Science*, 118, pp. 538-546, 2010.

7. P. Natkanski, P. Kustrowski, A. Bialas, Z. Piwowarska and M. Michalik, "Controlled swelling and adsorption properties of polyacrylate/montmorillonite composites," *Materials Chemistry and Physics*, 136, pp. 1109-1115, 2012.

8. A. Popova, G. Geoffroy, M.-F. Renou-Gonnord, P. Faucon and E. Gartner, "Interactions between polymeric dispersants and calcium silicate hydrates," *Journal of the American Ceramic Society*, 83(10), pp. 2556-2560, 2000.

9. F. Merlin, H. Lombois, S. Joly, N. Lequeux, J.-L. Halary and H. Van Damme, "Cement-polymer and clay-polymer nano- and meso-composites: spotting the difference," *Journal of Materials Chemistry*, 12, pp. 3308-3315, 2002.

10. R. Khoshnazar, J. J. Beaudoin, L. Raki and R. Alizadeh, "Interaction of 2-, 3- and 4-nitrobenzoic acid with the structure of calcium-silicate-hydrate," *Materials and Structures*, under review, 2014.

11. R. Khoshnazar, J. J. Beaudoin, L. Raki and R. Alizadeh, "Durability and mechanical properties of C-S-H/nitrobenzoic acid composite systems," under review, 2014.

12. R. Khoshnazar, J. J. Beaudoin, L. Raki and R. Alizadeh, "Charactristics and engineering performance of C-S-H/aminobenzoic acid composite systems," under review, 2014

13. R. Khoshnazar, J. J. Beaudoin, L. Raki and R. Alizadeh, "Dynamic Mechanical analysis of organically modified calcium-silicate-hydrate systems," under preparation, 2014.

14. J. H., Yeum, "Novel poly(vinyl alcohol)/clay nanocomposite microspheres via suspension polymerization and saponification," *Polymer-Plastics Technology and Engineering*, 50, pp. 1149-1154, 2011.

15. D. J., Greenland, "Adsorption of polyvinyl alcohols by montmorillonite," *Journal of Colloidal Science*, 18, pp. 647-664, 1963.

16. J. Billingham, C. Breen and Yarwood J., "Adsorption of polyamine, polyacrylic acid and polyethylene glycol on montmorillonite: An in situ study using ATR-FTIR," *Vibrational Spectroscopy*, 14, pp. 19-34, 1997.

17. Khoshnazar R, Beaudoin JJ, Raki L, Alizadeh R, Volume stability of C-S-H/polyaniline nanocomposites in aqueous salt solutions. ACI Mat J. (accepted for publication), 2014.

18. R. Khoshnazar, J. J. Beaudoin, R. Alizadeh and L. Raki, "Volume stability of calcium sulfoaluminate phases," *Journal of the American Ceramic Society*, 95(12), pp. 3979-3984, 2012.

19. P. Yu, R. J. Kirkpatrick, B. Poe, P. McMillan and X. Cong, "Structure of calcium silicate hydrate (C-S-H): Near-, mid-, and far-infrared spectroscopy," *Journal of the American Ceramic Society*, 82(3), pp. 742-748, 1999.

20. A. M. Shanmugharaj, K. Y. Rhee and S. H. Ryu, "Influence of dispersing medium on grafting of aminopropyltriethoxysilane in swelling clay materials," *Journal of Colloid and Interface Science*, 298, pp. 854-859, 2006.

21. J. Minet, S. Abramson, B. Bresson, C. Sanchez, V. Montouillout and N. Lequeux, "New layered calcium organosilicate hybrids with covalently linked organic functionalities," *Chemistry of Materials*, 16, pp. 3955-3962, 2004.

22. S. Madakbas, E. Cakmakcı, M. V. Kahraman, K. Esmer, "Preparation, characterisation, and dielectric properties of polypyrrole-clay composites," *Chemical Papers*, 67(8), pp. 1048-1053, 2013.

23. K. Anuar, S. Murali, A. Fariz and H. N. M. M. Ekramul, "Conducting polymer/clay composites: Preparation and characterization," *Materails Sience*, 10(3), 2004, pp. 255-258.

Chapter 10

Volume Stability and Durability of C-S-H/Polyaniline Nanocomposites

The volume stability of phase pure C-S-H and C-S-H/polyaniline nanocomposites prepared with two different Ca/Si ratios (0.8 and 1.2) was assessed in $MgSO_4$, $MgCl_2$, LiCl and NaCl aqueous solutions. The change in the crystalline structure of the samples with the time of immersion was also explored using the X-ray diffraction, scanning electron microscopy and thermal gravimetric analysis techniques. It was observed that the modification of the C-S-H samples with polyaniline significantly enhanced their volume stability and durability in all the salt solutions. The beneficial effect of the polyaniline modification was more pronounced in the C-S-H host with higher Ca/Si ratio (Ca/Si =1.2). The longitudinal expansion of the C-S-H/polyaniline nanocomposites with Ca/Si = 1.2 in the salt solutions was about 30% of that of the pure C-S-H with a similar Ca/Si ratio. In addition, the polyaniline modification of C-S-H samples reduced the rate of formation of gypsum, brucite and other reaction products in the samples.

10.1 Introduction

The development of new C-S-H-polyaniline nanocomposites has recently been reported by Alizadeh et al. [1]. The synthesis involved an in-situ polymerization technique that allows for an initial interaction of monomers with the C-S-H followed by polymerization using an external oxidant. The C-S-H/aniline and C-S-H/polyaniline samples were characterized by the X-ray diffraction, ^{29}Si NMR, thermal analysis, Fourier transform infrared spectroscopy

and scanning electron microscopy techniques. Evidence was obtained in support of the view that the aniline and polyaniline were formed in two different locations of the C-S-H i.e. grafted on the surface and partially intercalated in the interlayer regions. It was also suggested that the polyaniline might be arranged between the C-S-H layers in a way that the benzene ring was oriented parallel to the sheets. The monomer molecules, however, had random positions in various directions. A schematic picture of aniline monomer (C_6H_7N) and polyaniline $(C_6H_7N)_n$ are presented in Figure 10-1.

Figure 10-1- Schematic picture of aniline monomers (C_6H_7N) and polyaniline $(C_6H_7N)_n$

Key objectives inherent in the development of C-S-H nanocomposites are the realization of enhanced engineering properties and improvement in the durability characteristics of cement-based materials. This chapter focuses on the latter. The primary objective is to demonstrate that polymer C-S-H nanocomposites can improve the volume stability of cement-based materials in aggressive media. The results of length-change and microstructural change of C-S-H/polyaniline nanocomposites in aqueous salt solutions ($MgSO_4$, $MgCl_2$, LiCl and NaCl) typical of those central to many durability issues are reported. An assessment of the ability of the polymer to 'seal' the C-S-H system from the ingress of deleterious ionic species is presented.

10.2 Experimental program

10.2.1 Materials

Phase pure C-S-H and C-S-H/polyaniline nanocomposites (Ca/Si = 0.8 and 1.2) as synthesized by Alizadeh et al. were used in this study. The synthesis method described by these researchers was as follows [2]. Stoichiometric amounts of calcium oxide (CaO) and silica (SiO_2) were mixed in excess water (water/solid mass ≈ 10) in order to prepare the

phase pure C-S-H. The CaO was freshly calcined from the reagent grade calcium carbonate (Sigma-Aldrich) at 900 °C. Reactive SiO_2 (CAB-O-SIL®, grade M-5 from Cabot Corporation) was heated at 110 °C in order to remove any surface adsorbed water. De-ionized out-gassed water was added to the solid mixture of CaO and SiO_2. C-S-H/aniline powder was also prepared in a method similar to that used for the phase pure C-S-H except that the water contained aniline monomer (2 ml of aniline in 75 ml of water). This solution was, then, added to the dry mix of the CaO and SiO_2 in the high density polyethylene (HDPE) bottles to initiate the pozzolanic reaction. All the bottles were mounted on a rotating rack (speed = 16 rpm). The solution was filtered after 90 days. The drying procedure of these samples included two steps; four days of vacuum drying followed by conditioning in desiccators at the relative humidity of 11%. Both steps were performed at room temperature (about 24 °C). The samples were considered to be in equilibrium when they reached a constant mass.

Ammonium persulfate ($(NH_4)_2S_2O_8$ from Sigma-Aldrich, 98% purity) was used as an external oxidant in order to polymerize the aniline monomers. Dried C-S-H/aniline powder (0.5 g) was first mixed in 100 ml of water using a magnetic stirrer. Then, 0.228 g of ammonium persulfate was added during stirring the suspension solution. The stirring was continued for three days at room temperature. The final material was filtered and washed to remove the unreacted ions. It was, then, dried under vacuum at room temperature for four days, and then equilibrated at the relative humidity of 11%. It was estimated, based on the thermal analysis, that the polyaniline content was about 3% in the C-S-H/polyaniline preparations.

10.2.2 Test solutions

The test solutions prepared for the dimensional stability and durability assessments included $MgSO_4$ (hepahydrate), $MgCl_2$ (decahydrate), LiCl and NaCl with the concentration of 15 g/l. All the salts were reagent grade.

10.2.3 Experiments

Circular compacted samples of the phase pure and modified C-S-H powders with the porosity of about 30% were prepared by the technique described in chapter 3. Prisms (5 mm × 25 mm × 1 mm) were cut from the compacted discs and mounted on modified Tuckerman extensometers with an accuracy of 1 microstrain. These were, then, placed in small containers including the test solutions so that the specimens were completely immersed. The ratio of the solid to the solution was 1 g of solid per 50 ml of the solution. The whole set-up was placed in sealed desiccators containing the same salt solution as the test solution to avoid evaporation. The length-change of the samples in each solution was measured at least for 7 days as almost all the samples exhibited a plateau in the length-change versus time curves at this age. A schematic of the set-up for length-change measurements was presented in Figure 3-5. The length-change measurements were repeated two times on two different samples.

In addition to the length-change measurements, several samples of the C-S-H preparations were immersed in the test solution for 2 h, 8 h, 1 d, 3 d and 24 d to investigate any change in the microstructure of the samples during the time of immersion. The solid/solution ratio in this case was exactly the same as the one in the length-change measurements. The solution was filtered, and the powder was kept at the relative humidity of 11% for 48 hours to reach equilibrium before starting the characterization by the X-ray diffraction (XRD), scanning electron microscopy (SEM), and thermal gravimetric analysis (TGA).

The XRD patterns were obtained using a Scintag XDS 2000 diffractometer. The patterns were collected with a diffraction angle range of $6^\circ < 2\theta < 60^\circ$ using a step size of 0.08° at a 5 second count interval. Intensities were, then, normalized according to the mass of the samples. SEM images were collected using a Hitachi S-4800 Field Emission Scanning Electron Microscope. Surface structure images were taken using a beam current of 10 mA at 3.2×10^{-16} J (2 kV). Images were obtained at a working distance of 4 mm. TGA was performed using a TA Instruments SDT Q-600. About 30 mg of the sample was heated from room temperature to 1000 °C at a rate of 10 °C/min under the flow of nitrogen gas

(10 ml/min). The derivative mass loss and heat flow were analyzed using Universal Analysis 2000 software.

10.3 Results and discussions

10.3.1 Length-change measurements

All the samples expanded following immersion in the salt solutions. The amount of expansion, however, was noticeably different for the pure C-S-H samples and the nanocomposites. It is suggested based on the length-change versus time curves plotted in Figure 10-2 that the expansion of pure C-S-H(1.2) samples was quite significant in all the solutions. The expansion of this sample in $MgSO_4$, for example, was about 3.4% after 7 days. The expansion of modified C-S-H(1.2) samples in all the test solutions was considerably lower than that of the C-S-H(1.2) itself. The 7-day expansion of the C-S-H(1.2)/aniline samples in different solutions was about 37% to 52% of that observed for the phase pure C-S-H(1.2). The C-S-H(1.2)/polyaniline samples were even more stable. The expansion of the C-S-H(1.2)/polyaniline samples after 7 days was about 20% to 30% of the expansion of phase pure C-S-H (1.2).

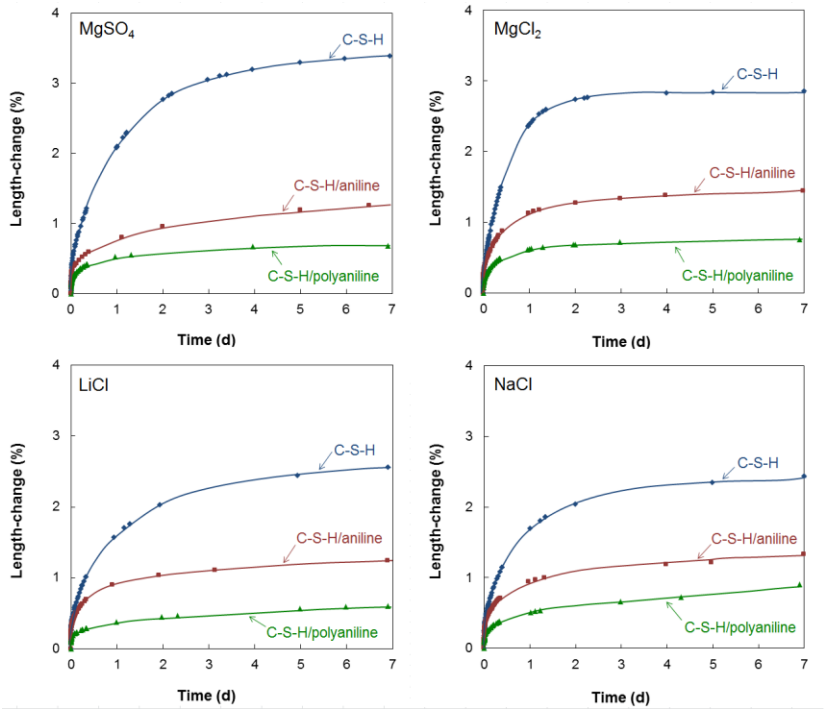

Figure 10-2- Length-change of the pure C-S-H, C-S-H/aniline and C-S-H/polyaniline samples (Ca/Si = 1.2) in the aqueous solutions

It is suggested that dissolution and leaching of lime from the structure is likely the main mechanism responsible for the expansion of C-S-H preparations in the salt solutions. The dissolution process of porous materials, which includes break-down of the structure and leaching of the constituent ions into the solution [3], was previously shown to be an expansive process for porous glass samples immersed in sodium hydroxide and cement paste samples treated with acids [4, 5]. It was suggested that expansion accompanying dissolution can be caused by changes to the surface free energy of the solid phase, gradients in the concentration of dissolved species in the pore solution resulting in osmotic-like pressures, disjoining pressure resulting from double layer effects outside the surface generating repulsive forces and release of strain-energy stored in the sample [5]. Beaudoin et al. [6, 7] also suggested that samples of cement paste or calcium hydroxide can expand in aggressive solutions due to the dissolution process.

Intercalation of some water molecules into the layered structure of C-S-H may be a source of expansion although at 11% relative humidity many of the interlayer positions are filled [8]. Lime leaching, however, results in some defect points in the structure of C-S-H which can facilitate the entry of water molecules and ionic species into the interlayer space. The entry of ionic species into the interlayer region of the C-S-H structure can also cause expansion [9]. Adsorption on hydrated silicate surfaces is generally expansive. This is commonly known as the Bangham effect which relates length-change to change in surface free energy [8]. It has, however, been previously shown that the effect of surface adsorption on the expansion of hydrated Portland cement is less significant than the effect of lime-leaching and intercalation phenomena [8, 10]. Formation of gypsum and brucite crystals on the samples immersed in the sulfate and magnesium salt solutions may also be expansive. There is not, however, a general agreement on the possibility of expansion of C-S-H due to the formation of these crystals [9, 11, 12]. The formation of these crystalline products on the samples will be discussed in greater detail later.

The lower expansion of modified C-S-H(1.2) samples is possibly due to its higher level of silicate polymerization, and the fewer defects in their structure due to the shielding effect of organic materials adsorbed at the defect locations on the surface of the C-S-H [1, 13]. The defects can serve as the access points for the migration of water molecules and ionic species into the layered structure of C-S-H. The fewer the defects, the lower the rate of

entry of water molecules and ionic species into the interlayer space. In addition, the rate of dissolution of lime from the C-S-H structure would be slower as the entry of the interlayer water occurs primarily at the end of the layers [10]. Either of these mechanisms can result in the reduction of the expansion.

The length-change versus time of immersion in the salt solutions for the pure and modified C-S-H(0.8) samples is presented in Figure 10-3. C-S-H(0.8)/polyaniline nanocomposites had an improved volume stability compared to the phase pure C-S-H(0.8). The expansion of C-S-H(0.8)/polyaniline nanocomposite samples after 7 days of immersion in the salt solutions was about 40% to 50% of that observed for the pure C-S-H samples depending on the type of the salt solutions. The intercalation of aniline monomers was not as effective as the polymers. The expansion of C-S-H(0.8)/aniline was about 80% to 95% of that of the phase pure C-S-H.

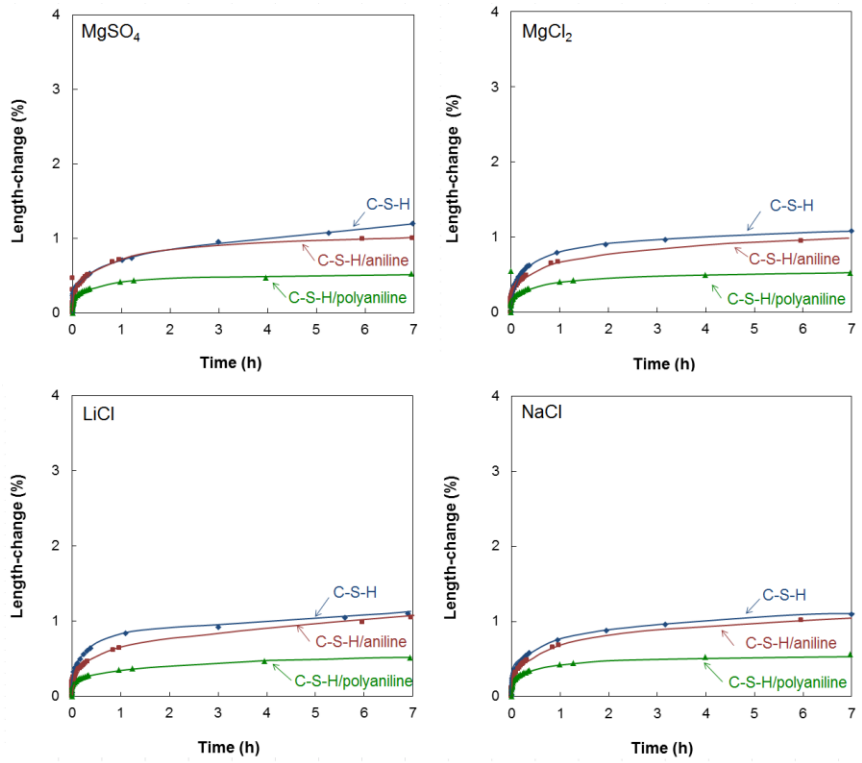

Figure 10-3- Length-change of the pure C-S-H, C-S-H/aniline and C-S-H/polyaniline samples (Ca/Si = 0.8) in the aqueous solutions

The influence of aniline and polyaniline intercalation in the control of the expansion of C-S-H(0.8) is also likely due to its effect on increasing the silicate polymerization level as described above for the C-S-H(1.2). It should also be noted based on comparison of Figure 10-2 and Figure 10-3 that the expansion of pure and modified C-S-H(0.8) samples was generally lower than that of the samples with Ca/Si = 1.2. This was expected considering the higher silicate chain length and the greater frequency of bridging tetrahedra occurring in the structure of low lime C-S-H(0.8) [13] which in turn makes its structure more resistant to the intercalation of water molecules and ionic species.

10.3.2 Microstructural characterization of samples with Ca/Si = 1.2

Immersion in $MgSO_4$ solution

The microstructure of phase pure C-S-H, C-S-H/aniline and C-S-H/polyaniline samples was characterized by the XRD, TGA and SEM after 2 h, 8 h, 1 d, 3 d and 7 d of immersion in the $MgSO_4$ solution. Sharp peaks of gypsum crystals were detected in the XRD pattern of phase pure C-S-H as early as 2 h after immersion in $MgSO_4$ solution. No gypsum peaks were detected in the XRD pattern of the samples with aniline and polyaniline at this early immersion time. These peaks with very low intensity, however, were detected in the XRD patterns of C-S-H/aniline and C-S-H/polyaniline samples after 8 h as shown in Figure 10-4. In addition to gypsum, brucite was also formed in the pure C-S-H(1.2) sample, but not in the samples modified by aniline or polyaniline after 8 h of immersion in $MgSO_4$ (Figure 10-4). The formation of gypsum and brucite crystals is an indication of lime-leaching from the phase pure C-S-H sample. It is, therefore, suggested that the lime-leaching would be limited in the C-S-H/aniline and C-S-H/polyaniline samples.

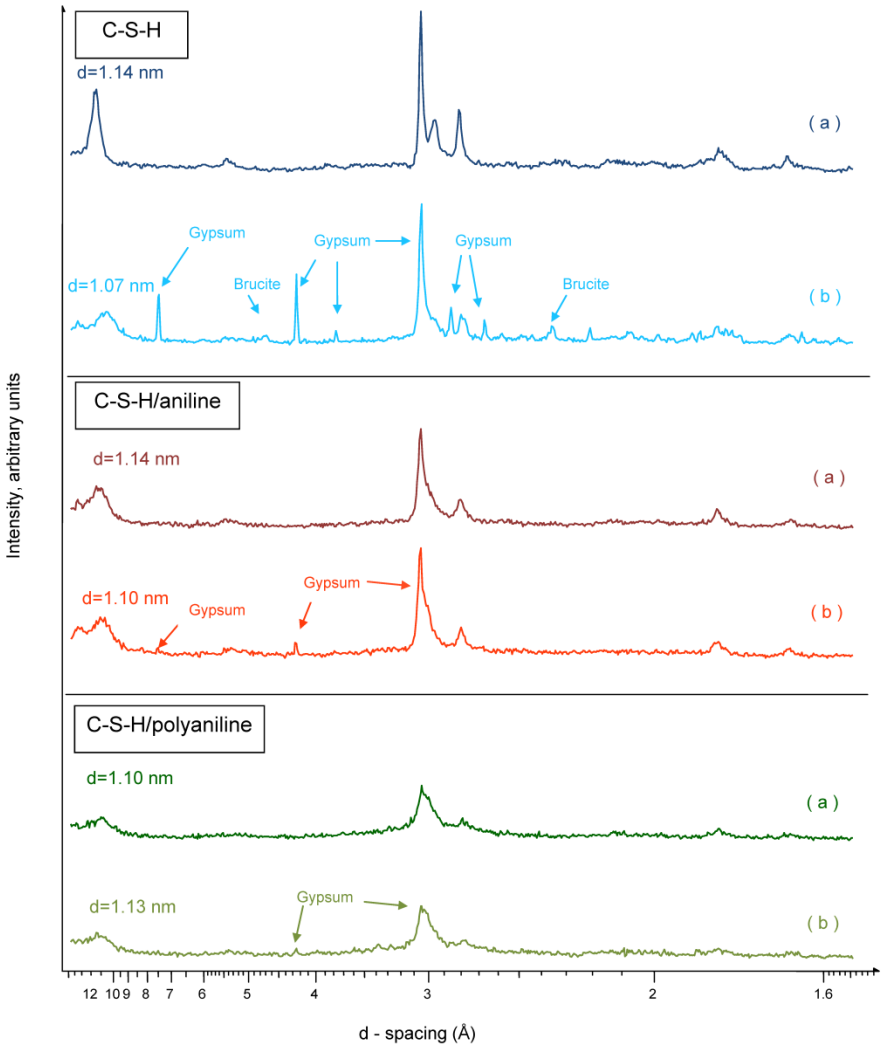

Figure 10- 4- XRD patterns of (a) control phase pure C-S-H, C-S-H/aniline and C-S-H/polyaniline samples (Ca/Si = 1.2), and (b) the samples immersed in the $MgSO_4$ solution for 8 h

It was also suggested based on the XRD patterns of Figure 10-4 that the intensity of the peak at the basal spacing of 1.14 nm of the pure C-S-H(1.2) was significantly reduced once the sample was immersed in the $MgSO_4$. This indicates the reduction of the crystallinity of the pure C-S-H sample after immersion in the $MgSO_4$ solution which can be caused by leaching of lime from this sample. The intensity of the peak corresponding to the d_{002} basal spacing of the C-S-H(1.2)/aniline and C-S-H(1.2)/polyaniline, however, was not noticeably changed by the immersion in the $MgSO_4$ solution.

The SEM micrographs for the samples immersed in $MgSO_4$ after 8 h of immersion are presented in Figure 10-5. Gypsum crystals are detected in the phase pure C-S-H and C-S-H(1.2)/aniline samples. No sign of the formation of gypsum crystals was detected in the C-S-H(1.2)/polyaniline sample tested by the SEM.

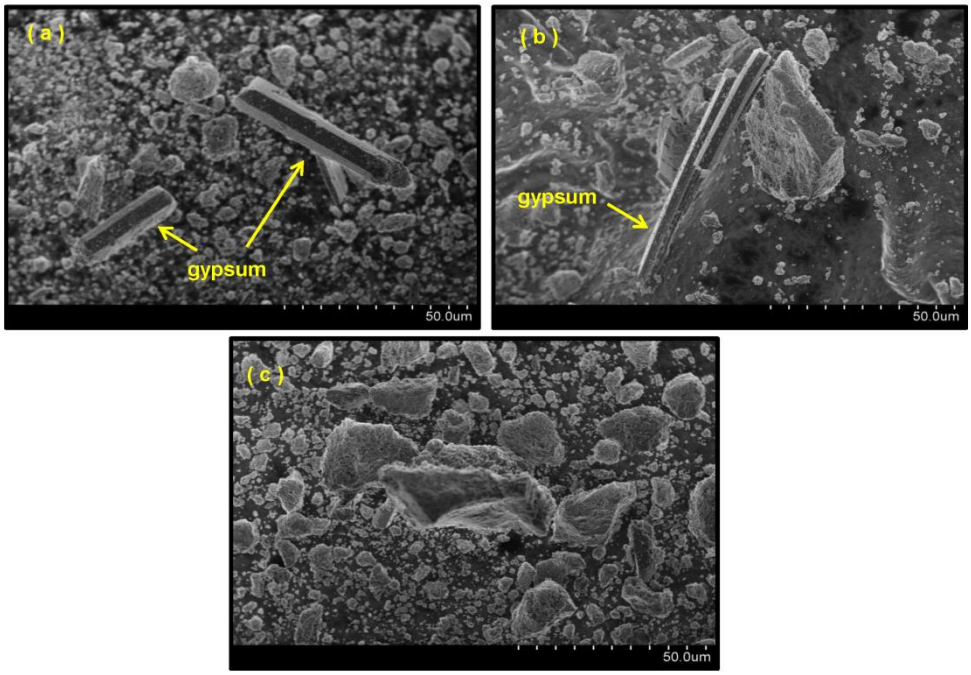

Figure 10-5- SEM micrographs of (a) phase pure C-S-H, (b) C-S-H/aniline and (c) C-S-H/polyaniline samples (Ca/Si = 1.2) immersed in the $MgSO_4$ solution for 8 h

The formation of new crystalline products due to the immersion of the samples in $MgSO_4$ solution was quantitatively examined using the TGA technique (Figure 10-6). The percentages of gypsum and brucite formed on the samples are provided in Table 10-1. It is known that gypsum decomposes at temperatures of about 130 °C [14]. Brucite decomposes at a temperature of about 385 °C [15]. It is possible to capture the formation of even a small percentage of these crystals in the sample by the TGA. It is suggested that about 7.3% of gypsum and 1.1% of brucite was formed in the phase pure C-S-H(1.2) after 8 h of immersion in $MgSO_4$. These amounts were reduced to 1.1% (gypsum) and 0.58% (brucite) for the sample with aniline, and 0.90% (gypsum) in the sample with polyaniline. No brucite was detected by the TGA in the C-S-H(1.2)/polyaniline.

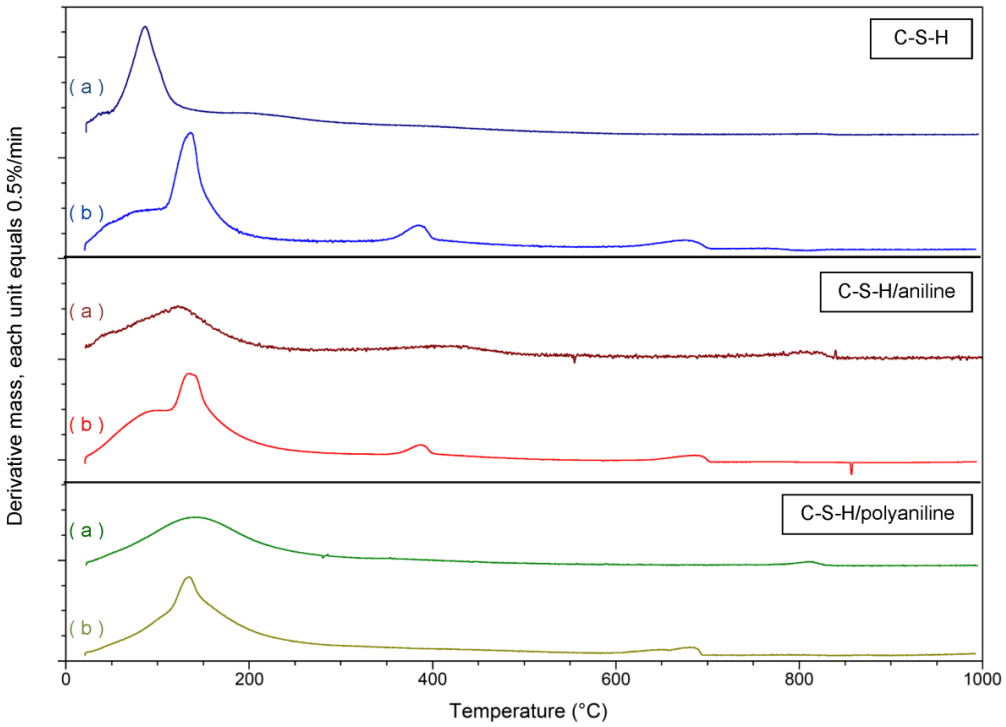

Figure 10-6 - TGA curves of (a) control phase pure C-S-H, C-S-H/aniline and C-S-H/polyaniline samples (Ca/Si = 1.2), and (b) the samples immersed in the $MgSO_4$ solution for 8 h.

Table 10-1 - Percentage of gypsum and brucite crystals formed in the C-S-H(1.2) preparations due to the 8 h of immersion $MgSO_4$ estimated by the TGA technique

Sample	**Amount of gypsum and brucite formed (% by mass)**	
	Gypsum	**Brucite**
C-S-H	7.3	1.1
C-S-H/aniline	1.1	0.58
C-S-H/polyaniline	0.9	-

Immersion in $MgCl_2$ solution

The XRD patterns of pure and modified C-S-H(1.2) immersed in $MgCl_2$ for 7 days are presented in Figure 10-7. The intensity of the d_{002} basal spacing of the phase pure C-S-H(1.2) sample was significantly reduced due to the immersion in the $MgCl_2$ solution which is an indication of significant lime-leaching and collapse of the microstructure of this sample. In addition, peaks corresponding to brucite were detected on this sample. The d_{002} basal spacing of the C-S-H(1.2)/aniline sample was also reduced in intensity due to the immersion in $MgCl_2$ due to the lime-leaching. No brucite, however, was detected in this sample by the XRD. The d_{002} basal spacing of the C-S-H(1.2)/polyaniline sample was unchanged by the immersion in the $MgCl_2$ solution. Brucite peaks were not detected in this sample either. This is in conformity with the length-change results suggesting the significant enhancement of volume stability of C-S-H(1.2)/polyaniline samples compared with that of the C-S-H/aniline and the pure C-S-H samples with similar Ca/Si ratios.

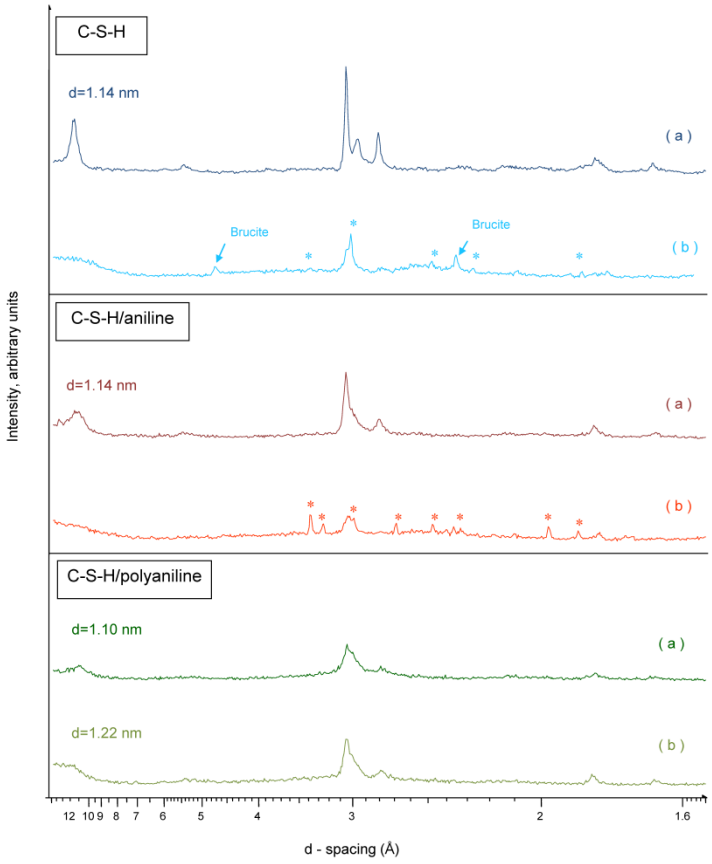

Figure 10-7- XRD patterns of (a) control phase pure C-S-H, C-S-H/aniline and C-S-H(1.2)/polyaniline samples, and (b) the samples immersed in the $MgCl_2$ solution for 7 d. * These peaks correspond to calcium carbonate crystals.

Additional peaks were observed in the XRD patterns of the samples immersed in $MgCl_2$, especially in the XRD patterns of C-S-H and C-S-H/aniline. These peaks correspond to calcium carbonate crystals which were formed due to the reaction of calcium leached out of the sample and carbonate in the air during the preparation of the samples for the test. The rapid formation of calcium carbonate crystals in the samples is also a result of lime-leaching. The rate of formation of calcium carbonate crystals is also affected by the specific surface area of the samples. The nitrogen Brunauer-Emmett-Teller (BET) surface area of C-S-H(1.2)/aniline was 107.6 m^2/g which was considerably higher than that for phase pure C-S-H (41.4 m^2/g) and C-S-H/polyaniline (54.3 m^2/g) with similar Ca/Si ratio. No significant change could be detected by the SEM in the morphology of these samples after the immersion except the formation of some calcium carbonate crystals on the surface of the samples (Figure 10-8). Calcium carbonate crystals were mainly formed in the form of calcite and aragonite on the phase pure C-S-H and C-S-H/polyaniline samples, respectively. Both of these crystals were, however, detected on the C-S-H/aniline sample. This might be due to the changes in the surface area of the samples, concentration of lime leached out of the samples as well as the pH in different solutions which could favor the formation of one crystal rather than the other.

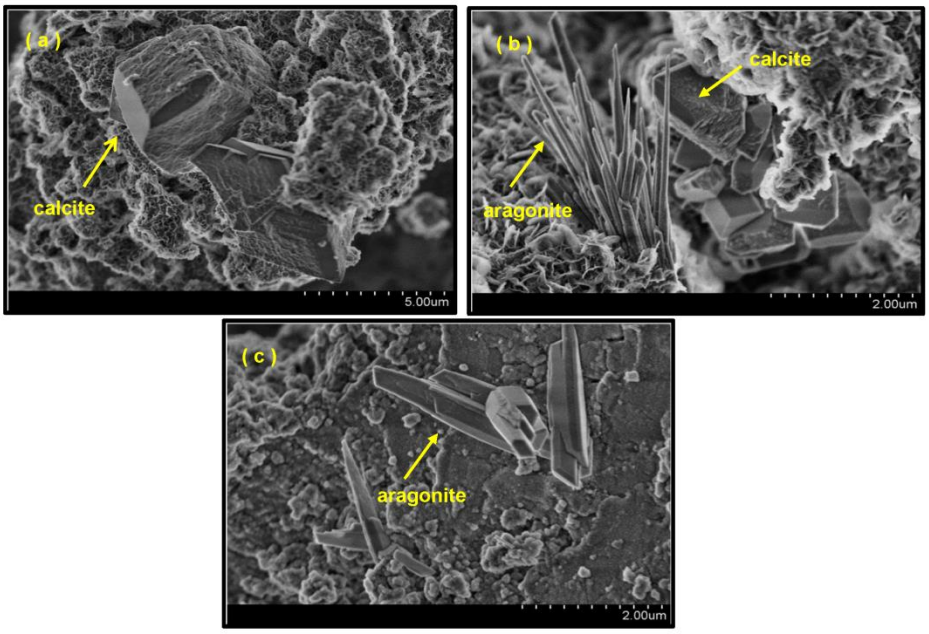

Figure 10-8- SEM micrographs of (a) phase pure C-S-H, (b) C-S-H/aniline and (c) C-S-H(1.2)/polyaniline samples immersed in the $MgCl_2$ solution for 7 d.

Results obtained using the TGA technique for the C-S-H(1.2)-based samples immersed in $MgCl_2$ were also in conformity with those of the other techniques suggesting the greater resistance of C-S-H/aniline and especially C-S-H/polyaniline samples to the formation of new crystalline products compared to that of phase pure C-S-H (Figure 10-9). The amount of brucite based on the TGA was estimated as 1.7% for the phase pure C-S-H(1.2) and 0.28% for the C-S-H(1.2)/aniline. No brucite was detected in the sample with polyaniline.

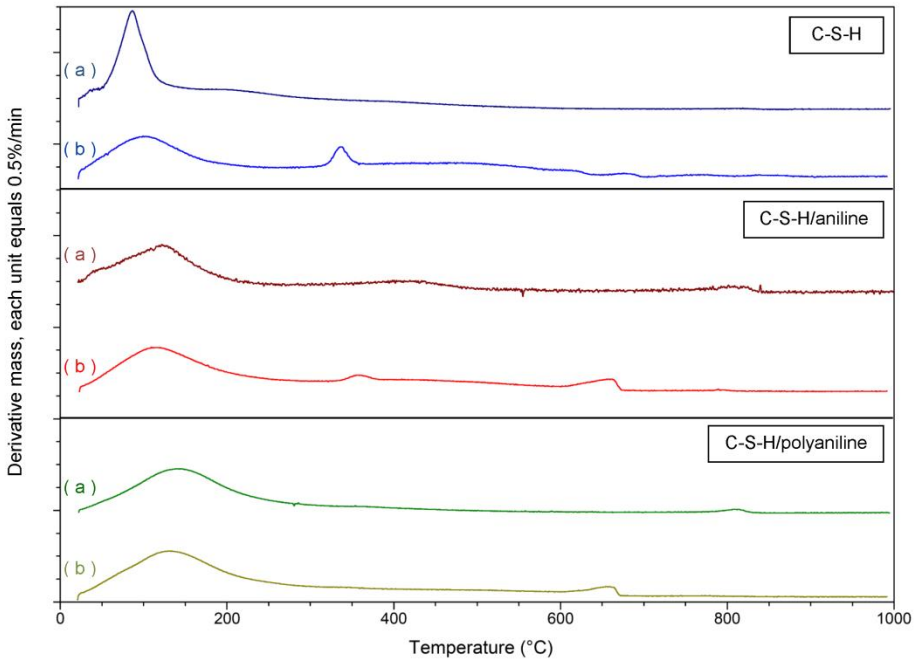

Figure 10-9- TGA curves of (a) control phase pure C-S-H, C-S-H/aniline and C-S-H(1.2)/polyaniline samples, and (b) the samples immersed in the $MgCl_2$ solution for 7 d.

Immersion in LiCl and NaCl solutions

The XRD patterns of the C-S-H(1.2) samples immersed in the LiCl and NaCl solutions after 7 days did not show any significant change in the crystalline structure except the formation of some calcium carbonate peaks which had a considerably lower intensity in the C-S-H/polyaniline compare to that in phase pure C-S-H and C-S-H(1.2)/aniline. The XRD patterns of these samples immersed in LiCl solution for 7 days are presented in Figure 10-10. Less damage to the crystalline structure of the samples immersed in LiCl and NaCl solutions compared to those in $MgSO_4$ and $MgCl_2$ solutions is in conformity with the

length-change measurements suggesting the greater volume stability of the samples immersed in the two former solutions.

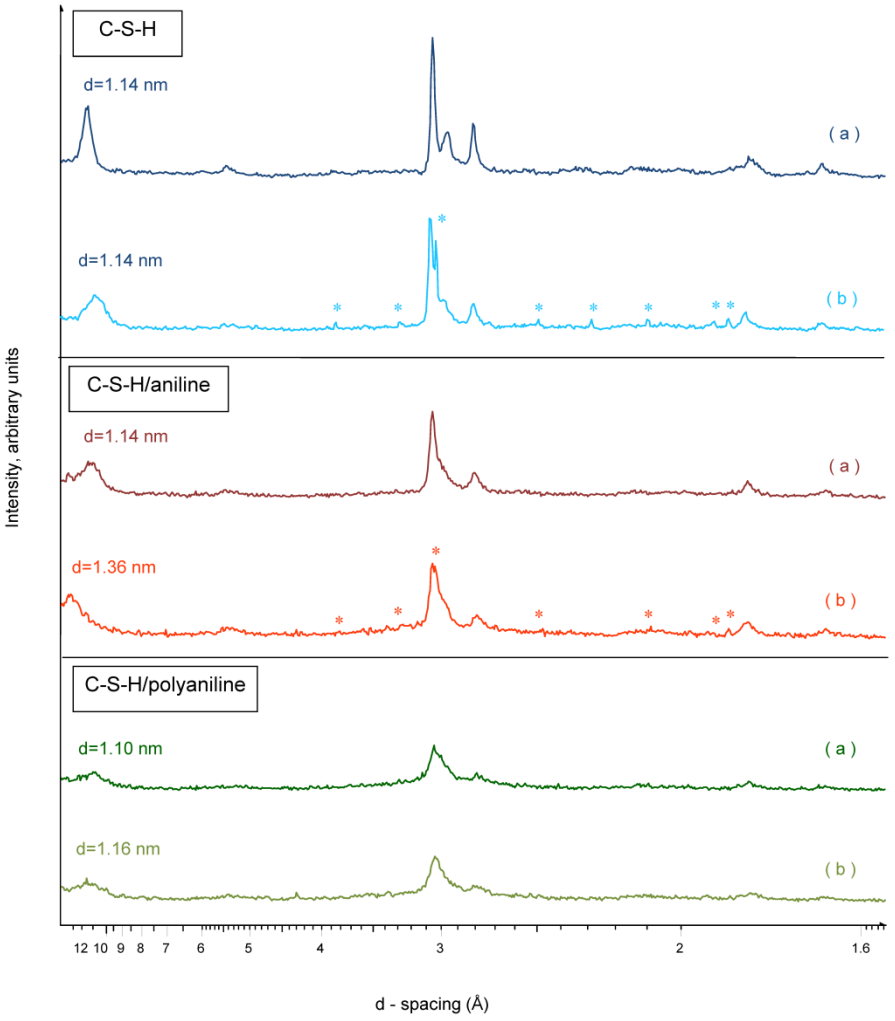

Figure 10-10- XRD patterns of (a) control pure C-S-H, C-S-H/aniline and C-S-H/polyaniline samples (Ca/Si = 1.2), and (b) the samples immersed in the LiCl solution for 7 d. * These peaks correspond to calcium carbonate crystals.

The results of SEM and TGA techniques for the C-S-H(1.2)-based samples immersed in LiCl and NaCl solutions did not show any significant change in the microstructure of the samples except the formation of calcium carbonate crystals. The quick formation of these crystals is an indication of lime-leaching of the samples. The results of these two techniques also support the argument that the amount of calcium carbonates formed on the C-S-H(1.2)/polyaniline was considerably less that that formed in phase pure C-S-H(1.2) and C-S-H(1.2)/aniline sample.

10.3.3 Microstructural Characterization of samples with Ca/Si = 0.8

Characterization by the XRD, SEM and TGA was also performed on the C-S-H(0.8) preparations immersed in various aggressive solutions for different time intervals (2 h to 7 d). No evidence of formation of new products was detected by the XRD technique for the C-S-H(0.8) samples after 8 hours of immersion in $MgSO_4$. The XRD patterns showed that gypsum crystals were formed on the pure C-S-H(0.8) sample after 1 day of immersion. The gypsum formation, however, was delayed to about 3 days for the C-S-H/aniline and to about 7 days for the C-S-H(0.8)/polyaniline samples. The XRD patterns of pure and modified C-S-H(0.8) samples immersed in $MgSO_4$ for 7 days are compared in Figure 10-11. It is suggested, based on the data in the figure, that the modified C-S-H(0.8) performed better than the pure C-S-H(0.8) in the $MgSO_4$ solution. The gypsum peaks formed after 7 days in the C-S-H(0.8)/aniline sample were significantly less intense than those formed in the phase pure C-S-H(0.8) sample. These peaks were almost negligible for the C-S-H(0.8)/polyaniline sample after 7 days of immersion. No brucite peaks were detected on any of the samples even after 7 days. These results were also confirmed by the SEM and TGA.

The microstructure of the samples (the phase pure or the modified C-S-H(0.8) sample) was almost unchanged up to 7 days of immersion in other solutions. The improvement of the durability of the C-S-H(0.8) samples by the aniline or polyaniline modification was not, therefore, readily discernible although the length-change curves provide clear evidence that modified systems are superior. It is suggested that the damage to the microstructure of the samples with Ca/Si = 0.8 was generally less than that of the samples with Ca/Si = 1.2 samples. It confirms the results of the length-change measurements. It is due to the higher degree of polymerization in the samples with lower Ca/Si ratio.

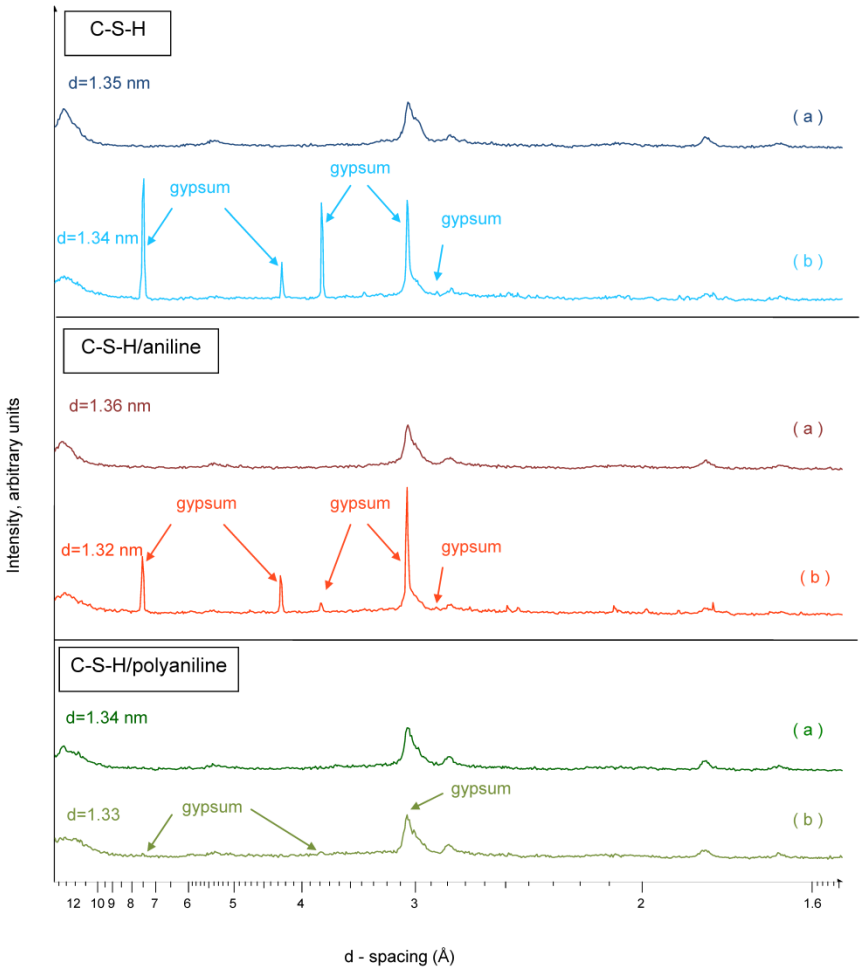

Figure 10-11- XRD patterns of (a) control phase pure C-S-H, C-S-H/aniline and C-S-H/polyaniline samples (Ca/Si = 0.8), and (b) the samples immersed in the $MgSO_4$ solution for 7 d

10.4 Conclusions

The length-change of the phase pure C-S-H and C-S-H modified with aniline and polyaniline due to immersion in the $MgSO_4$, $MgCl_2$, LiCl and NaCl aqueous solutions was assessed. The formation of crystalline products on the samples was also explored by the XRD, SEM and TGA techniques. Two different Ca/Si ratios (Ca/Si = 0.8 and 1.2) were considered. The main conclusions are as follows:

1. Lime-leaching from the structure of C-S-H samples, especially from the high lime samples, is likely to be a main mechanism underlying their expansion in the salt solutions studied.

2. The formation of new products, e.g. gypsum and brucite, and generation of pressure due to crystal growth or swelling pressure due to intercalation phenomena are possible additional mechanisms that may contribute to expansion.
3. The expansion of C-S-H nanocomposites in the test solutions was considerably lower than that of the pure C-S-H.
4. The formation of crystalline products, e.g. gypsum and brucite, was limited in the C-S-H/aniline and C-S-H/polyaniline samples.
5. Modification of C-S-H with aniline and polyaniline is more effective in improving the volume stability when the host C-S-H has a higher Ca/Si ratio.
6. Intercalation of polyaniline within the C-S-H layers (for both Ca/Si ratios) had a greater effect on the volume and microstructural stability of the C-S-H samples compared to that of aniline monomers.

References

1. R. Alizadeh, J. Beaudoin, L. Raki and V. Terskikh, "C-S-H/polyaniline nanocomposites prepared by in situ polymerization," *Journal of Materials Science*, 46(2), pp. 460-467, 2011.
2. R. Alizadeh, Nanostructure and engineering properties of basic and modified calcium silicate hydrate systems, PhD Thesis, University of Ottawa, 2009.
3. S. Békri, J. F. Thovert, P. M. Adler, "Dissolution of porous Media," *Chemical Engineering Science*, 50, pp. 2765-2791, 1995.
4. G. G. Litvan, "Volume instability of porous solids: Part 1"; In Proceedings of the 7th International Congress on the Chemistry of Cement, Paris, Vol. III, pp. 46-50, 1980.
5. G. G. Litvan, "Volume instability of porous solids: Part 2. Dissolution of porous silica glass in sodium hydroxide," *Journal of Materials Science*, 19(8), pp. 2473-2480, 1984.
6. J. J. Beaudoin, S. Catinaud, J. Marchand and T. Sato, "Volume stability of hydrated Portland cement exposed aggressive solutions," *Industria Italiana del Cemento*, 72, pp. 954-967, 2002.

7. J. J. Beaudoin, S. Catinaud and J. Marchand, "Volume stability of calcium hydroxide in aggressive solutions," *Cement and Concrete Research*, 31(1), pp. 149-151, 2001.

8. R. F. Feldman, "Sorption and length change scanning isotherms of methanol and water on hydrated Portland cement," In Proceedings of the 5th International Symposium on the Chemistry of Cement, Tokyo, Vol. III, pp. 53-66, 1986.

9. H. Drame´, J. J. Beaudoin and L. Raki, "Comparative study of the volume stability of C-S-H (I) and Portland cement paste in aqueous salt solutions," *Journal of Materials Science*, 42, pp. 6837-6846, 2007.

10. J. J. Beaudoin, B. Patarachao, L. Raki, J. Margeson and R. Alizadeh, "Length-change of C-S-H of variable composition immersed in aqueous solutions," *Advances in cement Research*, 22(1), pp. 15-19, 2010.

11. B. Tian and M. D. Cohen, "Does gypsum formation during sulfate attack on concrete lead to expansion?" *Cement and Concrete Research*, 30(1), pp. 117-123, 2000.

12. M. D. Cohen and B. Mather, "Sulfate attack on concrete - Research needs," *ACI Materials Journal*, 88(1), pp. 62-69, 1991.

13. J. J. Beaudoin, L. Raki and R. Alizadeh, "A ^{29}Si MAS NMR study of modified C-S-H nanostructures," *Cement and Concrete Composites*, 31(8), pp. 585-59, 2009.

14. V. S. Ramachandran, R. M. Paroli, J. J. Beaudoin and A. H. Delgado, Handbook of Thermal Analysis of Construction Materials, Noyes Publication, New York, 2002.

15. V. S. Ramachandran, D. Phil, Applications of differential thermal analysis in cement chemistry, Chemical publishing company, INC. New York, 1969.

Chapter 11

Dynamic Mechanical Thermal Analysis of C-S-H/Polyaniline Nanocomposites

The focus of this chapter is on the dynamic mechanical thermal analysis (DMTA) of C-S-H/polyaniline nanocomposites. DMTA experiments were recently performed by Alizadeh [1] on the synthetic C-S-H/polyaniline nanocomposites (Ca/Si = 0.8 and 1.2). The variations of the storage modulus (E') and internal friction (tan δ) were reported upon heating to 200 °C. A discussion of the results obtained is provided in this chapter. The results are also compared with the DMTA results obtained for the C-S-H systems modified with nitrobenzoic acid or aminobenzoic acid (chapter 7). It is suggested that the polyaniline compounds likely reinforce the C-S-H layered structure during the dehydration up to about 45 °C. No improvement, however, occurs at higher temperatures.

11.1 Introduction

Characterization of the nanostructure of C-S-H has been the focus of numerous research investigations in the past two decades as it is considered fundamental to the ultimate resolution of problems associated with the durability and sustainability of concrete infrastructure [2-4]. The possibility of 'tailoring' the nanostructure of C-S-H in cement binders to improve mechanical behavior and resistance to aggressive media is feasible and rapidly evolving. Examples include 'designing' the Ca/Si ratio of the C-S-H in cement paste through the use of C-S-H 'seeds' and the development of organo-C-S-H nanocomposites [5, 6].

The C-S-H-polyaniline nanocomposites are among the novel organically modified C-S-H systems. These nanocomposites have been recently developed by Alizadeh et al. [1, 6] using an in-situ polymerization technique. The synthesis procedure included an initial interaction of aniline monomers with the C-S-H structure followed by polymerization using ammonium persulfate as the oxidant. The synthetic C-S-H/polyaniline systems were characterized by various analytical techniques. Evidence of the interaction of aniline and polyaniline with the nanostructure of C-S-H (i.e. surface grafting and partially intercalation) was reported. Preliminary results of the physical and mechanical stability of the C-S-H/polyaniline nanocomposites in comparison with those of the phase pure C-S-H were also reported [1]. The main objective of this chapter is to provide detailed discussions of the dynamic mechanical thermal analysis of the C-S-H/polyaniline nanocomposites based on the experimental data previously obtained for these nanocomposites or pure polyaniline as well as those determined in this thesis for the C-S-H systems modified with nitrobenzoic acid or aminobenzoic acid (chapter 7).

11.2 Experiments

Materials **-** Phase pure C-S-H and C-S-H/polyaniline nanocomposites (Ca/Si = 0.8 and 1.2) as synthesized by Alizadeh et al. [1, 7] were used in this study. The synthesis method included a pozzolanic reaction technique. Aniline monomer was pre-dissolved in water (2 ml of aniline in 75 ml of water) to prepare the C-S-H/aniline systems. The solutions (for phase pure C-S-H or C-S-H/aniline systems) were filtered after 90 days of hydration. The drying procedure of these samples included two steps; four days of vacuum-drying followed by conditioning in desiccators at the relative humidity of 11%. Both steps were performed at room temperature. In order to synthesize the C-S-H/polyaniline systems, 0.5 g of the C-S-H/aniline powder was mixed in 100 ml of water using a magnetic stirrer. Then, 0.228 g of ammonium persulfate was added during stirring the suspension solution. The stirring was continued for three days at room temperature. The final material was filtered and washed to remove the unreacted ions. It was, then, dried under vacuum at room temperature for four days, and then conditioned at the relative humidity of 11%.

Tests – The phase pure C-S-H and C-S-H/polyaniline powders (at a relative humidity of 11%) were compacted in order to obtain rectangular prisms. The compaction pressure was adjusted to reach a porosity of about 30%. The thickness of the samples was about 0.8 and 1.2 mm depending on the type of the material. The length and width of all specimens were 58.9 and 12.97 mm, respectively. The compacted samples were conditioned at 11% RH for one more week. The dynamic mechanical response of the compacted samples was evaluated at various temperatures using a Rheometrics RSA II instrument using the three-point bending method. An initial static load of 3 g was applied on the specimen. The temperature was increased from 26 °C to 200 °C (increase rate = 2 °C/min). Measurements were made at 2 °C increments. At each increment, a frequency range of 0.1 to 10 Hz (for a strain of 0.01%) was applied. The storage modulus (E') and internal friction (tan δ) of samples were recorded at each temperature and frequency. All the tests were repeated at least two times, and similar results were obtained in all cases [1, 7].

11.3 Discussion of the results

The results of the DMTA for the phase pure C-S-H(0.8) and C-S-H(0.8)/polyaniline nanocomposite at two frequencies of 0.25 and 2.5 Hz are presented in Figures 11-1 and 11-2, respectively. As it is observed in these figures, the general trend for the E' and tan δ curves versus temperature was not dependant of the test frequency. The results obtained at the frequency of 0.25 Hz are used for the quantitative analysis in this section.

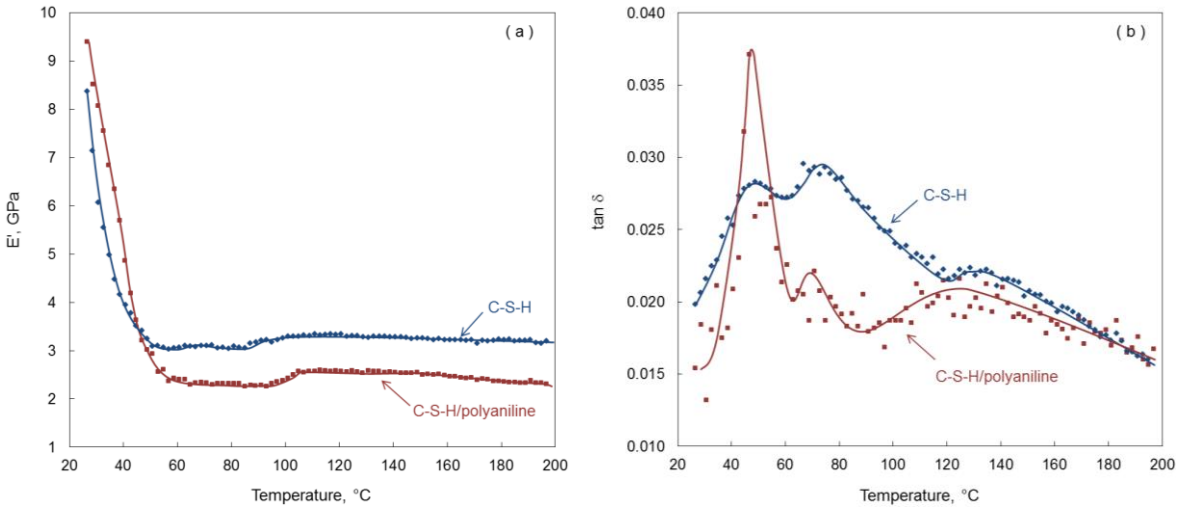

Figure 11-1- DMTA responses of phase pure and polyaniline-modified C-S-H(0.8) systems at f = 0.25 Hz

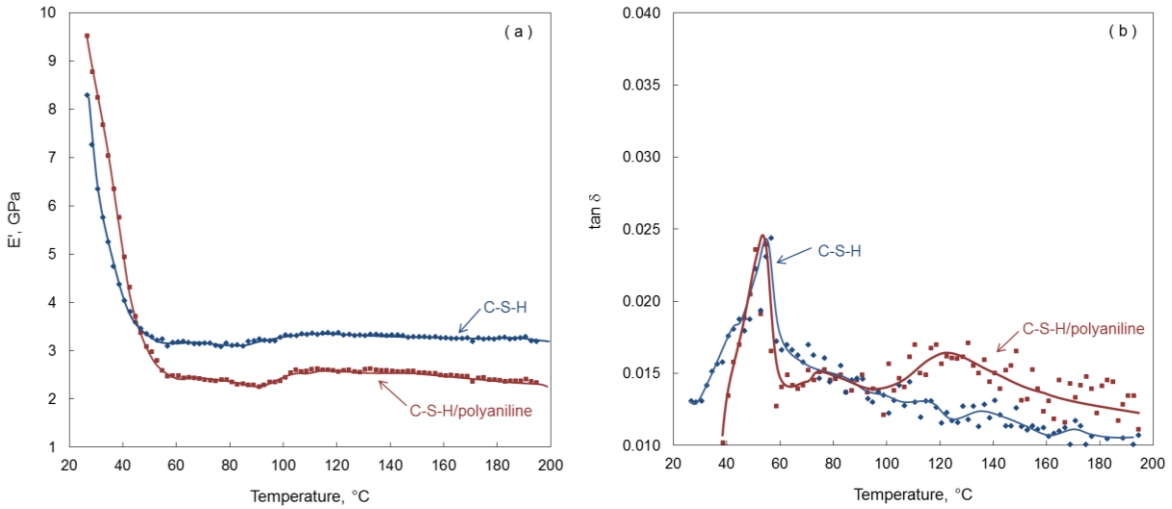

Figure 11-2- DMTA responses of phase pure and polyaniline-modified C-S-H(0.8) systems at f = 2.5 Hz

Modification of C-S-H(0.8) with polyaniline improved the storage modulus and reduced the internal friction of the samples at the room temperature and 11% RH (Figure 11-1). The C-S-H(0.8)/polyaniline nanocomposite, however, exhibited a more rapid loss of storage modulus upon the first stage of drying (from room temperature to the first inflection point) compared to the phase pure C-S-H(0.8) (Figure 11-1(a)). The modulus-loss in this stage of drying of C-S-H systems is normally assigned to the removal of most of the interlayer water of the systems. The E' of the C-S-H(0.8)/polyaniline sample was about 23% lower than that of phase pure C-S-H at the end of this stage although it was initially higher by about 12%. The storage modulus of the C-S-H/polyaniline sample started to increase again at the temperature of about 90 °C. The strain recovery of the sample was possibly due to the cross-linking of the polyaniline in addition to that occurring between the silicate chains. It resulted in the formation of a sharper peak in the E' curve of the C-S-H/polyaniline sample in this region compared to that in the phase pure C-S-H. The E' of the C-S-H/polyaniline was, however, still lower than the pure C-S-H by about 25% by the end of the test. A significant decrease of the E' values during the first stage of drying was also observed for the C-S-H/NBA or C-S-H/ABA systems in chapter 7. It was assigned to the break-down of some possible hydrogen bonding between the structure of the organic and inorganic phases in addition to the removal of the interlayer water of C-S-H. It is possible

that a similar mechanism contributed to the significant reduction of the E' values of the C-S-H(0.8)/polyaniline nanocomposite systems.

It is also noted that the inflection points in the DMTA curves of the C-S-H/polyaniline sample were shifted to the higher temperatures. The change in the location of these points is likely to be further evidence for the intercalation of polyaniline in the interlayer of C-S-H and fewer defects in the microstructure of the organically modified C-S-H. A similar result was obtained in chapter 7 for the C-S-H/NBA composite systems.

Modification of C-S-H with polyaniline also improved the initial elastic properties of the C-S-H(1.2) sample with (Figures 11-3 and 11-4). The E' of the C-S-H(1.2)/polyaniline sample initially was about 14% higher than that of the phase pure C-S-H (Figure 11-3(a)). The tan δ of the C-S-H/polyaniline sample was also significantly lower at the starting point. The elastic properties of the C-S-H(1.2)/polyaniline sample were stable up to about 32 °C. The storage modulus, however, was reduced significantly so that it was even slightly lower than that of pure C-S-H at the temperature range of 45 to 60 °C. A noticeable relaxation was, then, observed in the DMTA curves of the C-S-H(1.2)/polyaniline sample in the temperature ranging 60 to 145 °C. The E' either could not be recorded in this region as the sample lost its contact with the upper fixture in the DMA instrument or very low values for the E' was recorded when the contact was satisfied. The specimen, however, regained its rigidity at the higher temperatures. It had a storage modulus close to that of phase pure C-S-H at the temperature of about 150 °C to end of the test (at 200 °C).

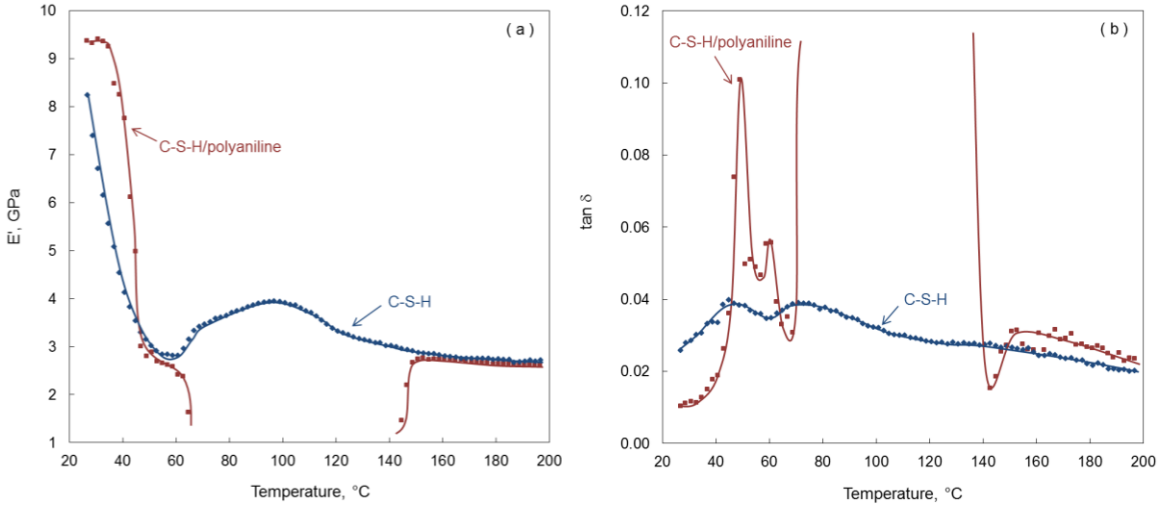

Figure 11-3- DMTA responses of phase pure and polyaniline-modified C-S-H(1.2) systems at f = 0.25 Hz

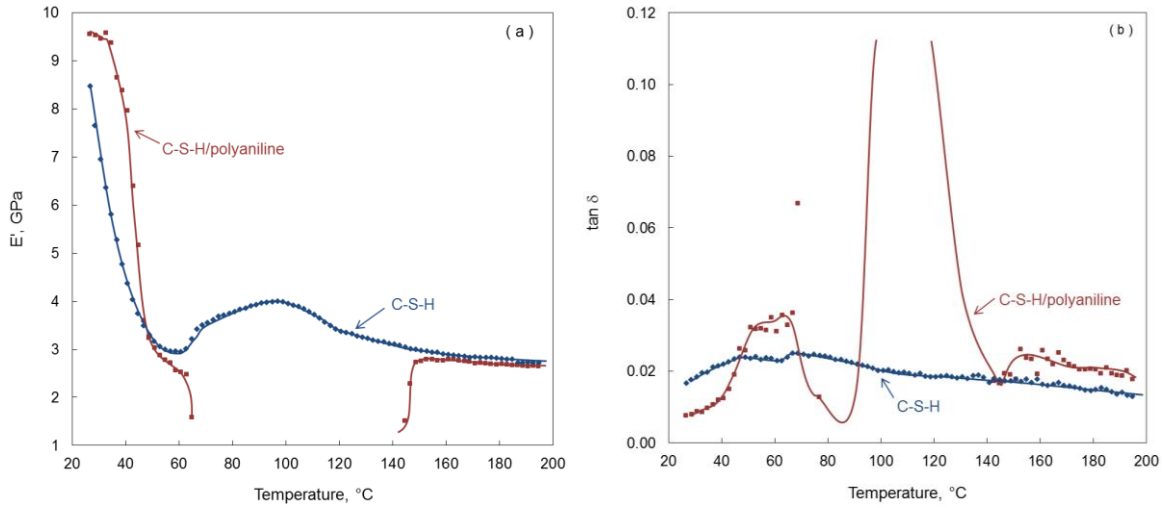

Figure 11-4- DMTA responses of phase pure and polyaniline-modified C-S-H(1.2) systems at f = 2.5 Hz

The source of the unexpected relaxation in the temperature range 60 to 150 °C is likely related to the difference in the elastic response of the polyaniline and C-S-H in this temperature range. The E' of the phase pure C-S-H(1.2) was increased to about 3.95 GPa likely due to the cross-linking of silicate chains in the temperature between 60 to 150 °C (Figure 11-3(a)). The E' of the polyaniline intercalated in the layered structure of C-S-H likely tends to decrease in this temperature range. The significant difference of the elastic properties of these two phases possibly resulted in the extreme relaxation of the C-S-H(1.2)/polyaniline sample. In order to illustrate this behavior, a typical DMTA curve of an emeraldine-base polyaniline film at the frequency of 5 Hz (Rodrigures and Akcelrud [8]) is presented in Figure 11-5. It has been previously shown that the DMTA of polyaniline is dependent on the synthesis procedure and the dopant nature [9, 10]. However, although the location of the inflection points may vary, it is likely that at least three different regions can be recognized in the E' curve of the polyaniline (undoped or doped) film. The E' of polyaniline film, as it is shown in Figure 11-5, decreases in the first region of the curve. The E' values drops more rapidly in the second region which is followed by a recovery due to the cross-linking of the polyaniline [8] in the third region. The comparison of Figures 11-3 to 11-5 shows that at the temperatures that the second peak of E' of the host C-S-H are likely to occur, the E' of polyaniline is likely to reduce noticeably resulting in the significant difference of these two E' values.

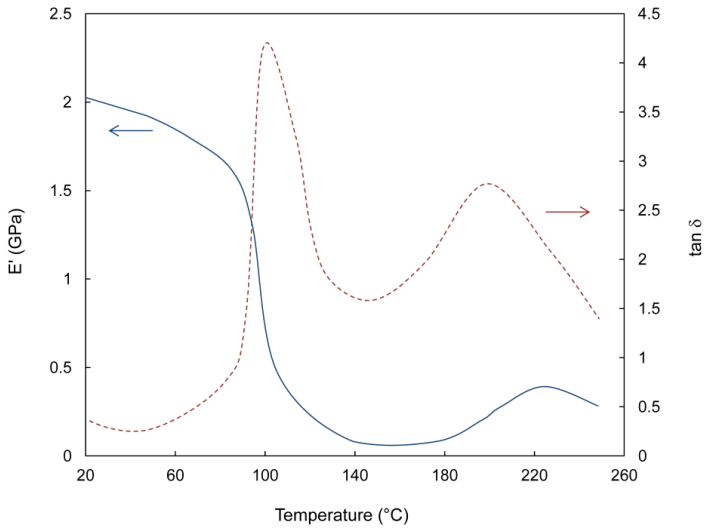

Figure 11-5- DMTA responses of emeraldine-base polyaniline film at f = 5 Hz [8]

It is suggested based on the comparison of the curves in Figure 11-1 and Figure 11-3 that the elastic behavior (E' and tan δ values) of the C-S-H sample with Ca/Si = 1.2 was more influenced by the polyaniline intercalation than that of the sample with Ca/Si = 0.8. This is in conformity with the results of the change of the d_{002} spacing of the C-S-H/polyaniline samples due to drying in Ref. [7] as well as the volume stability in aggressive solutions provided in chapter 10. This is possibly due to the greater number of defect points in the high-lime hosting C-S-H. A higher amount of polyaniline, therefore, is likely to fill these defect points resulting in a greater enhancement of the engineering properties and resulting durability characteristics. The higher relaxation of the C-S-H(1.2)/polyaniline sample in the temperature ranging of 60 to 150 °C can also be explained by the higher value of the E' of the C-S-H host, and the greater difference in the elastic properties of C-S-H and polyaniline for the sample with Ca/Si = 1.2 in this temperature range.

The comparison of the E' and the tan δ curves in Figures 11-1 and 11-3 also shows that the change in the tan δ curves of the C-S-H systems due to polymer modification is likely to be in the opposite direction to that of the E' curve. This was expected as the E' and tan δ generally act in opposite directions in the cement-based systems [11-14].

11.4 Conclusions

The discussion of the DMTA results provided new information about the mechanism of stability of the organically-modified C-S-H systems at elevated temperatures. The initial storage modulus of the C-S-H/polyaniline nanocomposites with both Ca/Si ratios was improved. No evidence of the enhanced mechanical performance, however, was obtained at the temperatures above 45 °C. The C-S-H modification with organic polymers is likely to be more effective in the C-S-H host with Ca/Si = 1.2 as detected by these experiments.

References

1. R. Alizadeh, Nanostructure and engineering properties of basic and modified calcium silicate hydrate systems, PhD thesis, University of Ottawa, 2009.
2. I. G. Richardson, "Tobermorite/jennite- and tobermorite/calcium hydroxide-based models for the structure of C-S-H: applicability to hardened pastes of tricalcium silicate, Portland cement, and blends of Portland cement with blast-furnace slag, metakaolin, or silica fume," *Cement and Concrete Research*, 34(9), pp. 1733-1777, 2004.
3. D. Viehland, L. J. Yuan, Z. Xu, X. D. Kong and R. J. Kirkpatrick, "Structural studies of jennite and 1.4nm tobermorite. Disordered layering along the [100] of jennite", *Journal of the American Ceramic Society*, 80(12), pp. 3021-3028, 2005.
4. H. F. W. Taylor, Hydration of the calcium silicate phases, Cement Chemistry, Chapter 5, Thomas Telford Publishing, London, 1997.
5. R. Alizadeh, L. Raki, J. M. Makar, J. J. Beaudoin and I. Moudrakovski, "Hydration of tricalcium silicate in the presence of synthetic calcium-silicate-hydrate," *Journal of Materials Chemistry*, 19(42), pp. 7937-7946, 2009.
6. R. Alizadeh, J. Beaudoin, L. Raki and V. Terskikh, "C-S-H/polyaniline nanocomposites prepared by in situ polymerization," *Journal of Materials Science*, 46(2), pp. 460-467, 2011.

7. R. Khoshnazar, R. Alizadeh, J. J. Beaudoin and L. Raki, "The physico-mechanical stability of C-S-H/polyaniline nanocomposites," *Materials and Structures*, in-press, DOI: 10.1617/s11527-013-0168-4, 2013.
8. P. C. Rodrigues and L. Akcelrud, "Networks and blends of polyaniline and polyurethane: correlations between composition and thermal, dynamic mechanical and electrical properties," *Polymer*, 44(22), pp. 6891-6899, 2003.
9. D. Lesueur, X. Colin, G. Camino and N. D. Alberola, "Dynamic mechanical behaviour and thermal degradation of undoped polyaniline," *Polymer Bulletin*, 39(6), pp. 755-760, 1997.
10. S. Chen and H. Lee, "Structure and properties of poly(acry1ic acid)-doped Polyaniline," *Macromolecules*, 28, pp. 2858-2866, 1995.
11. F. Radjy and C. W. Richards, "Effect of curing and heat treatment history on the dynamic mechanical response and the pore structure of hardened cement paste," *Cement and Concrete Research*, 3, pp. 7-21, 1973.
12. E. J. Sellevold and F. Radjy, "Drying and resaturation effects on internal friction in hardened cement pastes," *Journal of the American Ceramic Society*, 59, pp. 256-258, 1976.
13. F. Radjy and C. W. Richards, "Internal friction and dynamic modulus transitions in hardened cement paste at low temperatures," *Materials and Structures*, 2, pp. 17-22, 1969.
14. F. Radjy and C. W. Ricahrds, "Effect of curing and heat treatment history on the dynamic mechanical response and the pore structure of hardened cement paste," *Cement and Concrete Research*, 3, pp. 7-21, 1973.

Chapter 12

Volume Stability of Calcium Sulfoaluminate Phases in Aqueous Solutions

The volume stability of calcium sulfoaluminate phases exposed to water, lime and gypsum-rich environments was investigated. The length changes of compacted specimens of synthetic monosulfate and ettringite were monitored in de-ionized water, lime-saturated water, gypsum-saturated water, and saturated water vapor. The X-ray diffraction analysis was also performed on the samples to assess the changes in the crystalline structure of each phase. Evidence was provided in support of the significant role of dissolution of monosulfate and ettringite, and the leaching of their constituent ions on the expansion of these phases.

12.1 Introduction

Ettringite ($3CaO.Al_2O_3.3CaSO_4.32H_2O$) and monosulfate ($3CaO.Al_2O_3.CaSO_4.12H_2O$) are the two common forms of calcium sulfoaluminate phases present in the hydrated cement paste. Ettringite is known to have a column and channel-like structure in which the columns have the empirical chemical formula of $[Ca_3Al(OH)_6.12H_2O]^{3+}$, and the SO_4^{2-} anions and water molecules occupy the intervening channels [1]. The formation of ettringite is a key factor in the setting process of the cement paste. Ettringite normally converts to monosulfate as the cement hydration continues [2]. Monosulfate has a lamellar crystalline

structure. Its main layers are composed of $[Ca_2Al(OH)_6]^+$, and the SO_4^{2-} anions and water molecules are located between the layers [3].

The characteristics of ettringite and monosulfate are of significant importance, from the durability point of view, as these phases may exhibit considerable expansion due to the environmental conditions. The expansions related to the calcium sulfoaluminate phases have long been studied by cement chemists and researchers since the investigation of Michaelis in 1892 [4]. The mechanisms controlling these expansions are, however, still under debate.

The formation of ettringite in sulfate rich environments has been widely accepted as a main cause of expansion referred to as sulfate attack [5-8]. The anisotropic growth of ettringite crystals, according to this theory, is an expansive phenomenon which can result in the deterioration of cement paste. Mehta [9-11], however, reported that the expansion of ettringite does not necessarily occur in the presence of high sulfate concentrations. He attributed the expansion of ettringite crystals of colloidal dimensions to the imbibition of liquid water. The observed expansion in this case could be considerably greater than the expansions due to the ettringite formation itself [9]. Other proposed mechanisms include the expansion of ettringite associated with the osmotic forces, similar to those responsible for the swelling of the clay particles [12].

There remains no general agreement on the theories of expansion of ettringite. In addition, very few investigations have been conducted on the volume stability of monosulfate itself. The published studies have focused mainly on the conversion of monosulfate to ettringite in the sulfate environments [6, 13] although other mechanisms may also be associated with the expansion of these phases. Dissolution of ettringite and monosulfate, for example, is a possible source of expansion that is not widely recognized.

The solid phase of porous materials can gradually breakdown to release individual ions into the pores through a dissolution process [14]. It has been suggested that dissolution of porous materials and leaching out of ions into the liquid phase is an expansive process. The results of previous investigations by Litvan [15, 16], Dent Glasser and Kataoka [17] and Feldman and Sereda [18] support this argument. Specifically, Litvan [15] investigated the volume stability of porous silica glass specimens (1 – 8 mm thick) in NaOH solutions (0.1

to 6.4 M) for an exposure period of about 24 h. The expansion of the samples was quite significant (e. g. 0.70 % for a 1 mm thick glass sample in the 0.4 M NaOH solution). These length changes far exceed the length change of porous glass saturated with water (about 0.16%). In addition, Dent Glasser and Kataoka observed significant expansions of silica gel in a NaOH solution. Feldman and Sereda also reported a 0.19% expansion of porous silica glass during alkali treatment.

Litvan [15, 16] further demonstrated that leaching of lime from cement paste results in expansion as does the partial dissolution of cement paste by a 1 N aqueous solution of HCl. He suggested that dimensional changes accompanying dissolution can possibly result for the following reasons: changes to the surface free energy of the solid phase; transient length changes due to gradients in the concentration of dissolved species in the pore solution generating osmotic-like pressures; disjoining pressure resulting from double layer effects outside the surface generating repulsive forces; release of strain-energy stored in the sample. Beaudoin et al. [19] also suggested that cementitious materials can expand in aggressive solutions due to the dissolution process.

The intent of this chapter is to further investigate the details of mechanisms responsible for the volume stability of calcium sulfoaluminate phases. The experiments were designed to determine the length change of synthetic monosulfate and ettringite in de-ionized water, and in presence of lime and gypsum solutions. The observed expansions were, then, compared with the changes of the pH of the solutions as well as the crystalline structure and the morphology of the specimens in order to explore the possible origins of these expansions.

12.2 Experimental Program

12.2.1 Preparation of Materials

Monosulfate was synthesized according to Kuzel [20]. Ettringite was prepared by a method described by Struble and Brown [21]. The details of the synthesis techniques were provided in chapter 3.

12.2.2 Tests

Porous solid bodies in the form of circular discs (32 mm in diameter × 1 mm thick) were prepared by powder compaction. The compaction pressure was adjusted to reach a porosity of 10% for the samples. Then, prisms measuring 5 × 25 × 1 mm were cut from the compacted samples, and mounted on modified Tuckerman extensometer (see Figure 3-4).

The prepared samples were placed in the test solutions, and the length-changes were measured continuously. De-ionized water, lime-saturated water, gypsum-saturated water and saturated water vapor were used as the test solutions. For the liquid solutions, the ratio of solid sample to the solution was 1 g of solid per 50 ml of the solution. The whole set-up was placed in desiccators containing the test solution in order to avoid evaporation. The pH of the test solutions were monitored using a VWR-SP90M5 pH meter for the first 24 h after immersion of the samples in the test solutions.

Parallel to the length-change and pH measurements, samples of the solid compacts were immersed in the solution for X-ray diffraction (XRD) analysis at various times. The solid/solution ratio in this case was exactly the same as the one in the length-change measurements. The sample was removed from the solution, and ground to get the powder 10 minutes before starting the XRD measurements. The X-ray diffraction measurements were performed using a Scintag XDS 2000 diffractometer using CuK_{α} radiation. The spectra were obtained in the range $6^{\circ} < 2\theta < 60^{\circ}$ using a step size of 0.08° at 5 second intervals. They were, then, normalized according to the mass of the samples.

Changes to the morphology of the samples were observed using the scanning electron microscopy (SEM) techniques. SEM images were collected using a Hitachi S-4800 Field Emission Scanning Electron Microscope. The surface structure images were acquired using a beam current of 10 mA at 3.2×10^{-16} J (2 kV) at the working distance of 8 mm.

All the tests were performed at room temperature (24 - 26 °C). The compacted samples were kept in desiccators at a relative humidity of 11%. They were all examined using XRD, prior to immersing in the solutions, to verify that the crystalline structures corresponded to those of $3CaO.Al_2O_3.3CaSO_4.30\text{-}32H_2O$ [24, 25] and $3CaO.Al_2O_3.CaSO_4.12H_2O$ [24, 25]. In the cases where a decrease of the main basal-spacing of the monosulfate samples was

observed, the humidity of the sample was adjusted to revert it to the $3CaO.Al_2O_3.CaSO_4.12H_2O$.

12.3 Results and discussion

The results are presented for the monosulfate and ettringite separately. In each part, the length-change of the samples is discussed with reference to the changes in the pH of the solution, and the crystalline structure and morphology of the samples detected by the XRD and SEM techniques. The associated mechanisms of expansion are discussed.

12.3.1 Expansion of monosulfate

Monosulfate specimens exhibited a significant expansion immediately after immersion in de-ionized water (Figure 12-1). The rate of expansion was significantly reduced about 20 min after the immersion. The amount of expansion, however, was quite large as the total expansion of monosulfate was 2.7% after 8 h. The observed expansion was possibly due to the dissolution of monosulfate, and the release of its ions to the de-ionized water. The rate of the dissolution decreases as the dissolution continues, due to the increased ion concentrations in the solution, likely resulting in a decrease of the rate of expansion. Expansion due to the change in the surface energy of the samples (due primarily to sorption phenomena) seems to be insignificant as the samples were conditioned at the relative humidity of 11% before starting the tests. The surface of the samples was, consequently, covered with water molecules prior to immersion in the de-ionized water. Length change of porous bodies due to flattening of menisci that occurs on adsorption of water vapor at a partial pressure generally greater than 0.45 is also minimized when a sample is directly immersed in liquid water [16].

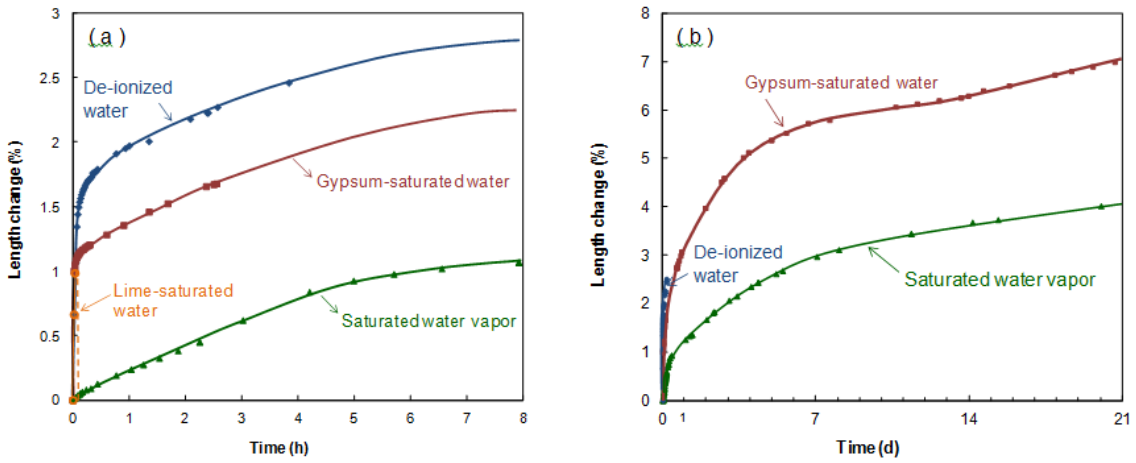

Figure 12-1- Length-change of monosulfate specimens in de-ionized water, lime-saturated water, gypsum-saturated water and saturated water vapor – (a) up to 24 h, (b) up to 21 d

The data for the change in the pH with time of immersion in de-ionized water also supports the role of dissolution of monosulfate and the leaching out of the ions associated with the observed expansion. It is suggested based on the results shown in Figure 12-2 that the initial reduction of pH of the de-ionized water immediately after immersion of the monosulfate sample is an indication of leaching of sulfate ions from the interlayer space of monosulfate structure into the de-ionized water. The pH, then, oscillated between 7.0 and 7.4 due to the competing effects of leaching of both sulfate and lime. The release of sulfate ions was, however, reduced after about 40 min, and the pH continued to increase due to the leaching of lime to the solution.

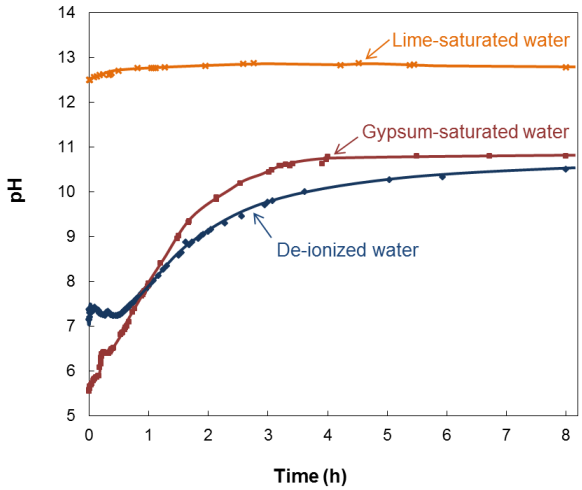

Figure 12-2- Changes in pH with time of immersion of monosulfate specimens of de-ionized water, lime-saturated water and gypsum-saturated water

The expansion of monosulfate in the gypsum-saturated water was significantly lower than in de-ionized water. Sulfate ions and calcium ions were available in the gypsum solution which possibly reduced the solubility of these ions due to the common-ion effect, and, consequently, decreased the expansion. It is also indicated from the results of Figure 12-2 that the pH of the gypsum-saturated solution did not decrease (during the first 40 minutes) after immersion of the monosulfate sample in it. In addition, the pH of the gypsum-saturated solution exceeded that of the de-ionized water after about 1 h as the effect of lime leaching on the increase of the pH was not compensated for by that of the sulfate leaching occurring in the de-ionized water solution.

The expansion of monosulfate in the lime-saturated water was very quick, and the sample disintegrated a couple of minutes after the immersion (Figure 12-1(a)). The pH of lime-saturated water did not significantly change after the immersion of the monosulfate sample in it (Figure 12-2). The leaching out of lime from the monosulfate sample is minimized in the lime-saturated water. Some sulfate ions likely leached out from the sample, and resulted in a part of the expansion. The amount of sulfate leaching, however, was not large enough to change the pH of the solution; especially as the lime-saturated water has a high alkaline buffer capacity which makes it more resistant to change of the pH compared to the de-ionized water. Aluminum leaching possibly also played a role in the expansion and the disintegration of the monosulfate sample in the lime-saturated water. Aluminum can leach out in the form of $Al(OH)^-$ in the solutions with high values of pH. As aluminum is a main component in the microstructure of monosulfate layers, leaching of even a small amount of aluminum can likely result in large expansions leading to the disintegration of the sample.

The significant role of the dissolution of monosulfate in the aqueous solutions as it pertains to volume stability was also supported by the length-change measurements on a monosulfate sample in a solution containing both aluminum sulfate hydrate (25 g/l) and gypsum (2.8 g/l). The results, which are not presented here, suggested that the expansion of monosulfate sample in this solution, containing dissolved ions of calcium, aluminum and sulfate, was about 1×10^{-3} % after 3 minutes. It was considerably lower than the expansion observed for the monosulfate samples immersed in the other solutions for a similar period of time (about 1 % after 3 minutes) emphasizing that all three of these ions can have a role

in the volume stability of monosulfate depending on the composition of the aqueous solution.

Dissolution of monosulfate also occurs, at a lower rate, in the saturated water vapor (Figure 12-1). The ions, especially those that are near the surface, could gradually leach out, resulting in the expansion.

The XRD patterns of monosulfate in de-ionized water are presented in Figure 12-3. The figure shows that the dissolution of monosulfate resulted in the gradual growth of the ettringite peak in the sample so that after 21 days the ettringite peak was significantly more dominant than the monosulfate peak. The appearance of ettringite due to the dissolution of monosulfate in de-ionized water was also reported by Atkins et al. [24]. The concentration of sulfate ion increases in both the pore solution and the bulk solution as a result of the leaching process tending towards an equilibrium concentration in a few hours. The increased concentration of sulfate ions in the sample pores, due to the dissolution of monosulfate, could result in the formation of ettringite which is more stable than monosulfate in water at 25 °C [24, 25].

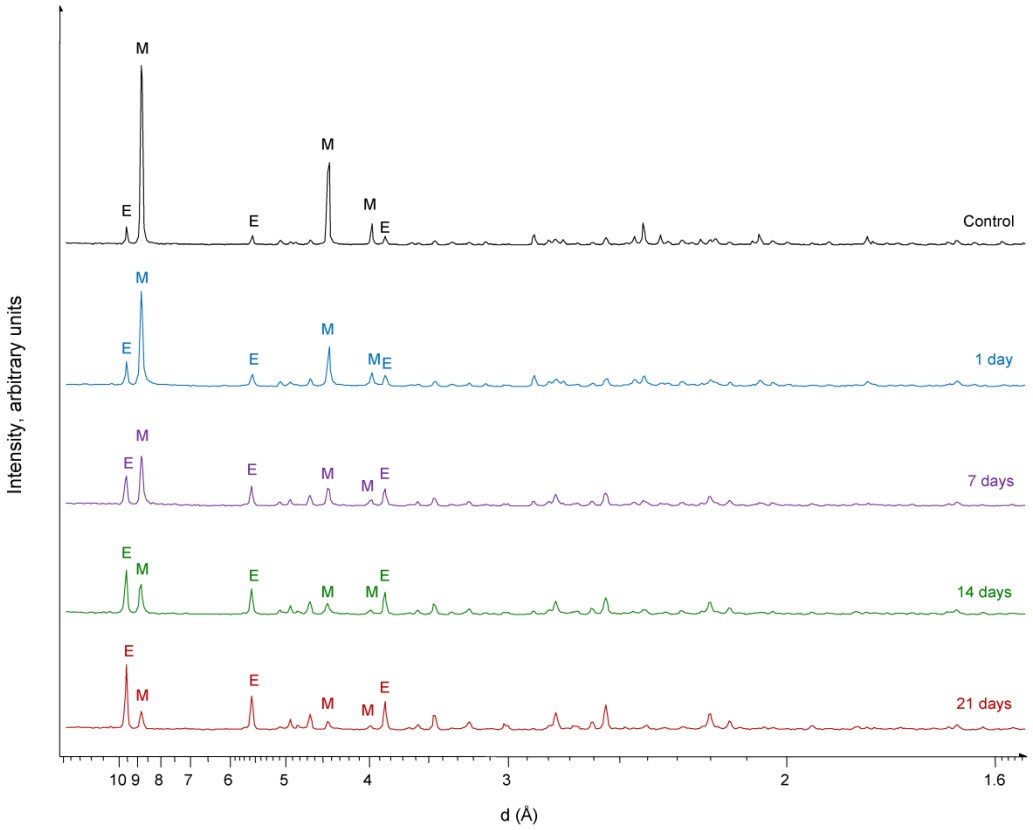

Figure 12-3- XRD patterns of monosulfate in de-ionized water – E: Ettringite, M: Monosulfate

The growth of ettringite peaks occurred more slowly in the lime-saturated water compared to that in the de-ionized water (Figures 12-3 and 12-4). It was also observed that the sulfate leached out of the monosulfate sample reacted with the calcium cations available in the lime-saturated solution and formed gypsum crystals after three weeks. The formation of gypsum crystals is an indication of some sulfate leaching from the interlayer of the monosulfate sample even though the pH of the solution did not significantly change during the first 8 h (Figure 12-2).

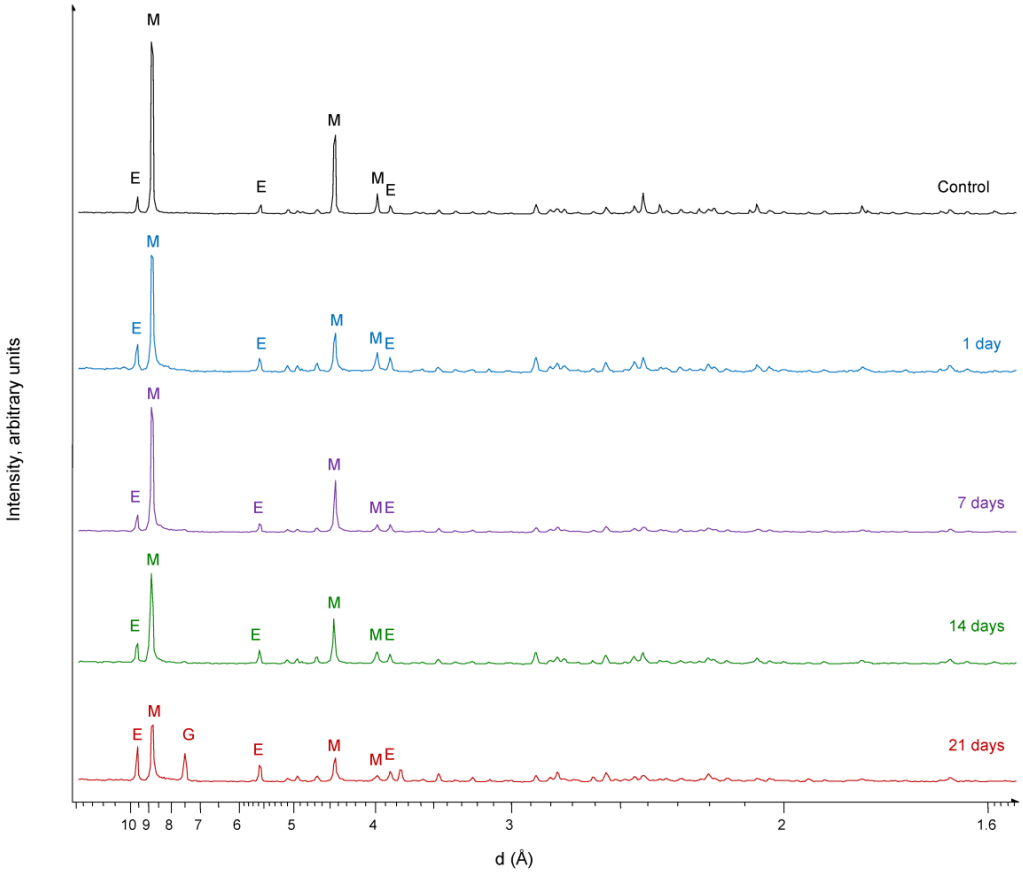

Figure 12-4- XRD patterns of monosulfate in lime-saturated water – E: Ettringite, M: Monosulfate, G: Gypsum

The XRD pattern of the monosulfate samples immersed in the gypsum-saturated water is shown in Figure 12-5. As expected, the formation of ettringite was accelerated in the presence of gypsum solution. However, in spite of the higher rate of ettringite formation, the gypsum-saturated water resulted in less expansion compared to the de-ionized water and the lime-saturated water (Figure 12-1(a)). In addition, the sample did not disintegrate, and did not exhibit evidence of macro- cracking even though it exhibited more than 7% expansion (Figure 12-1(b)). The higher resistance of the sample to disintegration in the gypsum-saturated water may be related to the limited amount of ions leached out of the sample. The XRD patterns of Figure 12-5 together with the expansion curve of Figure 12-1-b suggest that the monosulfate sample in the saturated-gypsum solution exhibited about 6% longitudinal expansion before its complete conversion to ettringite. About half of this expansion occurred in the first day of the experiments, although a significant growth of

ettringite crystals occurred after this period. This also suggests that the dissolution of the sample is a main source of expansion. In addition, the length change curve of the ettringite formed through the dissolution process of the monosulfate sample is concave up (Figure 12-1(b)) corresponding to the length-change curves of the synthetic ettringite presented in the following section.

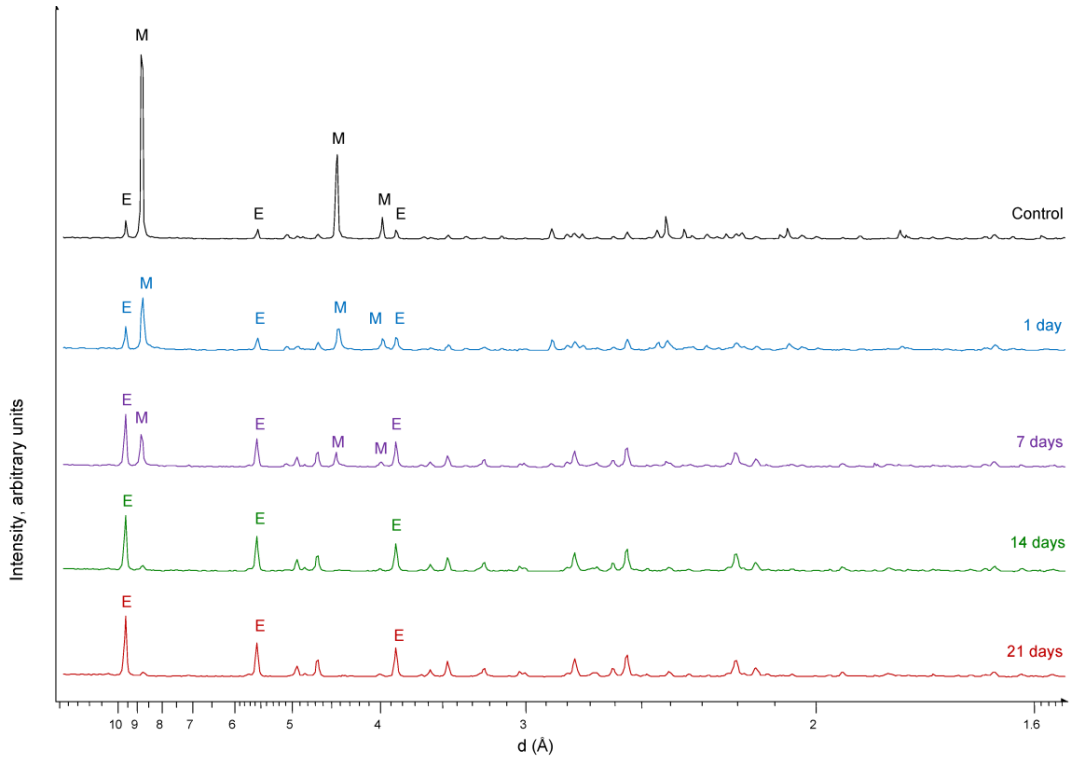

Figure 12-5- XRD patterns of monosulfate in gypsum-saturated water– E: Ettringite, M: Monosulfate

The XRD patterns of the sample in the saturated water vapor show that the expansive behaviour of monosulfate in the water vapor is very similar to that in the de-ionized water, but the expansion occurs at a lower rate (Figures 12-6 and 12-3).

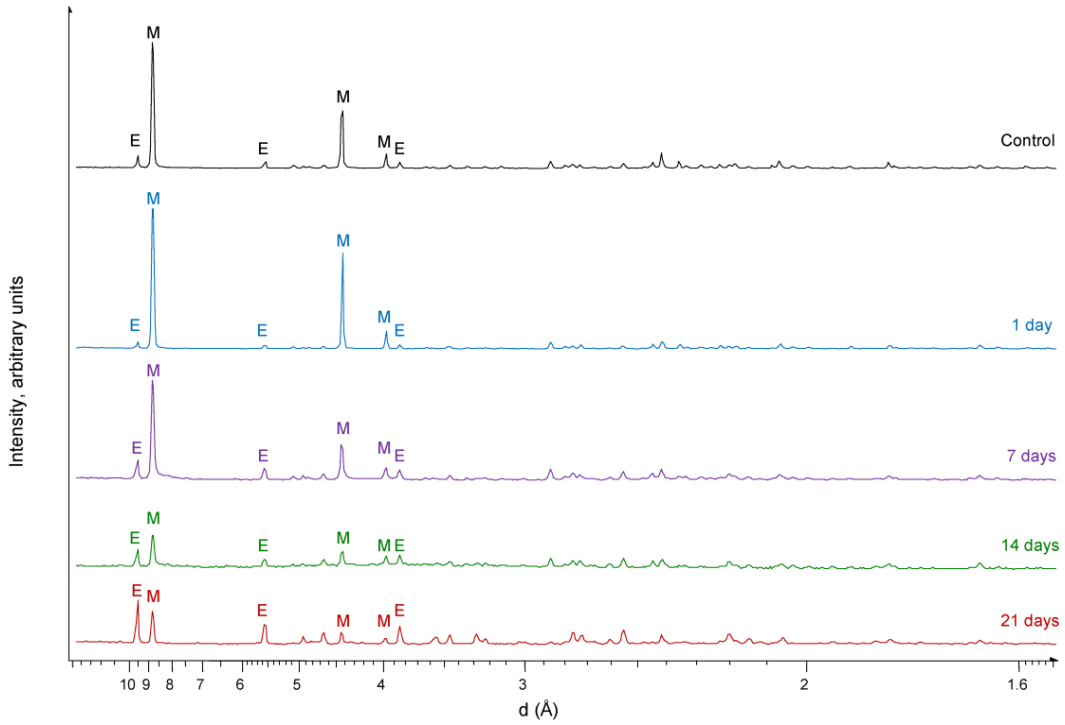

Figure 12-6- XRD patterns of monosulfate in saturated water vapor– E: Ettringite, M: Monosulfate

The SEM micrographs of the monosulfate samples after 24 h immersion in the de-ionized water, lime-saturated water, gypsum-saturated water and water vapor are shown in Figure 12-7. It was observed that the surface texture and the hexagonal morphology of the monosulfate plates were altered following immersion in the test solutions for 24 h. The ettringite crystals are likely formed on the surface of the samples, especially on the one immersed in the gypsum-saturated water. It can also be seen that the particles exhibiting plate-like morphology for the monosulfate sample immersed in the lime-saturated water are smaller than in the other test solutions. The alterations to the surface of the monosulfate sample in the water vapor were less than those in the other solutions as was expected.

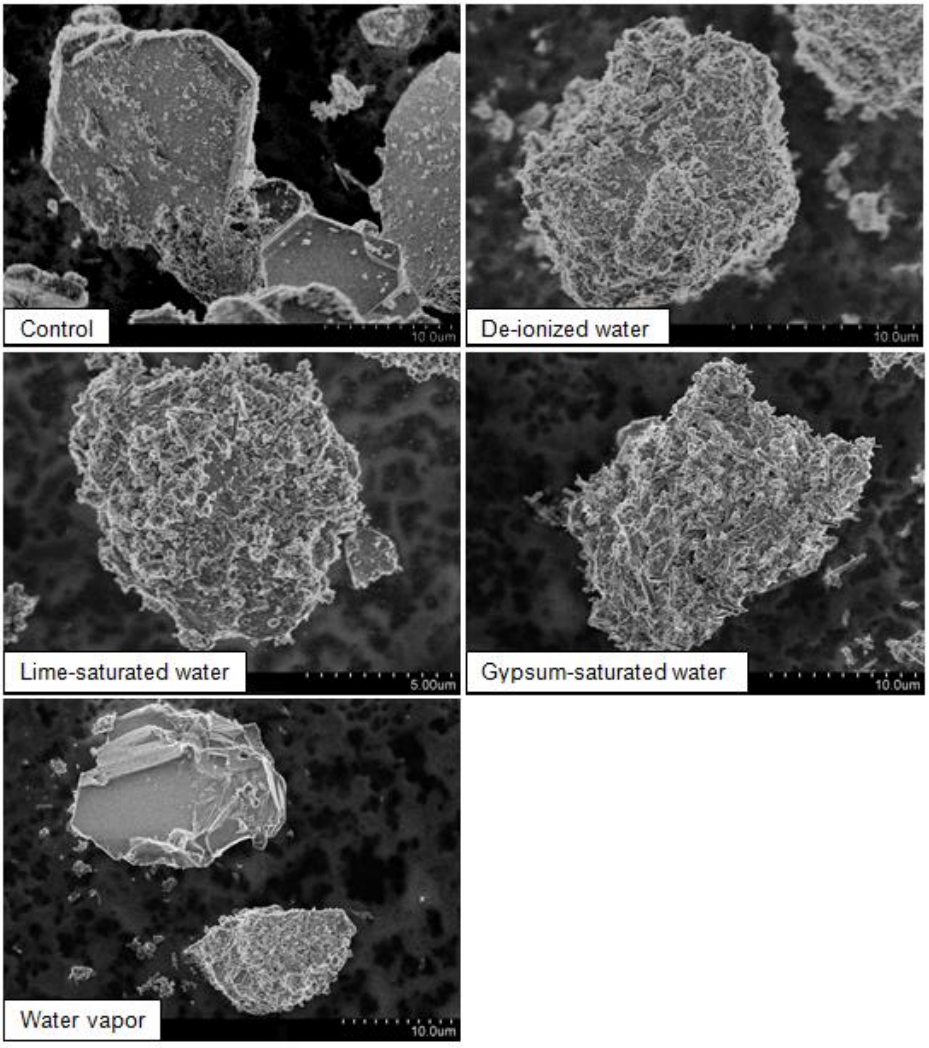

Figure 12-7- SEM micrographs of monosulfate specimens immersed in de-ionized water, lime-saturated water, gypsum-saturated water and saturated water vapor for 24 h

12.3.2 Expansion of ettringite

Ettringite also exhibited a significant expansion when it was exposed to the de-ionized water (Figure 12-8). The expansion of ettringite in the lime-saturated water was very similar to that in the de-ionized water. The samples, in both solutions, disintegrated after about 40 minutes. The expansion of ettringite in the gypsum-saturated water was lower than that in de-ionized water and lime-saturated water. In addition, the sample had a higher resistance to the disintegration in the gypsum-saturated water, and it did not disintegrated for a period of up to about 100 minutes. The ettringite sample also expanded in the water

vapor at a lower rate compared to those in the other solutions. The expansion of ettringite sample, however, was still significant so that the total length change of ettringite in the saturated water vapor was about 1.3% after 8 h.

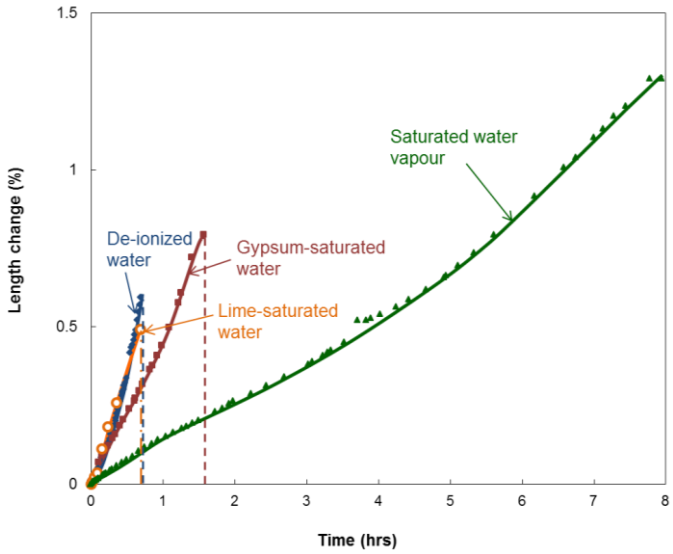

Figure 12-8- Length change of ettringite specimens in de-ionized water, lime-saturated water, gypsum-saturated water and saturated water vapor

It is suggested that the expansion of ettringite in the aqueous solutions is also associated with the dissolution process. Data from the pH versus time of immersion curves in Figure 12-9 supports this argument. It is suggested that the reduction in pH of the de-ionized water, from 7.0 to 6.7, 40 minutes after immersion of the ettringite sample is due to the leaching of sulfate ions from the intercolumnar space of the ettringite structure. Ghorab et al. [26, 27] reported that a total of about 0.2 g/l of sulfate ions are available in an equilibrated ettringite-water solution at 30 °C. The pH, then, gradually increased to 9.14 after 8 h due to the leaching of lime into the solution.

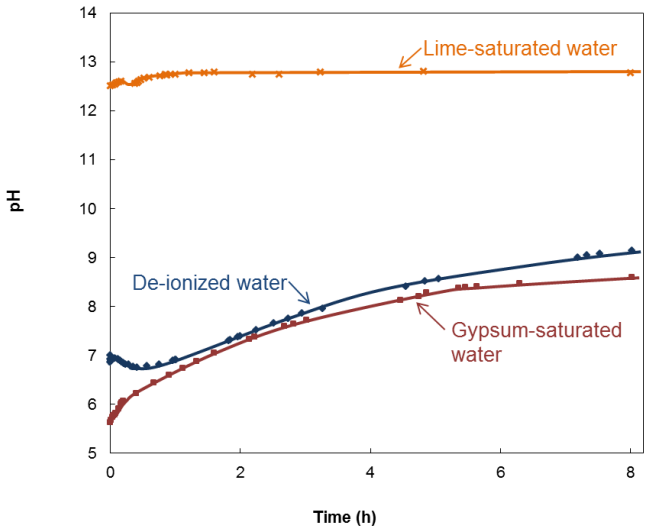

Figure 12-9- Changes in pH with time of immersion of ettringite specimens of de-ionized water, lime-saturated water and gypsum-saturated water

The pH of lime-saturated water did not significantly change after the immersion of ettringite. Lime-leaching from the ettringite sample is minimized in the lime-saturated water. The sulfate leaching is also lower in the lime-saturated water. Some sulfate, however, likely leached from the ettringite sample and resulted in some expansion although it did not noticeably decrease the pH of the solution. Ghorab et al. [27] also suggested that the concentration of sulfate ions was lower in the presence of lime solution. The 1:1 ettringite-lime water solution, however, contained about 0.045 g/l sulfate ions. It is possible that aluminum leaching in the form of $Al(OH)^{-}$, which is likely accelerated in the alkaline solutions, was also responsible for some of the expansion and especially for the disintegration of the ettringite sample. Aluminum has a critical location in the structure of ettringite columns. Only a small amount of aluminum leaching is likely required to result in the significant expansion, and loss of integrity of the ettringite sample.

The pH of gypsum-saturated water did not decrease after the immersion of ettringite as expected. It only gradually increased due to the lime leaching. These results are in good conformity with the length-change curves of Figure 12-8. A lower expansion and higher resistance to the disintegration of the ettringite sample in the gypsum-saturated water compared to that in the de-ionized water and lime-saturated water are shown.

The data presented in Figure 12-10 indicates that no significant change was observed in the XRD patterns of ettringite samples in the test solutions up to 21 days. The comparison of Figure 12-8 and Figure 12-10 indicates that the dissolution of ettringite, and especially the leaching of sulfate ions located between the columns of the ettringite structure, plays an important role in the expansion of ettringite in the test solutions. Leaching of sulfate ions did not affect the general nature of the channelled structure of ettringite. It, however, resulted in considerable expansion that could contribute to cracking and the disintegration of the ettringite sample. In addition, leaching of aluminum is likely to be very expansive and may result in the disintegration of the ettringite sample. Defects in the crystalline structure of ettringite due to the leaching of aluminum cannot be necessarily detected by the XRD technique as it may affect only a small percentage of the ettringite crystals. Ghorab et al. [26] also suggested that no significant change in the XRD patterns of the ettringite samples immersed in the de-ionized water does not guarantee that there is no damage to the structure of the ettringite crystal.

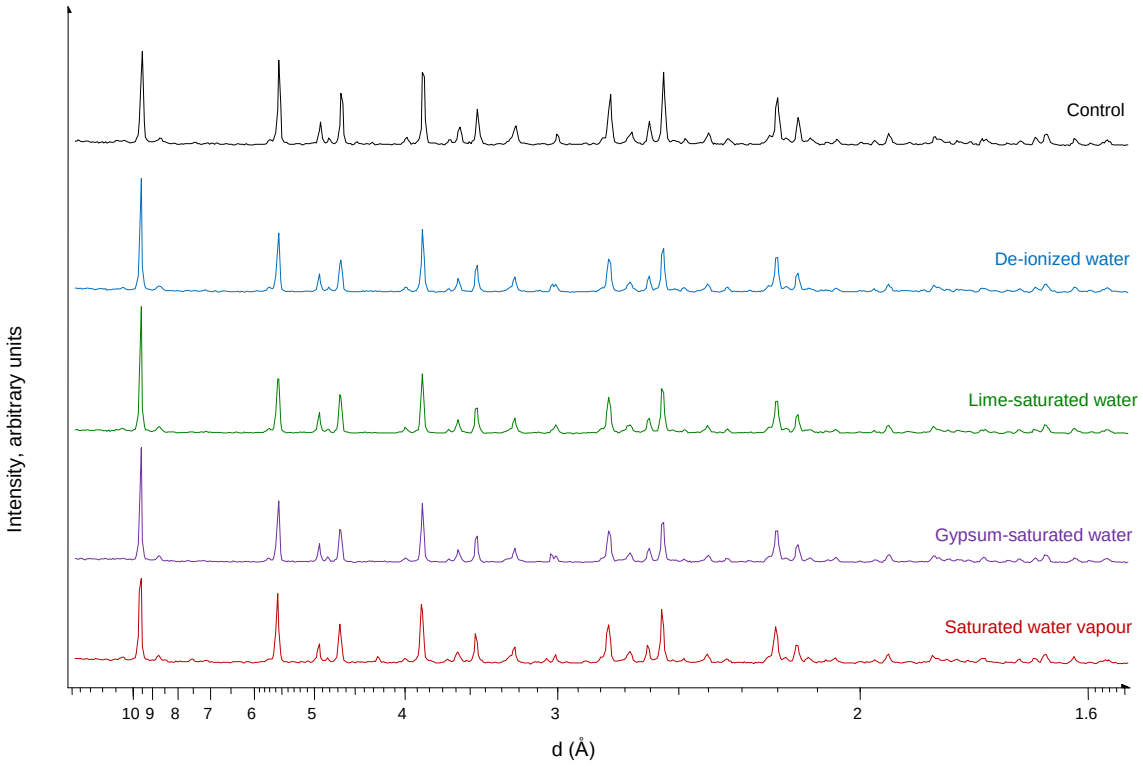

Figure 12-10- XRD patterns of ettringite specimens after 21 days immersion in de-ionized water, lime-saturated water, gypsum-saturated water and saturated water vapor

The SEM micrographs of ettringite samples immersed in the de-ionized water, lime-saturated water, gypsum-saturated water and water vapor for 24 h are presented in Figure 12-11. The size of the ettringite crystals resulting from exposure to the test solutions is smaller than that in the control sample. In addition, gypsum crystals formed near the surface of the ettringite crystals exposed to the water vapor. This is an indication of sulfate and calcium leaching from the ettringite sample.

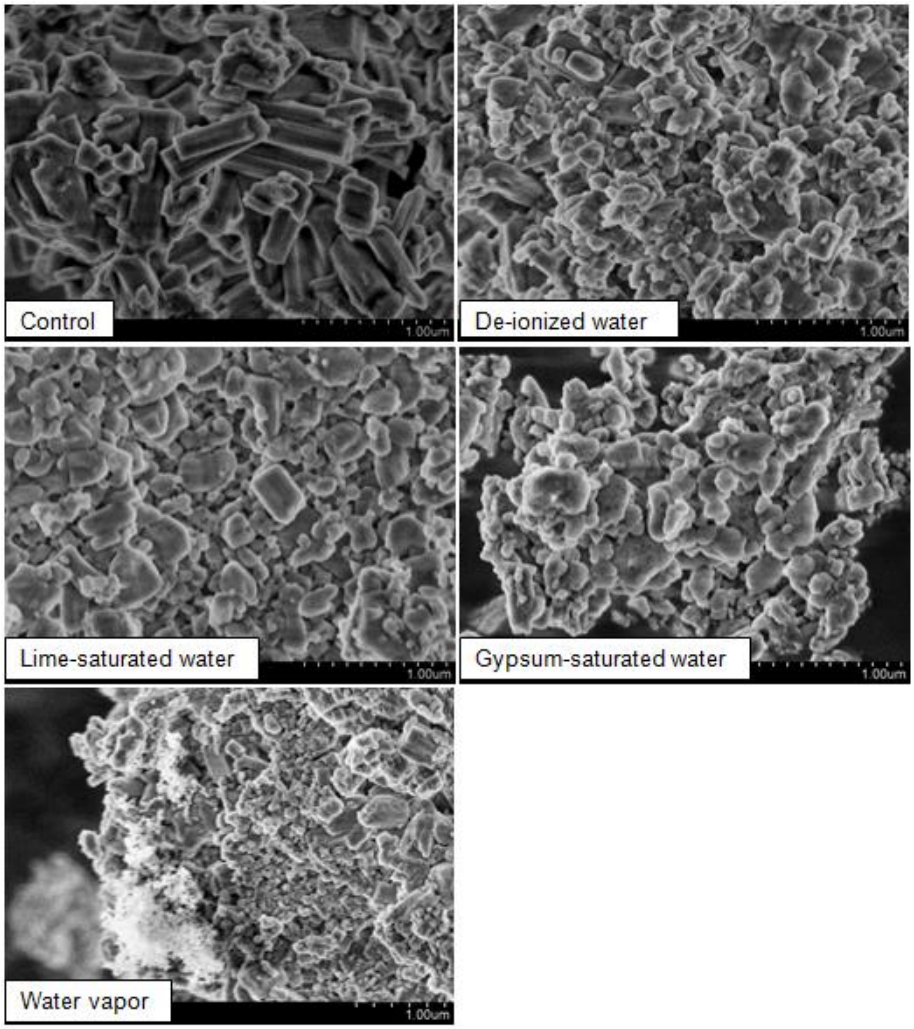

Figure 12-11- SEM micrographs of ettringite specimens immersed in de-ionized water, lime-saturated water, gypsum-saturated water and saturated water vapor for 24 h

The comparison of Figure 12-1 and Figure 12-8 indicates that the expansion of ettringite in de-ionized water is considerably lower than monosulfate which is also in conformity of the previous published investigations on the lower solubility of ettringite (at 25 °C) compared to that of monosulfate [24].

12.4 Conclusions

In this study, mechanisms of expansion of monosulfate and ettringite in de-ionized water and in presence of lime and gypsum solutions were investigated. The main conclusions are as follows:

- Dissolution of ettringite and monosulfate phases in the aqueous solutions results in significant expansion.
- A dissolution mechanism may be also a significant source of expansion in cement paste.
- Expansion of monosulfate and ettringite can occur in aqueous solutions containing no sulfate ions.
- Monosulfate exhibited larger expansion than ettringite in the test solutions which may be related to the higher solubility of monosulfate.
- Leaching of the sulfate ions which occurred immediately after the exposure to all the test solutions resulted in a significant expansion. The effect was not detected in the XRD patterns as these ions leached out of the interlayer of monosulfate structure or channels of the ettringite structure.
- Leaching of aluminum and calcium ions from the structure of monosulfate and ettringite cannot be detected by the XRD technique when it affects only a small percentage of the crystals. The leaching of these ions, especially aluminum, however, likely results in a significant expansion.
- Monosulfate and ettringite also expanded when they were exposed to the saturated water vapor. The mechanism of expansion is similar to that of exposure in de-ionized water but the expansion occurs at a lower rate.

References

1. E. A. Moore and F. W. Taylor, "Crystal structure of ettringite," *Acta Crystallographica Section B: Structural Science,* 26, pp. 386-393, 1970.

2. S. N. Ghosh, Advances in Cement Technology: Chemistry, Manufacture and Testing, Second Edition, Tech Books International, New Delhi, India, 2002.

3. R. Allmann, "Refinement of the hybrid layer structure $[Ca_2Al(OH)_6]^+ \cdot [1/2SO_4 \cdot 3H_2O]^-$," *Neues Jahrbuch fur Mineralogie Monatsheft*, pp. 136-44, 1977.

4. W. Michaelis, "Cement Bacillus," *The Engineering Record*, 16, p. 110, 1892.

5. W. C. Hansen, "Attack on Portland cement concrete by alkali soils and waters - A critical review," *Highway Research Record,* 113, pp. 1-32, 1966.

6. I. Odler and M. Gasser, "Mechanism of sulfate expansion in hydrated Portland cement," *Journal of the American Ceramic Society*, 71, pp. 1015-1020, 1988.

7. B. Mather, "A Discussion of the Paper 'Mechanism of Expansion-Associated Ettringite Formation' by P.K. Mehta," *Cement and Concrete Research*, 3, pp. 651-652, 1973.

8. W. C. Hansen, "A Discussion of the Paper 'Scanning Electron Microscopic Studies of Ettringite Formation' by P.K. Mehta," *Cement and Concrete Research*, 6, pp. 595-596, 1976.

9. P. K. Mehta, "Mechanism of Expansion Associated with Ettringite Formation," *Cement and Concrete Research*, 3, pp. 1-6, 1973.

10. P. K. Mehta and F. Hu, "Further evidence for expansion of ettringite by water adsorption," *Journal of the American Ceramic Society*, 61, pp. 179-181, 1978.

11. P. K. Mehta and S. Wang, "Expansion of ettringite by water adsorption," *Cement and Concrete Research*, 12, pp. 121-122, 1982.

12. T. Thorvaldson, "Chemical Aspects of the Durability of Cement Products," in Proceedings of the 3rd International Symposium on the Chemistry of Cement, Cement and Concrete Association, London, p. 463, 1952.

13. M. Collepardi, "Ettringite Formation and Sulfate Attack on Concrete," In supplementary papers, Proceedings of the 5th CANMET/ACI International Conference on Durability of Concrete, Barcelona, Spain, pp. 25-42, 2000.

14. S. Békri, J. F. Thovert and P.M. Adler, "Dissolution of porous Media," *Chemical Engineering Science*, 50, pp. 2765-2791, 1995.

15. G. G. Litvan, "Volume instability of porous solids: Part 2. Dissolution of porous silica glass in sodium hydroxide," *Journal of Materials Science*, 19(8), pp. 2473-2480, 1984.

16. G. G. Litvan, "Volume instability of porous solids: Part 1"; In Proceedings of the 7th International Congress on the Chemistry of Cement, Paris, Vol. III, pp. 46-50, 1980.

17. L. S. Dent Glasser and N. Kataoka, "The chemistry of alkali-aggregate reaction," *Cement and Concrete Research*, 11, pp. 1-9, 1981.

18. R. F. Feldman and P. J. Sereda, "Characteristics of sorption and expansion isotherms of reactive limestone aggregate," *Journal of the American Concrete Institute*, 58(2), pp. 203-214, 1961.

19. J. J. Beaudoin, S. Catinaud, J. Marchand and T. Sato, "Volume stability of hydrated Portland cement exposed aggressive solutions," *Industria Italiana del Cemento*, 72, pp. 954-67, 2002.

20. H. J. Kuzel, "Synthesis and X-Ray Study of the Crystalline Composition $3CaO.Al_2O_3.CaSO_4.12H_2O$," *Neues Jahrbuch Mineral Monatsh*, 7, pp. 193-197, 1965.

21. L. J. Struble and P. W. Brown, "An evaluation of ettringite and related compounds for use in the solar energy storage," NBSIR 82-253, USA, US Department of Commerce, p. 11, 1982.

22. H. F. W. Taylor, The Chemistry of Cements, Academic Press, London and New York, 1964.

23. L. Zhang and F. P. Glasser, "Critical examination of drying damage to cement pastes," *Advances in Cement Research*, 12, pp. 79-88, 2000.

24. M. Atkins, F. P. Glasser and A. Kindness, "Cement hydrate phases: solubility at 25 °C," *Cement and Concrete Research*, 22, pp. 241-6, 1992.

25. M. Atkins, D. Macphee, A. Kindness and F. P. Glasser, "Solubility properties of ternary and quaternary compounds in the CaO-Al_2O_3-SO_3-H_2O system," *Cement and Concrete Research*, 21, pp. 991-998, 1991.

26. H. Y. Ghorab and E. A. Kishar, "Studies on the stability of the calcium sulfoaluminate hydrates. Part I: Effect of temperature on the stability of ettringite in pure water," *Cement and Concrete Research*, 15, 93-99, 1985.

27. H. Y. Ghorab, E. A. Kishar and S. H. Abou Elfetouh, "Studies on the stability of the calcium sulfoaluminate hydrates. Part II: Effect of allite, lime and monocarboaluminate hydrate," *Cement and Concrete Research*, 28, 53-61, 1998.

Chapter 13

Solvent-Exchange in Sulfoaluminate Phases – Part I: Ettringite

The change in the microstructure of ettringite and concomitant changes in volume due to the application of organic solvent-exchange methods were investigated. Ettringite samples conditioned to 11% relative humidity were treated with methanol, ethanol and isopropanol, and were examined by different analytical techniques including XRD, FTIR, TGA, SEM and nitrogen BET surface area measurement to explore the limitations of using these organic solvents in the study of ettringite microstructure. The results suggest that methanol interacts with ettringite. It, therefore, is not recommended for the characterization of this sulfoaluminate phase. Ethanol and isopropanol did not significantly change the crystalline structure of ettringite. They, however, resulted in the higher surface area of the treated sample compared with the surface area of the untreated one. Length-change of ettringite in these alcohols was also determined in addition to the microstructure study, and the results are presented.

13.1 Introduction

Solvent replacement techniques have been used by several researchers to characterize the microstructure of hydrated cement systems [1-4]. An organic liquid, miscible with water, but with higher vapor pressure is used in this technique to remove water from the investigated system [5]. Some alcohols, such as methanol and isopropanol, and also acetone are examples of the commonly used solvents. It is often assumed that these organic solvents

are inert with respect to the hydrated cement solid, and do not affect the results of microstructural investigation [6, 7]. Some evidence, however, has been published indicating that this assumption is not always correct [8, 9].

Beaudoin [10] suggested that treatment with alcohol resulted in the microstructural changes of calcium silicate hydrate (C-S-H) systems which were detectable by the X-ray diffraction (XRD) and thermal analytical techniques. In addition, the nitrogen surface area and pore size distribution of cement paste systems were largely affected by the alcohol treatment. Evidence provided by the length-change measurement of calcium hydroxide (CH) compacts in methanol and isopropanol demonstrated that it is not only the C-S-H phase in cement paste that is influenced by the alcohol treatment [11]. Day [12] also suggested that methanol reacts with calcium hydroxide forming calcium methoxide or a carbonate like product. The investigation performed by Beaudoin [13] supported the hypothesis that methanol reacts with calcium hydroxide at 22 °C.

The suggestion that organic solvents react with cementitious phases is not accepted by all researchers. Some authors [7, 14] suggested that methanol exchange was suitable for the pore structure investigation. Hansen and Gran [15] also reported that no evidence of chemical interaction between ethanol and cement paste solids was detected by the ^{13}C NMR spectroscopy. In addition to the controversy regarding the validity of using organic solvent for the microstructure study of C-S-H and CH, it is noted that very few papers have been published on the application of solvent-exchange methods in the study of sulfoaluminate phases. The influence of other drying techniques such as vacuum drying and desiccant drying on the structure of sulfoaluminate phases has been investigated recently by Zhang and Glasser [5]. The validity of utilizing organic solvent-exchange methods for this purpose has not been confirmed. Its use is not fully understood.

The intent of this chapter was to investigate the influence of aliphatic alcohols on the microstructure of ettringite ($3CaO.Al_2O_3.3CaSO_4.30\text{-}32H_2O$). Part II to be reported in the following chapter will focus on a similar investigation of the monosulfate phase ($3CaO.Al_2O_3.CaSO_4.12H_2O$). The interaction between methanol, ethanol and isopropanol, as the solvent, and these sulfoaluminate phases was explored by the X-ray diffraction (XRD), thermal gravimetric analysis (TGA), Fourier transform infrared spectroscopy

(FTIR), scanning electron microscopy (SEM), nitrogen BET surface area and length-change measurements.

13.2 Experimental Program

Ettringite was synthesized by a method described by Struble and Brown [16] (see chapter 3). The ettringite powder was kept in desiccators over saturated lithium chloride solution, at a relative humidity of 11%, until equilibrium was obtained prior to conducting the experiments. The powder was immersed in the solvent for different intervals of 15 minutes to 24 hours. Methanol, ethanol and isopropanol were used as the solvent, and the solid-solvent ratio was 1 gr of solid per 50 ml of the solvent in all the experiments. The solvent was discharged when the immersion time was completed, and the solid was vacuum-dried for about 2 minutes. The experiments performed are described in the following paragraphs. All these experiments were performed on the powder, except the FTIR spectroscopy and the length-change measurements which required compacted samples. The compaction procedure for these two tests is described in the corresponding sections.

XRD - XRD measurements were performed using a Scintag XDS 2000 diffractometer and CuK_α radiation. The spectra were collected with a diffraction angle range of $6^\circ < 2\theta < 60^\circ$ using a step size of 0.08° at 5 second count interval with an accelerating voltage of 45 kV and current of 35 mA. Intensities were, then, normalized according to the mass of the samples.

FTIR spectroscopy - Samples were ground to a fine powder with potassium bromide, and compacted into a disk of 10 mm diameter using a 10 ton load. FTIR spectra were collected on a Tensor 27 spectrometer in direct transmission mode between 4000 and 400 cm^{-1}. Each FTIR spectrum represented the average of 50 scans at 4 cm^{-1} resolution. Air was used as a background for the measurements.

TGA - The TGA was performed using a TA Instruments SDT Q-600. About 25 mg of the sample was heated from ambient temperature to 1000 °C at a rate of 10 °C/min under the flow of nitrogen gas (10 ml/min). The derivative mass loss and heat flow were analyzed

using Universal Analysis 2000 software. NETZSCH Peak Separation software, version 2010.09, was also used to analyse the overlapping peaks in the derivative mass-loss curve.

BET surface area - Nitrogen BET surface area measurement was performed using the Quantachrome instrument, NOVA 2200e surface area and pore size analyzer. The samples were vacuum-dried at 40 °C for one hour prior to starting the measurements.

SEM - The SEM images were collected using a Hitachi S-4800 Field Emission Scanning Electron Microscope. Surface structure images were taken using a beam current of 10 mA at 3.2×10^{-16} J (2 kV). Images were acquired at a working distance of 8 mm.

Length-change measurements - The ettringite powder was compacted to produce porous bodies in the form of circular discs (32 mm in diameter × 1 mm thick). The compaction pressure was adjusted to have a porosity of 10% for the samples. Then, prisms, 5 × 25 × 1 mm thick, were cut from the compact samples, and mounted on modified Tuckerman extensometers. The prepared samples were placed in each alcohol with the same solid/solvent ratio as the other tests, and the length-change was continuously measured for up to 14 days.

13.3 Results and discussion

13.3.1 XRD

The XRD patterns of ettringite samples immersed in methanol for various intervals are given in Figure 13-1. The intensity of the ettringite peaks was reduced significantly even after 15 minutes immersion in methanol. Small peaks of ettringite crystals were still present in the sample after 2 and 6 hours. The peaks, however, completely disappeared after 24 hours suggesting that solvent-exchange with methanol likely resulted in the breakdown of the crystalline structure of ettringite and formation of an amorphous material.

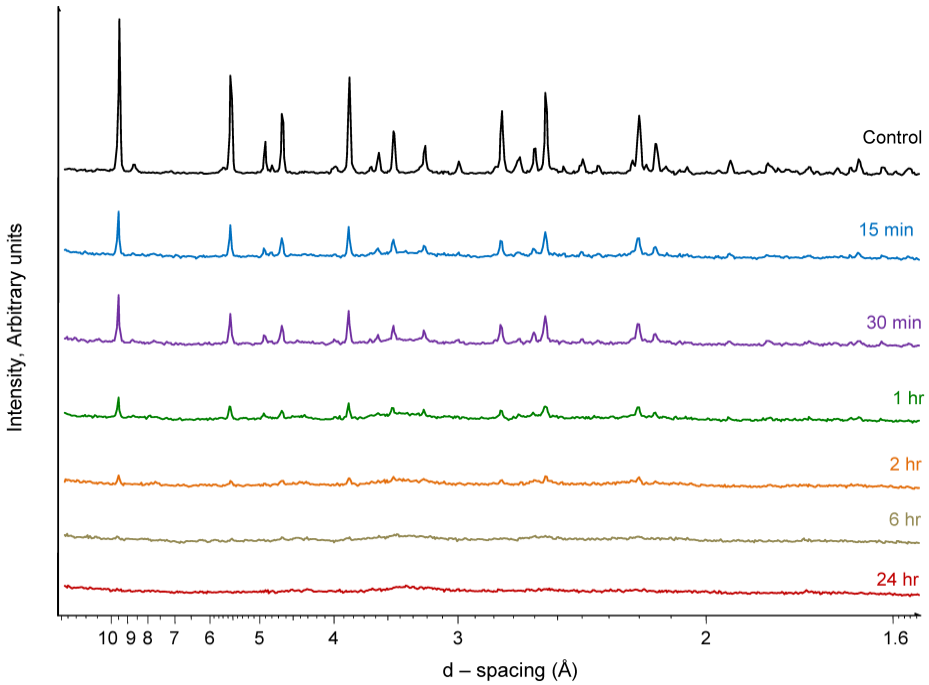

Figure 13-1- XRD patterns of ettringite samples immersed in methanol for various periods

The intensity of the 9.73 Å peak, associated with the intercolumn distances in the ettringite structure [17], was dramatically reduced due the methanol treatment. This indicates that the intercolumn bonds have been disturbed. Methanol molecules are of small size (3.6 Å in diameter), and likely entered the intercolumnar space of the ettringite structure in addition to adsorption on the surface. In addition, the hydroxyl group of methanol possibly replaced some of the hydroxyl groups of the ettringite structure. The two structural columns of ettringite include 24 water molecules which are attached to the calcium polyhedra, half of them in the main vertices and the other half in the additional vertices of the trigonal prisms, and six hydroxyl groups which form the aluminum and calcium polyhedra [18]. Skoblinskaya et al. [17] suggested that the intensity of XRD peaks of ettringite ($3CaO.Al_2O_3.3CaSO_4.30H_2O$) was reduced due to the removal of 12 water molecules located in the additional vertices of the calcium polyhedra. The crystalline structure of ettringite, however, was still retained in the sample with 18 molecules of water. They, however, reported that ettringite became likely amorphous due to the removal of water molecules from the main vertices of the calcium polyhedra, and the 9.73 Å peak was not present in the ettringite sample with 12.8 water molecules. These dehydration theories

corroborated by the XRD patterns of Figure 13-1 suggest that methanol possibly replaced even some of the water molecules in the main vertices resulting in the significant distortion of the ettringite crystals.

The hydrogen atoms of water molecules located in the main vertices of the calcium polyhedra are arranged in horizontal planes, and, therefore, are capable of forming hydrogen bonds with the sulfate and water molecules in the intercolumnar channels [18] as well as with the surface adsorbed water [19]. These atoms could also participate in hydrogen bonding with methanol molecules possibly resulting in some change in the crystalline structure of ettringite. It is, however, possible that the hydroxyl group of methanol had formed a hydrogen bond with these hydrogen atoms through its oxygen, and with the hydroxyl group of aluminum polyhedra through its hydrogen atom; the new structured material was not as well crystalline as the ettringite itself. The chemical bonding of the 24 hour methanol treated ettringite was studied by the IR spectroscopy technique in order to explore the details of formation of new bonds due to the chemical interaction of methanol with ettringite. This is reported in the following section 13.3.2.

The XRD patterns of ettringite samples after 24 hours immersion in methanol, ethanol and isopropanol are compared in Figure 13-2. In contrast with the XRD pattern associated with the methanol treatment, no significant change in the XRD pattern of ettringite samples was observed due to the solvent-exchange with ethanol and isopropanol. The absence of a diffraction line broadening or reduction of the intensity of the 9.73 Å peak for the ethanol and isopropanol treated samples suggests that the intercolumnar distances did not significantly change during the treatment.

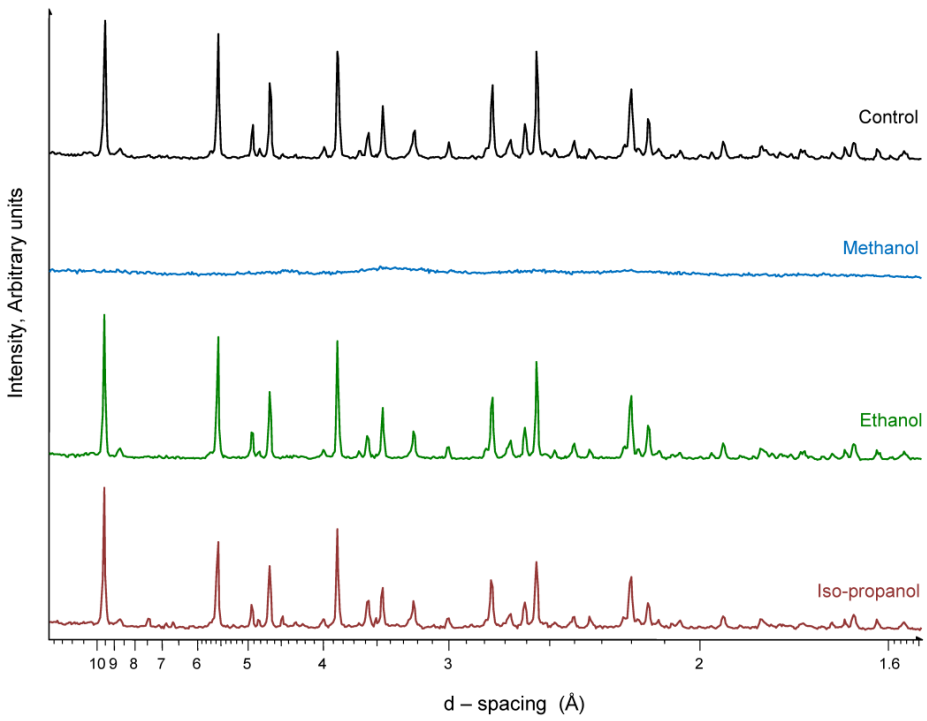

Figure 13-2- XRD patterns of the ettringite sample immersed in methanol, ethanol and isopropanol for 24 h

13.3.2 FTIR spectroscopy

The FTIR spectra of the methanol-treated sample suggest that the intensity of the bond with a frequency of 3630 cm^{-1} was lower in the methanol treated ettringite compared to in pure ettringite (Figure 13-3). This peak corresponds to the free hydroxyl group which is likely assigned to the Ca-bonded groups [20, 21] that do not form a hydrogen bond. The reduction in the intensity of this bond is in conformity with the XRD results suggesting that the water molecules in the additional vertices of the calcium polyhedra were partially replaced with methanol.

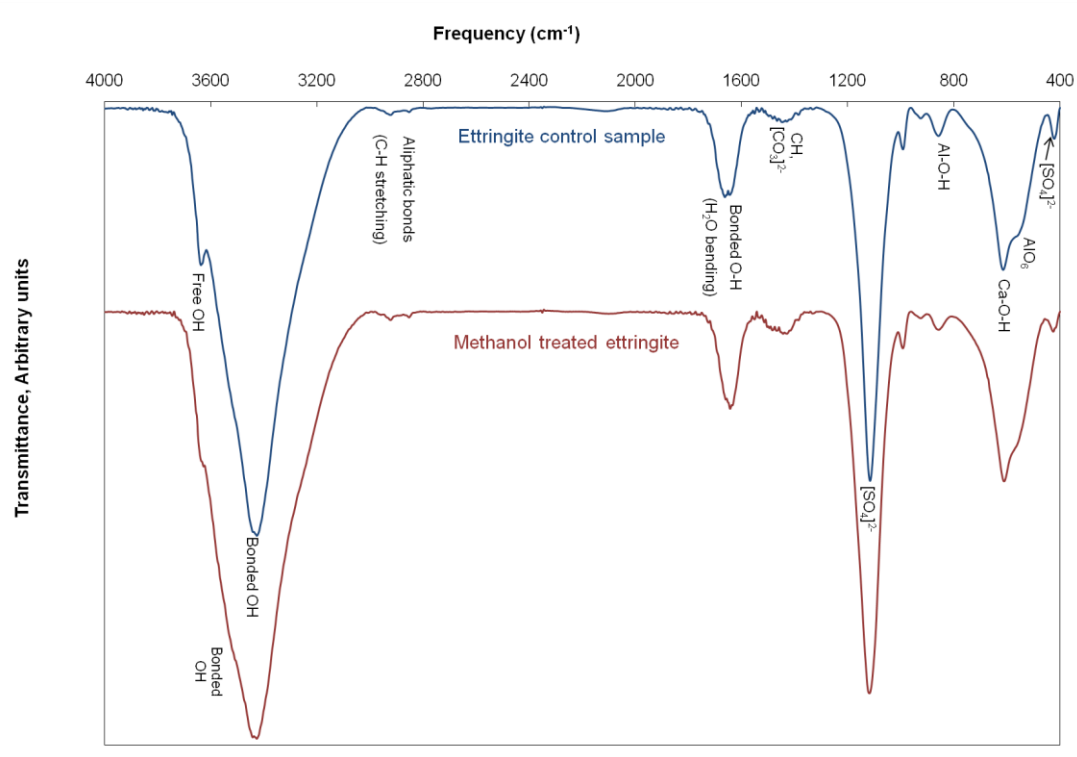

Figure 13-3- FTIR spectra of the ettringite sample and the 24-hour methanol-treated ettringite sample

A new bond is formed due to the methanol treatment at a frequency of about 3530 cm^{-1} which likely corresponds to the hydrogen-bonded hydroxyl group of methanol [22]. This hydrogen bond is possibly formed between methanol and the free water of ettringite, and/or replaces some of the hydrogen bonds in the ettringite structure. The peaks between 1400 and 1500 cm^{-1} likely correspond to the $(CO_3)^{-2}$ [23, 24] and C-H bonds [25]. The peaks between 2800 to 3000 cm^{-1} also represent aliphatic bonds [25] and possibly some aluminum methoxy groups [26]. The presence of organic peaks in the control sample is due to the use of the sucrose solution in the synthesis of ettringite. The intensity of these peaks, however, was increased due the methanol treatment. The asymmetric broadening of the peak at 1128 cm^{-1} in the methanol treated sample is possibly due to the presence of C=O bond at about 1149 cm^{-1} [22].

13.3.3 TGA

Ettringite normally loses its water at temperatures lower than 500 °C, mainly at about 120 °C and 230 °C, during the TGA experiment [27]. The peaks that appear between 550 to 1000 °C likely correspond to the release of some sulphur oxides which occur during the TGA experiment of ettringite synthesized in sucrose solution [28] and natural ettringite [29]. FTIR spectra of the ettringite sample after heating up to 1000 °C during the TGA technique, data not presented here, suggest that the intensity of the SO_4^{2-} peak was significantly reduced.

The derivative of mass-loss curves for the ettringite sample and the methanol treated ettringite samples at different intervals are presented in Figure 13-4. The peak appearing at about 40 to 60 °C corresponds to the release of the adsorbed methanol. The decrease of the area of the peaks at 120 and 230 °C in the methanol treated samples suggests that the methanol treated samples had significantly lower water content compared to the control one. Further decrease of the water content of the sample was observed by increasing the time of immersion in methanol. A large amount of water, however, was removed from the ettringite sample in the first 15 minutes of immersion. The mass-loss percentage of the ettringite sample immersed in different alcohols due to the release of water molecules in the TGA experiment is presented in Figure 13-5. The peaks corresponding to water and the alcohols were separated using the NETZSCH Peak Separation software. Assuming 30-32 molecules of water for the control sample, it is estimated that the ettringite sample had about 21 water molecules after 15 minutes of immersion in methanol. The water content of the methanol treated samples was likely reduced to about 18.5, 14 and 10.7 water molecules, respectively, after immersion for 1, 2 and 24 hours. These results are in good conformity with the XRD spectra indicating the damage of ettringite crystals is due to the removal of water molecules from the main structure of the ettringite crystals. Additional XRD and TGA experiments were performed on the 24 hour methanol treated ettringite sample after 6 months exposure to the room humidity conditions. The results were similar to the results presented in Figures 13-1 and 13-4, suggesting that the distortion of the crystalline structure of ettringite and the loss of water content due to the methanol interaction is likely irreversible.

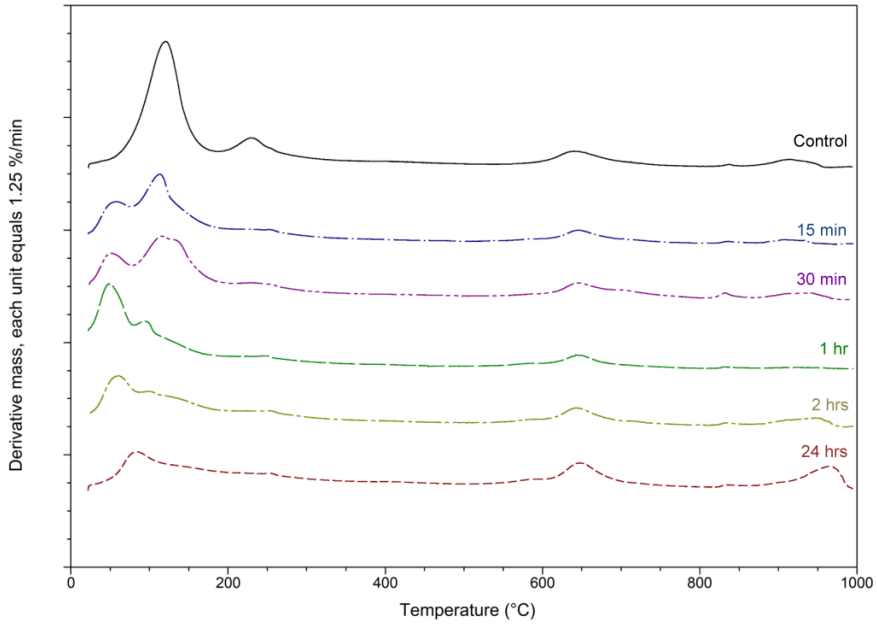

Figure 13-4- Derivative of mass-loss curves in the TGA experiment for the control ettringite sample and the samples immersed in methanol for different time intervals

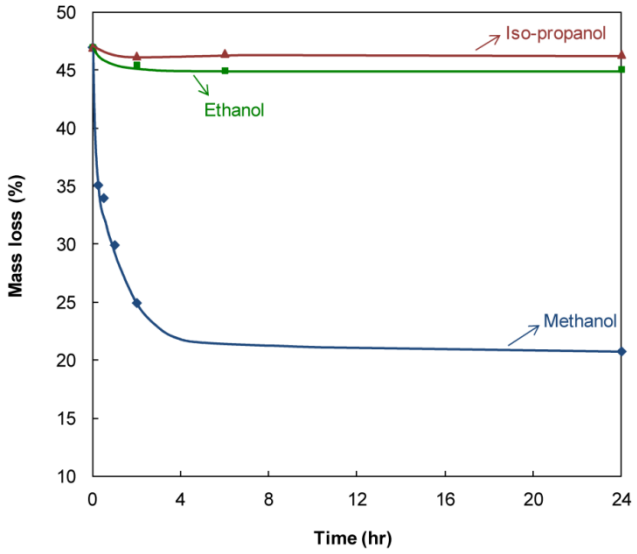

Figure 13-5- Mass loss due to the release of water molecules during the TGA experiment for the ettringite samples immersed in methanol, ethanol and isopropanol

The derivative of mass-loss curves for the ettringite samples after 24 hours immersion in methanol, ethanol and isopropanol are summarized in Figure 13-6. This figure together with the mass-loss curves of Figure 13-5 suggests that it was mainly the surface water that

was replaced due to the treatment with ethanol and isopropanol. In the case of ethanol treatment, some of the intercolumn water was possibly also replaced. No signs of change in the structural water of ettringite were, however, observed due to the solvent-exchange with ethanol or isopropanol.

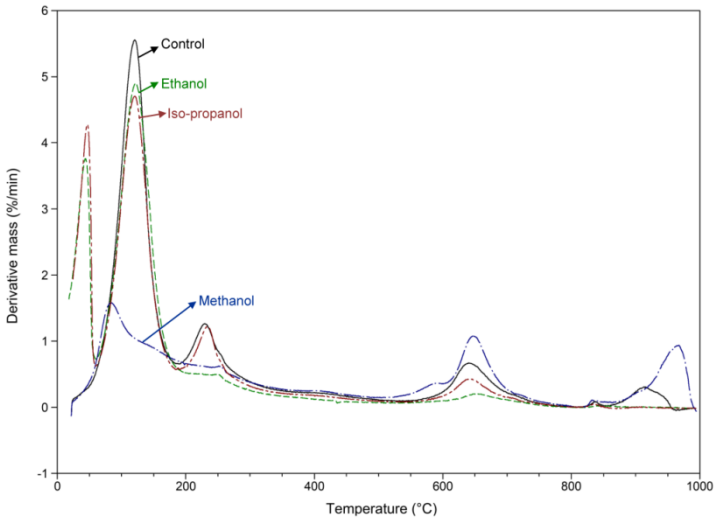

Figure 13-6- Derivative of mass loss curves in the TGA experiment for the ettringite samples immersed in methanol, ethanol and isopropanol for 24 h

13.3.4 BET Surface area

Nitrogen BET surface area of ettringite was significantly increased due to the methanol treatment. Figure 13-7 suggests that the ettringite sample immersed in methanol for 24 hours had a surface area of about 10 times higher than the surface area of the control sample. The high surface area of the methanol treated sample was expected due to the amorphous structure and lower water content of the formed material.

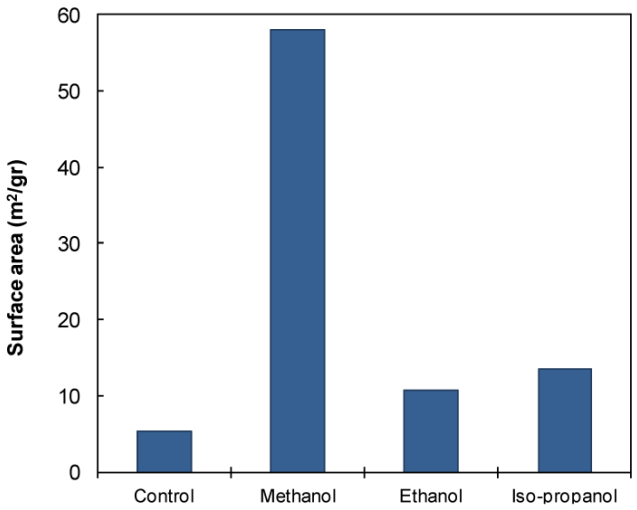

Figure 13-7- Nitrogen BET surface area of the ettringite samples immersed in methanol, ethanol and isopropanol for 24 h

Solvent-exchange with ethanol and isopropanol also increased the surface area of ettringite samples (Figure 13-7). The increase of the surface area of ettringite due to the treatment with ethanol and isopropanol was, however, significantly lower than the increase of the surface area due to the methanol treatment.

13.3.5 SEM

SEM images of ettringite before and after the solvent-exchange with methanol, ethanol and isopropanol are presented in Figure 13-8. The figure suggests that the methanol-treated sample was composed of mainly amorphous particles and some ettringite-shaped particles with smaller size compared to the size of ettringite crystal in the control sample. No significant change was observed in the ettringite texture due to the solvent-exchange with ethanol and isopropanol.

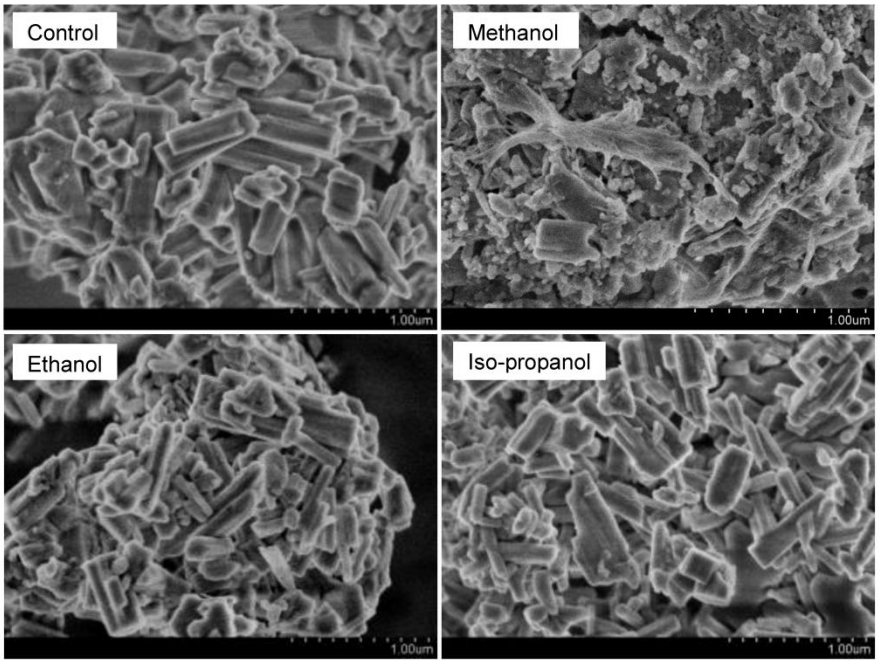

Figure 13-8- SEM images of the ettringite samples immersed in methanol, ethanol and isopropanol for 24 h

13.3.6 Length-change measurements

The ettringite sample significantly expanded due to the immersion in methanol (Figure 13-9) which is possibly due to the decrease of the surface energy of the ettringite sample due to replacement of the surface water with the solvent. The theoretical details of the length-change of solids due to the adsorption process in general, based on the Gibbs's and Bangham equations, are provided by Feldman [30]. He applied the Bangham equation to the hydrated cement-water system to account for the expansion from the physically adsorbed water. The Bangham effect can also be operative in other porous materials such as compacted ettringite samples. In addition to the Bangham effect, the entry of methanol between the ettringite columns may also be a significant source of expansion. The replacement of water with methanol in the columnar structure is likely expansive due to the larger molecular size of methanol. Formation of hydrogen bonding between methanol and ettringite may also be a source of expansion. The expansion of the ettringite sample in methanol followed by a contraction after three days (Figure 13-9(b)) suggests that the

material formed due to this interaction possibly has a higher density compared to the density of the untreated ettringite sample.

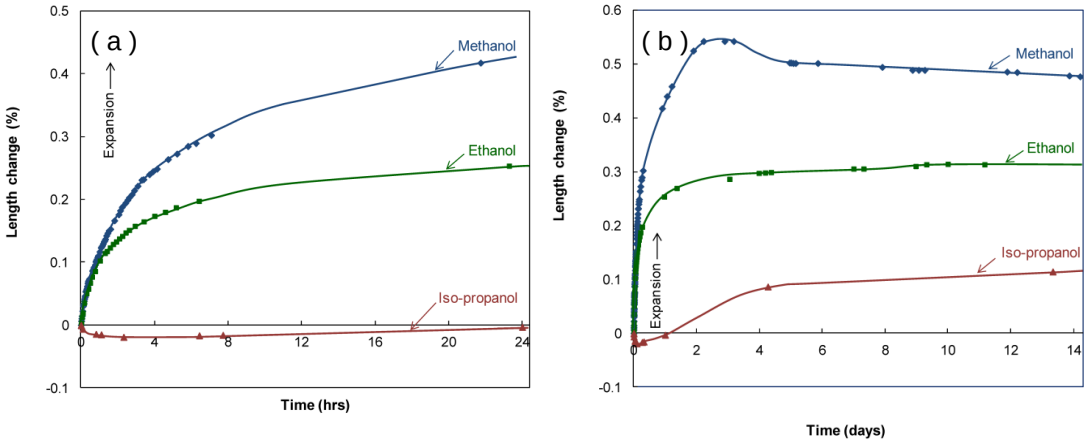

Figure 13-9- Length change of ettringite sample immersed in methanol, ethanol and isopropanol up to (a) 24 h, (b) 14 d

The expansion of ettringite in ethanol is likely due to the decrease of surface energy. The size of the ethanol molecule (4.5 Å) is larger than the size of methanol molecule (3.6 Å), and it is unlikely that it enters the intercolumn space of the ettringite structure.

The length-change curve of ettringite in isopropanol shows contraction followed by the expansion after about 24 hours. The surface energy of ettringite is possibly increased in the first day of immersion in isopropanol resulting in the slight contraction. The expansion after one day of immersion may be due to the formation of some new hydrogen bonds.

13.4 Conclusions

The microstructure of ettringite samples treated with methanol, ethanol and isopropanol was investigated. The main conclusions are as follows:

- Methanol reacts with ettringite. It replaces some of the water molecules in the structure of ettringite, and forms some hydrogen bonds with the ettringite structure.

- The methanol treated ettringite was poorly crystalline. It had lower water content and significantly higher surface area compared to the water content and the surface area of ettringite itself.
- The expansion of ettringite in the test alcohols was in the following order: methanol > ethanol > isopropanol. Differences are due to the greater chemical interaction following immersion in methanol, surface energy considerations and the relative size of the alcohol molecules.
- The crystalline structure of the ettringite samples as detected by the XRD technique was unaffected by treatment with ethanol and isopropanol.
- There are some limitations on the use of methanol, ethanol and isopropanol for the surface area determination of ettringite. The surface area of the sample, however, was less affected by ethanol and isopropanol compared with methanol.

References

1. J. J. Beaudoin, B. Tamtsia, J. Marchand and H. R. Myers, "Solvent exchange in partially saturated and saturated microporous systems - Length change anomalies," *Cement and Concrete Research*, 30(3), pp. 359-370, 2000.
2. L. J. Parrot, "Effect of drying history upon the exchange of pore water with methanol and upon subsequent methanol sorption behaviour in hydrated alite paste," *Cement and Concrete Research*, 11(5), pp. 651-658, 1981.
3. R. F. Feldman and J. J. Beaudoin, "Pretreatment of hardened hydrated cement pastes for mercury intrusion measurements," *Cement and Concrete Research*, 21(2), pp. 297-308, 1991.
4. R. F. Feldman, "Diffusion measurements in cement paste by water replacement using propan-2-ol," *Cement and Concrete Research*, 17(4): pp. 602-612, 1987.
5. L. Zhang and F. P. Glasser, "Critical examination of drying damage to cement paste," *Advances in Cement Research*, 12(2), pp. 79-88, 2000.

6. R. S. Mikhail and S. A. Selini, "Adsorption of organic vapors in relation to the pore structure of hardened Portland cement pastes", Symposium on Structure of Portland Cement Paste and Concrete, Highway Research Board Special Report 90, pp. 122–134 Washington, 1966.

7. L. Parrot, "Thermogravimetric and sorption studies of methanol exchange in an alite paste," *Cement and Concrete Research*, 13(1), pp. 18-22, 1983.

8. H. F. W. Taylor and A. B. Turner, "Reactions of tricalcium silicate paste with organic liquids," *Cement and Concrete Research*, 17(4), pp. 614–662, 1987.

9. J. J. Beaudoin, "A comparison of mechanical properties of compacted calcium hydroxide and Portland cement paste systems," *Cement and Concrete Research*, 13, pp. 319-324, 1983.

10. J. J. Beaudoin, "Interaction of aliphatic alcohols with cement systems," *Il Cemento*, 83, pp. 199-210, 1986.

11. J. J. Beaudoin, P. Gu, J. Marchand, B. Tamtsia, R. E. Myers and Z. Liu, "Solvent replacement studies of hydrated Portland cement systems: The role of calcium hydroxide," *Advances in Cement Based Materials*, 8(2), pp. 56-65, 1998.

12. R. L. Day, "Reactions between methanol and Portland cement paste," *Cement and Concrete Research*, 11(3), pp. 341-349, 1981.

13. J. J. Beaudoin, "Validity of using methanol for studying the microstructure of cement paste," *Materials and Structures*, 20(115), pp. 27-31, 1987.

14. M. D. A. Thomas, "The suitability of solvent exchange techniques for studying the pore structure of hardened cement paste," *Advances in Cement Research*, 2(1), pp. 29-34, 1989.

15. E. W. Hansen and H. C. Gran, "Carbon NMR used in probing the exchange of ethanol with water in water-saturated cement pastes," *Magnetic Resonance Imaging*, 14, pp. 903-904, 1996.

16. L. J. Struble and P. W. Brown, "An evaluation of ettringite and related compounds for use in the solar energy storage," NBSIR 82-253, USA, US Department of Commerce, p. 11, 1982.

17. N. N. Skoblinskaya, K. G. Krasilnikov, L. V. Nikitina and V. P. Varlamov, "Change in the crystal structure of ettringite due to dehydration. Part 2," *Cement and Concrete Research*, 5, pp. 419-432, 1975.

18. E. A. Moore and F. W. Taylor, "Crystal structure of ettringite," *Acta Crystallographica Section B: Structural Science*, 26, pp. 386-393, 1970.

19. N. N. Skoblinskaya and K. G. Krasilnikov, "Change in the crystal structure of ettringite due to dehydration. Part 1," *Cement and Concrete Research*, 5, pp. 381-394, 1975.

20. D. Gastaldi, F. Canonico and E. Boccaleri, "Ettringite and calcium sulfoaluminate cement: investigation of water content by near-infrared spectroscopy," *Journal of Materials Science*, 44, pp. 5788-5794, 2009.

21. M. A. Trezza and A. E. Lavat, "Analysis of the system $3CaO.Al_2O_3$-$CaSO_4.2H_2O$-$CaCO_3$-H_2O by FT-IR spectroscopy," *Cement and Concrete Research*, 31, pp. 869-872, 2001.

22. J. Kotrla, D. Nachtigallova, L. Kubelkova L, L. Heeribout, C. Doremieux-Morin and J. Fraissard, "Hydrogen bonding of methanol with bridged OH groups of zeolite: Ab Initio calculation," ^1H NMR and FTIR studies, *The Journal of Physical Chemistry B*, 102(14), pp. 2454-2463. 1998.

23. R. B. Perkins and C. D. Palmer, "Solubility of ettringite ($Ca_6[Al(OH)_6]_2(SO_4)_3.26H_2O$) at 5-75 °C", *Geochimica et Cosmochimica Acta*, 63(13/14), pp. 1969-1980, 1999

24. E. Ciliberto, I. Salvatore and F. Manuella, "Ettringite and thaumasite: A chemical route for their removal from cementitious artefacts," *Journal of Cultural Heritage*, 9, pp. 30-37, 2008.

25. C. Flengo, A. Carati and C. Perego, "Methanol interaction with mesoporous silica-aluminas," *Microporous and Mesoporous Materials*, 44-45, pp. 733-744, 2001.

26. Z. Jiang, "In situ FTIR studies of extra framework aluminum bound methoxy species in H-ZSM-5 zeolites," *Journal of Molecular Catalysis*, 121(1), pp. 63-68, 1997.

27. H. F. W. Taylor, The Chemistry of Cements. 2nd edition, Thomas Telford, New York, 1997.

28. F. Goets-Neunhoeffer, J. Neubauer and P. Schwesig, "Mineralogical characteristics of ettringites synthesized from solutions and suspensions," *Cement and Concrete Research*, 36, pp. 65-70, 2006.

29. S. M. Antao, M. J. Duane and I. Hassan, "DTA, TG, and RD studies of sturmanite and ettringite," *The Canadian Mineralogist*, 40, pp. 1403-1409, 2002.

30. R. F. Feldman, "Sorption and length-change scanning isotherms of methanol and water on hydrated Portland cement," Proceeding of the 5th International Symposium on the Chemistry of Cement, Tokyo, Vol. III, pp. 53-66, 1968.

Chapter 14

Solvent-Exchange in Sulfoaluminate Phases – Part II: Monosulfate

The influence of organic solvent-exchange techniques on the microstructure and the dimensional stability of monosulfate ($3CaO.Al_2O_3.CaSO_4.12H_2O$) was critically investigated. Monosulfate samples were treated with methanol, ethanol and isopropanol, and examined by different analytical techniques including XRD, FTIR, TGA and SEM. Nitrogen BET surface area measurements and length-change of the monosulfate samples in the solvents were also recorded. Evidence was obtained that indicates monosulfate was readily dehydrated from 12 water molecules to 10 water molecules once it was treated by the investigated alcohols. The alcohol molecules, however, likely intercalated into the monosulfate structure limiting an expected decrease in the interlayer distance of the monosulfate structure. Methanol had the greatest damaging effect on the monosulfate microstructure. Ethanol, however, resulted in higher long-term expansion due to its intermediate molecular size and reactivity with monosulfate compared to methanol and isopropanol.

14.1 Introduction

The solvent-exchange technique is one of the common drying methods for the study of hydrated cement phases [1-4]. An organic liquid like methanol or isopropanol, which is miscible with water but has a higher vapor pressure, is used in this technique to remove water from the system [5]. There, however, remains controversy as to the possibility of interaction of these organic solvents with the hydrated cement paste phases [6-11]. Some evidence of the reaction of organic solvents with the calcium silicate hydrate (C-S-H) and calcium hydroxide phases (CH) in cement paste has been reported [12-15]. It, however, is not accepted by all the researchers [6, 7].

It is noted that very few investigations have been performed on the application of solvent-exchange methods in the study of sulfoaluminate phases. The influence of using methanol, ethanol and isopropanol on the microstructural characteristics and the dimensional stability of ettringite was studied in chapter 13. Evidence was obtained on the interaction of methanol with ettringite resulting in the formation of a semi-amorphous material with significantly lower water content compared to ettringite itself. No permanent effect of ethanol and isopropanol on the microstructure of ettringite was, however, observed.

The published investigations on the influence of drying techniques on the monosulfate characteristics are even fewer than those published on ettringite. Difficulty with the synthesis of pure monosulfate [5] is possibly a reason for this. Zhang and Glasser [5] examined the influence of vacuum drying, d-drying and desiccant drying on the structure of ettringite and monosulfate. They suggested that monosulfate is more sensitive than ettringite to changes in the hydration state during drying.

The intent of this investigation was to explore the validity of using aliphatic alcohols for drying monosulfate ($3CaO.Al_2O_3.CaSO_4.12H_2O$). The influence of methanol, ethanol and isopropanol on the monosulfate microstructure was examined by the XRD, thermal gravimetric analysis (TGA), Fourier transform infrared spectroscopy (FTIR) and scanning electron microscopy (SEM) techniques. The nitrogen BET surface area values were determined and length-change measurements of monosulfate in these alcohols were also recorded.

14.2 Experimental Program

Monosulfate was synthesized by a method described by Kuzel [16]. It consisted of reacting stoichiometric amounts of tricalcium aluminate (C_3A) and gypsum ($CaSO_4.2H_2O$) in an excess amount of water in a hydrothermal pressure vessel as described in chapter 3. The monosulfate powder with a relative humidity of 11% was immersed in the solvent for periods of 1, 2, 6 and 24 hours. Methanol, ethanol and isopropanol were used as the solvent, and the solid-solvent ratio was 1 g of solid per 50 ml of the solvent in all the experiments. The solvent was discharged after the treatment time was completed, and the solid was vacuum-dried for about 2 minutes. The dried powder was, then, used in the experiments described in the following sections. It is noted that the FTIR spectroscopy and the length-change measurements were performed on compacted samples. The compaction procedure for these two experiments is described in the corresponding sections.

XRD - A Scintag XDS 2000 diffractometer and CuK_α radiation was used for obtaining the XRD spectra. The spectra were collected with a diffraction angle range of $6^\circ < 2\theta < 60^\circ$ using a step size of 0.08° at a 5 second count interval. Intensities were, then, normalized according to the mass of the samples.

FTIR spectroscopy - Monosulfate powder was ground with potassium bromide, and compacted into a disk of 10 mm diameter using a 98 kN load. FTIR spectra were collected on a Tensor 27 spectrometer in direct transmission mode between 4000 and 400 cm^{-1}. Each FTIR spectrum represented the average of 50 scans at 4 cm^{-1} resolution. Air was used as a background for the measurements.

TGA - Simultaneous thermogravimetric analysis and differential scanning calorimetry (TGA-DSC) experiments were performed using a TA Instruments SDT Q-600. About 25 mg of the sample was heated from ambient temperature to 1000 °C at a rate of 10 °C/min under the flow of nitrogen gas (10 ml/min). The derivative mass loss and heat flow were analyzed using Universal Analysis 2000 software. NETZSCH Peak Separation software, version 2010.09, was also used for the deconvolution of the overlapping peaks in the derivative mass-loss curve.

BET surface area - The nitrogen BET surface area of the samples was determined using the Quantachrome instrument, NOVA 2200e surface area and pore size analyzer. The samples were vacuum-dried at 40 °C for one hour prior to starting the measurements.

SEM - SEM images were collected using a Hitachi S-4800 Field Emission Scanning Electron Microscope. The surface structure images were acquired at the working distance of 8 mm using a beam current of 10 mA at 3.2×10^{-16} J (2 kV).

Length-change measurements - The monosulfate powder was compacted to form circular discs (32 mm in diameter × 1 mm thick). The compaction pressure was adjusted to reach a porosity of about 10% for the samples. The porosity of the samples was determined using a Beckman helium pycnometer. Prisms, with the dimension of 5 × 25 × 1 mm, were cut from the compact samples, and mounted on modified Tuckerman extensometers with an accuracy of 1 microstrain. The prepared samples were placed in each alcohol with the same solid/solvent ratio as the other experiments. The length-change was continuously measured for up to 14 days.

14.3 Results and discussion

14.3.1 XRD

The XRD patterns of the methanol treated samples at different time intervals are presented in Figure 14-1. The basal spacing of 8.93 Å in these spectra corresponds to the interlayer distance of monosulfate with 12 molecules of water ($3CaO.Al_2O_3.CaSO_4.12H_2O$ or AFm-12). Six of these water molecules build the main layers of the monosulfate structure, and the remaining water molecules are located between the layers [17]. Allmann [17] suggested that two thirds of the interlayer water molecules are bound to the calcium atoms of the main layers, and the other one third is likely free in the interlayer space of the monosulfate structure. Removal of the two unbonded water molecules of AFm-12 is known to reduce its basal spacing from 8.93 Å to 8.15 Å [5, 18].

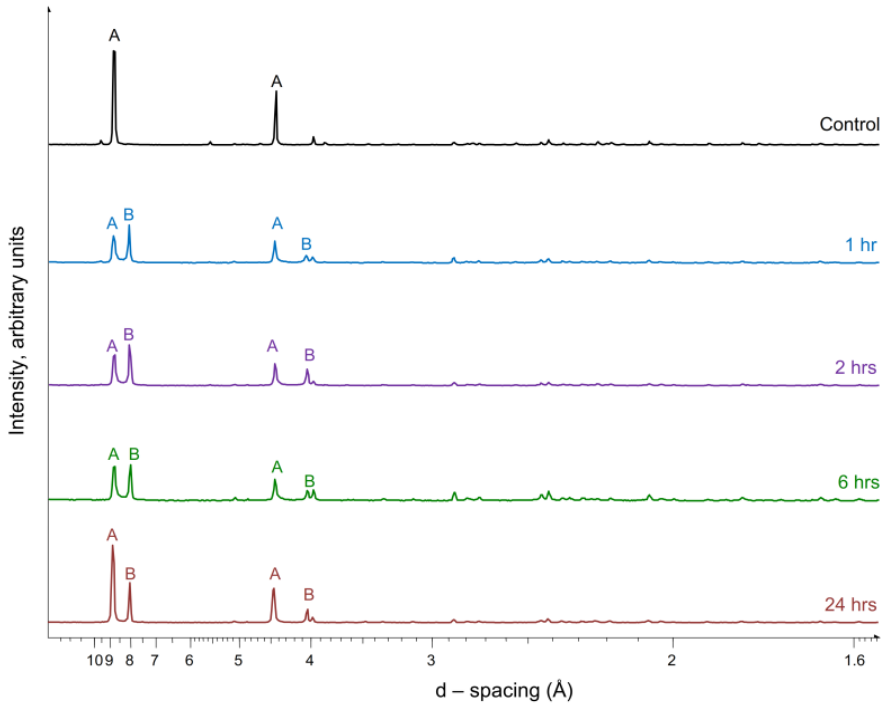

Figure 14-1- XRD patterns of the monosulfate sample immersed in methanol for different time intervals. A and B represent the basal spacing of monosulfate containing 12 and 10 water molecules respectively

The appearance of the 8.15 Å basal spacing, corresponding to the monosulfate with 10 molecules of water (AFm-10), in the one-hour methanol treated sample suggests that the two unbonded water molecules were removed from the interlayer of the monosulfate structure, and the AFm-12 was partially converted to the AFm-10 after one hour treatment with methanol. The intensity of the 8.15 Å peak was still more dominant than that of the 8.93 Å peak after 2 hours of methanol treatment indicating the presence of a relatively large portion of AFm-10 in the sample. In addition to the removal of water, methanol molecules possibly entered the interlayer of the monosulfate structure resulting in the re-generation of the intensity of the 8.93 Å basal spacing after 24 hours. The replacement by methanol at sites occupied by the water molecules occurs by counterdiffusion, and likely does not occur in discrete steps. It is, however, a time-dependent process. It is possible that there is a delay in the time required for the methanol molecules to reach the interlayer sites. It is suggested, based on the re-generation of the peak at 8.93 Å, that methanol molecules, which are only slightly larger than the size of water molecules, can gradually enter all the interlayer space vacated by the two molecules of water.

The XRD patterns of ethanol treated samples for different time intervals are very similar to those of the control sample (Figure 14-2). It is possible that some water molecules in the interlayer of the AFm-12 structure were exchanged with ethanol. The expected decrease of the interlayer spacing was, however, compensated by the possible increase of the interlayer spacing due to the intercalation of the ethanol molecules in the interlayer region. The larger molecular size of ethanol compared to that of methanol in addition to its lower reactivity appears to support this argument.

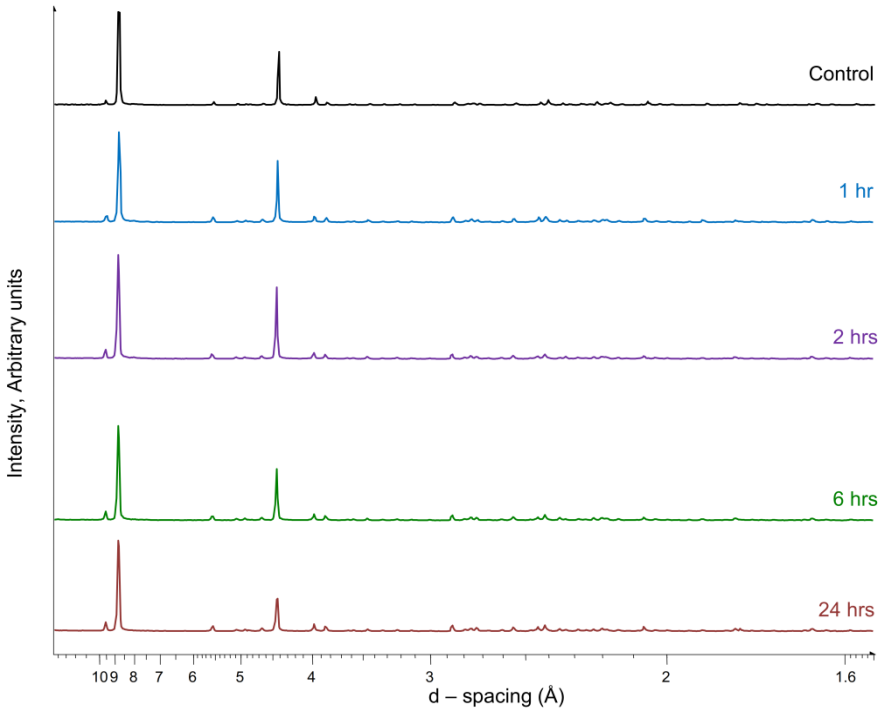

Figure 14-2- XRD patterns of the monosulfate sample immersed in ethanol for different time intervals

The interlayer distance of monosulfate was also altered by the isopropanol treatment. The XRD spectra in Figure 14-3 indicate that a small peak was formed at the basal spacing of 8.15 Å due to the treatment of the sample with isopropanol for only one hour. The intensity of this peak gradually increased with the duration of the isopropanol treatment up to 24 hours.

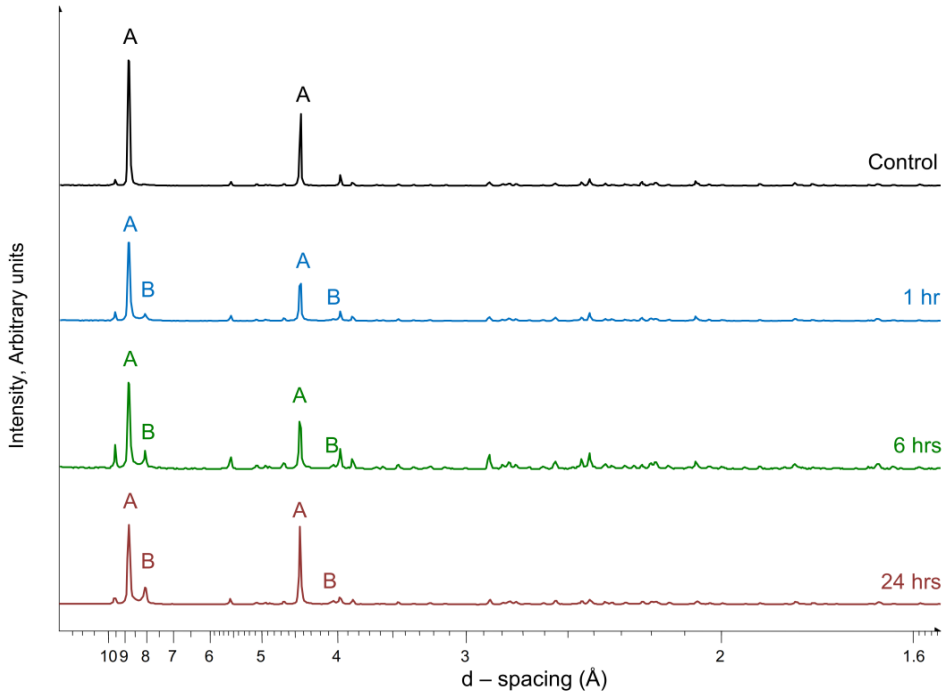

Figure 14-3– XRD patterns of the monosulfate sample immersed in isopropanol for different time intervals. A and B represent the basal spacing of monosulfate containing 12 and 10 water molecules respectively

An additional XRD experiment was performed on the 24 hour methanol treated monosulfate sample after 6 months exposure to the room humidity conditions. The obtained diffraction pattern, not presented here, was similar to the one of the untreated monosulfate sample. This result suggests that the removal of the two water molecules of AFm-12 is readily reversible. The reversibility of dehydration of AFm-12 to AF-10 has also been reported by other researchers [5, 18].

14.3.2 FTIR spectroscopy

The possibility of any chemical interaction between the alcohols and monosulfate samples after 24 hour alcohol treatment was explored by the FTIR technique. The peak corresponding to the bonded hydroxyl group was shifted from the frequency of 3443 cm^{-1} to the frequency of 3483 cm^{-1} once the monosulfate sample was treated with methanol (Figure 14-4). It is suggested that the hydroxyl groups in the methanol treated sample were less tightly bonded compared to the hydroxyl groups in the control sample which is likely

due to the slight change of the position of the water molecules in the monosulfate structure. It is also possible that the hydroxyl group of methanol has formed some hydrogen bonds with the monosulfate layers (either new bonds or the replacement of the existing bonds). The hydrogen bonds that form may be slightly weaker compared with the hydrogen bonds of the monosulfate itself.

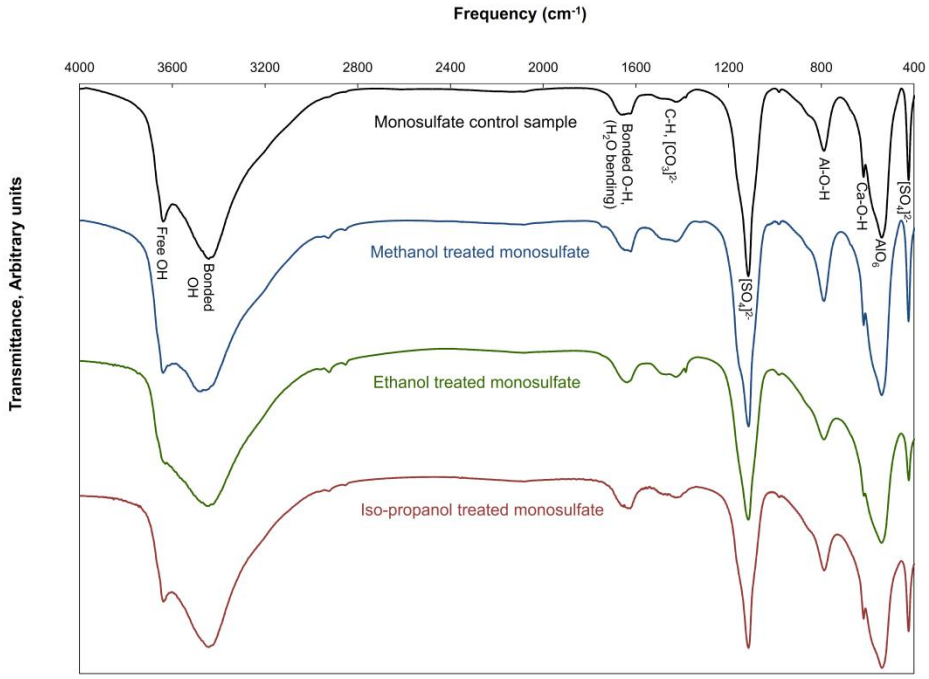

Figure 14-4- FTIR spectra of the monosulfate control sample and the samples immersed in methanol, ethanol and isopropanol for 24 h

The position of the 3443 cm^{-1} peak was not significantly changed once the monosulfate sample was treated with ethanol for 24 hours. A shoulder, however, was formed at the frequency of about 3474 cm^{-1} in the spectra of the ethanol treated sample which is likely an indication of some hydrogen bonding between ethanol and the monosulfate structure. In addition, the intensity of the peak at the frequency of 3640 cm^{-1}, corresponding to the free hydroxyl group, was noticeably reduced due to the ethanol treatment. It is an indication of partial replacement of surface adsorbed water and the free interlayer water of monosulfate structure with ethanol although no significant change of the basal spacing of the sample was detected by the XRD technique.

No significant change in the intensity or broadening of the peak at the frequency of 3443 cm^{-1} was observed in the spectra of the 24 hour isopropanol treated sample. It is suggested that the bonded hydroxyl groups in the structure of the 24 hour isopropanol treated monosulfate sample were likely located at the similar positions as in the structure of the untreated monosulfate sample. The free water content of the isopropanol treated sample, however, was lower than that in the untreated one.

The peaks at the frequencies between 2800 and 3000 cm^{-1} in the alcohol treated sample likely correspond to CH_3 stretching of aliphatic bonds. The frequencies of these peaks in the methanol treated sample are likely greater than those expected for the CH_3 stretching in the unreacted methanol [19]. These peaks in addition to the peaks formed at the frequencies of about 1743, 1323 and 1030 cm^{-1} are similar to those observed in the interaction of methanol with calcium hydroxide [13] and in the reaction of monosulfate with aliphatic sulfonate anions [20]. The formation of these peaks is possibly an indication of some interaction between methanol and the monosulfate structure. The aliphatic peaks in the monosulfate samples which were treated with ethanol and isopropanol can be assigned either to the reacted or unreacted alcohols. The intensities of these peaks, however, are relatively small in the isopropanol treated sample.

14.3.3 TGA

The mass-change, its derivative and the heat flow curves of the pure monosulfate sample are presented in Figure 14-5. The derivative of the mass loss curve is compared, in Figure 14-6, with that of the samples treated with methanol, ethanol and isopropanol for 24 hours. The total mass-loss of the pure monosulfate sample was 34.7% during the TGA experiment which corresponds to 12 molecules of water in the monosulfate structure. Six of these water molecules, likely the interlayer ones, were released once the sample was heated from room temperature to about 220 °C. The remaining six water molecules, likely the ones located in the main layers, were removed at higher temperatures. Leisinger et al. [21] also suggested that the peaks observed up to 260 °C in the TGA derivative mass-loss curve of AFm-10 are associated with the dehydration of the interlayer of the monosulfate structure.

The peaks beyond this temperature are, then, associated with the dehydration of the main layers.

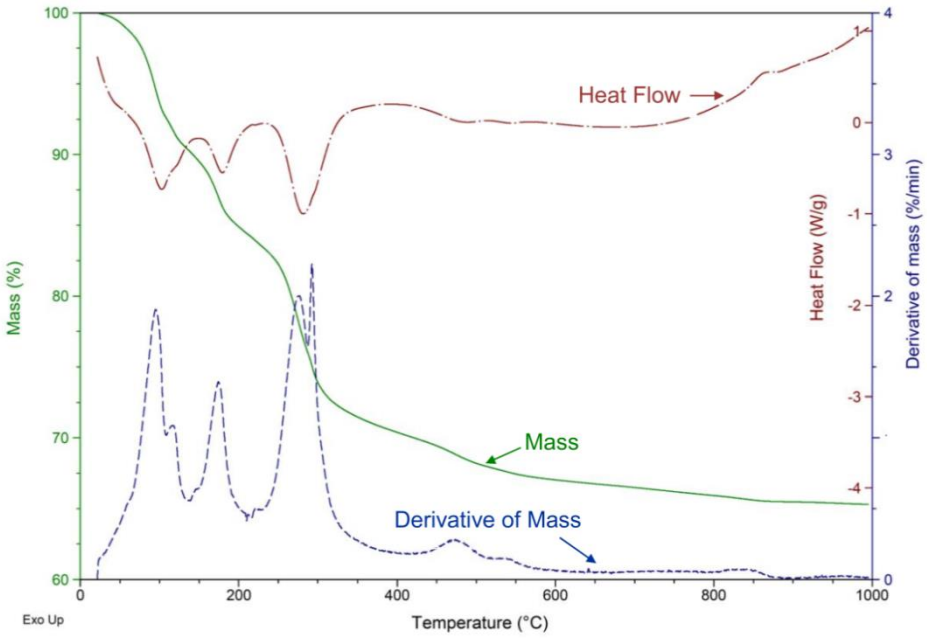

Figure 14-5- Mass, derivative of mass and heat flow of the monosulfate control sample during the TGA experiment

Two additional peaks were observed in the mass-loss derivative of the alcohol treated samples (Figure 14-6). The peak at the temperature of about 47 °C likely corresponds to the release of the unbonded alcohol molecules while the peaks formed at the temperatures between 65 to 75 °C are possibly associated with the removal of the alcohol molecules that interacted with the monosulfate structure. In addition, the area of the peak between 90 to 100 °C was mainly reduced due to the alcohol treatment. This peak likely corresponds to the release of the unbonded and the loosely bonded water molecules in the interlayer of the monosulfate structure. Reduction of the area of this peak confirms the partial removal of the interlayer water by the alcohol treatment.

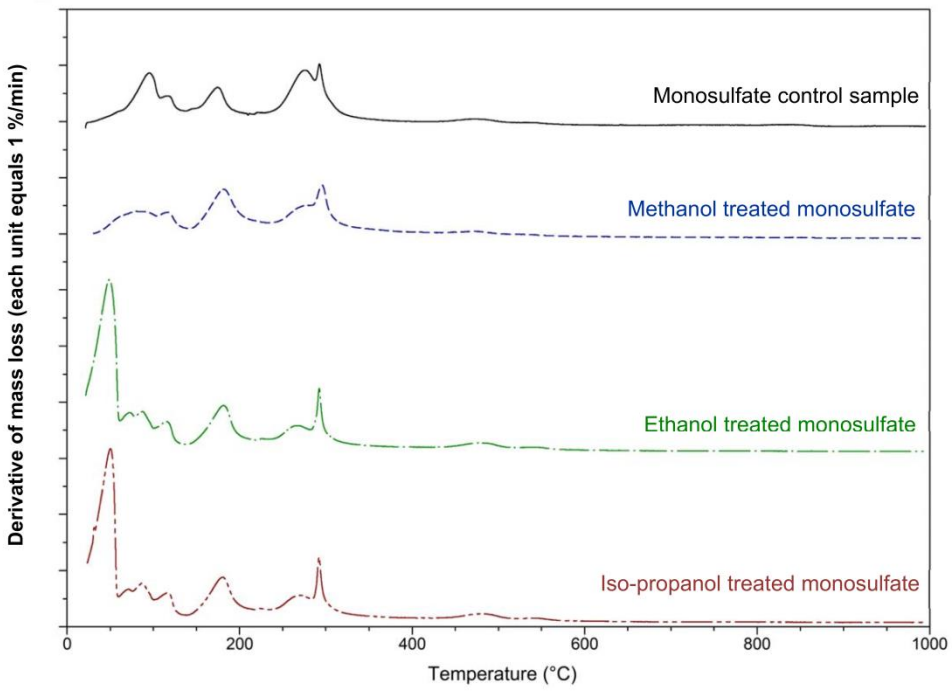

Figure 14-6- Derivative of mass loss curves in the TGA experiment for the monosulfate control sample and the samples immersed in methanol, ethanol and isopropanol for 24 h

The areas associated with different peaks in the derivative mass loss curves were deconvoluted using the NETZSCH Peak Separation software. It is estimated that an average of about 10 water molecules were available in the samples which were treated with methanol or ethanol after 24 hours. The estimated number of water molecules was, however, higher (about 11 molecules) in the 24-hour isopropanol treated sample. This result was expected due to the lower reactivity of isopropanol compared to that of methanol and ethanol.

The estimated number of water molecules in the alcohol treated samples based on the TGA experiment was lower than the one that might be expected based on the XRD results. This was especially the case for the ethanol treated sample, although the TGA experiments suggest that about two water molecules were released due to the ethanol treatment, the peaks associated with the AFm-10 were not detected by the XRD technique in the 24-hour ethanol treated sample (Figure 14-2). The dehydration of AFm-12 to AFm-10 by ethanol treatment was also confirmed by the FTIR results (Figure 14-4). It is possible that the alcohol molecules intercalated the layered structure of monosulfate, and prevented the

expected decrease of the basal-spacing of monosulfate normally detectable by the XRD technique. It is estimated, based on the TGA results, that about 3.5 ethanol molecules were present in the 24-hour ethanol treated sample. Most of these ethanol molecules are likely unbonded i.e. adsorbed on the surface of monosulfate sample or intercalated the interlayer space. It is, however, estimated that about 0.5 ethanol molecules possibly formed hydrogen bonding with the monosulfate structure. It is also likely that about 2.2 isopropanol molecules were present in the 24-hour treated sample. The number of interacted isopropanol molecules was, however, likely negligible.

14.3.4 BET Surface area

Nitrogen BET surface area of monosulfate was significantly increased due to the treatment with methanol. The results of Figure 14-7 suggest that the surface area of the 24-hour methanol treated monosulfate sample was about 5 times higher than that of the untreated sample which possibly occurred due to some interaction of monosulfate sample with methanol. The surface area of the samples which were treated with ethanol or isopropanol for 24 hours was also greater (relative to the control sample) by about 50%. This is likely due to the removal of some interlayer water of monosulfate structure and its partial replacement with the alcohols.

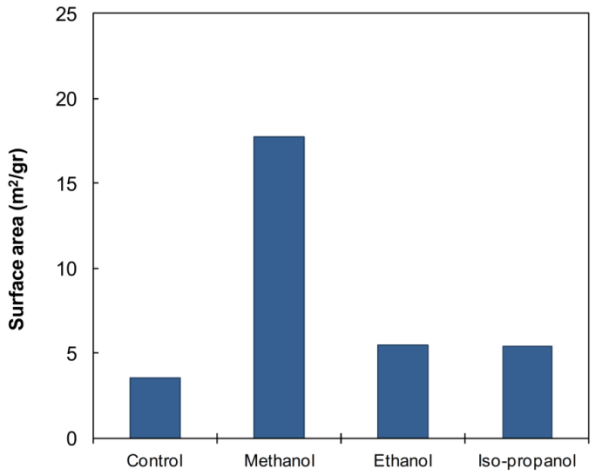

Figure 14-7- Nitrogen BET surface area of the monosulfate control sample and the samples immersed in methanol, ethanol and isopropanol for 24 h

14.3.5 SEM

SEM images of monosulfate before and after the solvent-exchange with methanol, ethanol and isopropanol are presented in Figure 14-8. The hexagonal plate morphology of the layered structure of monosulfate was observed. Some interaction of methanol with the surface of the monosulfate sample is also observed in this figure. The surface defects, however, were not uniformly distributed throughout the sample. No significant change of the samples treated with ethanol and isopropanol was detected by the SEM technique.

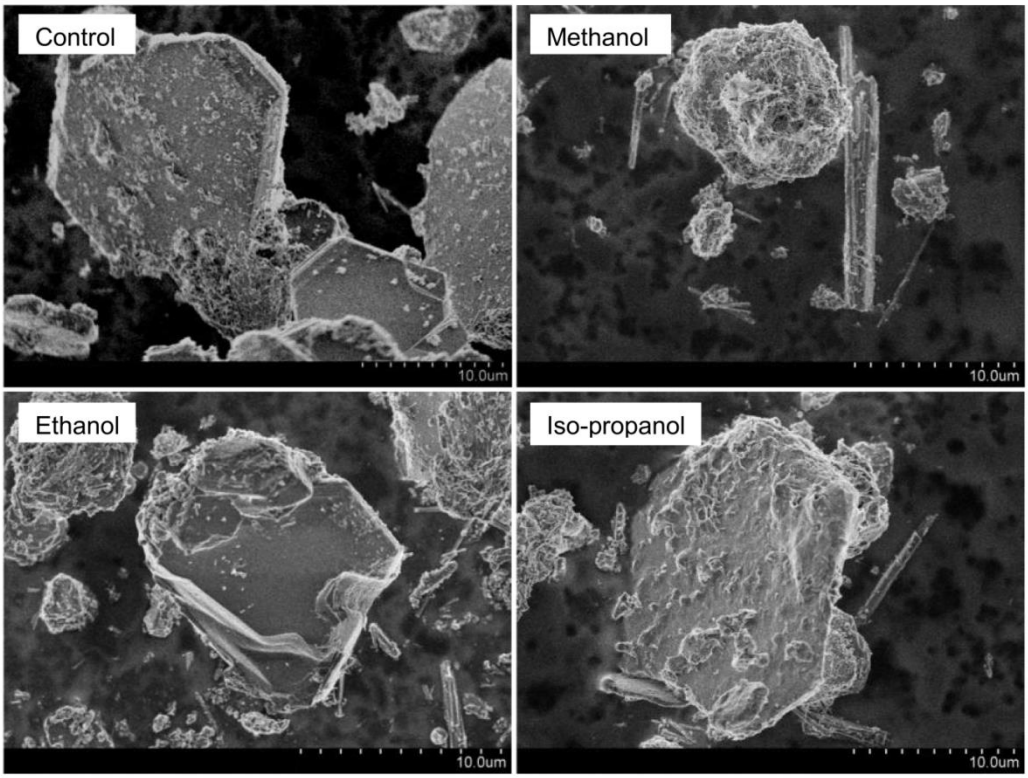

Figure 14-8– SEM images of the monosulfate control sample and the samples immersed in methanol, ethanol and isopropanol for 24 h

14.3.6 Length-change measurements

The monosulfate sample expanded once it was immersed in the methanol solvent (Figure 14-9(a)). The decrease of the surface energy of the monosulfate sample due to replacement of its surface water with the solvent possibly resulted in the immediate expansion of the sample in methanol. It is likely that the expansion due to the decrease of

the surface energy of the monosulfate sample exceeded the expected contraction due to the removal of water from the interlayer space of the monosulfate structure. The expansion continued up to 14 days (Figure 14-9(b)) due to the intercalation of methanol between the layers of monosulfate structure. Formation of new bonds between methanol and monosulfate may also be a source of expansion.

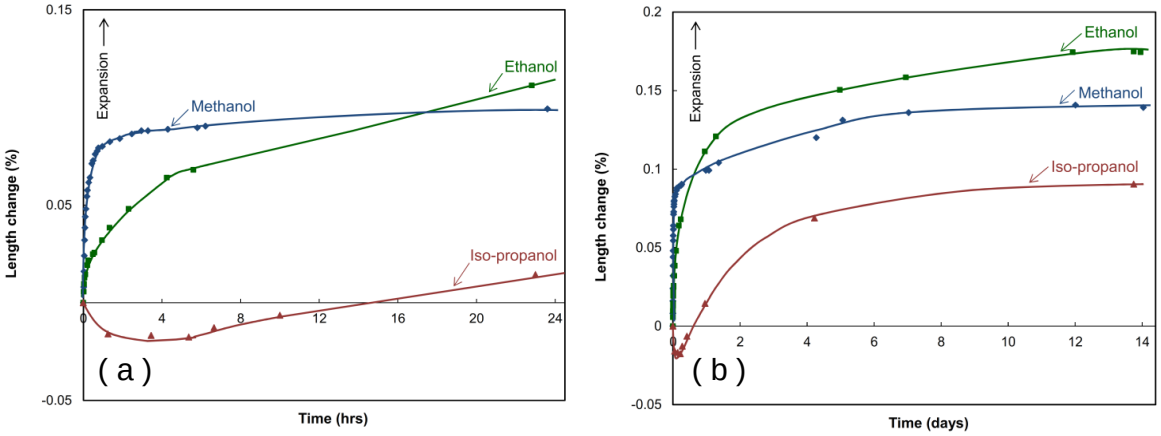

Figure 14-9- Length-change of monosulfate samples immersed in methanol, ethanol and isopropanol up to (a) 24 h (b) 14 d

The monosulfate sample also expanded in ethanol. The immediate expansion of the monosulfate sample in ethanol occurred due to the decrease of the surface energy of the sample once it was immersed in the ethanol solvent. The ethanol molecules likely intercalated the monosulfate structure and resulted in the expansion of the sample up to 14 days. The expansion of monosulfate sample immersed in ethanol exceeded that of the sample immersed in methanol after about 18 hours of immersion. Ethanol molecules are about 4.5 Å in dimension which is larger than the dimension of the methanol molecules (3.6 Å). Their intercalation, thus, possibly results in higher expansion of the monosulfate sample.

The monosulfate sample exhibited an immediate contraction followed by an expansion due to the immersion in isopropanol. The contraction was possibly due to the removal of some of the interlayer water molecules or an increase of the surface energy of the monosulfate sample. The entry of some isopropanol molecules between the monosulfate layers likely resulted in the long-term expansion of the sample.

The immediate expansion or contraction of the monosulfate samples due to the change of the surface energy of the samples in the alcohols was lower than that of the ettringite sample, presented in chapter 13. It was expected due to the lower surface area of monosulfate compared to that of ettringite.

14.4 Conclusions

The influence of methanol, ethanol and isopropanol on the microstructure and dimensional stability of monosulfate was investigated. The main conclusions are as follows:

- Monosulfate dehydrated easily from 12 H_2O to 10 H_2O on immersion in each of the alcohols investigated.
- The XRD technique has limitations in detecting the change in the basal-spacing of the monosulfate due to removal of interlayer water when solvent-exchange methods are used due to the intercalation of the solvent into the interlayer space of the monosulfate structure.
- Methanol is the most reactive of the alcohols investigated when in contact with the monosulfate structure. It likely forms some methoxy bonds with the monosulfate structure. The hydroxyl bonds in the methanol-treated monosulfate are possibly weaker than those in the untreated one.
- Ethanol possibly formed some hydrogen bonds with the monosulfate structure. Isopropanol is, however, unlikely to interact with the main layer hydrates.
- The immediate expansion of monosulfate was higher in methanol compared to that in ethanol largely due to surface energy considerations. The long-term expansion due to intercalation effects, however, was higher in ethanol as a result of its larger molecular size.
- The application of drying using methanol, ethanol and isopropanol for the surface area determination of monosulfate is not recommended. Treatment with these alcohols results in an overestimation of the surface area.

- The application of isopropanol for a limited time likely has the lowest damaging effect on the microstructure of monosulfate compared to that of methanol and ethanol.

References

1. J. J. Beaudoin, B. Tamtsia, J. Marchand and H. R. Myers, "Solvent exchange in partially saturated and saturated microporous systems - Length change anomalies," *Cement and Concrete Research*, 30(3), pp. 359-370, 2000.
2. L. J. Parrot, "Effect of drying history upon the exchange of pore water with methanol and upon subsequent methanol sorption behaviour in hydrated alite paste," *Cement and Concrete Research*, 11(5), pp. 651-658, 1981.
3. R. F. Feldman and J. J. Beaudoin, "Pretreatment of hardened hydrated cement pastes for mercury intrusion measurements," *Cement and Concrete Research*, 21(2), pp. 297-308, 1991.
4. R. F. Feldman, "Diffusion measurements in cement paste by water replacement using propan-2-ol," *Cement and Concrete Research*, 17(4): pp. 602-612, 1987.
5. L. Zhang and F. P. Glasser, "Critical examination of drying damage to cement paste," *Advances in Cement Research*, 12(2), pp. 79-88, 2000.
6. M. D. A. Thomas, "The suitability of solvent exchange techniques for studying the pore structure of hardened cement paste," *Advances in Cement Research*, 2(1), pp. 29-34, 1989.
7. E. W. Hansen and H. C. Gran, "Carbon NMR used in probing the exchange of ethanol with water in water-saturated cement pastes," *Magnetic Resonance Imaging*, 14, pp. 903-904, 1996.
8. R. S. Mikhail and S. A. Selini, "Adsorption of organic vapors in relation to the pore structure of hardened Portland cement pastes", Symposium on Structure of Portland Cement Paste and Concrete, Highway Research Board Special Report 90, pp. 122–134 Washington, 1966.

9. L. Parrot, "Thermogravimetric and sorption studies of methanol exchange in an alite paste," *Cement and Concrete Research*, 13(1), pp. 18-22, 1983.

10. H. F. W. Taylor and A. B. Turner, "Reactions of tricalcium silicate paste with organic liquids," *Cement and Concrete Research*, 17(4), pp. 614-662, 1987.

11. J. J. Beaudoin, "A comparison of mechanical properties of compacted calcium hydroxide and Portland cement paste systems," *Cement and Concrete Research*, 13, pp. 319-324, 1983.

12. J. J. Beaudoin, "Interaction of aliphatic alcohols with cement systems," *Il Cemento*, 83, pp. 199-210, 1986.

13. J. J. Beaudoin, "Validity of using methanol for studying the microstructure of cement paste," *Materials and Structures*, 20(115), pp. 27-31, 1987.

14. J. J. Beaudoin, P. Gu, J. Marchand, B. Tamtsia, R. E. Myers and Z. Liu, "Solvent replacement studies of hydrated Portland cement systems: The role of calcium hydroxide," *Advances in Cement Based Materials*, 8(2), pp. 56-65, 1998.

15. R. L. Day, "Reactions between methanol and Portland cement paste," *Cement and Concrete Research*, 11(3), pp. 341-349, 1981.

16. H. J. Kuzel, "Synthesis and X-Ray Study of the Crystalline Composition $3CaO.Al_2O_3.CaSO_4.12H_2O$," *Neues Jahrbuch Mineral Monatsh*, 7, pp. 193-197, 1965.

17. R. Allmann, "Refinement of the hybrid layer structure $[Ca_2Al(OH)_6]^+\cdot[1/2SO_4\cdot 3H_2O]^-$," *Neues Jahrbuch fur Mineralogie Monatsheft*, pp. 136-44, 1977.

18. H. F. W. Taylor, Cement Chemistry, Academic Press, London, 1990.

19. R. Lu, W. Gan, B. Wu, Z. Zhang, Y. Guo and H. F. Wang, "C-H stretching vibrations of methyl, methylene and methine groups at the vapor/alcohol (N = 1-8) interface," *Journal of Physical Chemistry B*, 109, pp. 14118-14129, 2005.

20. H. Pöllman, S. Stefan and E. Stern, "Synthesis, Characterization and reaction behaviour of lammelar AFm phases with aliphatic sulfonate-anions," *Cement and Concrete Research*, 36, pp. 2039-2048, 2006.

21. S. M. Leisinger, B. Lothenbach, G. Le Saot and C. A. Johnson, "Thermodynamic modeling of solid solutions between monosulfate and monochromate $3CaO.Al_2O_3.Ca[(CrO_4)_x(SO_4)_{1-x}].nH_2O$," *Cement and Concrete Research*, 42, pp. 158-165, 2012.

Chapter 15

Mechanisms of Thaumasite and Ettringite Sulfate Attack and Novel Mitigation Techniques

Pure thaumasite was synthesized and its volume stability in de-ionized water and in saturated gypsum or lime solutions was compared with that for ettringite. It was observed that these two phases, in spite of similarities in their structure, have different patterns of expansion in the aqueous solutions although a dissolution mechanism is likely to contribute significantly to the expansion of both these phases. In addition, bi-component systems comprised of the phase pure C-S-H and thaumasite or ettringite were prepared and tested for the length-change measurements in the same test solutions. The influence of the modification of the nanostructure of C-S-H with nitrobenzoic acid isomers on the length-change measurements of these bi-component systems was also investigated. The results in this chapter have application to concrete structural elements which are exposed to a high sulfate concentration environment and are subjected to wetting and drying. Information on the long-term performance of thaumasite or ettringite formed during the initial cycles of wetting and drying is provided. Novel methods to mitigate the damage due to the presence of thaumasite or ettringite in such concrete elements are also suggested.

15.1 Introduction

Thaumasite is a naturally occurring mineral with an approximate formula of $3CaO.SiO_2.CO_2.SO_3.15H_2O$. It has a column and channel-like structure similar to that of ettringite. The columns have a composition of $[Ca_3Si(OH)_6.12H_2O]^{4+}$. The sulfate and

carbonate ions are also located between the columns [1, 2]. The thaumasite mineral was discovered more than a hundred years ago in materials collected from the copper mines in Sweden [3]. The first case of damage to concrete elements due to thaumasite formation, however, was identified by Erlin and Stark in 1965 [4]. The mechanisms of thaumasite formation in concrete structures have received significant attention among material scientists and civil engineers especially since 1998 when serious damage as a result of thaumasite sulfate attack to the buried elements of a thirty-year old highway bridge in the UK was reported [5].

It has been suggested that the formation of thaumasite in concrete structures is usually accompanied by the decomposition of C-S-H phases. This would result in the softening and strength-loss of concrete materials [6]. In addition, crystallization of thaumasite in concrete pores could generate stresses at the boundaries of the pores and ultimately cracking of concrete elements [7].

The mechanisms of formation of thaumasite and its stability in concrete elements have been widely investigated during the past two decades [8-12]. The number of investigations on the mechanisms of the damage caused by the expansion of the existing pure thaumasite, however, is very limited. A reason might be that pure thaumasite is very difficult to synthesize [13-17]. Successful synthesis of almost pure thaumasite has been recently reported by a few researchers [15-17]. Blanco-Varela et al. [16] investigated the influence of various organic admixtures on the formation of thaumasite. The formation of solid solutions between ettringite, carbonated ettringite and thaumasite was also examined by Matschei [17].

The main objective of the current study is to explore the mechanisms of the volume stability of pure thaumasite in aqueous solutions and to compare these mechanisms with those suggested for the phase pure ettringite. The results can provide insight to our understanding of the damage to concrete elements containing thaumasite crystals during re-wetting. In addition to the phase pure thaumasite, compacted bi-component systems comprised of 10% of either thaumasite or ettringite and 90% of the phase pure C-S-H were prepared in order to simulate the presence of these phases in the actual cement-based elements. The volume stability of these bi-component systems in the aqueous test solutions

was studied. In addition, the influence of the modification of the nanostructure of C-S-H with nitrobenzoic acid isomers (see chapters 4 and 5) on the volume stability and the service-life of the bi-component systems was considered.

15.2 Experimental program

Pure thaumasite was synthetized using a method described by Blanco-Varela et al. [16]. It consisted of mixing two sugary solutions (a sugary solution containing sodium salts of silicate, sulfate and carbonate, and a sugary solution of calcium oxide) at 5 °C for three months. The mixing proportions of the reactants based on Ref. [16] were also provided in Table 3-1. The thaumasite powder conditioned to a relative humidity of 11% was compacted into circular samples with a porosity of about 10% as determined using volumetric measurements from a helium pycnometer. The samples were then cut into rectangular prisms for the length-change measurements. The length-change values were determined up to 7 days in de-ionized water as well as in gypsum-saturated and lime-saturated water. The change in the microstructure of the thaumasite samples was also examined by the X-ray diffraction (XRD), thermal gravimetric analysis (TGA) and scanning electron microscopy (SEM) techniques.

In order to simulate the presence of these hydrated sulfate-based phases in concrete, compacted bi-component systems comprised of 10% of thaumasite or ettringite (synthesis is described in chapters 12 and 14) with 90% of the phase pure C-S-H (produced with a Ca/Si ratio of 1.5 according to synthesis methods described in chapters 4 to 11) were prepared. The compaction pressure was adjusted to reach a porosity of about 30% as determined by the helium pycnometer technique. The length-change of the samples up to 21 days was determined in de-ionized water, gypsum-saturated water and lime-saturated water. Additional samples were also prepared using the modified C-S-H/nitrobenzoic acid systems (prepared with a NBA/Ca = 0.01 according to the method described in chapter 4). These multicomponent samples were also tested for the length-change measurements in the same test solutions in order to determine the efficiency of the modification of C-S-H with organic compounds as a mitigation technique of the expansions associated with the presence of thaumasite or ettringite.

15.3 Results and discussion

15.3.1 Mechanisms of expansion of pure thaumasite

Length-change measurements - The length-change measurements of thaumasite samples in the test solutions are presented in Figure 15-1. The thaumasite sample expanded by 0.65% after 20 minutes of immersion in de-ionized water. No significant expansion was, then, observed for this sample up to 7 days of immersion. The expansion of the sample immersed in lime-saturated water was about 0.83% after 20 min of immersion. It increased to 1.16% at the end of the length-change measurement (7 d). The expansion of the sample in gypsum-saturated water was very quick, and exceeded 0.4% after only 2 minutes. This resulted in the disintegration of the sample.

A dissolution mechanism similar to that proposed in chapter 12 for the expansion of ettringite and monosulfate phases is likely to be responsible for the expansion of the thaumasite samples as well. Leaching of carbonate and sulfate ions from the intercolumnar space as well as calcium and silicon-based anions from the columns of the thaumasite microstructure could result in the release of energy, and possibly also generation of some osmotic-like pressure. This could cause the expansion of the sample immediately following the immersion in the de-ionized water. The sample, then, likely reached equilibrium, and as a consequence no more expansion was observed.

Leaching of calcium ions would be limited in the lime-saturated water and gypsum-saturated water due to the common ion effect. It is, however, known that amorphous silica is more soluble in solutions with high pH or low pH than in those with neutral pH [18]. A relatively high expansion was also previously observed by Beaudoin et al. [19] for the synthetic C-S-H samples due to the immersion in lime-saturated water attributed to a possible dissolution of silicate network in these samples. Silicon has also a critical role in the structure of thaumasite. A possible increase in the leaching of silicon-based anions could, therefore, result in the higher expansion of the samples immersed in the lime-saturated or gypsum-saturated water compared to that in de-ionized water. It was also suggested in chapter 12 that the expansion of ettringite samples was higher in lime-saturated water compared to that in de-ionized water or gypsum saturated water, likely as a result of higher solubility of aluminum ions in high-pH solutions. A similar role of silicon

in the structure of thaumasite to that of aluminum in the ettringite structure is another evidence of the role of dissolution in the length-changes observed for these samples. It is also known that carbonate ions are released readily and hydrolyzed in low-pH solutions. The possible hydrolysis of the carbonate ions in the structure of thaumasite accompanied by the higher leaching of silicon-based anions likely resulted in the immediate disintegration of the sample in gypsum-saturated water.

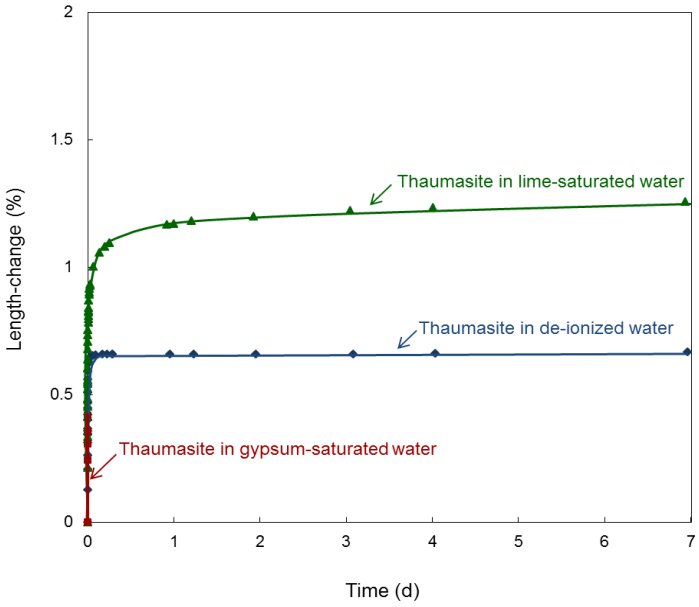

Figure 15-1- length-change measurements for thaumasite samples in the aqueous solutions

XRD - The XRD patterns of thaumasite samples before and after the immersion in the aqueous solutions are presented in Figure 15-2. The intensity of the main peak at 9.56 Å was reduced after immersion in the aqueous solutions. This peak corresponds to the intercolumnar space in the thaumasite structure. It is likely that the columns in the structure of thaumasite broke-down to shorter columns after the immersion in the aqueous solutions resulting in a lower intensity of this peak. The damage to the crystallinity of the samples was more pronounced after the immersion in the lime-saturated water. It is noted that the release and hydrolysis of carbonate ions which is expected to be more significant in the gypsum-saturated water would occur from the intercolumnar space. It is not, therefore, detected by the XRD technique.

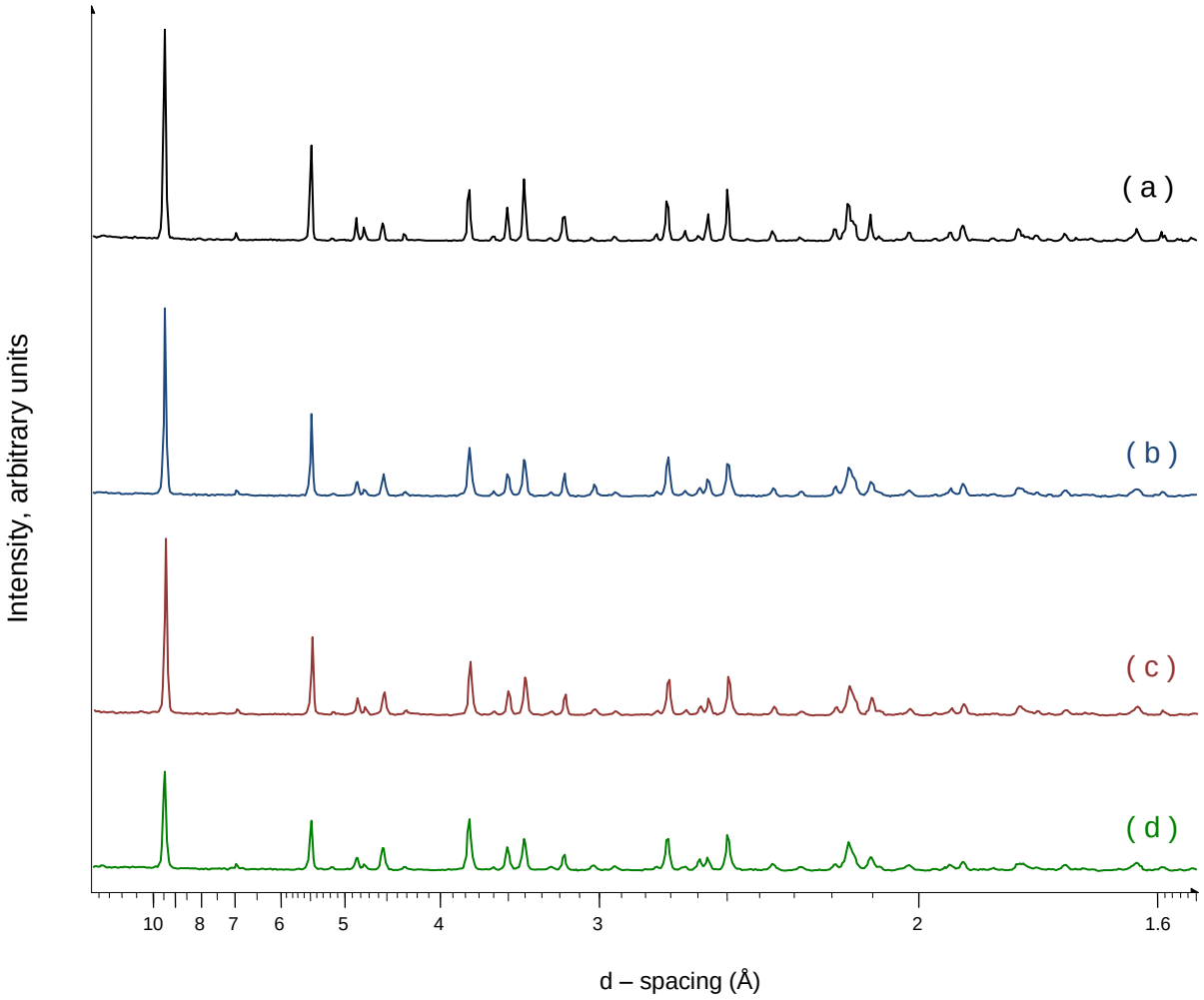

Figure 15-2- XRD patterns for the thaumasite (a) control sample, (b), (c) and (d) after the immersion in de-ionized water, gypsum-saturated water and lime-saturated water, respectively.

TGA - The derivative of mass-loss curves for the thaumasite samples before and after the immersion in the aqueous solutions are presented in Figure 15-3. The peaks observed in the TGA curve of the pure thaumasite sample were very similar to that reported by Matschei [17]. The peak with a maximum at about 132 °C is a typical peak corresponding to the removal of water and some hydroxyl groups from the structure of thaumasite. Other peaks at higher temperatures are only slightly discernible. The very small peak at about 415 °C also likely corresponds to the decomposition of the hydroxyl groups [17]. Drabik and Galikova [20] also suggested that dehydration and dehydroxylation of natural thaumasite occurs in two steps up to about 300 °C. The peak with a maximum at 690 °C likely corresponds to the release of carbon dioxide as also suggested in Ref. [17] and [20].

Kirov [21], however, performed XRD and IR analysis on the natural thaumasite samples heated at 200, 360, 550, 725, 800, 900, and 1150 ° C. He suggested that that carbon dioxide is continuously released over a large temperature interval. Most of it, however, is released between 200 and 500 °C and between 900 and 1150 °C. The heating of thaumasite samples in this reference, however, was conducted in air not under the N_2 flow.

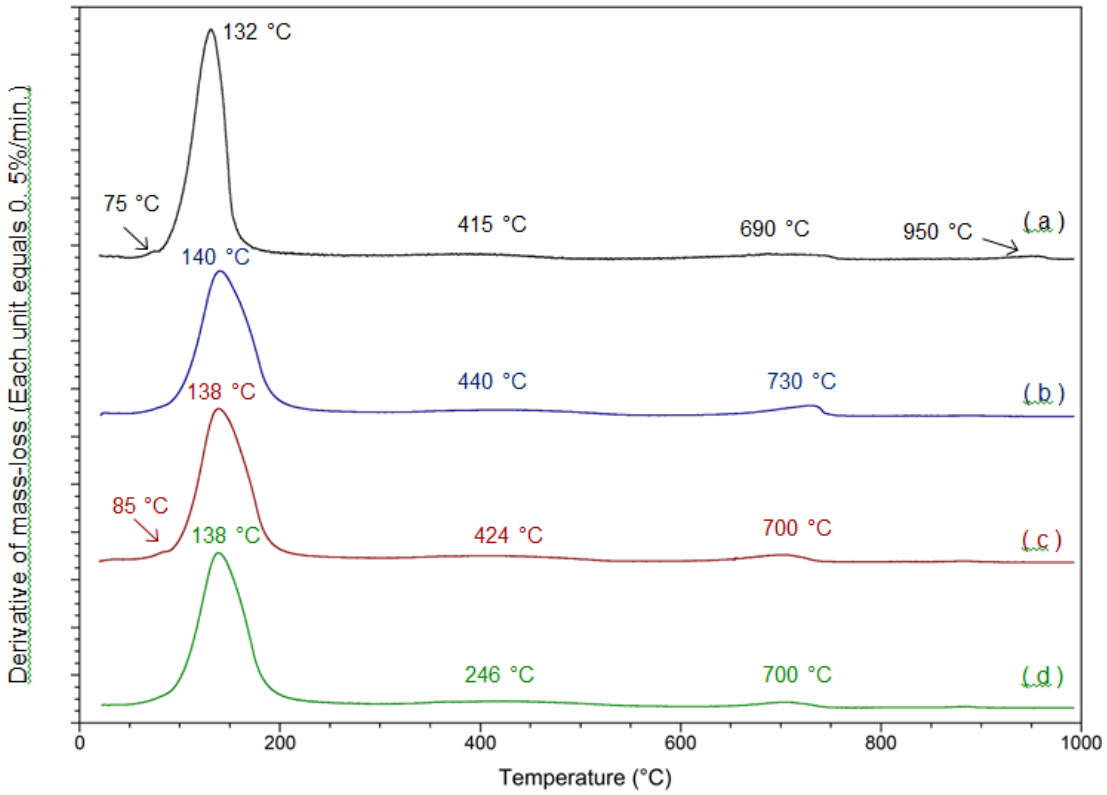

Figure 15-3- TGA curves for the thaumasite (a) control sample, (b), (c) and (d) after the immersion in de-ionized water, gypsum-saturated water and lime-saturated water, respectively.

The peak with a maximum at 950 °C observed for pure thaumasite likely corresponds to the decomposition of the sulfate ions based on the results obtained for ettringite in chapter 13. Matschei [17] suggested two possiblities for the occurance of this peak; release of SO_2 or the remaining CO_2. The former is consistent with the results obtained in chapter 13 of this study and those reported by Götz-Neunhöfer for ettringite specimens [22]. The latter also supports the results obtained by Drabik and Galikova [20]. In addition to these four major peaks detected in the TGA curve of the pure thaumasite sample, a small peak was also observed at the very beginning of the TGA experiment (with a maximum at about 75 °C).

This peak was previously observed in the thermal studies of thaumasite by Martucci and Cruciani [23]. It was suggested by these researchers that it might be due to "an initial hysteresis of the cell parameter variation" or "an experimental uncertainty".

The main peak corresponding to the dehydration of thaumasite (with a maximum at about 132 °C) became slightly broader for the thaumasite samples exposed to the aqueous solutions (Figure 15-3). The maximum of this peak was also shifted to higher temperatures (~ 140 °C). The maximum of the second peak of dehydration/dehydroxylation was also shifted from about 415 °C to 440, 424 and 426 °C after the immersion in de-ionized water, gypsum-saturated water and lime-saturated water, respectively. These changes could have occurred due to the dissolution of the thaumasite samples in the aqueous solutions resulting in a possible rearrangement in the structure of these samples. In addition, the area of the peak associated with the release of CO_2 was larger in the samples immersed in the aqueous solutions. The larger area of this peak is an evidence of the precipitation of some calcite following the dissolution of thaumasite in the aqueous solutions. The area associated with this peak was the largest for the sample immersed in de-ionized water.

The peak at about 950 °C observed in the TGA experiment of the thaumasite sample was only detected as a hump after the immersion in the aqueous solutions. This peak, as previously suggested, likely corresponds to the decomposition of the sulfate ions available in the intercolumnar space of thaumasite structure. These ions could have been readily released to the test solution after the immersion. It is also noted that the small peak at about 75 °C was not detected in the TGA curves of the samples after immersion in de-ionized water or in lime-water. It is suggested that a small amount of the carbonates in the structure of thaumasite were possibly hydrolyzed (Although it has been previously suggested that none of the carbonate oxygens in the thaumasite structure are hydrated or hydroxylated [24].). These could have been dehydroxylated at the very beginning of the TGA experiments. Partial hydrolysis of the carbonates of the intercolumnar space of thaumasite is expected for the sample immersed in gypsum-saturated water. This is reflected in the TGA experiments at about 85 °C.

SEM - Examples of SEM micrographs of the thaumasite samples before the immersion in the aqueous solutions are presented in Figure 15-4(a) and (b). Long needle-shaped crystals with hexagonal cross-sections are observed in these figures. The SEM micrographs of the thaumasite sample after the immersion in de-ionized water and the calcite crystals formed on this sample are presented in Figures 15-4(c) and 15-4(d), respectively. The SEM micrographs after the immersion in the gypsum-saturated water and lime-saturated water are also presented in Figures 15-4(e) and 15-4(f), respectively. It was observed that the thaumasite samples were generally reduced in crystallinity due to the immersion in the aqueous solutions. This was more pronounced in the sample immersed in the lime-saturated water. These observations are in conformity with the results obtained by the XRD technique.

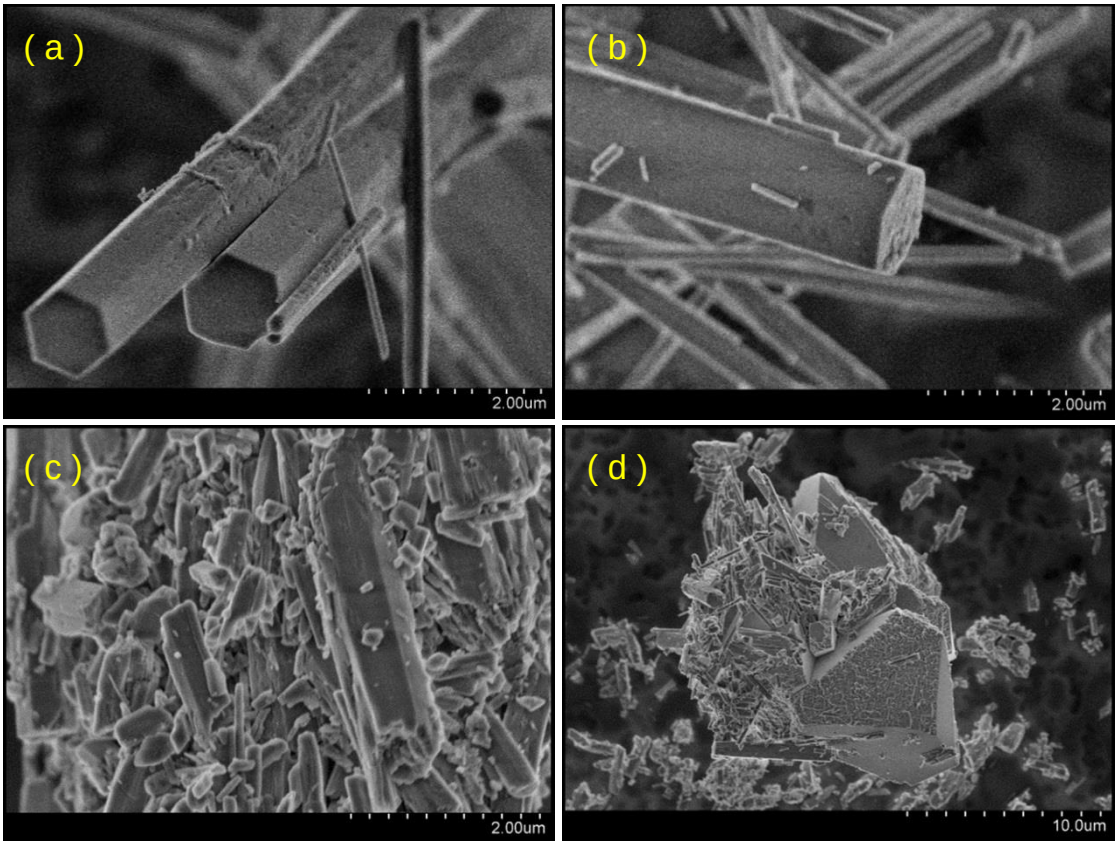

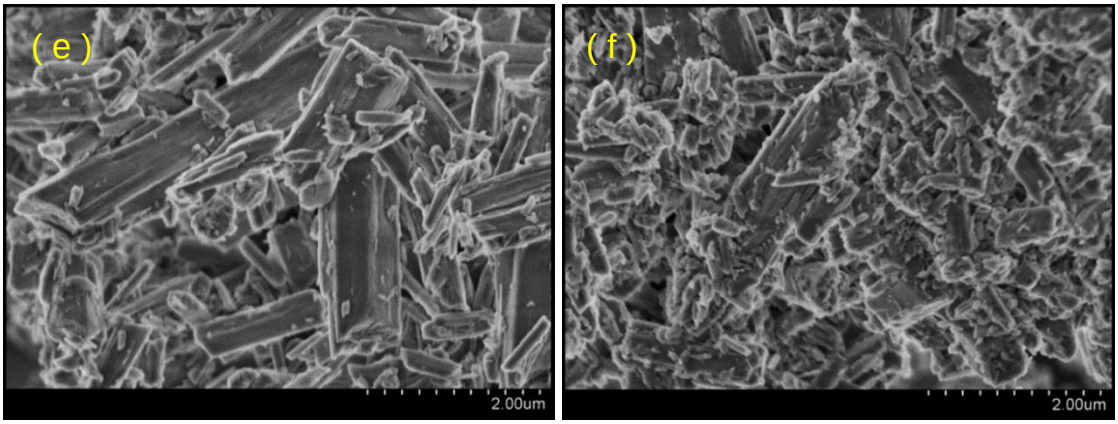

Figure 15-4- SEM micrographs for (a), (b) thaumasite control sample, (c) thaumasite sample after the immersion in de-ionized water (d) calcite formed on the thaumasite sample after the immersion in de-ionized water (e) thaumasite sample after the immersion in the gypsum-saturated water and (f) after the immersion in the lime-saturated water.

15.3.2 Length-change measurements of the bi-component systems

The length-change values of the bi-component systems (composed of the phase pure C-S-H and thaumasite or ettringite) in the aqueous solutions are compared with those of the phase pure C-S-H in Figure 15-5. The length-change of the samples containing either of thaumasite or ettringite was higher than that of the phase pure C-S-H in de-ionized water. The sample containing thaumasite had the highest length-change values compared to the other two samples during the first 10 days of immersion. The length-change curves for this sample and the mono-component C-S-H sample reached a plateau eventually after about 7 days of immersion. The length-change curve of the sample containing ettringite, however, did not include a plateau even after 21 days. It is suggested that dissolution of the investigated systems is the primary mechanism underlying their expansion following the immersion in de-ionized water. For the mono-component C-S-H sample and that containing thaumasite, a solid-solution equilibrium was likely attained a few days after the immersion. The rate of the expansions could have been reduced as a result of this equilibrium. For the sample including ettringite, however, dissolution of the bi-component system is likely followed by the re-precipitation of ettringite crystals. Precipitation of ettringite in this case can generate forces resulting in the significant rate of expansions even after 21 days.

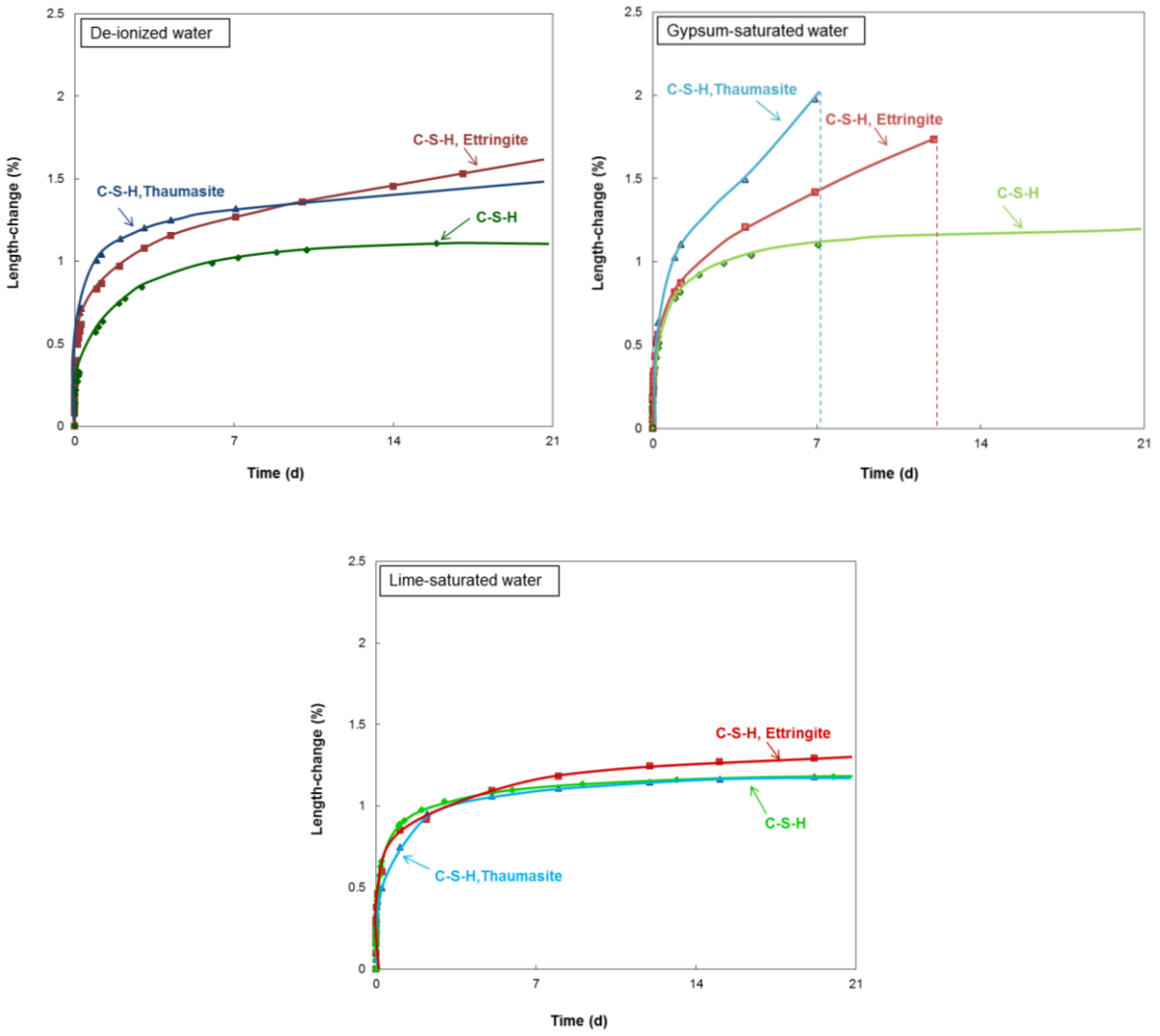

Figure 15-5- length-change of the bi-component systems comprised of the phase pure C-S-H and ettringite or thaumasite in de-ionized water, gypsum-saturated water and lime-saturated water

The length-change values of the bi-component systems in gypsum-saturated water were significantly higher than that observed for the mono-component C-S-H system. The sample with thaumasite had significantly high length-change values. In addition, a plateau, similar to that observed for this sample in de-ionized water, did not occur in the gypsum-saturated water. An inflection point was also detected in this curve after about four days. The rate of the expansion was, then, increased after this point and the sample disintegrated after about three additional days. This inflection could have occurred due to the significant growth of the cracks in this sample. Partial re-precipitation of thaumasite crystals is also possible in this case. A crystal growth mechanism could also be responsible for the higher expansion

of ettringite in the gypsum-saturated water compared to that in de-ionized water. The ettringite containing sample also disintegrated about 12 days following the immersion in the gypsum-saturated water.

The initial length-change values of the mono-component C-S-H system in the lime-saturated water were generally slightly higher than that observed in de-ionized water or in gypsum-saturated water. It is likely due to the partial break-down of the silicate tetrahedra in the high pH solutions [19]. The length-change values of the bi-component system containing thaumasite were not significantly different from that without thaumasite. It is possible that the effect of leaching of silicon-based anions from the thaumasite structure was similar to that occurring from the C-S-H structure. No larger expansion was, therefore, observed for this system. The ettringite containing system had slightly higher length-change values compared to the other two systems likely due to the leaching of aluminum ions or possibly the crystal growth mechanism.

It is noted, based on the results of Figure 15-5, that the presence of only 10% of thaumasite or ettringite in the cement-based phases could contribute to large length-change values during the exposure to the aqueous solutions. A significant amount of expansion, especially in the high-concentration gypsum environment, could result in the disintegration of the whole system. The efficiency of the use of the organically modified C-S-H systems rather than the phase pure C-S-H in improving the volume stability of these systems in de-ionized water and in gypsum-saturated water is described in the following section.

15.3.3 Effect of modification of C-S-H with nitrobenzoic acid isomers on the length-change measurements of multicomponent systems containing thaumasite or ettringite

The length-change measurements of the multicomponent systems including the C-S-H/4NBA systems and thaumasite in de-ionized water and in gypsum-saturated water are presented in Figure 15-6. The length-change values for the sample containing the modified C-S-H system were lower than those obtained for the unmodified system by about 15% in de-ionized water. The sample including the C-S-H/4NBA system had also lower length-change values in the gypsum-saturated water. The inflection point was also delayed from about 4 days to about 9 days for the modified system. In addition, this sample did not

disintegrate until about 23 days. It was previously suggested in chapter 5 that the 4-nitrobenzoic acid molecules likely fill the gaps in the nanostructure of C-S-H. This reduces the rate of the dissolution of the C-S-H-based systems, and limits the entry of the aqueous or alcohol-based solutions into the porous structure of these systems. A similar mechanism is likely responsible for improving the volume stability of the multicomponent systems of Figure 15-6. In addition to reducing the expansions due to the dissolution of the C-S-H-based phases in the multicomponent system, it is possible that the 4-nitrobenzoic acid isomer could be partially adsorbed on the surface of the thaumasite columns and reduce its expansion. The whole system also has a better resistance to the crack growth and disintegration.

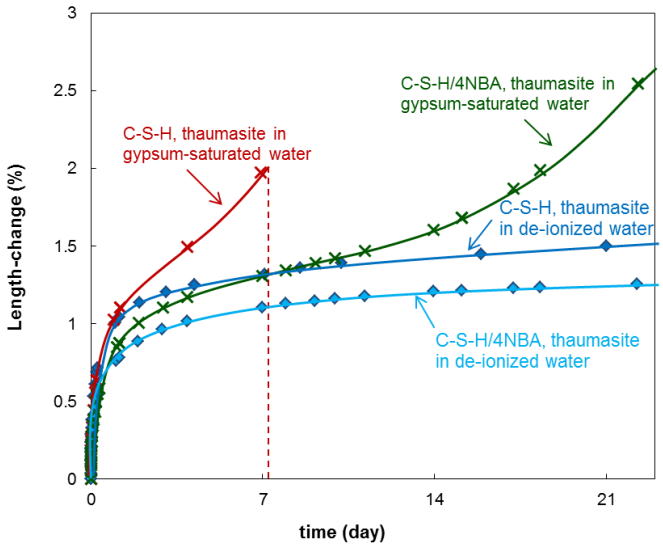

Figure 15-6- length-change of the thaumasite containing multicomponent systems in de-ionized water and in gypsum-saturated water; effect of modification of C-S-H with 4-nitrobenzoic acid isomer

The length-change values of the multicomponent samples comprised of the C-S-H/4NBA systems and ettringite are presented in Figure 15-7. It is suggested that the modification of C-S-H with the 4-nitrobenzoic acid isomer was not effective in limiting the length-change values associated with the presence of ettringite. It, however, significantly increased the service-life of the investigated sample in the gypsum-saturated water. It is suggested that the crack growth occurred at a slower rate in the sample containing the modified C-S-H system. This ultimately increased the service-life of this sample.

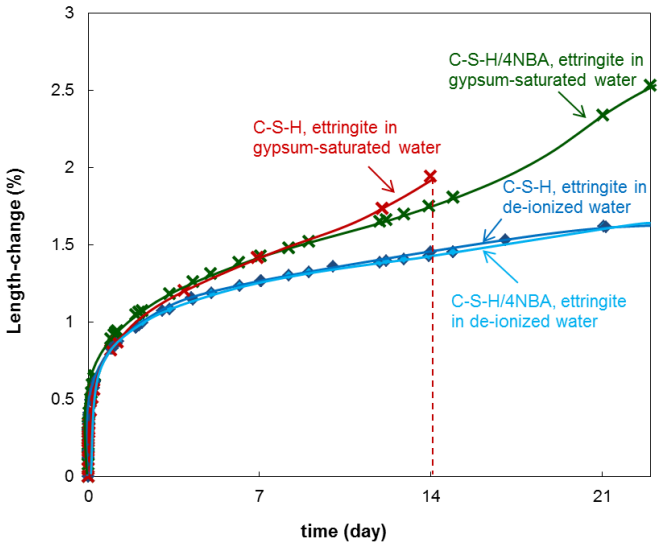

Figure 15-7- length-change of the ettringite containing multicomponent systems in de-ionized water and in gypsum-saturated water; effect of modification of C-S-H with 4-nitrobenzoic acid isomer

It was previously suggested in chapter 5 that the 4-nitrobenzoic acid isomer was the most effective isomer in reducing the length-changes of the phase pure C-S-H in the aqueous salt solutions. The influence of the modification of C-S-H with 2- and 3-nitrobenzoic acid isomers on the length-changes of the ettringite containing systems was, however, also investigated in this chapter (see Figures 15-8 and 15-9). No significant reduction of the length-change values was observed due to the modification of C-S-H with 2-nitrobenzoic acid isomer. It, however, increased the resistance of the multicomponent system to disintegration in the gypsum-saturated water. The 3-nitrobenzoic acid isomer was significantly effective in reducing the length-change values and increasing the service-life of the multicomponent system. It was previously suggested that the C-S-H/3NBA systems is composed of two different phases; a possible intercalated nanocomposite and a phase in which the 3-nitrobenzoic acid molecules are mainly adsorbed on the layers surfaces or between the stacked layers of C-S-H. The more weakly bonded 3-nitrobenzoic acid could have been adsorbed on the surface of the ettringite columns and contributed to the reduction of the length-change values.

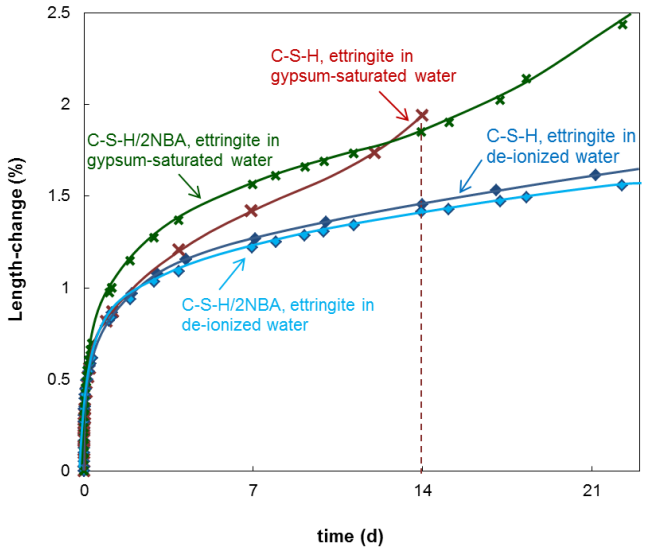

Figure 15- 8- Length-change of the ettringite containing multicomponent systems in de-ionized water and in gypsum-saturated water; effect of modification of C-S-H with 2-nitrobenzoic acid isomer

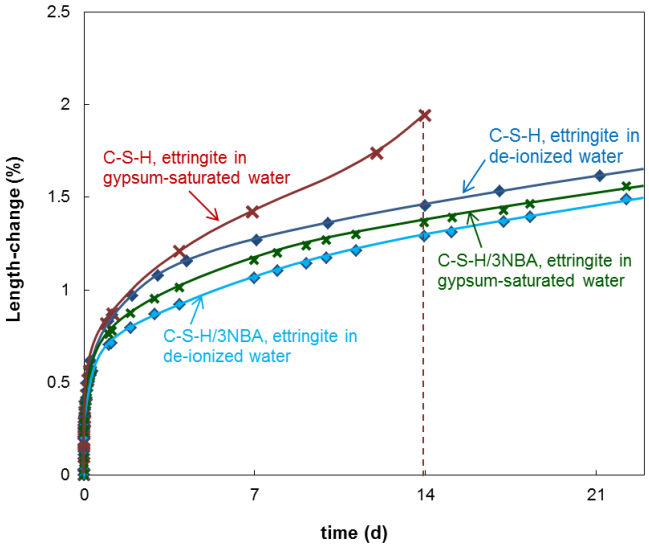

Figure 15- 9 Length-change of the ettringite containing multicomponent systems in de-ionized water and in gypsum-saturated water; effect of modification of C-S-H with 3-nitrobenzoic acid

15.4 Concluding remarks

The mechanisms underlying the expansion of thaumasite as well as the multicomponent systems comprising C-S-H (the phase pure or organically modified C-S-H) and selected secondary hydrated cement phases (thaumasite or ettringite) in de-ionized water and in presence of high concentration of gypsum or lime was investigated. The concluding remarks are as follows:

- Dissolution is likely a primary mechanism underlying the expansion of the hydrated cement-based phases especially during the short-term after the exposure of these phases to the aqueous solutions.
- No evidence of the crystal growth of the pure thaumasite samples was obtained under the test conditions of this study. Re-precipitation of thaumasite or ettringite crystals, however, likely contributed to some expansion of the multicomponent systems especially in the gypsum-saturated water.
- The damage due to the presence of 10% of either thaumasite or ettringite was very significant resulting in the disintegration of the whole sample in the gypsum-saturated water.
- Modification of the C-S-H nanostructure with any of the nitrobenzoic acid isomers was effective in increasing the service-life of the multicomponent systems in the gypsum-saturated water. Lower length-change values were also observed in some cases.

References

1. R. A. Edge and H. F. Taylor, "Crystal Structure of Thaumasite, $[Ca_3Si(OH)_6.12H_2O](SO_4)(CO_3)$," *Acta Crystallographica B*, 27, pp. 594-601, 1971.
2. H. Effenberger, A. Kirfel, G. Will and E. Zobetz, "A further refinement of the crystal structure of thaumasite, $Ca_3Si(OH)_6CO_3SO_4.12H_2O$," *Neues Jahrbuch für Mineralogie, Monatshefte*, 2: 60–68, 1983.
3. A. E. Nordenskiöld, "Sur une nouvelle espèce minérale nommée thaumasite," *Comptes Rendus Hebdomadaires des Séances de l'Académie des Sciences*, 87, pp. 313-314, 1878.

4. B. Erlin and D. C. Stark, "Identification and occurrence of thaumasite in concrete," Symposium on the effects of aggressive fluids in concrete, Highway Research Record No. 11, pp. 108-113, 1965.

5. N. Loudon, "A review of the experience of thaumasite sulfate attack by the UK Highways Agency," *Cement and Concrete Composites*, 25, pp. 1051-1058, 2003.

6. J. Skalny, Sulfate Attack on Concrete, Spon Press, London, 2002.

7. G. D. Gatta, G. J. McIntyre, J. G. Swanson and S. D. Jacobsen, "Minerals in cement chemistry: A single-crystal neutron diffraction and Raman spectroscopic study of thaumasite, $Ca_3Si(OH)_6(CO_3)(SO_4)\cdot 12H_2O$," *American Mineralogist*, 97, pp. 1060-1069, 2012.

8. D. W. Hobbs and M. G. Taylor, "Nature of the thaumasite sulfate attack mechanism in field concrete," *Cement and Concrete Research*, 30, pp. 529-533, 2000.

9. V. Tesch and B. Middendorf, "Occurrence of thaumasite in gypsum lime mortars for restoration," *Cement and Concrete Research*, 36, pp. 1516-1522, 2006.

10. N. J. Crammond, "The thaumasite form of sulfate attack in the UK," *Cement and Concrete Composites*, 25, pp. 809-818, 2003.

11. N. J. Crammond, "The occurrence of thaumasite in modern construction - a review," *Cement and Concrete Composites*, 24, pp. 393-402, 2002.

12. D. W. Hobbs, "Thaumasite sulfate attack in field and laboratory concretes: implications for specifications," *Cement and Concrete Composites*, 25, pp. 1195-1202, 2003.

13. L. J. Struble and P. W. Brown, "An evaluation of ettringite and related compounds for use in the solar energy storage," NBSIR 82-253, USA, US Dept. of Commerce, pp. 11, 1982.

14. J. Aguilera, M. T. Blanco Varela and T. Va´zquez, "Procedure of synthesis of thaumasite," *Cement and Concrete Research*, 31, pp. 1163-1168, 2001.

15. S. Martinez-Ramirez, M. T. Blanco-Varela and J. Rapazote, "Thaumasite formation in sugary solutions: Effect of temperature and sucrose concentration," *Construction and Building Materials*, 25, pp. 21-29, 2011.

16. M. T. Blanco-Varela, P. M. Carmona-Quiroga, I. F. Sáez del Bosque and S. Martínez-Ramírez, "Role of organic admixtures on thaumasite precipitation," *Cement and Concrete Research*, 42(7), pp. 994-1000, 2012.

17. T. Matschei, Thermodynamics of cement hydration, PhD thesis, University of Aberdeen, 2007.

18. P. Meyers, "Behaviour of Silica in Ion Exchange and Other Systems," The International Water Conference, Pittsburgh, 1975.

19. J. J. Beaudoin, B. Patarachao, L. Raki, J. Margeson and R. Alizadeh, "Length change of C-S-H of variable composition in aqueous solutions," *Advances in Cement Research*, 22 (1), pp. 15-20, 2010.

20. M. Drabik and L. Galikova, "Methods of thermal analysis in the detection of thaumasite and its presence in the sufate attacked concrete," *Solid State Phenomena*, 90-91, pp. 33-38, 2003.

21. G. N. Kirov, "On the infra-red spectrum and thermal decomposition products of thaumasite $Ca_3H_2(CO_3/SO_4)SiO4.13H_2O$," *Mineralogical Magazine*, 36(283), pp. 1003-1011, 1968.

22. F. Götz-Neunhöffer, J. Neubauer, P. Schweswig, "Mineralogical characteristics of Ettringites synthesised from solutions and suspensions," *Cement and Concrete Research*, 36, pp. 65-70, 2006.

23. A. Martucci and G. Cruciani, "In situ time resolved synchrotron powder diffraction study of thaumasite," *Physics and Chemistry of Minerals*, 33, pp. 723-731, 2006.

24. S. D. Jacobsen, J. R. Smyth and R. J. Swope, "Thermal expansion of hydrated six-coordinate silicon in thaumasite, $Ca_3Si(OH)_6(CO_3)(SO_4).12H_2O$," *Physics and Chemistry of Minerals*, 30, pp. 321-329, 2003.

Chapter 16

Summary and Recommendations for Future Research

The specific concluding remarks for each part of this research were presented in the relevant chapters. The most remarkable achievements are "the potential of selected organic compounds (e.g. nitrobenzoic acid isomers and polyaniline) to improve the durability and mechanical performance of C-S-H-based systems" and "the primary role of a dissolution mechanism in the volume stability of hydrated cement-based phases". The concluding remarks of the various chapters are summarized in this chapter. Recommendations for future advanced research in this area of cement science are also given.

16.1 Summary

This research was designed to elucidate the primary mechanisms governing the durability of hydrated cement phases and to produce novel construction materials with enhanced engineering performance. The efficiency of the modification of the nanostructure of C-S-H systems on their engineering performance was studied in chapters 4 to 11. The mechanisms of expansion of sulfoaluminate and related phases were also explored in chapters 12 to 15. A summary of the achievements of each chapter is as follows:

Chapter 4 – The mechanisms of interaction of nitrobenzoic acid (NBA) isomers with the structure of C-S-H were investigated. The C-S-H/NBA systems with various concentrations of the nitrobenzoic acid isomers were synthesized and characterized using several analytical techniques. A model for the nanostructure of the resulting C-S-H/NBA systems was suggested. Based on this model, the nitrobenzoic acid isomers with a concentration of

0.01 mol. per mol. of calcium are able to interact with the C-S-H nanostructure by partial intercalation, adsorption on the surface and edges of the layers or between the stacked layers of C-S-H. The interaction of higher concentrations of nitrobenzoic acid isomers with the nanostructure of the host C-S-H, however, was limited. Local accumulation of the nitrobenzoic acid on the surface of the C-S-H layers or between the stacked layers of C-S-H is expected for these systems.

Chapter 5 – Durability and mechanical properties of the C-S-H/NBA systems synthesized in chapter 4 were assessed in this chapter. The experiments included measurement of length-change and calcium-ion leaching in potentially aggressive salt solutions, and mass-change measurements in anhydrous isopropanol. A microindentation technique was also used to determine the creep modulus and hardness of these systems. Evidence of the superior durability and creep modulus of the C-S-H/NBA systems with NBA/Ca = 0.01 was provided. The systems prepared with 3- or 4-nitrobenzoic acid generally had a better engineering performance compared to the one prepared with 2-nitrobenzoic acid. The C-S-H/NBA systems with a higher concentration of nitrobenzoic acid, however, had poor engineering performance.

Chapter 6 – The focus of this chapter was on the characterization and assessment of the engineering performance of C-S-H/aminobenzoic acid systems. Evidence of the interaction of the organic and inorganic phases was provided. It was also suggested that the C-S-H systems with 3- and 4-aminobenzoic acid had improved durability and creep modulus. No significant difference was obtained between the effects of these two aminobenzoic acid isomers.

Chapter 7 – Dynamic mechanical thermal analysis was employed in order to determine the resistance of the phase pure and modified C-S-H systems to the change of the dynamic mechanical properties upon heating to 300 °C. Evidence was provided on the structural role of the nitrobenzoic acid isomers in the modified C-S-H systems. The aminobenzoic acid isomers also had a structural role although they were not as effective as the nitrobenzoic acid isomers especially at high temperatures.

Chapter 8 – The resistance of the phase pure and modified C-S-H systems to the change of the storage modulus and fracture under repetitive dynamic loading was studied. A dynamic

mechanical analysis technique using a strain-controlled set-up was employed for the study. It was suggested that the C-S-H systems modified with nitrobenzoic acid and those with lower Ca/Si ratios or increased hydration time had significantly better performance under dynamic loading.

Chapter 9 – The influence of three different organic polymers (polyvinyl alcohol (PVA), polyacrylic acid (PAA) and polymethylmethacrylate (PMM)) on the structure and engineering performance of C-S-H systems was investigated. Improvement of the engineering performance of the resulting C-S-H systems was expected based on the previous publications. No evidence of the improved performance of the C-S-H systems due to the incorporation of these polymers was, however, obtained in the current study. The only improvement observed was the increase of the microindentation creep modulus of the C-S-H/PMM (PMM/Ca = 0.01) by about 20%. In addition to the polymers, several organic compounds (with a possible application in the formulation of chemical admixtures) were also selected and their potential for the modification of the C-S-H structure and the improvement of its volume stability was investigated. No evidence of significant improvement was obtained for these organics. Most of these organics, however, had significantly larger molecular sizes compared to that for the nitro- and amino-nitrobenzoic acid compounds studied in the previous chapters. It may have been a case of limited interaction of the organic and inorganic phases in these systems.

Chapter 10 – Volume stability and the change in the microstructure of the C-S-H/polyaniline nanocomposites exposed to the aqueous solutions were investigated in this chapter. Evidence on the superior performance of the C-S-H/polyaniline nanocomposites compared to that of the phase pure C-S-H was obtained. A larger improvement was attained for the C-S-H-based systems with higher Ca/Si ratio.

Chapter 11 – This chapter provides a discussion of the recent experimental results on the dynamic mechanical thermal analysis of C-S-H/polyaniline nanocomposites at temperatures ranging from 25 to 200 °C. The results were compared with those obtained for the C-S-H systems modified with nitro- or amino-benzoic acid (chapter 7). It was suggested that C-S-H/polyaniline nanocomposites had improved dynamic mechanical performance at

temperatures up to about 45 °C. No improvement, however, was observed at higher temperatures.

Chapter 12 – The mechanisms of volume stability of ettringite and monosulfate in aqueous solutions were studied in this chapter. It was proposed that dissolution of these phases have a primary role in there expansion during the exposure to the aqueous solutions. Other mechanisms such as growth of ettringite crystals may also contribute to some expansion. It, however, mainly occurs during the long-term immersion in the solution.

Chapter 13 – The mechanisms of dehydration of ettringite using the solvent-exchange technique were investigated. Three different alcohol-based solvents (methanol, ethanol and isopropanol) were used in this chapter. It was demonstrated that the use of methanol for only 15 minutes resulted in the decomposition of ettringite in addition to its dehydration. Formation of a new product due to this interaction was also possible. Ethanol likely also formed some hydrogen bonding with the ettringite structure. Isopropanol, however, had the least damaging effect.

Chapter 14 – This chapter was designed as a continuation of chapter 13 with a focus on the dehydration of monosulfate due to the solvent-exchange technique. It was suggested that dehydration of monosulfate occurred readily due to the exposure to these alcohol-based solvents. No evidence of the decomposition of monosulfate was, however, obtained.

Chapter 15 – The mechanisms of expansion of thaumasite in aqueous solutions was explored. These mechanisms were compared with those underlying the expansion of ettringite. Evidence was provided for the primary role of a dissolution mechanism in the expansion of thaumasite samples. In addition, it was concluded that multicomponent systems comprised of organically modified C-S-H systems (rather than the phase pure C-S-H) and either thaumasite or ettringite had increased service-life in a highly concentrated sulfate environment.

16.2 Recommendations for future research

In spite of the comprehensive research performed in this study on the "mechanisms of durability and mechanical performance of hydrated cement phases" and the "possibility of the development of novel C-S-H-based materials with enhanced engineering performance", there is still considerable potential for research in this area of construction materials. Additional research should also be conducted to bring this research closer to application in concrete industry. A few recommendations for future research as a corollary to this study are listed as follows:

1. The primary mechanisms of fatigue behaviour of pure hydrated cement phases can be investigated using dynamic mechanical analysis and other experimental techniques. The fatigue behaviour of porous glass (which is considered as an ideal silica-based system) has been long-studied. It was, however, the first time that the fatigue behaviour of the phase pure C-S-H was investigated. Fundamental research on the mechanisms of crack propagation and fatigue fracture of pure hydrated cement phases can provide insight to those responsible for the fracture of cement-based infrastructure at a larger scale.
2. The effect of aging of pure hydrated cement phases on their durability and mechanical performance can be studied.
3. Dynamic mechanical analysis can be employed to provide information about the mechanical stability of secondary hydrated cement phases.
4. Mechanisms of crack initiation and propagation in pure hydrated cement-based phases due to the application of repetitive dynamic loading, prolonged static loading, thermal gradients or diffusion of ionic species e.g. sulfate ions can be studied and compared.
5. Freeze-thaw of pure hydrated cement phases can be studied using advanced techniques such as thermal mechanical analysis technique.
6. Mechanisms of volume stability of pure secondary hydrated phases under long-term wetting and drying cycles can be studied.
7. Mechanisms of durability and mechanical properties of multicomponent systems comprised of C-S-H, calcium hydroxide and sulfoaluminate phases can be studied.

Appendix: Vita

Rahil Khoshnazar received her B.Sc. degree in Civil Engineering and M.Sc. degree in Civil Engineering/Structural Engineering, both from the University of Tehran in 2008 and 2010, respectively. Her M.Sc. thesis was entitled "Instability in self-consolidating concrete, evaluation methods and mitigation techniques". It was awarded the prize for the best thesis in the field of construction materials by the Iranian Concrete Institute in 2010. She was admitted to the doctoral program in Civil Engineering at the University of Ottawa in 2011. Her doctoral research focused on the application of nanotechnology for the durability assessment and improvement of hydrated cement phases. She conducted her research in the state-of-the-art facilities at the National Research Council of Canada. Her doctoral research contributed to the following publications and presentations:

Refereed Journal Papers:

1. R. Khoshnazar, R. Alizadeh, J. J. Beaudoin and L. Raki, "The physico-mechanical stability of C-S-H/polyaniline nanocomposites," *Materials and Structures*, 48(1-2), pp. 67-75, 2015.
2. R. Khoshnazar, J. J. Beaudoin, L. Raki and R. Alizadeh, "Volume stability of C-S-H/polyaniline nanocomposites in aqueous salt solutions," *ACI Materials Journal*, 111(6), pp. 623-632, 2014.
3. R. Khoshnazar, J. J. Beaudoin, L. Raki and R. Alizadeh, "Interaction of 2, 3 and 4-nitrobenzoic acid with the structure of calcium-silicate-hydrates (C-S-H)," *Materials and Structures*, in-press, DOI: 10.1617/s11527-014-0513-2, 2014.
4. R. Khoshnazar, J. J. Beaudoin, L. Raki and R. Alizadeh, "Solvent-exchange in sulfoaluminate phases – Part I: ettringite," *Advances in Cement Research*, 25(6), pp. 314-321, 2013.

5. R. Khoshnazar, J. J. Beaudoin, L. Raki and R. Alizadeh, "Solvent-exchange in sulfoaluminate phases – Part II: monosulfate," *Advances in Cement Research*, 25(6), pp. 322-331, 2013.
6. R. Khoshnazar, J. J. Beaudoin, R. Alizadeh and L. Raki, "Volume stability of calcium sulfoaluminate phases," *American Ceramic Society*, 95(12), pp. 3979-3984, 2012.
7. R. Khoshnazar, J. J. Beaudoin, L. Raki and R. Alizadeh, "Durability and mechanical properties of C-S-H/nitrobenzoic acid nanocomposites", *Materials and Structures*, under review, 2015.
8. R. Khoshnazar, J. J. Beaudoin, L. Raki and R. Alizadeh, "Characterization, durability and engineering performance of C-S-H/aminobenzoic acid nanocomposites", under review, 2015.

Journal papers under preparation:

1. R. Khoshnazar, J. J. Beaudoin, L. Raki and R. Alizadeh, "Volume stability of thaumasite in aqueous solutions"
2. Khoshnazar R., Beaudoin J.J., Raki L. and Alizadeh R., "Fatigue resistance of organically modified C-S-H systems"
3. Khoshnazar R., Beaudoin J.J., Raki L. and Alizadeh R., "Dynamic mechanical thermal analysis of organically modified calcium-silicate-hydrates"
4. Khoshnazar R., Beaudoin J.J., Raki L. and Alizadeh R., "Interaction of high molecular weight polymers with the structure of C-S-H prepared with the pozzolanic reaction technique"

Conference Presentations:

1. Khoshnazar R., Beaudoin J.J., Raki L. and Alizadeh R., "Dynamic mechanical performance of organically modified C-S-H/systems," *American Concrete Institute Fall Convention*, Washington, DC, USA, 2014.

2. Khoshnazar R., Beaudoin J.J., Raki L. and Alizadeh R., "Durability and engineering performance of calcium-silicate-hydrate systems modified with nitrobenzoic acid," *American Ceramic Society Meetings - 5th Advances in Cement-based Materials Symposium*, Tennessee Technological University, TN, USA, 2014.
3. Khoshnazar R., Beaudoin J.J., Raki L. and Alizadeh R., "Thaumasite and ettringite sulfate attack: similarities and distinctions," *American Concrete Institute Spring Convention*, Reno, NV, USA, 2014.
4. Khoshnazar R., Beaudoin J.J., Raki L. and Alizadeh R., "Durability and volume stability of C-S-H/polyaniline nanocomposites," *American Ceramic Society Meeting - 4th Advances in Cement-based Materials Symposium*, University of Illinois at Urbana-Champaign, IL, USA, 2013.
5. Khoshnazar R., Beaudoin J.J., Raki L. and Alizadeh R., "Solvent-exchange damage to ettringite microstructure," *American Concrete Institute Fall Convention*, Toronto, Canada, 2012.

Seminar:

1. Khoshnazar R., Beaudoin J.J., Raki L. and Alizadeh R., "Organically modified calcium-silicate-hydrate systems," Purdue University, IN, USA, 2014.
2. Khoshnazar R., Beaudoin J.J., Raki L. and Alizadeh R., "Development, characterization and durability assessment of cement-based nanocomposites," Northwestern University, IL, USA, 2013.